Synergistic Integration of Life Cycle Assessment and Life Cycle Costing for a Performance-Oriented Structural Design with Advanced Cement-Based Materials

Davide di Summa

Doctoral dissertation submitted to obtain the academic degrees of
Doctor of Civil Engineering (UGent) and Doctor of Structural, Seismic and Geotechnical Engineering (PoliMi)

Supervisors

Prof. Nele De Belie, PhD* - Prof. Liberato Ferrara, PhD**

* Department of Structural Engineering and Building Materials
Faculty of Engineering and Architecture, Ghent University

** Dipartimento di Ingegneria Civile e Ambientale
Politecnico di Milano, Italy

May 2024

GHENT UNIVERSITY

POLITECNICO MILANO 1863

Synergistic Integration of Life Cycle Assessment and Life Cycle Costing for a Performance-Oriented Structural Design with Advanced Cement-Based Materials

Davide di Summa

Doctoral dissertation submitted to obtain the academic degrees of
Doctor of Civil Engineering (UGent) and Doctor of Structural, Seismic and Geotechnical Engineering (PoliMi)

Supervisors
Prof. Nele De Belie, PhD* - Prof. Liberato Ferrara, PhD**

* Department of Structural Engineering and Building Materials
Faculty of Engineering and Architecture, Ghent University

** Dipartimento di Ingegneria Civile e Ambientale
Politecnico di Milano, Italy

May 2024

GHENT UNIVERSITY

POLITECNICO MILANO 1863

ISBN 978-94-6355-835-8
NUR 955, 971
Wettelijk depot: D/2024/10.500/40

Members of the Examination Board

Chairs

Prof. Em. Luc Taerwe, PhD, Ghent University
Prof. Giovanni Muciaccia, PhD, Politecnico di Milano, Italy

Other members entitled to vote

Prof. Eddie Koenders, PhD, Technische Universität Darmstadt, Germany
Prof. Erik Schlangen, PhD, Technische Universiteit Delft, the Netherlands
Philip Van den Heede, PhD, Ghent University

Supervisors

Prof. Nele De Belie, PhD, Ghent University
Prof. Liberato Ferrara, PhD, Politecnico di Milano, Italy

“A volte penso che non esiste niente.
E che tutta la mia vita e` un’invenzione di fatti, sentimenti e persone.
Ma se ripenso a certe albe e al bene che mi scambio con qualcuno,
mi dico che anche se fosse così, mi andrebbe bene.”

“Sometimes I think nothing exists.
And my whole life is an invention of facts, feelings and people.
But if I think back to certain dawns and the love I exchange with someone,
I tell myself that even if it were like that, it would be fine with me.”

Research Funding

This dissertation has been developed as part of the following project:

SMARTINCS

SELF-HEALING - MULTIFUNCTIONAL - ADVANCED REPAIR TECHNOLOGIES IN CEMENTITIOUS SYSTEMS

This project has received funding from the European Union’s Horizon 2020 research and innovation programme under the Marie Skłodowska-Curie grant agreement No 860006.

Acknowledgements

A first sincere thanks goes to the European Commission for having provided the financial support for this investigation within the framework of the Marie Skłodowska Curie grant. This gave to me the possibility of foster both my professional and personal growth. In an increasingly fragmented world, this experience convinced me that "the future is Europe" and no other ways are possible.

I would like to express an immense gratitude to my supervisors, Nele and Liberato, for selecting me for this PhD opportunity. Their unwavering support, guidance, and encouragement throughout my thesis journey have been invaluable. More than mere supervisors, they have been inspiring mentors who positively influenced my academic and professional development every step of the way. I am truly grateful for the opportunity to learn from you both.

My deepest appreciation also extends to the jury members for dedicating part of their time to contribute and improve the overall quality of this manuscript. Their insights have greatly enhanced the quality of my research outputs.

The Smartincs project has been an unforgettable experience, leaving a profound impact on both my professional growth and personal connections. Beyond its professional benefits, it provided me with the chance to extend my family. Yasmina and Vanessa have been my house when needed, becoming like family. Our shared experiences and conversations about our evolving families have added immense value to this journey, something I will always cherish. Lais and Mert have been my comfort/therapeutic zone whenever needed, often accompanied by a Belgian beer (but without fries…since we are still unable to order them in Dutch). Through this experience, I also had the pleasure of meeting Tim and Niranjan, whose friendship enriched the entire experience even further. I hope to have you all in my future!

Ghent did not welcome me with bright sunshine. However, it gave me the opportunity to meet Nati, Carolina, Luiza, Balsa, Mirko, Ivana, Mert Y, Michiel and Jolien. Thanks for having turned this cloudy piece of world into a sunny place where I always felt at home!

I would also like to express my heartfelt thanks to the entire PoliMi group, for making my experience there more enriching thank the expectations.

Since part of this work has been carried out at the Labo Magnel, I also want to express my gratitude to the technicians who assisted me during my lab activities: Nathan, Tom, Stefan, Tommy, and Jens. Their support, along with the constant happiness of Marijke and Christel, has been invaluable. Thanks for always being there to provide help whenever needed.

Aside from my Belgian colleagues, I would also like to extend my appreciation to those who were always there for me, even with a simple phone call. Mary, Roberta, Sara, Stefano, Andrea, Donato e Domenico. Their unwavering support and friendship have enriched my life in countless ways. I am profoundly grateful for your constant presence, proudness and encouragement and I will do my best to have you all in next chapters.

I certainly owe a thought to my family. On one side, there is my grandmother: a tireless presence who floods me daily with boundless love. On the other, there are my sister and my parents. This achievement is a milestone that my parents made possible every time they told me they were by my side. Whenever, wherever. From them, I did not inherit my eyes, but rather my perspective on the world; learning from their legs, though different from mine, never to stop. If tomorrow I am able to be for my daughter even just 1% of what they have been for me, I will know I am on the right path. Vi voglio bene.

A special section must be dedicated to Alessandra. This journey began, like everything else over the past 14 years, alongside her. We have watched the sun rise and set together in so many places that I have now lost count. But, fortunately, there is still a whole world to discover. Thank you for giving me the certainty that our family will be perfect simply because you will be Diana's mother. If she read these words one day, I want her to know that I don't believe anyone can be fully prepared to be a dad. However, I have learned that "in teaching, you will learn, and in learning, you will teach." And if there's one thing she taught me even before her birth, it is the gratitude feeling.

Thank you, Diana, for choosing this family for your earthly experience in this life. I promise “I will help your dreams crossing the sea faster than eagles, because you're a special being, and I’ll take care of you”.

Gand,
27th of May 2024.

Ringraziamenti

Un primo sincero ringraziamento va alla Commissione Europea per aver finanziato questa ricerca nell’ambito dei progetti di dottorato Marie Skłodowska Curie, dandomi la possibilita` di crescere sia professionalmente che personalmente. In un mondo sempre più frammentato, questa esperienza mi ha convinto sempre piu` che “il futuro è Europa” e non sono possibili altre strade.

Un ringraziamento va anche ai miei supervisors, Nele e Liberato, per avermi innanzitutto scelto per questa opportunita` di dottorato. La loro guida, assieme al costante incoraggiamento e supporto, sono stati inestimabili. Sono stati per me dei mentori che hanno influenzato quotidianamente e positivamente il mio percorso accademico e professionale. Grazie per avermi dato l’occasione di apprendere da voi.

Un sentito ringraziamento va anche ai membri del comitato di valutazione per aver dedicato parte del loro tempo per contribuire e migliorare la qualità complessiva di questo manoscritto, migliorando, con i loro suggerimenti, la qualita` dell’intero lavoro.

Il progetto Smartincs è stata un'esperienza indimenticabile, con ricadute sia professionali che personali, che mi ha dato la possibilita` di allargare la mia famiglia. Yasmina e Vanessa sono state la mia casa quando necessario, diventando come una famiglia. Le nostre esperienze condivise e le conversazioni sulle nostre famiglie in evoluzione hanno aggiunto un valore immenso a questo viaggio, qualcosa che apprezzerò sempre. Lais e Mert sono stati, poi, la mia comfort zone ogni volta che ne avevo bisogno, spesso accompagnati da una birra belga (ma senza patatine fritte...visto che non possiamo ancora ordinarle in fiammingo). Ho avuto anche il piacere di incontrare Tim e Niranjan, la cui amicizia ha arricchito ulteriormente l'intero viaggio. Spero di avervi tutti nel mio futuro!

Sebbene Gand e il Belgio non mi abbiano accolto con un sole splendente, mi hanno dato l'opportunità di incontrare Nati, Carolina, Luiza, Balsa, Mirko, Ivana e Mert Y. Grazie per aver trasformato questo nuvoloso pezzo di mondo in un luogo soleggiato dove mi sono sempre sentito a casa!

Desidero inoltre esprimere i miei ringraziamenti a tutto il gruppo PoliMi, per aver reso la mia esperienza lì migliore di ogni aspettativa.

Parte di questo lavoro è stato svolto presso il Labo Magnel e voglio pertanto esprimere la mia gratitudine anche nei confronti dei tecnici che mi hanno assistito durante le mie attività di laboratorio: Nathan, Tom, Stefan, Tommy e Jens. Il loro sostegno, insieme alla costante felicità di Marijke e Cristiel non ha eguali. Grazie per aver fornito sempre aiuto quando necessario.

Oltre ai miei colleghi belgi, sono grato anche a coloro che sono sempre stati lì per me anche con una semplice chiamata. Mary, Roberta, Sara, Stefano, Andrea e Domenico. Il loro sostegno e la loro amicizia mi hanno arricchito in modi innumerevoli. Vi sono riconoscente per il costante incoraggiamento e l'indiscutibile presenza e faro` di tutto affinche` possiate esserci in tutti i capitoli futuri.

Un pensiero lo devo, poi, sicuramente alla mia famiglia. Da un lato c'è mia nonna: una presenza instancabile che mi inonda quotidianamente di sconfinato amore. Dall'altro ci sono i miei genitori con mia sorella. La tappa di oggi è un traguardo che mamma e papa` hanno reso possibile ogni volta che mi hanno ripetuto d'essere al mio fianco. Sempre e ovunque. Da loro non ho ereditato gli occhi, ma lo sguardo verso il mondo; imparando dalle loro gambe, per quanto diverse dalle mie, a non fermarmi mai. E se domani riuscirò ad essere per mia figlia anche solo l'1% di quello che loro sono state per me, saprò di essere sulla strada giusta. Vi voglio bene.

Questo viaggio è iniziato, come tutto il resto negli ultimi 14 anni, insieme ad Alessandra. Abbiamo visto il sole sorgere e tramontare insieme in così tanti posti che ormai ho perso il conto. Ma, per fortuna, c'è ancora tutto un mondo da scoprire. Grazie di avermi donato la certezza che la nostra famiglia sarà perfetta semplicemente perché tu sarai la mamma di nostra figlia Diana. Se un giorno leggesse queste parole, voglio che sappia che non credo che nessuno possa davvero credersi pronto per essere un buon padre. Tuttavia, mi suggeriscono che "insegnando imparerai e imparando insegnerai". E se c'è una cosa che mi ha insegnato ancor prima della sua nascita, è il sentimento di gratitudine.

Grazie, Diana, per aver scelto proprio questa famiglia per la tua esperienza terrena in questa vita. Ti prometto che aiuterò i tuoi sogni ad "attraversare il mare più velocemente di aquile. Perché sei un essere speciale, ed io avro` cura di te".

Gand,
27 Maggio 2024

Table of contents

Samenvatting

Beton is een van de meest gebruikte bouwmaterialen vanwege zijn mechanische eigenschappen, eenvoudige installatie, kosteneffectiviteit en veelzijdigheid in vormgeving die bijdraagt tot esthetische constructies. Het vertoont echter ook zwaktes, met name een lage treksterkte, wat in veel gevallen de incorporatie van stalen wapeningsstaven noodzakelijk maakt, en vatbaarheid voor scheuren, toe te schrijven aan factoren zoals krimp op jonge leeftijd en mechanische belasting. Deze zwaktes kunnen de duurzaamheid ervan compromitteren: corrosieproducten van staal (en gerelateerde uitzettingsfenomenen) en de vorming van scheuren hebben niet alleen invloed op de mechanische prestaties van het materiaal, maar creëren ook paden voor schadelijke stoffen vanuit de omgeving. In dit kader moet ook worden overwogen dat, met een groeiende wereldbevolking, de vraag naar huisvesting en infrastructuur toeneemt, wat zal leiden tot een hoger betonverbruik in de nabije toekomst. Bovendien neemt beton een belangrijke plaats in binnen ons wereldwijde erfgoed en heeft het een intrinsieke identiteitswaarde, met name binnen bepaalde architecturale stijlen. Bijvoorbeeld, de brutalistische architectuur, populair sinds de jaren 1950 (met Le Corbusier als een van de voornaamste voorstanders), kenmerkt zich door het gebruik van zichtbeton. Al deze factoren benadrukken de noodzaak om innovatieve cementgebonden materialen te ontwikkelen die de prestaties en duurzaamheid van traditionele materialen overtreffen. Deze materialen zijn niet alleen essentieel voor nieuwe bouwprojecten, maar ook voor het renoveren van bestaande structuren. Over het algemeen zouden ze het concept van "minder is meer" moeten omarmen, waarbij hun hoge prestaties worden benut om niet alleen de onderhoudsbehoeften te minimaliseren, maar ook de afmetingen van structurele elementen te verminderen dankzij hun verbeterde mogelijkheden, waardoor de hoeveelheid benodigde grondstoffen wordt verminderd. Deze materialen moeten ook voldoen aan de opkomende markteisen, afgestemd op een groter bewustzijn van de milieugevolgen van de bouwsector op elk niveau: lokaal, regionaal en mondiaal. Dit resulteert in een groeiende vraag naar duurzamere materialen, in het kader van een holistisch duurzaamheidsperspectief dat milieutechnische, economische en sociale gevolgen omvat.

Het voorliggend onderzoek heeft tot doel het dwingende belang te belichten van het kiezen van het meest geschikte materiaal om zowel structurele als duurzaamheidsdoelen te bereiken, door een "a priori" benadering te

hanteren, waarbij levenscyclusanalyse (Life Cycle Assessment, LCA) en levenscycluskosten (Life Cycle Costing, LCC) worden geïntegreerd in de ontwerpfase van de constructie om het besluitvormingsproces te ondersteunen. De eerste poging om een levenscyclusbenadering toe te passen om de milieuprestaties van een product te beoordelen, dateert uit eind jaren 1960. Deze methodologieën zijn tegenwoordig gestandaardiseerd door internationale normen ISO 14040 en ISO 14044 en worden veel gebruikt in de bouwsector om de efficiëntie van de gehele toeleveringsketen te verbeteren. Ondanks de uitgebreide literatuur die beschikbaar is over traditionele cementgebonden materialen, blijven gegevens over geavanceerde bouwmaterialen schaars. Dergelijke gegevens zijn doorgaans beperkt tot de productiefase en missen vaak schattingen van de materiaalprestaties in de loop van de tijd en bij grootschalige toepassing.

Een eerste deel van dit werk is daarom gericht op een diepgaande analyse van de stand van zaken op het specifieke gebied, met een focus op de te gebruiken methodologieën en de belangrijkste uitdagingen, zoals het gebrek aan gegevens met betrekking tot het gebruik en de einde-levensfase wanneer nieuwe materialen op een structurele schaal worden toegepast. Hier wordt de introductie van een methodologie voor het maken van duurzaamheidsbeoordelingen cruciaal. Deze benadering heeft tot doel de levensduur en veerkracht van structuren tegen degradatiemechanismen te maximaliseren door duurzaamheids-overwegingen vroeg in het ontwerpproces te integreren. Door op potentiële degradatiemechanismen te anticiperen en structurele oplossingen dienovereenkomstig aan te passen, kan de prestatie van structuren gedurende hun levenscyclus worden verbeterd. Het overkoepelende doel is om de behoefte aan onderhoud en reparaties in de loop van de tijd te minimaliseren, wat indirect zowel LCA- als LCC-resultaten ten goede komt. De effectiviteit van deze benadering is echter gebaseerd op de beschikbaarheid van uitgebreide gegevens, wat een grote uitdaging vormt, met name voor nieuwe materialen, vanwege hun gebrek eraan.

Om dit doel te bereiken, zijn experimenten en gegevensverzameling cruciaal, met name met betrekking tot duurzaamheid bij blootstelling aan agressieve omgevingen. Deze werden uitgevoerd voor bepaalde materialen geëvalueerd binnen het kader van het SMARTINCS-project (of andere gerelateerde projecten zoals ISAP en RESHEALIENCE). Zo werden specifieke geavanceerde betontypes, waaronder beton met superabsorberende polymeren (SAP) of beton met CEM III en kristallijne toeslagstoffen (CA), beoordeeld om een gegevensbibliotheek te creëren die dient als een van de belangrijkste exploiteerbare resultaten van dit onderzoek voor toekomstige duurzaamheidsinschattingen. Meer specifiek zijn chloridemigratie en -diffusietesten uitgevoerd voor ongescheurd SAP-gebaseerd beton en beton met CEM III + CA, en ook in de gescheurde toestand voor beton met CEM III + CA. Chloridediffusietesten zijn uitgevoerd op een leeftijd van 6 en 12 maanden door monsters onder te dompelen in een oplossing met 33 g/l natriumchloride. Bovendien is voor CEM III + CA-beton natuurlijke carbonatatie getest voor monsters die gedurende 6 en 12 maanden aan de buitenlucht werden blootgesteld.

De studie duikt vervolgens in verschillende gevalstudies, van microscopische schaal tot grootschalige toepassingen. Microcapsules en aluminium nanovezels werden onderzocht op hun potentieel om zelfhelende prestaties te verbeteren. Voor de microcapsules werd het opgeschaalde productieproces via membraanemulsificatie beoordeeld. In dit proces worden capsules gevormd uit een olie-in-water-emulsie (waarvan de oliefase een dispersie is van een waterafstotend middel op basis van een alkoxysilaan met lage viscositeit en isoforon diisocyanaat) gevolgd door de vorming van een polyurethaanschaal. Dit deel van de studie is uitgevoerd samen met Claire Riordan, ESR 2 van het SMARTINCS-project. Nog steeds vanuit een microscopisch perspectief werden geconcentreerde aluminiumnanovezeldispersies onderzocht. Dit type product, ontwikkeld door NAFENTM, wordt geleverd in een 10% concentratie waterige suspensie. Aluminium nanovezels, zoals degene die hier zijn geanalyseerd (met diameters variërend van 4-11 nm en lengtes van 100-900 nm), bieden potentiële voordelen in ultrahoogwaardig beton (UHPC). Ze vergemakkelijken spanningsherverdeling in de gescheurde toestand, waardoor smalle scheuren ontstaan. Samen met hun hydrofiele eigenschappen stimuleren deze vezels de uitgestelde hydratiereacties, waardoor het herstel zowel qua scheurafdichting als mechanische eigenschappen na materiaalschade wordt verbeterd en versneld. Voor zowel de microcapsules als de 10% dispersie van aluminium nanovezels werd de milieuduurzaamheid gekwantificeerd en gepresenteerd met behulp van de EPD (Environmental Product Declaration) 2018-methodologie. Dit is bedoeld om aan te tonen dat deze materialen commercieel levensvatbaar en concurrerend kunnen zijn op de markt, aangezien een EPD een document is dat meestal vereist is om ervoor te zorgen dat milieubeweringen zijn gebaseerd op consistente en betrouwbare informatie.

De studie verplaatst zich vervolgens naar een macroscopische schaal, waarbij het gebruik van een 3D-geprint vasculair netwerk ingebed in een betonnen balk, blootgesteld aan een chloride-omgeving, is geanalyseerd. Daarnaast wordt het gebruik van beton met SAP's in wanden als onderdeel van tunnelelementen, evenals de toepassing van UHPC en R-UHPC (respectievelijk met traditionele of gerecycleerde granulaten) voor het construeren van een bassin met geothermisch water, onderzocht. Uiterst agressieve scenario's werden beoordeeld, zoals chloride-omgeving en zuuraantasting (XS en XA blootstellingsklassen volgens de Eurocode). Onderzoek naar het 3D-printen van vasculaire netwerken werd uitgevoerd in samenwerking met Yasmina Shields en Vanessa Giaretton Cappellesso (ESRs 1 en 11 van het SMARTINCS-project), terwijl het deel betreffende R-UHPC werd uitgevoerd samen met Niranjan Prabhu (ESR10).

Het onderzoek gaat vervolgens verder met de beoordeling van materialen met een hogere prestatie voor een strategische structuur zoals de waterzuiveringsinstallatie (een van de grootste in Europa), gelegen in Genua, Italië. Deze laatste werd gedeeltelijk geconstrueerd met behulp van beton met CA en is blootgesteld aan carbonatatie en chloride-aantasting. Deze studie is verder gericht op een beter begrip van de sociale implicaties voor de hele gemeenschap, die voortvloeien uit het gebruik van geavanceerde bouwmaterialen. Alle hierin behandelde gevalstudies benadrukken de consistente voordelen van het gebruik van geavanceerde bouwmaterialen vergeleken met meer traditionele oplossingen. Dit geldt zowel voor milieuduurzaamheid als economische duurzaamheid. Zo heeft de integratie van een 3D-geprint vasculair netwerk van Nylon/PLA ingebed in een betonmatrix, in combinatie met de injectie van helende middelen bij optreden van scheuren, geleid tot verminderingen tot wel 50% voor ecologische impact en kosten. Beton met superabsorberende polymeren toonde een vermindering van de milieueffecten tot wel 67% en een verbetering van wel 22% bij de economische beoordeling, voornamelijk toe te schrijven aan de aanzienlijk verbeterde duurzaamheid en bijgevolg verminderde onderhoudsactiviteiten. Op een vergelijkbare manier toonde UHPC voordelen tot wel 63% in milieubeoordelingen en 46% in economische beoordelingen, terwijl gerecyclede-UHPC, met 100% gerecyclede granulaten, leidde tot respectievelijk 50% en 33% vermindering. Evenzo vertoonde beton met CEM III + kristallijne toevoeging (CA) verminderingen tot wel 40% wat betreft milieugevolgen bij blootstelling aan carbonatatie als belangrijkste degradatiefenomeen.

Echter, het effectief communiceren van de voordelen van geavanceerde cementgebonden materialen (of andere specifieke materialen) ten opzichte van alternatieven, vanwege hun verbeterde algehele duurzaamheid, kan een uitdaging vormen. Om deze uitdaging aan te pakken en een duidelijke communicatie te vergemakkelijken, met name naar geïnteresseerde stakeholders, richt de studie zich vervolgens op de ontwikkeling van duurzaamheidsindices. Deze indices, te gebruiken op zowel materiaal- als constructieniveau, overwegen een reeks aspecten van materiaalprestaties zoals duurzaamheid, mechanische parameters, evenals LCA- en LCC-resultaten. Het doel is om een meer gestroomlijnde en efficiënte methode te bieden om duurzaamheid te communiceren door één unieke numerieke waarde te verstrekken.

Zoals eerder vermeld, zijn LCA- en LCC-methodologieën niet nieuw als instrument bij het beoordelen van duurzaamheid, maar de reikwijdte van dit werk gaat verder dan hun conventioneel gebruik. Hier wordt hun rol gedemonstreerd bij het vormgeven van de toekomstige koers van de bouwsector. Synergetisch geïntegreerd in een prestatiegericht constructief ontwerp, evolueren deze methodologieën van louter evaluatie-instrumenten naar beslissingsondersteunende instrumenten, met als doel een eco-bestendige bouwsector te vormen.

Sommario

Il calcestruzzo è uno dei materiali da costruzione più utilizzati grazie alle sue proprietà meccaniche, alla facilità di installazione, al costo contenuto e alla sua versatilità nell'acquisire le forme piu` svariate. Tuttavia, la sua bassa resistenza alla trazione, (che richiede l'incorporazione di barre di armatura in acciaio), e la suscettibilità alle fessurazioni rappresentano sicuramente una debolezza che ne inficia la durabilita`. I prodotti della corrosione dell'acciaio (e i relativi fenomeni di espansione) non solo influiscono sulle prestazioni meccaniche del materiale, ma favoriscono anche l'ingresso di agenti aggressivi provenienti dall'ambiente esterno. Bisogna inoltre osservare che, con la crescita della popolazione mondiale, la domanda di abitazioni e infrastrutture è in aumento, generando quindi, nel prossimo futuro, consumi di calcestruzzo sempre crescenti. Quest'ultimo e` inoltre un materiale che puo` portare con sé un valore identitario intrinseco, in particolare all'interno di alcuni stilemi architettonici: ad esempio, l'architettura brutalista, resa popolare a partire dagli anni '50 (con Le Corbusier tra i suoi principali esponenti) è identificata con l'utilizzo di calcestruzzo a faccia vista.

Quanto sopra evidenzia la necessita` di sviluppare materiali cementizi innovativi piu` performanti, con piu` elevate prestazioni di durabilita` rispetto a quelli tradizionali, da utilizzarsi non solo per le nuove costruzioni ma anche per la manutenzione di quelle esistenti. Tali materiali dovranno impiegarsi non solo perche' possano ridurre al minimo le esigenze di manutenzione attraverso le loro elevate prestazioni, ma anche perche` le loro proprieta` meccaniche possano consentire di ridurre le dimensioni degli elementi strutturali, riducendo, quindi, la quantità di materie prime necessarie. Oltre a questo, dovranno anche soddisfare le richieste di un mercato sempre piu` sensibile alla sostenibilita` ambientale del settore delle costruzioni a ogni livello: locale, regionale e globale.

In quest'ottica, questo lavoro di ricerca mira a fornire una metodologia per identificare il materiale più adeguato al raggiungimento di obiettivi sia strutturali che di sostenibilità olistica, integrando le metodologie Life Cycle Assessment (LCA) e Life Cycle Costing (LCC) con la progettazione strutturale. La prima analisi a ciclo di vita per valutare la prestazione ambientale di un prodotto (LCA) risale alla fine degli anni '60. Tuttavia, queste metodologie sono oggi standardizzate dalle norme internazionali ISO 14040 e ISO 14044 e ampiamente utilizzate nel campo delle costruzioni per migliorare l'efficienza dell'intera supply-chain. Nonostante, l'ampia

letteratura disponibile sui materiali tradizionali a base di cemento, i dati sui materiali da costruzione avanzati rimangono scarsi e in genere limitati alla fase di produzione, spesso mancando di stime delle prestazioni degli stessi nel tempo e su un'applicazione su larga scala.

Una prima parte di questo lavoro è quindi incentrata su un'analisi approfondita dello stato dell'arte nel campo delle valutazioni di sostenibilita`, con un focus sulle metodologie da impiegare e sulle principali sfide da superare, quali la mancanza di dati riguardanti le fasi di utilizzo e di fine vita. Questo, soprattutto per strutture realizzate con materiali di nuova tecnologia. Qui, l'introduzione di una metodologia di progettazione basata sulla valutazione della durabilità assume un ruolo cruciale. Quest'ultima, infatti, mira a massimizzare longevità e resilienza delle strutture, integrando considerazioni sulla durabilità nelle prime fasi del processo di progettazione. Pertanto, i meccanismi di degrado vengono analizzati gia` nella fase progettuale, adattando di conseguenza le soluzioni strutturali con lo scopo di ridurre al minimo la necessità di manutenzione nel tempo, con benefici diretti sia per l'LCA che per l'analisi LCC. Tuttavia, l'efficacia di questo approccio si basa sulla disponibilità di dati che, come detto prima, soprattutto per i materiali di nuova generazione, rappresentano una sfida significativa, in quanto spesso mancanti. A questo scopo, per alcuni dei materiali valutati nell'ambito del progetto SMARTINCS (o di altri progetti correlati come iSAP e ReSHEALiencE), sono stati condotti esperimenti al fine di raccogliere dati, in particolare riguardo alla durabilità quando esposti ad ambienti aggressivi. Pertanto, calcestruzzo contenente polimeri superassorbenti (SAPs) o, in alternativa, contenente CEM III e additivo cristallino (CA), sono stati analizzati al fine di realizzare una libreria di dati che, di fatto, rappresenta uno dei primi expolitable results di questa ricerca. Più nel dettaglio, sono state effettuate prove di migrazione e diffusione dei cloruri per calcestruzzi non fessurati contenenti SAPs e per calcestruzzi con CEM III+CA (per quest'ultimi anche allo stato fessurato). Le prove di diffusione dei cloruri sono state effettuate immergendo i campioni in una soluzione con 33 g/l di cloruro di sodio per 6 e 12 mesi. Inoltre, per il calcestruzzo CEM III + CA, e` stata testata anche la carbonatazione naturale su provini esposti all'aria aperta per un periodo di 6 e 12 mesi.

La ricerca approfondisce poi diversi casi studio, dalla scala microscopica alle applicazioni su larga scala. In prima istanza sono state studiate le microcapsule e le nanofibre di allumina (addizionate al calcestruzzo per il loro potenziale di migliorare le prestazioni di autoriparazione). Per le microcapsule e` stato valutato il processo di produzione in larga scala tramite "*membrane emulsification*". In questo processo, le capsule vengono formate da un'emulsione olio in acqua (la cui fase oleosa è una dispersione di un agente idrorepellente alcossisilano a bassa viscosità e isoforone diisocianato) seguita dalla formazione dell'involucro di poliuretano. Questa parte dello studio è stata svolta assieme a Claire Riordan, ESR 2 del progetto SMARTINCS. Sempre in una prospettiva microscopica, sono state esaminate le nanofibre di allumina in dispersione acquosa. Questo tipo di prodotto, sviluppato da NAFEN™ , viene fornito in sospensione acquosa con concentrazione al 10%. Le nanofibre di allumina, come quelle analizzate qui (con diametri che vanno da 4-11 nm e lunghezze da 100-900 nm), offrono potenziali vantaggi nel calcestruzzo ad altissime prestazioni (Ultra-High performance concrete). Facilitano la ridistribuzione delle tensioni nello stato fessurato e, insieme alle loro caratteristiche idrofile, favoriscono reazioni ritardate di idratazione del legante, migliorando e accelerando così sia la sigillatura delle crepe che il recupero nelle proprietà meccaniche. Sia per le microcapsule che per la dispersione al 10% di nanofibre di allumina, la sostenibilità ambientale è stata quantificata utilizzando, per presentare i risultati dell'analisi LCA, la metodologia EPD (Dichiarazione Ambientale di Prodotto) 2018 con lo scopo di fornire una prova che questi materiali possono essere competitivi sul mercato e pronti per essere commercializzati.

Lo studio si concentra poi su scala macroscopica, dove è stato analizzato l'utilizzo di una rete vascolare stampata in 3D incorporata in una trave di calcestruzzo, esposta ad un ambiente ricco in cloruri. Successivamente, viene esaminato l'uso del calcestruzzo con SAPs per realizzare muri, anch'essi esposti ad attacco di cloruri, nonché l'applicazione di UHPC e Recycled-UHPC (rispettivamente con aggregati tradizionali o riciclati) per la costruzione di una vasca contenente acqua geotermica. In genere, sono valutati scenari estremamente aggressivi, come ambiente ricco di cloruri o caratterizzato da attacco acido (classi di esposizione XS e XA secondo l'Eurocodice). La ricerca sulla stampa 3D delle reti vascolari è stata condotta in collaborazione con Yasmina Shields e Vanessa Giaretton Cappellesso (rispettivamente ESR 1 e 11 del progetto SMARTINCS), mentre la parte riguardante R-UHPC è stata svolta in sinergia con Niranjan Prabhu (ESR10). Lo studio ha, inoltre, valutato le prestazioni di una struttura strategica come l'impianto di depurazione (uno dei più grandi d'Europa) situato a Genova, in Italia. Quest'ultimo è stato in parte realizzato mediante l'utilizzo di calcestruzzo con additivo cristallino ed è sottoposto all'attacco della carbonatazione e dei cloruri. L'obiettivo, per questo caso, e` stato quello di comprendere meglio le implicazioni sociali per l'intera comunità derivanti dall'uso di materiali da costruzione avanzati che possano comportare una maggiore durabilita` della struttura.

Tutti i casi studio citati hanno evidenziato vantaggi consistenti nell'uso di materiali da costruzione avanzati rispetto a soluzioni più tradizionali. Ciò vale sia in termini di sostenibilità ambientale che economica. Ad esempio, l'integrazione di reti vascolari in nylon/PLA stampate in 3D ed incorporate nel calcestruzzo (per la successiva iniezione di agenti atti a favorire la chiusura delle fessure), ha prodotto riduzioni fino al 50% degli impatti ecologici e dei costi. Il calcestruzzo con polimeri superassorbenti ha mostrato riduzioni degli impatti ambientali fino al 67% e miglioramenti fino al 22% nelle valutazioni economiche, attribuiti principalmente alla durabilità significativamente migliorata e alla conseguente riduzione delle attività di manutenzione. Allo stesso modo, l'UHPC ha dimostrato benefici fino al 63% nelle valutazioni ambientali e del 46% in quelle economiche, mentre l'UHPC che incorpora il 100% di aggregati riciclati, ha generato riduzioni rispettivamente del 50% e del 33%. In modo analogo, il calcestruzzo contenente CEM III + additivo cristallino ha mostrato riduzioni fino al 40% per alcuni indicatori di impatto ambientale quando soggetto alla carbonatazione come principale fenomeno di degrado.

Tuttavia, comunicare in modo efficace i vantaggi derivanti della pronunciata sostenibilità dei materiali avanzati a base di cemento (o di un materiale in genere) rispetto alle alternative, può rappresentare una sfida. Per facilitare una comunicazione chiara ed efficace verso gli stakeholders interessati, lo studio approfondisce poi lo sviluppo di indici di sostenibilità. Questi indici, da utilizzarsi sia sulla scala del materiale (ad esempio, il m^3) che su scala strutturale, includono parametri prestazionali dei materiali come la durabilità, i parametri meccanici, nonché i risultati derivanti dalle analisi LCA e LCC. L'obiettivo è offrire un metodo efficiente per comunicare la sostenibilità fornendo un unico valore numerico.

Come accennato, sebbene le metodologie LCA e LCC non siano nuove nel campo della sostenibilità, questo lavoro va oltre il loro uso convenzionale per dimostrando la loro capacita` nell'influenzare il futuro del settore delle costruzioni. Integrate sinergicamente in una progettazione strutturale basata sulle prestazioni, questa ricerca propone una metodologia olistica in cui, da meri strumenti di valutazione divengono strumenti di supporto alle decisioni, con l'obiettivo di creare un settore delle costruzioni eco-resiliente.

Summary

Concrete is one of the most widely used construction materials due to its mechanical properties, ease of installation, cost-effectiveness, and versatility in shaping, which can also enhance architectural aesthetics if needed. However, it also exhibits weaknesses, notably its low tensile strength, necessitating in many cases the incorporation of steel reinforcing bars, and susceptibility to cracking, attributable to factors like early age shrinkage and loading conditions. These weaknesses may compromise its durability: corrosion products from steel (and related expansion phenomena) and cracks formation, not only impact the mechanical performance of the material, but also create pathways for harmful substances from the external environment. In this framework, it must be also considered that, with a growing global population, the demand for housing and infrastructures is increasing, leading to higher concrete consumption in the near future. Furthermore, concrete holds a significant place in our global heritage and carries intrinsic identity value, particularly within certain architectural styles: as an example, brutalist architecture, popularized since the 1950's (with Le Corbusier among its foremost proponents) is characterized by the use of fair-faced concrete. All these factors highlight the imperative for developing innovative cement-based materials that surpass the performance and durability of traditional ones. These materials are essential not only for new construction projects but also for retrofitting existing structures. In general, they should embrace the concept of "less is more", leveraging their high performance not only to minimize maintenance needs but also to reduce the dimensions of structural elements thanks to their enhanced capabilities, thereby reducing the amount of needed raw materials. These materials must also meet the emerging market demands, tailored to a greater awareness of the environmental implications of the construction sector at every level: local, regional, and global. This results in a growing demand for more sustainable materials, encompassing a holistic sustainability perspective that includes environmental, economic and social ramifications. This research aims to shed light on the imperative need of choosing the most proper material to achieve both structural and sustainability goals, adopting an "a priori" approach, integrating Life Cycle Assessment (LCA) and Life Cycle Costing (LCC) into the structural design phase to support the decision making process. The first attempt to apply a life cycle thinking to assess the environmental performance of a product, dates back to the late 1960's. However, these methodologies are nowadays standardized by international standards ISO 14040 and ISO 14044 and

largely employed in the field of construction to improve the efficiency of the entire supply-chain. Despite the extensive literature available on traditional cement-based materials, data on advanced construction materials remains scarce. Typically, such data are limited to the production stage, often lacking estimations of material performance over time and at a large scale application.

A first part of this work is then directed to a deep analysis of the state of the art in the specific field, with a focus on the methodologies to be employed and on the main challenges to be addressed, like lack of data regarding the usage and end-of-life phases when novel materials are implemented on a structural scale. Here, the introduction of durability assessment-oriented design methodology becomes pivotal. This approach aims to maximize the longevity and resilience of structures against degradation mechanisms by integrating durability considerations early in the design process. By anticipating potential degradation mechanisms and tailoring structural solutions accordingly, the performance of structures can be enhanced throughout their lifecycle. The overarching goal is to minimize the need for maintenance and repairs over time, indirectly benefiting both LCA and LCC outcomes. However, the effectiveness of this approach is based on the availability of comprehensive data, which poses a significant challenge, particularly for novel materials, due to their lack. To this purpose, experiments and data collection, especially regarding durability when exposed to aggressive environments, have been carried out for certain of these materials assessed within the framework of the SMARTINCS project (or other related ones as ISAP and RESHEALIENCE). Thus, concrete including superabsorbent polymers (SAP) or, alternatively, containing CEM III and crystalline admixture (CA), have been assessed to create a data library to serve as one of the key exploitable results of this research, for future durability estimations. More specifically, chlorides migration and diffusion tests have been carried out for uncracked SAP-based concrete and concrete with CEM III + CA and also in the cracked state for concrete with CEM III + CA . Chloride diffusion tests have been carried out at the age of 6 and 12 months, by submerging specimens in a solution with 33 g/l of sodium chloride. Moreover, for CEM III + CA concrete, natural carbonation has been tested for specimens exposed to open air at the age of 6 and 12 months. The study delves then into various case studies, from the microscopic scale to large-scale applications. Microcapsules and alumina nanofibers are examined for their potential to enhance self-healing performance. For the microcapsules, the scaled production process through membrane emulsification, is assessed. In this process, capsules are formed from an oil-in-water emulsion (the oil phase of which is a dispersion of a low viscosity alkoxysilane water repellent agent and isophorone diisocyanate) followed by polyurethane shell formation. This part of the study has been performed together with Claire Riordan, ESR 2 of the SMARTINCS project. Still employing a microscopic perspective, the concentrated alumina nanofiber dispersions are examined. This type of product, developed by NAFEN™, is provided in a 10% concentration aqueous suspension. Alumina nanofibers, like the ones analyzed here (with diameters spanning from 4-11 nm and lengths from 100-900 nm), offer potential benefits in ultra-high performance concrete (UHPC). They facilitate stress redistribution in the cracked state, creating narrow cracks. Coupled with their hydrophilic characteristics, these fibers encourage delayed binder hydration reactions, thereby enhancing and expediting recovery in both crack sealing and mechanical properties following material cracking. For both the microcapsules and the 10% dispersion of alumina nanofibers, environmental sustainability has been quantified and presented using the EPD (Environmental Product Declaration) 2018 methodology. This is aimed at providing a proof that these materials can be commercially viable and competitive in the market, since EPD is a document usually required to ensure that environmental claims are based on consistent and reliable information.

The study moves then to a macroscopic scale, where the utilization of a 3D-printed vascular network embedded into a concrete beam, exposed to a chloride environment, has been analyzed. Additionally, use of concrete with SAPs in building walls as part of tunnel elements, as well as the application of UHPC and Recycled-UHPC (with traditional or recycled aggregates respectively) for constructing a basin containing geothermal water, are examined. Extremely aggressive scenarios are assessed, such as chloride environment and acid attack (XS and XA exposure classes according to the Eurocode). Research involving the 3D printing of vascular networks was conducted in collaboration with Yasmina Shields and Vanessa Giaretton Cappellesso (ESRs 1 and 11 of the SMARTINCS project), whereas the part concerning R-UHPC was undertaken alongside Niranjan Prabhu (ESR10). The research then continues with the examination of the performance resulting from the use of higher-performing materials for a strategic structure such as the wastewater treatment plant (one of the largest in Europe), located in Genoa, Italy. The latter has been partly constructed through the use of concrete with CA and it is subjected to carbonation and chloride attack. This is further aimed at better understanding the social implications for the entire community arising from the use of advanced construction materials.

All the case studies herein addressed highlighted consistent advantages in the use of advanced construction materials compared to more traditional solutions. This applies to both environmental and economic sustainability. For instance, the integration of a 3D printed Nylon/PLA vascular networks embedded into the concrete matrix, coupled with the injection of healing agents upon occurrence of cracks, yielded reductions of up to 50% in ecological impacts and costs. Concrete with Superabsorbent Polymers showcased environmental impact reductions of up to 67% and improvements of up to 22% in economic assessments, mainly attributed to the significantly enhanced durability and consequent reduction in maintenance activities. Similarly, UHPC demonstrated benefits of up to 63% in environmental assessments and 46% in economic assessments, while Recycled-UHPC, incorporating 100% recycled aggregates, was observed to generate reductions of 50% and 33% respectively. In a comparable way, concrete containing CEM III + Crystalline Admixture (CA) exhibited reductions of up to 40% concerning environmental ramifications when subjected to carbonation as main degradation phenomenon.

However, effectively communicating the advantages of advanced cement-based materials (or other specific materials) over alternatives, due to their enhanced overall sustainability, can pose a challenge. To address this challenge and facilitate a clear communication, particularly to interested stakeholders, the study delves then into the development of sustainability indices. These indices, to be used either on a material scale or on a structural scale, consider a series of material performance aspects such as durability, mechanical parameters, as well as LCA and LCC outcomes. Aim is to offer a more streamlined and efficient method of communicating sustainability by providing one unique numerical value.

As mentioned, while LCA and LCC methodologies are not new in the realm of sustainability, the scope of this work extends beyond their conventional use to demonstrate their role in shaping the future trajectory of the construction industry. Synergistically integrated into a performance-oriented structural design, these methodologies signify a transition from mere evaluation tools to decision-support tools, aiming at shaping an eco-resilient construction sector.

Notation index

LIST OF ABBREVIATIONS

ADP	Abiotic Depletion Potential
ADR	Advanced Dry Recovery
AP	Acidification Potential
AXF	Advanced Cross Flow
CMOD	Crack mouth opening displacement
DAD	Durability Assessment-oriented Design
DALYs	Disability Adjusted Life Years
EP	Eutrophication Potential
FAETP	Freshwater Aquatic Ecotoxicity Potential
FU	Functional Unit
GWP	Global Warming Potential
HTP	Human Toxicity Potential
IPDI	isophorone diisocyanate
ISO	International Organization for Standardization
KER	Key exploitable result
LCA	Life Cycle Assessment
LCC	Life Cycle Costing
LCI	Life Cycle Inventory
METP	Freshwater Aquatic Ecotoxicity Potential
ODP	Ozone Depletion Potential
PLA	Polylactic acid
POCP	Photochemical Ozone Creation Potential
rpm	revolutions per minute
SAPs	Super Absorbent Polymers
SAPs	SuperAbsorbent Polymers
SL	Service Life
TETP	Terrestrial Ecotoxicity Potential
TRL	Technology Readiness Level
UHPC	Ultra High Performance Concrete
UNI	Ente Nazionale Italiano di Unificazione

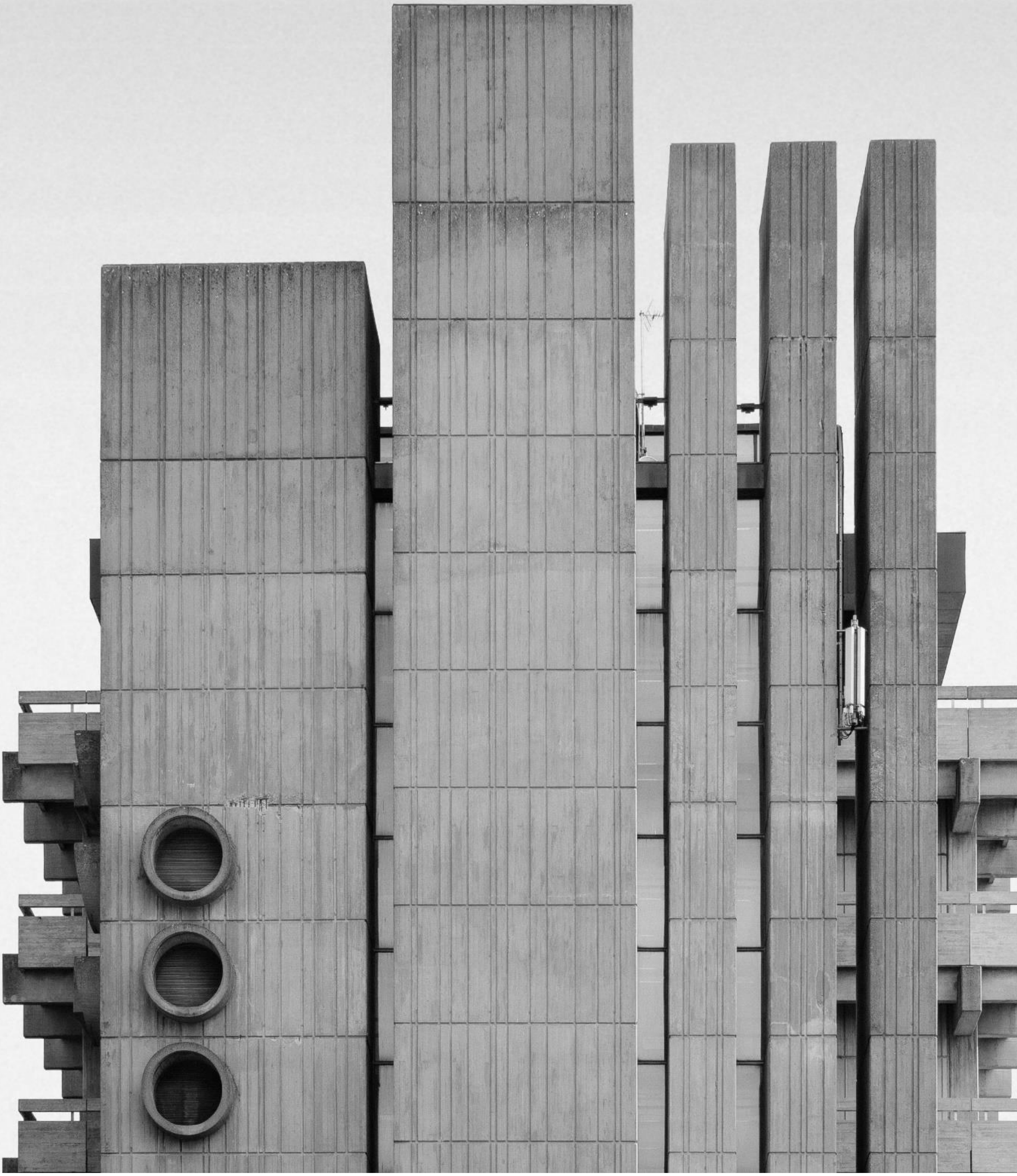

1 Introduction

This introduction chapter provides an overview of the contemporary challenges faced by the construction sector in terms of environmental, cost and social sustainability in modern society. It also includes scope and objective of this research and provides an overview of the thesis structure and organization. This investigation delves into exploiting advantages of advanced cement-based construction materials by employing a holistic life cycle design.

This chapter was redrafted after:

1] V. Cappellesso, D. di Summa, P. Pourhaji, N. Prabhu Kannikachalam, K. Dabral, L. Ferrara, M. Cruz Alonso, E. Camacho, E. Gruyaert, N. De Belie, A review of the efficiency of self-healing concrete technologies for durable and sustainable concrete under realistic conditions, International Materials Reviews (2023) 1–48. https://doi.org/10.1080/09506608.2022.2145747.

[2] D. di Summa, L. Ferrara, N. De Belie, How to account for benefits of Self-Healing concrete in design? A LCA/LCC perspective, in: M. di Prisco, A. Meda, G.L. Balazs (Eds.), Proceedings of the 14th Fib PhD Symposium in Civil Engineering, 2022: pp. 689–696.

[3] D. di Summa, M. Parpanesi, N. De Belie, L. Ferrara, How to address sustainability and economic viability of advanced cementitious based materials by means of Life Cycle Assessment (LCA) and Life Cycle Cost (LCC) tools integrated into a holistic design-wise approach., in: ICSHM2022 Milano -8thInternational Conference on Self-Healing Materials, 2022: p. 105.

[4] D. di Summa, M. Parpanesi, L. Ferrara, N. De Belie, Life Cycle Assessment (LCA) and Life Cycle Cost (LCC) analysis as crucial part of a holistic approach to the design of structures with advanced cement based materials, in: 76th RILEM Annual Week and International Conference on Regeneration and Conservation of Structures (ICRCS 2022), 2022.

[5] D. di Summa, M. Parpanesi, L. Ferrara, N. De Belie, A holistic life cycle design approach to enhance the sustainability of concrete structures, Structural Concrete 24 (2023) 7684–7704. https://doi.org/10.1002/suco.202300645.

[6] D. di Summa, J.R. Tenório Filho, Didier. Snoeck, Philip. Van den Heede, S. Van Vlierberghe, L. Ferrara, N. De Belie, Environmental and economic sustainability of crack mitigation in reinforced concrete with SuperAbsorbent polymers (SAPs), J Clean Prod 358 (2022). https://doi.org/10.1016/j.jclepro.2022.131998.

1.1 The sustainability challenges within the construction sector

The Human Right Council of the United Nations recognized, in 2021, globally and for the first time in history, the "human right to a clean, healthy and sustainable environment", followed by a more recent report (Human Rights Council United Nations, 2022) which better details the risk of the ongoing toxification of people and planet and raises awareness of the ensuing social injustices. More specifically, the report introduces the concept of "sacrifice zones" which are extremely contaminated areas where people, due to the contingent pollution issues, suffer human rights violations as well as physical and mental health consequences. The report also defines the boundaries of the problem which is actually of global interest. Indeed, places like the "Chemical Valley" in Canada and the city of Taranto in Italy, along with New Delhi in India or Bor in Serbia are mentioned because they are characterized by serious pollution and environmental degradation. Therefore, if on the one hand, this document strengthens the worldwide need for a more sustainable world (environmentally, economically and socially) with a new value, on the other hand, it also forces each production sector to re-think its future to change its current paradigm. In this regard, the construction sector requires specific attention not only because of its influence on the economy, since it represents around 9% of the EU Gross Domestic Product ("European Commission, 2016; Zhao et al., 2020) but also because it is estimated to be responsible of the consumption of 50% of the raw materials, of 36% of the global final energy use and of the generation of 25% of the total solid waste worldwide (Pérez-Lombard *et al.*, 2008; Yeheyis *et al.*, 2013). In this framework, concrete is one of the major players whose contribution to the transformation of the construction industry has, as such, aroused a growing scientific interest. As the most widely utilized construction material, accounting for approximately 30 billion tons in annual production (Miller *et al.*, 2018), concrete holds a significant environmental footprint due to the associated impacts of cement production, its primary component, contributing to approximately 7% of the world's total CO_2 emissions attributed to the concrete industry (Oh *et al.*, 2014). Therefore, the industry and academia efforts are focusing not only on the overall sustainability of the production of concrete, including the entire supply chain but also on the overall sustainability of the construction sector. This is possible only considering the entire Service Life (SL) of buildings and structures, until their decommissioning/demolition and treatment of constituent elements and materials, or even of the single building/structural elements and components (Ottosen *et al.*, 2021), as a waste or, alternatively, as recyclable materials and products. In this framework, the concept of material and structural durability has become one of the key factors to address the sustainability issue (di Summa *et al.*, 2022). About concrete, as an example, its inherent and unavoidable cracking in its structural service conditions, with the ensuing faster ingress of harmful substances inside the bulk of structural elements, accelerates the corrosion process of the steel reinforcement and, in case, the cementitious matrix degradation as well. The consequence is the degradation of the structural performance with the ensuing need to carry out the maintenance activities as soon as the front of the deterioration mechanism reaches a critical depth, e.g. concrete cover depth (Bartolini et al., 2004; Bartolini and Carsana, 2014). These maintenance activities, whose frequency may increase after the first one (Frangopol *et al.*, 1997), add up to further environmental impact and overall economic burden of the construction sector as a whole. To address the aforesaid problem, advanced cement-based materials have been developed which, ensuring the self-repair of the cracks upon occurrence or being extremely impervious to the penetration of harmful substances in aggressive environments, improve the durability of the structure they are built of or retrofitted with (De Belie *et al.*, 2018; Al-Obaidi *et al.*, 2020; Al Obaidi *et al.*, 2021; Liu *et al.*, 2021). It must be highlighted that durability represents a design target requisite which in current design codes (Folić and Zenunović, 2010), is achieved through "deemed to satisfy" prescriptions, including minimum water to cement ratio, minimum cement content and minimum concrete cover to guarantee the target service life. Nonetheless, because of the random and sometimes one-of-a-kind characteristics of structural service scenarios, this approach has resulted so far in a continuous need for repairing activities that have a huge incidence on the overall expenses, up to 50% (Zhang and Mailvaganam, 2006; Yang *et al.*, 2020).

Therefore, in the pursuit of fostering, in the construction industry, the implementation of materials and processes which can positively contribute to the sustainability signature of the sector as a whole, the significance of utilizing appropriate tools to measure the environmental impacts cannot be overstated. As stated before, at the core of this challenge stands the realization that conventional construction practices carry significant environmental consequences, stemming from raw material extraction, manufacturing processes, transportation, construction, usage, and disposal/recycling. Life Cycle Assessment (LCA) and Life Cycle Costing (LCC) emerge then as pivotal methodologies for quantifying the environmental and cost impact of construction materials and processes. Integrating both into the decision-making framework within the construction market is crucial, not only for evaluating the sustainability of individual projects but also for facilitating informed comparisons among diverse solutions. The concept of LCA, initially introduced around 1970 and primarily applied to scrutinize consumer products (Plati and Tsakoumaki, 2023), has evolved and been standardized by ISO 14040/44, which details its procedural steps (UNI, 2021a,b). LCA investigations often highlight the interplay between the embodied energy of materials and their operational energy (the energy required for maintaining buildings and associated activities) (Zhao *et al.*, 2020). As an example, deployed to assess new buildings, LCA aims to mitigate harmful emissions and decrease energy consumption during all phases between construction and end of life, establishing itself as a well-established approach for sustainability inquiries in the built environment (Peña *et al.*, 2021).

1.2 Scope and objective of the thesis

Aim of this investigation is to demonstrate the advantages offered by the application of sustainability analyses, such as LCA and LCC, in the design of structures made of (or in case retrofitted with) advanced cement-based materials. Additionally, the research seeks to explore the potential advantages of these materials in comparison to traditional ones and to identify the factors contributing to the potential improvements. Only through a structured and tailored LCA and LCC, extending beyond conventional metrics confined to material unit volume or mass, can the true improvements of advanced materials, particularly in terms of durability, be properly appreciated. To achieve this goal, the focus will be directed toward specific self-healing technologies, including SuperAbsorbent polymers (SAPs), microcapsules, crystalline admixture, and vascular networks, as well as Ultra High Performance Concrete (UHPC). The analyses will be conducted at various scales, ranging from the material level up to the structural element/structure scale. As the construction industry evolves towards innovative and sustainable solutions, understanding the environmental implications of these advanced materials is of paramount importance. Within this perspective, LCA and LCC evolve from mere postdesign (or even post-construction/post-production) assessment tools into essential decision-making tools within the structural design process with advanced (cement based) construction materials. The objective is then to push the boundaries of the aforesaid technologies and contribute to cultivating a more sustainable and environmentally conscious construction landscape in line with international agreements and standard frameworks.

1.3 Outline of the thesis

In alignment with the objectives before detailed, the work is organized within the following chapters as follows:

Chapter 2 concentrates on LCA and LCC methodologies, providing an overview of the state of the art for the advanced cement-based materials mentioned above, highlighting current limitations and challenges.

Chapter 3 addresses the existing information gap due to the novelty of these materials, proposing strategies to obtain data on durability through pertinent laboratory experiments. To this purpose, carbonation tests, chloride migration and diffusion tests have been carried out for various mix designs with the aim of creating a database regarding durability indicators to be specifically used for the scope of the sustainability analyses.

Chapter 4 presents a comprehensive overview of the diverse case studies examined for the research scope, encompassing evaluations at the material level, such as for microcapsules with healing agents, to the structural scale, exemplified by a UHPC water basin structure containing geothermal water.

Chapter 5 aims to establish an effective means of communicating the holistic sustainability of these materials to stakeholders by developing sustainability indices. This is deemed crucial for the successful penetration of these technologies into the construction market, as sustainability assessments play a pivotal role in shaping the commercialization strategy. The key exploitable results of this research are also presented.

Chapter 6 presents the main findings derived from this investigation, while also directing attention towards the challenges for future developments and the necessary follow-up of the current research.

2 Life Cycle Assessment and Life Cycle Costing for advanced construction materials

Life Cycle Assessment and Life Cycle Costing are worldwide recognized methodologies crucial for assessing and quantifying sustainability of a product or process throughout its entire life cycle. This chapter explores how they must be structured according to current international standards while also addressing the present obstacles in their application to advanced construction materials when assessed on a structural scale.

This chapter was redrafted after:

1] V. Cappellesso, D. di Summa, P. Pourhaji, N. Prabhu Kannikachalam, K. Dabral, L. Ferrara, M. Cruz Alonso, E. Camacho, E. Gruyaert, N. De Belie, A review of the efficiency of self-healing concrete technologies for durable and sustainable concrete under realistic conditions, International Materials Reviews (2023) 1–48. https://doi.org/10.1080/09506608.2022.2145747.

[2] D. di Summa, L. Ferrara, N. De Belie, How to account for benefits of Self-Healing concrete in design? A LCA/LCC perspective, in: M. di Prisco, A. Meda, G.L. Balazs (Eds.), Proceedings of the 14th Fib PhD Symposium in Civil Engineering, 2022: pp. 689–696.

[3] D. di Summa, M. Parpanesi, N. De Belie, L. Ferrara, How to address sustainability and economic viability of advanced cementitious based materials by means of Life Cycle Assessment (LCA) and Life Cycle Cost (LCC) tools integrated into a holistic design-wise approach., in: ICSHM2022 Milano -8thInternational Conference on Self-Healing Materials, 2022: p. 105.

[4] D. di Summa, M. Parpanesi, L. Ferrara, N. De Belie, Life Cycle Assessment (LCA) and Life Cycle Cost (LCC) analysis as crucial part of a holistic approach to the design of structures with advanced cement based materials, in: 76th RILEM Annual Week and International Conference on Regeneration and Conservation of Structures (ICRCS 2022), 2022.

[5] D. di Summa, M. Parpanesi, L. Ferrara, N. De Belie, A holistic life cycle design approach to enhance the sustainability of concrete structures, Structural Concrete 24 (2023) 7684–7704. https://doi.org/10.1002/suco.202300645.

[6] D. di Summa, J.R. Tenório Filho, Didier. Snoeck, Philip. Van den Heede, S. Van Vlierberghe, L. Ferrara, N. De Belie, Environmental and economic sustainability of crack mitigation in reinforced concrete with SuperAbsorbent polymers (SAPs), J Clean Prod 358 (2022). https://doi.org/10.1016/j.jclepro.2022.131998.

2.1 Life Cycle Assessment - basic principles

Life Cycle Assessment (LCA) is defined as 'the compilation and evaluation of the inputs, outputs and potential environmental impacts of a product system throughout its life cycle' (UNI, 2021a,b). In simpler terms, it can be considered as a tool for assessing the environmental impact of products at every stage of their life cycle, from creation to disposal/recycling. ISO 14040 and ISO 14044 standardize LCA methodology identifying 4 main steps: i) goal and scope definition, (ii) inventory analysis, (iii) impact analysis, and (iv) interpretation (UNI, 2021a,b).

2.1.1 Goal and scope definition

In the first stage, the objectives of the analysis must be worked out to provide a clear framework for the study. The intended audience must be identified along with a strategic approach for the effective communication of the results. Additionally, the relevance has to be emphasized of the chosen subject of the study, defined as Functional Unit (FU), better described in 2.1.1.1, that has to ensure the alignment with the overarching goals of the assessment. Besides the latter, the meticulous definition of the system boundary is also essential. This is because, as an example, different boundaries could lead to the inclusion or exclusion of indirect impacts (such as, e.g., those stemming from supply chain activities and end-user behaviour), affecting the outcomes of the analysis. Further details regarding the identification of the most appropriate system boundary are provided in 2.1.1.2.

2.1.1.1 Functional Unit Definition

As stated above, a crucial aspect involves the definition of the Functional Unit (FU), identified as the benchmark unit for the environmental impact assessment (Desmyter and Martin, 2001; UNI, 2021a). Existing literature highlights the variability of the FU scale in LCA analyses, ranging from the material level (i) to the structure level (ii):

(i) When assessing the environmental impact of diverse concrete mix designs, a small-scale FU at the material level may be appropriate. As observed in (Van den Heede, 2014) , an efficient metric, akin to that proposed by Damineli et al. (2010) can serve as an example. The latter introduced the binder intensity index as a measure of the total binder required per cubic meter of concrete to achieve 1 MPa of strength. This methodology establishes a unit of functional performance instead of relying on concrete volume or weight as the unit of measurement. Nevertheless, this kind of approach requires first of all appropriate considerations concerning the specified age at which this minimum strength has to be reached and hence to be taken into consideration. As an example, for structures like foundations, not immediately loaded, 90-days compressive strength could be taken into account and specified, instead of the conventional 28-day strength (Meyer, 2009). Additionally, this metric, to be considered exhaustive enough, must be correlated with a unit of service life. Thus, an alternative FU choice is the quantity of concrete required for a basic structural element (e.g., column, beam, slab, etc.) which has to resist the intended actions and must guarantee a predefined service life in a particular environment. This approach encompasses additional concrete manufacturing arising from replacements or repairs over time, as well as variations in strength. For example, opting for high-strength and high performance concretes (as UHPC) results in considerable reductions in structural dimensions and overall concrete volume, manifesting as an environmental benefit in the LCA output (di Summa *et al.*, 2023; Kannikachalam *et al.*, 2023).

(ii) In the evaluation of the environmental impact of a specific structure, the FU typically aligns with the structure or infrastructure itself. Several examples can be given in this respect. For instance, Sayagh et al. employed a 1 km pavement with a lane width of 3.5 m as the FU in a study on pavements, with a target service life of 30 years and a traffic load of 9.4 million trucks per lane within this period (Sayagh et al., 2010).Consideration on durability and mechanical load considerations was integrated into such studies. Similarly, Yang et al. (2015) evaluated the environmental and economic implications of incorporating recycled materials, in asphalt concrete pavement construction. The research considered as FU a roadway 1.6 km long with a varying service life depending on the specific asphalt mixture employed (Yang et al., 2015).In addition to infrastructure, entire buildings can be subjects of environmental evaluation. For instance, Xing et al. (2008) investigated the environmental impact differences between steel and concrete construction in office buildings with a 50-year lifespan. Bonamente and Cotana (2015) analyzed the carbon footprint besides the primary energy consumption of 1 m^3 of differently designed prefabricated industrial buildings throughout 50 years of life cycle. Above all, the work highlighted that the use phase can account for up to 76% of the overall environmental impacts. Similarly, Dsilva et al. (2023), carried out an LCA study based on an average prefabricated timber house produced in Germany, to specifically determine the environmental impacts of the production and construction stages.

2.1.1.2 System boundaries definition

LCA studies can be conducted at various levels within different boundaries. The cradle-to-gate boundary focuses solely on the impact stemming from raw material extraction till the point the finished product leaves the factory. However, this approach falls short when evaluating the environmental benefits of advanced cement-based materials, as it disregards aspects such as durability, demolition, and waste generation. In contrast, cradle-to-grave and cradle-to-cradle system boundaries, consider the entire life cycle of the material, incorporating aspects such as the use, end-of-life, and recycling phases. More specifically, the cradle-to-cradle approach is gaining prominence because extensive recycling and reuse are worldwide encouraged. This concept, as presented by McDonough and Braungart (2002), emphasizes designing products so that materials can be recycled at the end of their life cycle. An example is completely recyclable concrete (De Schepper *et al.*, 2014; Kannikachalam *et al.*, 2023), that, at the end of its life cycle, could be demolished and processed to obtain debris that can be reused in concrete production. Moreover, to encompass all influencing parameters, including, e.g., strength and durability, into the LCA, a modified cradle-to-gate approach is also possible. It aims to quantify the environmental impact of the total concrete amount required to produce and maintain a specific structure throughout its design service life. The latter excludes the end-of-life stage. However, it must be remarked that Wu et al. (2014) proposed to exclude 'use' and 'end of life' stages only if they affect LCA results by less than 1%. A detailed example of the possible system boundaries (and related inputs), employable for self-healing concrete, are reported in Figure 2.1 according to the life cycle stages outlined in (UNI, 2019). To conclude, it is noteworthy to mention the scales for concrete assessment suggested in (Van Den Heede, 2014):

(i) laboratory scale: focusing solely on the environmental impacts associated with the production of concrete constituents, this scale excludes transport and plant operation, making it ideal for comparing environmental impacts of different compositions but neglecting crucial aspects such as strength and durability aspects;
(ii) industrial scale: this stage includes transport and plant operation in the LCA but still excludes other aspects (e.g. strength and durability) from the study;
(iii) structure scale: the most comprehensive scale encompasses the entire life cycle of concrete, considering production, transport, plant

operation, on-site casting, use, maintenance, and end-of-life/recycling scenarios.

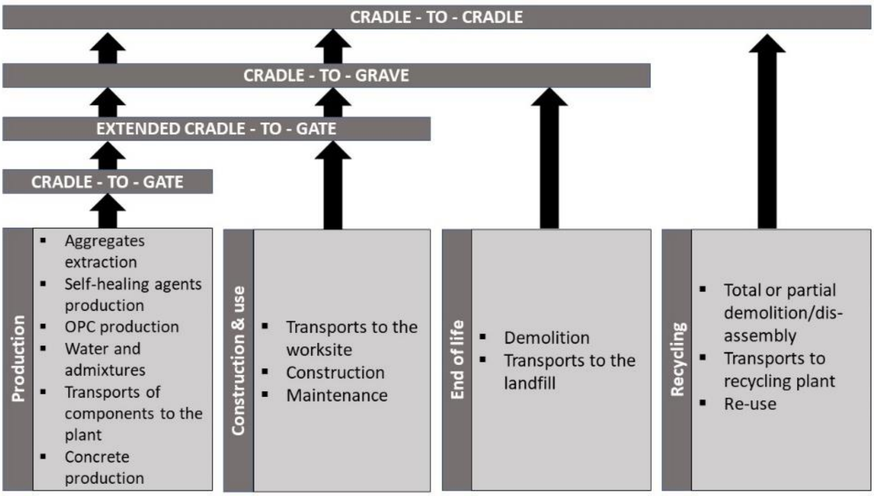

Figure 2.1: Possible LCA system boundaries for self-healing concrete.

Table 2.1: Life cycle stages for construction products – EN15804 (UNI, 2019).

PRODUCTION/ CONSTRUCTION					**USE**							**END OF LIFE/ BENEFITS**				
A1	**A2**	**A3**	**A4**	**A5**	**B1**	**B2**	**B3**	**B4**	**B5**	**B6**	**B7**	**C1**	**C2**	**C3**	**C4**	**D**
Raw materials supply	Transport	Manufacturing	Transport	Construction	Use	Maintenance	Repair	Replace	Refurbishment	Operation energy use	Operational water use	Demolition	Transport	Waste processing	Disposal	Reuse/Recovery/recycling

2.1.2 Inventory analysis

Once the subject of the study has been clearly defined, the subsequent step involves collecting data on all impacts associated with the chosen system boundary. First of all, the creation of the Life Cycle Inventory (LCI) necessitates substantial data from companies, encompassing activity data for both foreground processes directly linked to the product system and background processes not specifically tied to the product system (Bicalho *et al.*, 2017). These processes encompass input and output flows, covering consumed products, input of wastes, and resources from nature. Output flows include wastes, emissions, and final goods and services, with consideration given to various variables like productivity and types of transport used during data collection. The acquisition of essential information can occur either through comprehensive surveys directly from involved industries and stakeholders or by consulting publicly available annual environmental reports and environmental product declarations (EPDs). However, this type of data (defined as primary data) contributes to a more dependable life cycle inventory due to inherent risks of misinterpretation and double counting (Van Den Heede, 2014) Additionally, companies may not always provide firsthand data due to confidentiality concerns. In instances where primary data are unavailable, practitioners often turn to secondary data sources related to basic components. These datasets, commonly found in LCA databases like Ecoinvent, are vital for the development of LCA studies and are recognized as another crucial source (Frischknecht and Jungbluth, 2007). Thus, in consideration of the fact that data quality may largely affect LCA results (Guinee, 2002), the incorporation of a sensitivity analysis proves invaluable.

2.1.2.1 Allocation

During the inventory data collection process, careful attention must be given to the environmental burdens allocation, particularly when a system yields multiple products. Challenges arise when environmental impacts need to be distributed among different end products. Thus, inputs and outputs should be partitioned among the various products in a manner that reflects their underlying relationships. Allocation by mass or economic value can be used for this specific purpose (UNI, 2021b). Allocation becomes crucial when dealing with industrial by-products, including, e.g., blast furnace slag, fly ash, or silica fume. If no impact is attributed to them, they are regarded as waste. Alternatively, since these materials follow the requirements outlined by the European Union directive 2008/98/EC (European Parliament and Council of the European Union, 2008) they could be classified as a by-product. These criteria include certainty of further use, production as an integral part of a manufacturing process, direct usability without additional processing beyond normal industrial practice, and lawful use. Moreover, an investigation by Chen et al. (2010)(Chen et al., 2010), to assess the environmental impacts of blast furnace slag, fly ash, and silica fume, evaluated three different allocation procedures: no allocation, allocation by mass, and allocation by economic value. For the latter two, a mass allocation coefficient C_m and an economic allocation coefficient C_e have been developed, respectively. C_m and C_e are reported in Eq. (2.1) and (2.2) where m stands for mass and $(€ \cdot m)$ for economic value. However, it must be stressed that both allocation methodologies come with their own set of advantages and disadvantages. For instance, mass allocation might result in a substantial transfer of environmental impacts to the industrial by-product, potentially discouraging its further use. On the other hand, allocation based on economic value poses challenges as the economic value can fluctuate significantly over time, leading to consistently varying allocated burdens. Concerning the importance of choosing an appropriate allocation methodology, the work carried out by Seto et al. (2017) examined various concrete formulations with different proportions of fly ash as a cement replacement, considering different allocation scenarios. The obtained results indicated that concrete with higher fly ash content generally exhibits lower environmental impacts. However, the magnitude of these reductions depends on the chosen allocation scenario. Notably, both economic allocation and mass allocation scenarios yield higher environmental impacts than no allocation, highlighting the critical role of the allocation scenario in determining the environmental outcomes. Nevertheless, the study emphasized that it was the mass allocation scenario that produced the most substantial impacts.

$$Cm = \frac{m_{by-product}}{m_{main-product} + m_{by-product}} \qquad \text{Eq. 2.1}$$

$$Ce = \frac{(€ \cdot m)_{by-product}}{(€ \cdot m)_{main-product} + (€ \cdot m)_{by-product}} \qquad \text{Eq. 2.2}$$

2.1.3 Impact assessment

Scope of the impact assessment is to establish a connection between each LCI component and the corresponding environmental impacts. There are two distinct approaches which can be employed, as also identified by Jolliet et al. (2003) with a significant difference standing in the point at which the impacts are evaluated for the different environmental categories. The first approach, defined as a problem-oriented approach, positions the midpoint category indicators between the LCI results and the category endpoints. In short, midpoints serve as a link within the environmental impact mechanism, occurring before the endpoints, to derive indicators and portray the relative significance of emissions or extractions. These midpoint methods, such as the CML 2001, model quantitative aspects at the early stages of the cause-effect chain and, as detailed in 2.1.3.4, offer a problem-oriented perspective. For instance, the impact of a material on climate change is quantified in kilograms of CO_2-equivalents, serving as a quantification of emissions contributing to the climate change issue. Conversely, the second approach, defined as the damage-oriented one, puts higher emphasis on the endpoints, the terminals of the impact chains. Damage-oriented methods, such as Ecoindicator 99, model the damage based on the impact on human health, ecosystem health, or resource damage, but are often accompanied by higher uncertainties. Again, in the context of climate change, the damage to human health can be here quantified using disability-adjusted life years (DALYs), incorporating measures for Years Lived Disabled (YLD) and Years of Life Lost (YLL) due to this damage. There have been several discussions assessing the benefits and shortcomings of each approach. However, according to Benetto et al. (2004), the problem-oriented approach yields reliable results, although comparing them can be challenging. On the contrary, damage-oriented impact analysis allows for a more straightforward interpretation of LCA output but is considered less reliable. More details concerning some of the available assessment methodologies are reported in 2.1.3.2, 2.1.3.3 and 2.1.3.4.

2.1.3.1 Characterization/normalization/weighting

Before listing examples of damage-oriented and problem-oriented methodologies, it is worth clarifying the concepts of characterization, normalization, and weighting, included in each of them, as detailed in (European Commission, 2024). Characterization involves the quantification of environmental impacts related to inputs and outputs of a product or system. It entails converting raw data on emissions, resource usage, and other environmental releases into specific impact categories, representing concerns like climate change, human toxicity, or ecosystem damage. For instance, when considering climate change as an impact category, the emission data of greenhouse gases from a process are characterized using an indicator, often expressed as equivalent carbon dioxide emissions. This standardized representation allows for a uniform assessment of environmental impact, aiding in comparisons across different impact categories.

Normalization involves multiplying the life cycle impact assessment results by suitably defined factors to quantify and compare their contributions to impact categories relative to a reference unit. This process yields dimensionless, normalized results that indicate the burdens associated with a product in comparison to the reference unit. As an example, supposing the total greenhouse gas emissions of a product is equal to 10,000 kg CO_2 equivalent, and the average emissions per capita in the relevant region equal to 5,000 kg CO_2 equivalent, normalization would then express the impact as twice the average per capita emissions in that region. ISO 14040 standard considers normalization optional.

Weighting aids in interpreting and conveying the analysis results. During this stage, normalized outcomes undergo multiplication by a series of weighting factors (expressed in % and determined through stakeholder engagement or based on established environmental policies), representing the perceived relative significance of the considered life cycle impact categories. The weighted results for various impact categories can be compared to gauge their relative importance or aggregated to derive a comprehensive overall score. ISO 14040 standard also considers the weighting as an optional phase.

2.1.3.2 IPCC methodology

The IPCC 2001 methodology, developed by the International Panel on Climate Change, includes climate change factors within timeframes of 20, 100, and 500 years (*Climate Change 2007, the physical science basis . Contribution of Working Group I to the Fourth Assessment Report of the IPCC* , 2007). In the characterization process, the IPCC factors for the direct global warming potential of air emissions are outlined. However, certain aspects are not considered, (including, e.g., the indirect formation of dinitrogen monoxide from nitrogen emissions, radiative forcing due to emissions of NOx, water, sulphate). While the method includes CO_2 formation from CO emissions, it accounts for biogenic CO_2 uptake as a negative impact. Notably, normalization and weighting are excluded from this method.

The IPCC 2007 method is an updated version of the IPCC 2001 approach, retaining the climate change factors with timeframes of 20, 100, and 500 years. In the characterization stage, the IPCC factors for the direct (except CH_4) global warming potential of air emissions are highlighted. Similar to the IPCC 2001 method, certain considerations are not taken into account (e.g. the indirect formation of dinitrogen monoxide from nitrogen emissions, radiative forcing due to emissions of NOx, water, sulphate, etc.). Unlike the IPCC 2001 method, this approach does not include CO_2 formation from CO emissions. Biogenic CO_2 uptake and emission are not taken into account, focusing solely on biogenic methane release. As with the IPCC 2001 method, normalization and weighting are not incorporated into this approach.

The GWP index suggested by the IPCC is a problem-oriented metric as it solely quantifies greenhouse gas emissions (measured in kilograms CO_2 equivalents) and does not measure the resulting climate change-related damage (measured in DALYs) caused by these emissions.

2.1.3.3 Eco-indicator 99

Eco-indicator 99 comes after Eco-indicator 95, and both methodologies adopt a damage-oriented approach. The inception of the Eco-indicator 99 methodology initiated with the formulation of the weighting procedure (Goedkoop and Spriensma, 2001). Traditional life cycle assessments express the outcomes by employing 10 or more distinct impact categories. However, assigning meaningful weighting factors for this multitude of impact categories proves challenging for both expert panels and non-experts alike. Consequently, a panel of 365 individuals from a Swiss LCA interest group was tasked with evaluating the severity of three damage categories:

(i) damage to human health, quantified as the number of years of life lost and years lived with disability, combined as Disability Adjusted Life Years (DALYs), an index also employed by the World Bank and World Health Organization. In other terms, it takes into account respiratory and carcinogenic effects, impacts on climate change, ozone layer depletion, and ionizing radiation into a single value.
(ii) damage to ecosystem quality, expressed as the loss of species over a specific area during a designated period.
(iii) damage to resources, represented by the surplus energy required for future extractions of minerals and fossil fuels.

Normalization is carried out at the damage category level, with the data calculated on a European scale primarily using 1993 as the base year, and occasional updates for crucial emissions. Regarding weighting, the method employs a panel to assess three damage categories at the endpoint level

2.1.3.4 CML 2001 approach

In 2001, a team of scientists, led by the Center of Environmental Science at Leiden University (CML), introduced a set of impact categories and characterization methods for the impact assessment stage. The CML-IA methodology, implemented for the problem-oriented approach, foresees a normalization but lacks weighting schemes. The CML guide (Guinee, 2002) identifies the impact categories at the mid-point level as follows.

(i) depletion of abiotic resources: focuses on safeguarding human well-being, human health, and the health of ecosystems. It is related to the extraction of minerals and fossil fuels, stemming from inputs into the system. The Abiotic Depletion is calculated for each extraction event involving minerals and fossil fuels (measured in kilograms of antimony equivalents per kilogram of extraction). The geographical context for this indicator spans the global scale;
(ii) climate change: relates to emissions affecting ecosystem health, human health, and material welfare. The Global Warming Potential is expressed in kg carbon dioxide/kg emission, with a global scale
(iii) stratospheric ozone depletion: takes into account harmful effects due to increased UV-B radiation. The ozone depletion potential is expressed in kg CFC-11 equivalent/kg emission, globally and infinitely.
(iv) human toxicity: addresses toxic substance effects on the human environment. Human Toxicity Potentials (HTP) are calculated for an infinite time horizon, expressed as 1,4-dichlorobenzene equivalents/kg emission, with a variable geographic scale;
(v) fresh-water aquatic eco-toxicity: examines impacts on fresh water ecosystems. Eco-toxicity Potential (FAETP) is calculated for an infinite time horizon, expressed as 1,4-dichlorobenzene equivalents/kg emission, with a global/regional/local scope;
(vi) marine ecotoxicity: focuses on toxic substance impacts on marine ecosystems. It is characterized by a global/regional/local scope;
(vii) terrestrial ecotoxicity assesses impacts on terrestrial ecosystems. It is characterized by a global/regional/local scope;
(viii) photo-oxidant formation: involves the formation of reactive substances injurious to human health and ecosystems. The Photochemical Ozone Creation Potential (POCP) is calculated for a 5-day time span, with a variable geographic scope;
(ix) acidification: explores impacts of acidifying substances on various elements, calculated as Acidification Potential (AP), with eternity as the time span and a variable geographic scale.

(x) eutrophication: addresses impacts due to excessive nutrient levels. Eutrophication potential (EP) is expressed as kg PO_4 equivalents per kg emission, with eternity as the time span and a variable geographic scale.

Normalization, considered as optional for simplified LCA, becomes mandatory for detailed LCA. Baseline indicator normalization scores are calculated for reference situations in 1990 (world), 1995 (Europe), and 1997 (Netherlands), as outlined in (Huijbregts *et al.*, 2003).

2.1.3.5 EPD (2018)

This method is intended for generating Environmental Product Declarations (EPDs). An EPD is a comprehensive type of document that provides transparent and verified information about the environmental performance of a product throughout its life cycle, as per ISO 14025 (UNI, 2010). It is generally created and registered in the framework of a programme, such as the International EPD® system. This method includes the following categories:

(i) acidification potential;
(ii) eutrophication potential;
(iii) global warming potential;
(iv) photochemical oxidation potential;
(v) abiotic depletion potential for non- fossil resources;
(vi) abiotic depletion potential for fossil resources;
(vii) water scarcity and optionally;
(viii) ozone layer depletion.

The majority of impact categories, such as eutrophication, global warming, ozone depletion, and abiotic resource depletion, are directly adopted from the CML-IA baseline method. Normalization is not part of this method.

2.1.4 Interpretation

Scope of the interpretation stage is to exploits the results of the LCI and assessment phases to get reliable, verifiable, information. Both ISO 14040 and 14044 (UNI, 2021a,b) articulate these central objectives for life cycle interpretation: analyzing findings, drawing conclusions, discussing study limitations, and making recommendations based on earlier LCA stages. Simultaneously, the standards highlight the importance of transparently communicating the interpretation in a clear, comprehensive manner that aligns consistently with the defined goal and scope. The procedures for life cycle interpretation, as per ISO standards, include: i) identifying significant issues using LCIs; ii) evaluating sensitivity, completeness, and consistency, ii) concluding, making recommendations, and reporting results (*Industrial Waste Treatment Handbook*, 2006). In this regard, a technical report published by the European Commission (Zampori *et al.*, 2016) better details that the selected LCI must be scrutinized for its relevance to the goal and scope of the assessment, ensuring the consistency of the inclusion/exclusion of specific flows. Additionally, a thorough evaluation of different characterization models and normalization/weighting sets is crucial to achieve consistent and reliable results.

2.2 Life Cycle Cost (LCC) Assessment

Life Cycle Cost (LCC) assessment can be considered as a methodology which enables and facilitates comprehensive cost comparisons over a specific timeframe, taking into account pertinent economic factors. These include both initial costs and future operating costs, to optimize product performance and overall expenses throughout its lifespan (Jacob-Lopes *et al.*, 2021) In recent times, efforts to enhance the LCC methodology within industrial processes and integrate it into an environmental framework have emerged. As a result, LCC requires accurate considerations of all costs throughout the entire lifetime of the assessed FU, including purchase price and associated costs (e.g., delivery, installation), operating costs (energy, fuel, water usage, spares, maintenance), and end-of-life costs (such as decommissioning or disposal) or residual value (revenue from product sale). Moreover, LCC may also encompass indirect costs including, e.g., those related to greenhouse gas emissions, resource depletion, and water contamination, due to the implications for society in a broader perspective. The European Commission has responded to this by developing specialized LCC guidelines tailored to various sectors. These schemes are designed to facilitate LCC integration by public procurers in compliance with Article 68 of Directive 2014/24/EU and Article 83(2) of Directive 2014/25/EU (European Parliament and Council of the European Union, 2014; European Parliament and council of the European Union, 2014).

2.3 Advanced construction materials

Over the past decades, the construction sector has continually evolved with the emergence of new advanced construction materials, driven by increased awareness and knowledge about crucial aspects like sustainability, durability, and cost-effectiveness which have become material design governing variables of likewise importance as more Conventional mechanical performance parameters. In this respect, Dimov et al. (2018) emphasize the necessity to engineer concrete at the nanoscale to enhance its chemical and physio-mechanical properties. For instance, incorporating water-dispersed graphene (up to 8 grams per liter) with Portland cement can yield a remarkable increase of up to 146% in compressive strength and 79.5% in flexural strength, along with a 400% decrease in water permeability compared to conventional composites. However, when considering aggressive environmental scenarios, such as the ones identified by current standards (Cen,2002) (XC - corrosion induced by carbonation, XS - corrosion induced by chlorides from seawater, XF - freeze/thaw attack and XA – chemical attack), several advanced cement-based materials are nowadays available to fulfill the requirements. Makul (2020)performed a detailed (not-exhaustive) survey of the most recent advancements identifying: i) the reactive powder concrete; ii) the fiber-reinforced concrete, iii) the self-consolidating concrete, iv) the green concrete and v) the nano-concrete.

(i) reactive powder concrete is composed of fine grains, including cement, sand, quartz, and silica fume, along with superplasticizers and steel fibers. Achieving a dense matrix involves optimizing aggregates of dry fine powders, resulting in a highly compact composition that imparts ultra-high durability and strength to the composite. The average compressive strength typically ranges from 200 to 800 MPa while several techniques can be employed to enhance reactive powder concrete, as identified by Richard and Cheyrezy (1995): removal of coarse grains to improve homogeneity; use of the pozzolanic characteristics of silica fume to increase compressive strength and reduce water absorption; use of superplasticizer to lower water-cement ratio and improve workability; application of pressure to promote compaction; implementation of post-set heat-treatment to enhance the microstructure; incorporation of small-sized steel fibers to increase ductility.

(ii) with regard to fiber-reinforced concrete, it is widely acknowledged for its ability to be characterized by increased post-cracking tensile strength and crack propagation resistance, due to fiber presence. Furthermore, the latter have the potential to favour the creation of a dense network of microcracks instead of larger ones (Chalioris et al., 2019; Yang et al., 2019). Moreover, Al Obaidi et al. warned that the cost assessment of fiber-reinforced concrete (UHPC for the specific case of that study), usually made on the basis on the material cost per unit of volume, generates a misperception (Al-Obaidi *et al.*, 2022). This is because an estimation as such does not take into consideration the mechanical and durability properties which allow to use less raw materials, guaranteeing the same structural performance and a longer service life in comparison to a reference solution (Al-Obaidi *et al.*, 2022). In view of this, UHPC seems promising for obtaining important cost savings when scaled up to the level of a structure.

(iii) self-consolidating concrete exhibits a highly flowable and non-segregating nature, having as main advantage the fact that it does not necessitate mechanical vibration and can self-compact under its weight. This advanced concrete type operates independently of external compaction methods and relies on its weight to seamlessly fill all required formwork. To enhance workability, it may incorporate viscosity-modifying agents, high-range water reducers or superplasticizers.

(iv) with regard to what the author defines as green concrete, it is based on the idea that since Portland cement is associated with a huge quantity of CO_2 emissions, it must be partially replaced with low-carbon alternatives (e.g. fly ash or slag)(Maddalena *et al.*, 2018).

(v) nanomaterials can be used to enhance the durability and mechanical properties of cement-based materials (Shah *et al.*, 2016). Commonly employed nanomaterials include nanoscale spherical particles (such as nano-SiO_2, TiO_2, Al_2O_3, Fe_2O_3), nanotubes, and fibers (carbon nanotubes and carbon nanofibers) along with nanoplatelets (nanoclays, graphene, and graphite oxide) (Shah *et al.*, 2016). Two fundamental approaches guide the incorporation of nanotechnology: the creation of new products engineered at the nanometer scale for the concrete industry and the characterization and understanding of materials at the nano- and sometimes micro-scale through atomic modeling and advanced characterization techniques (Sobolev, 2016). Among the various nanomaterials, nano-silica stands out as a versatile element that improves the cement paste hydration process, creating a stronger microstructure. Researchers have successfully employed nano-silica to transform the rheological characteristics, strength, and longevity of Portland cement, showcasing significant improvements in compressive strength compared to a reference solution, up to 27% (Abreu *et al.*, 2017; Flores-Vivian *et al.*, 2017). Other researches (Cuenca et al., 2021a,b, 2022), explored the use of UHPC exposed to a chemical environment and containing crystalline admixtures (CAs) alongside alumina nanofibers (0.25% by weight of cement) and cellulose nanocrystals (0.15% by weight of cement). The results revealed that the presence of nano-additives not only improves mechanical properties, refines pore structure, and promotes cement hydration, but also improves self-sealing and self-healing capacity when exposed to an extremely aggressive environment (geothermal water rich in chlorides and sulphate ions, for the specific case of the cited study). This was due to the synergy between crack width control and the promotion of hydration and healing through internal curing mechanisms.

About concrete characterized by self-healing properties (a material on which the entire SMARTINCS research project focuses), it represents an innovation in the field of the construction sector that aroused great interest within the recent past. The significance of the topic in the scientific realm is discernible through Figure 2.2. The visual representation there provided can serve as an indicator of the impact of the subject within the scientific community. Moreover, a detailed overview of the various concrete healing technologies, below summarized, is provided in (De Belie *et al.*, 2018). The autogenous healing of cementitious materials is a fundamental process that leads to the partial or complete self-closure of cracks, resulting in the partial restoration of initial durability and physical-mechanical performances of the composites. Autogenous self-healing is primarily governed by the intricate interplay of physical, mechanical, and chemical mechanisms within the cementitious matrix. Figure 2.3 provides a schematic overview of the mechanisms contributing to autogenous healing when a crack is formed and exposed to water.

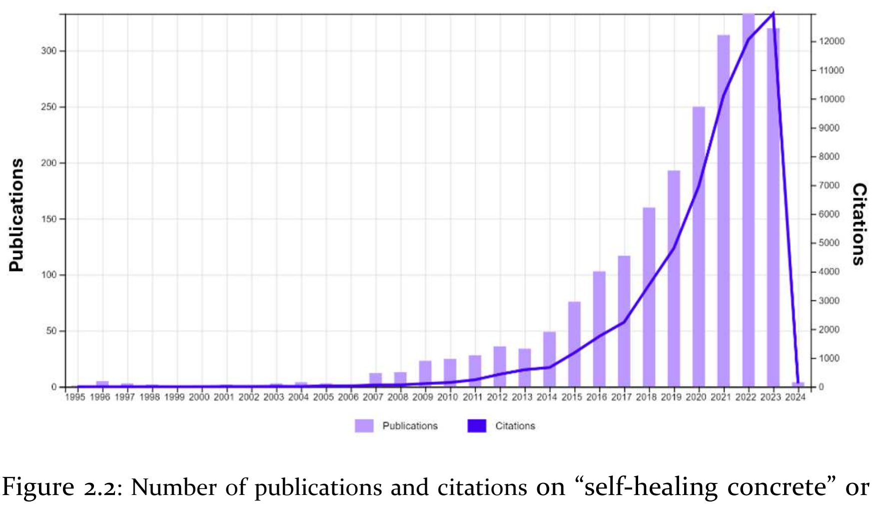

Figure 2.2: Number of publications and citations on “self-healing concrete” or “self-healing” in combination with ‘cement’ and ‘paste’ and ‘concrete’ and ‘mortar’ and ‘cementitious’ (Web of Science, 15 January 2024).

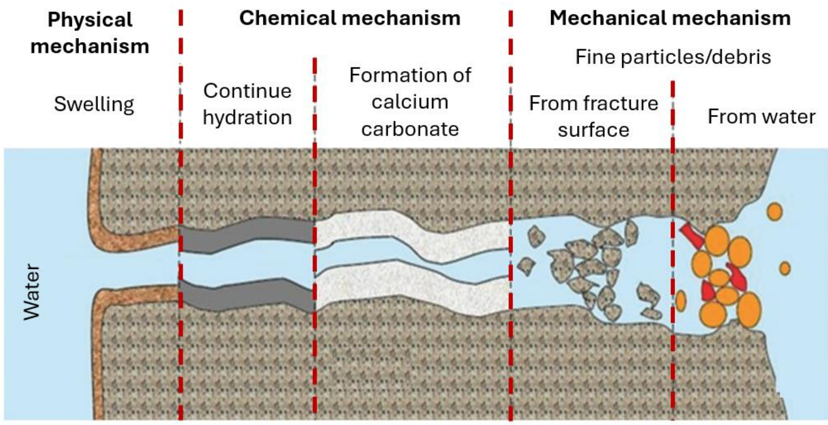

Figure 2.3 Mechanisms causing autogenous self-healing of cement-based materials. Redrafted after (de Rooij et al., 2013).

Two crucial chemical processes include the continuing hydration of un-hydrated cement grains and the precipitation of calcium carbonate crystals ($CaCO_3$) on the crack faces. In addition to these primary mechanisms, minor contributors to autogenous healing include the swelling of hydrated cement paste along crack walls and mechanical crack blocking by debris and fine concrete particles resulting from the cracking process or impurities in the entering water. Numerous experiments have been conducted to evaluate autogenous healing efficiency, with results indicating that it is effective for small cracks, typically in the range of 10–100 μm, and highly dependent on factors such as concrete composition, water presence, and crack characteristics. The intrinsic healing potential of concrete is mainly governed by its composition, including factors like cement type, silicate additions, aggregate type, concrete class, and age. Notably, water has been identified as a crucial factor for autogenous healing, influencing the chemical reactions and acting as a transport medium for fine particles. Lastly, the geometric characteristics of cracks, such as width, length, depth, and pattern, play a significant role in determining the degree of autogenous healing. Narrower cracks exhibit more efficient healing potential, suggesting that controlling crack width can substantially improve the intrinsic healing potential of cement-based composites. In this respect, fiber-reinforced composites have been developed to enhance crack control to favour the self-healing mechanism. Moreover, the autogenous healing can be achieved through ongoing hydration or crystallization, encompassing methods such as limiting crack width, providing water, and enhancing hydration or crystallization, all of which are regarded as stimulated autogenous healing. As said before, the work carried out by De Belie et al. (De Belie *et al.*, 2018), provides a detailed list of the various technologies whose characteristics can be summarized as follows.

(i) Use of mineral additions:

- contemporary cementitious materials commonly incorporate mineral additions, with a growing variety of types linked to global product development;

- the use of mineral additions, such as blast-furnace slag and fly ash, influences hydration kinetics, material properties, and autogenous self-healing potential.

- pozzolanic reactions, particularly those associated with additives such as fly ash, play a crucial role in promoting CSH polymerization reaction, thereby enhancing the autogenous self-healing mechanism.

(ii) Use of Crystalline Admixture (CA):

- crystalline additives designed for concrete often feature specific chemicals that react with the constituents of concrete during hydration process. Among these, tricalcium aluminate is a prevalent component that reacts with water, leading to the formation of calcium aluminate hydrate crystals. These crystals proliferate within the capillary pores and microcracks of the concrete matrix, establishing a protective barrier that hinders the infiltration of water, corrosive chemicals, and other detrimental substances;

- the generated water-insoluble precipitates block pores and cracks favouring the self-healing.

(iii) Use of Superabsorbent Polymers:

- Superabsorbent polymers (SAPs), known for their high fluid absorption capacity, are added to cementitious systems to mitigate autogenous shrinkage and to act as internal curing agents. They can also enhance freeze thaw resistance;

- SAPs absorb mixing water during concrete preparation and contract as the matrix hardens, resulting in the formation of macropores. These macro-pores become vulnerable points in the matrix, attracting and encouraging the occurrence of multiple cracks. Both phenomena contribute to the process of crack closure, as the cracks intersect with SAPs macropores, leading to the formation of narrower cracks.

(iv) Microencapsulation (<1 mm):

- Encapsulation of self-healing agents into microcapsules, with a diameter equal to or less than 1 mm, continues to be a widely embraced method for providing self-healing capacity to cementitious systems. Microcapsules must be incorporated into the matrix. When cracks develop, they draw in propagating cracks, rupture, and discharge their contents into the crack volume. The released agent subsequently reacts with a dispersed catalyst within the matrix, promoting the healing process of the crack.

(v) Macroencapsulation:

- macroencapsulation involves storing a larger amount of repairing agent compared to microencapsulation. The release of the healing agent is triggered by the formation of cracks, leading to the rupture of the embedded macrocapsule.

(vi) Vascular healing:

- vascular healing employs a biomimetic approach, mimicking human cardiovascular or plant vascular systems to deliver liquid healing agents to damaged areas;

- channels or networks are placed into concrete matrix to provide paths for continuous healing agent supply, overcoming challenges associated with encapsulation.

(vii) Self-healing bioconcrete:

- calcium carbonate $CaCO_3$ production through microbiological activity can be used as a self-healing mechanism;

- bacteria that stimulate the precipitation of $CaCO_3$ through various metabolic pathways have the potential to enhance self-healing by compacting the concrete matrix. Bacteria and nutrients can be either mixed directly into the concrete matrix during production or introduced via capsules or microcapsules;

- the efficiency of bacterial $CaCO_3$ precipitation is influenced by environmental factors, such as wet–dry conditions, and the control of crack width is crucial for faster and efficient healing.

2.4 LCA and LCC for advanced construction materials: state of the art

In light of recent advancements in the field of advanced cementitious materials, the necessity of employing methodologies such as LCA and LCC becomes even more pronounced. Both are crucial for comprehending the potential benefits that these materials can offer to the construction industry as a whole. Given the novelty of these materials and the incorporation of new components (e.g. chemical additives, healing agents etc.) the existing literature on the subject is relatively limited. Being this research carried out within the framework of European project SMARTINCS, focused on self-healing concrete, the following part addresses the specific case of the latter. However, it is important to note that the current limitations and challenges associated with these materials align with those encountered in the introduction of any new construction material. Compared to LCA studies for traditional concrete, the scientific literature about LCA of self-healing concrete is limited. Previous LCA studies focused mostly on sustainable concrete options like concrete containing incinerator ashes, marble sludge, blast furnace slag, recycled aggregates or fly ash (Colangelo et al., 2018; Colangelo et al., 2018; Kurda et al., 2018; Nath et al., 2018; Robayo-Salazar et al., 2018). This was motivated by the fact that cement-based composites are often associated with huge negative environmental impacts: the production of Portland cement only, can lead to 2 billion tons/year of CO_2 emissions (approximately equal to 8-10% of global anthropogenic emissions) (Szabó et al., 2006; McLellan et al., 2011; Turner and Collins, 2013; Ouellet-Plamondon and Habert, 2015)(McLellan et al., 2011; Ouellet-Plamondon & Habert, 2015; Szabó et al., 2006; Turner & Collins, 2013). Therefore, considering the consistent annual production of concrete, higher than 10 billion tons globally (Kline and Kline, 2015; Senaratne et al., 2016; Hache et al., 2020)(Hache et al., 2020; Kline & Kline, 2015; Senaratne et al., 2016), more sustainable solutions in this field can help to reduce negative environmental impacts related on a global, regional and local scale (Van den Heede & De Belie, 2012). The cited studies demonstrated that both the cement content and the extended service life had a significant impact on the overall environmental performance. More specifically, 36–43% and 36–38% of carbon footprint and energy consumption, respectively were avoided in the study developed by Nath et al. (2018) by replacing 40% of cement by fly ash and increasing the service life 1.6– 1.75 times. Robayo-Salazar et al. (2018)(Robayo-Salazar et al., 2018) used a natural volcanic pozzolan and granulated blast furnace slag, reaching 45% carbon footprint reduction. Thus, it is expected that LCA can also prove that self-healing concrete can achieve significant benefits from an environmental point of view due to the resulting extended service life (Van Belleghem et al., 2017)Van Belleghem et al., 2017).

Caruso et al. (2020) investigated the effect of the extended durability with a resulting service life of at least 30% longer on LCA output, developing a cradle-to-grave analysis for innovative cementitious materials exposed to aggressive ambient conditions. Here the authors assessed, in the construction of a basin for geothermal water settling, a high-performance fibre-reinforced cementitious composite with high content of slag (50% replacement by volume of cement) and 1.5% by volume of steel fibres (to obtain a strain hardening tensile behaviour) and autogenous healing stimulated by crystalline admixtures. They estimated a reduction of 71 and 87% for abiotic depletion and acidification, respectively. Similarly, Van den Heede et al. (Van den Heede *et al.*, 2019a,b) highlighted that the use of healing agents, together with PVA microfibres, allowed to save approximately 80% of global warming potential (GWP) if compared to Portland cement concrete due to the extended service life equal to 60 years (35 years longer than PC concrete). A cradle-to-gate system boundary was used by Van den Heede et al. (2018) for LCA of self-healing concrete containing different kinds of superabsorbent polymers. Here, the authors stressed two critical points, explaining why some studies are limited to the 'gate' stage: (i) the limited knowledge regarding the service life when exposed to a specific environmental condition and (ii) the lack of data regarding the life cycle inventory (LCI). Because of the absence of data related to the healing agent (due to confidentiality issues of the manufacturer), the authors combined data from the Ecoinvent database with information reported in the literature. Furthermore, the development of new materials in the laboratory (as for most of the healing agents currently used) is not an energy-efficient process. To this purpose the authors adjusted the LCI input by adopting the methodology by Piccinno et al. (2016) to go from the laboratory to the industrial scale. The proposed approach, focused on heated liquid phase batch reactions (identifying and streamlining the calculations related to the energy consumption during the reaction step, alongside specific purification and isolation procedures), provides formulas for computing values tailored to the specific case and based on literature and expert inputs. All of the available literature for LCA studies for self-healing concrete (as exemplified in Figure 2.4) uses a problem-related approach assessing up to 10 indicators in total: global warming (GWP); acidification (AP); eutrophication (EP); ozone depletion (ODP); photochemical oxidation (POCP); abiotic depletion potential (ADP); human toxicity potential (HTP); freshwater aquatic ecotoxicity potential (FAETP); marine aquatic ecotoxicity (MAETP) and terrestrial ecotoxicity potential (TETP). All the studies estimate promising results for self-healing concrete from the environmental point of view. The investigation by Rigamonti et al. (2019), which used a cradle-to-gate system boundary, cast a light on the better performance in terms of environmental impacts of self-healing concrete containing a crystalline admixture as an autogenous healing stimulator. In fact, impact indicators like AP, ODP, EP and POCP were reduced in a range between 5% - 15%. This was also the case in the study by Van Belleghem et al. (2017), where the same indicators were reduced by more than 50% because of the extended durability of concrete healed by encapsulated polyurethane. Due to the uncertainties associated with data quality, some studies highlighted the necessity to process further the results obtained by LCA analysis using a stochastic modeling approach, known as Monte Carlo simulation, to estimate the uncertainty and communicate the results in a probabilistic way (Nath *et al.*, 2018). Even in Van den Heede et al. (2019), considering the uncertainties related to maintenance and durability, the authors assumed a standard triangular error distribution that confirmed the sustainability of self-healing concrete with SAP (1 mass%/kg cement) and PVA microfibre (2 vol%). Finally, regarding the LCC assessment for self-healing concrete, only very few studies assessed the economic advantages of self-healing concrete compared to a conventional solution. In a work focused on the use of shape memory polymers to favour autogenous healing, Teall already addressed the potential cost reduction within a service life of 120 years due to the reduced maintenance activities (Teall, 2016). In line with this, another recent study highlighted the influence of the repairing activities throughout the service life, the cost of which for both the conventional and the self-healing solution, complying with ISO 16627:2015 (UNI, 2015), has to be actualized (Caruso *et al.*, 2020a). As a matter of fact, Life Cycle Costing outcomes are intricately tied to the timing of future costs since the value of money is contingent upon the specific date. Consequently, to aggregate present (e.g.

construction expenses) and future costs (e.g. the ones of the repairing activities to be carried out according to the estimations) a discount factor must be employed. The latter to reflect the diminished value in the year of transaction relative to the reference year. In this context, Equation 2.3 can be employed, where r is the annual real discount rate (usually assumed equal to 3% according to (Commission Delegated Regulation, 2012)) and T is the number of future years.

$$\text{Discount factor} = 1/(1 + r)^T \qquad \text{Eq. 2.3}$$

This highlights the need to further analyze these innovative materials from an economic point of view, the reason why Caruso et al. (2022), Gursel et al. (2014) and Colangelo et al. (2018) supported the idea of also assessing thoroughly economic performances to achieve a more holistic sustainable approach combining environmental and cost implications.

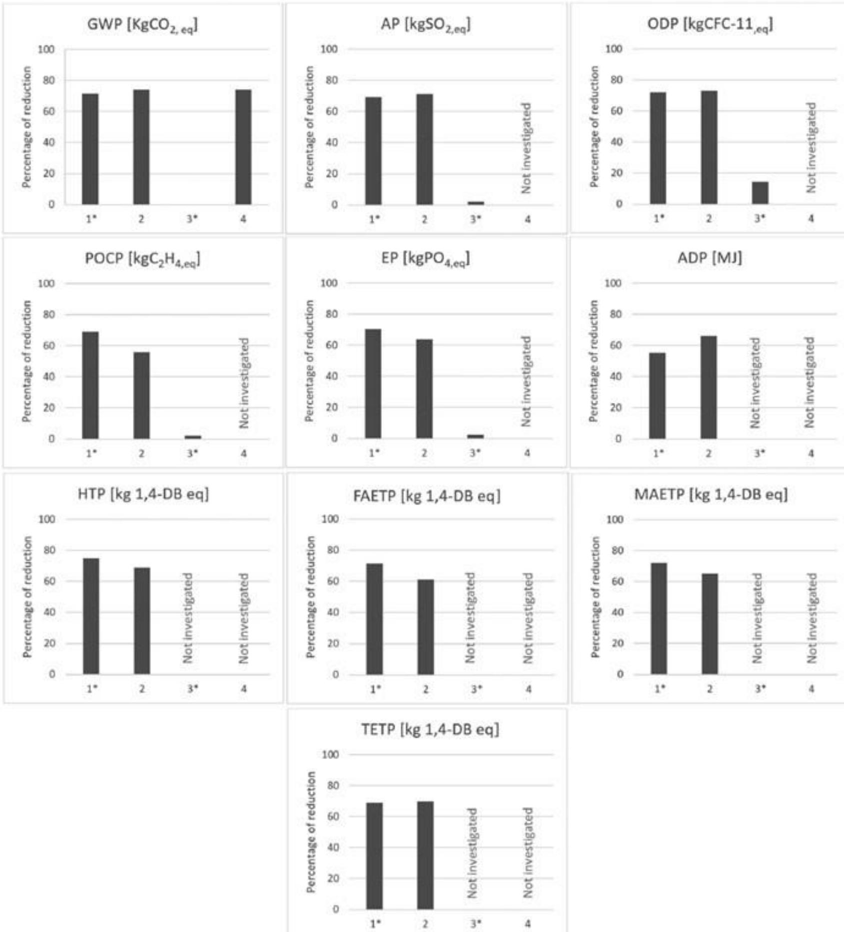

Figure 2.4: Comparison of the reduction of impacts in the available literature about LCA of self-healing concrete. (1) concerns concrete composites with 1 mass% of SAP and 2 vol% of PP microfiber, taking into account a FU with 100 years of service life (Van den Heede *et al.*, 2018); (2) similarly, but for self-healing concrete with polyurethane (Van Belleghem *et al.*, 2017); (3) concerns concrete with crystalline admixture using a cradle to gate system boundary (Rigamonti *et al.*, 2019); (4) concerns a concrete composite with 1 mass% of SAP and 2 vol% of PVA microfiber assuming 60 years of service life (Van den Heede *et al.*, 2019a). *Data here reported are obtained from 'Figure 2' and 'Figure 4' of the corresponding papers, respectively, as the exact value is not reported.

2.5 Conclusions

In the pursuit of advancing environmental sustainability within the construction industry, the use of robust tools to evaluate such sustainability is crucial. As mentioned earlier, conventional construction practices may have significant environmental consequences throughout their life cycle, not only because of the production/construction phase, but also due to maintenance and repair actions. Both Life Cycle Assessment and Life Cycle Costing methodologies emerge as pivotal tools for quantifying these environmental impacts. By integrating them into the decision-making framework, stakeholders can make informed comparisons among diverse solutions. Moreover, as the construction industry progresses toward innovative and sustainable solutions, understanding the environmental and cost implications of advanced materials is crucial. In this context, both LCA and LCC become allies in navigating the complexities of these materials. This seamlessly aligns with forward-looking perspectives and international sustainability goals outlined in international agreements and frameworks.

In the context of self-healing concrete and, more generally, of advanced cement-based materials, LCA studies represent an evolving field with limited literature compared to traditional concrete. The scientific literature on LCA for self-healing concrete highlights its potential environmental benefits, primarily due to extended service life and reduced maintenance activities. As a matter of fact, several studies demonstrate reductions in various environmental impact indicators, such as global warming potential, acidification, eutrophication, and more. In this framework, the emphasis on extended service life, coupled with rigorous assessments, positions self-healing concrete as a viable and environmentally friendly alternative, paving the way for a more sustainable future in construction practices. However, limited economic assessments carried out for the specific cases emphasize the need for a holistic sustainable approach, combining environmental, social, and economic considerations.

As research in this area continues to expand, a more thorough analysis is needed to contribute to an appropriate understanding, further promoting sustainable practices in the construction industry. Additionally, this work will go beyond the current state of knowledge. It will propose a new methodology that integrates LCA and LCC methodologies (whose role is essential for quantifying sustainability performance) into an omni-comprehensive design approach. This comprehensive framework will enable the assessment of the environmental and economic performance of advanced construction materials, including durability considerations and impacts associated with maintenance and end-of-life phase. The aim is to exploit the full potential of advanced cementitious materials, optimizing their performance while ensuring more accurate and dependable LCA and LCC outcomes. To this end, the forthcoming chapters will delve into the investigation of various case studies, illustrating the practical application of the proposed approach. The objective is to contribute to the evolution of construction practices, offering a comprehensive and integrated methodology that addresses the complex interplay between materials, design, and sustainability. Through the development of a groundbreaking approach, the following chapters aim to provide valuable insights and practical solutions for fostering a sustainable and resilient future in the field of civil engineering.

3 How to go beyond the “gate” stage: performance-oriented design and experimental setup to get a durability dataset

The lack of comprehensive data for novel materials presents a significant challenge, particularly concerning durability estimations, crucial for predicting their long-term performance. Addressing this challenge is of paramount importance, specifically when considering harsh environmental conditions that may lead to reiterated maintenance activities, whose entity and frequency has to be estimated by using reliable durability performance parameters. Thus, focus of this chapter is to bridge this data gap by highlighting the advantage of employing a performance-oriented design for which durability data are of the utmost importance. Given this, durability experiments for SAP-based concrete, as well as concrete consisting of CEM I or CEM III as binders and incorporating crystalline admixtures as healing stimulators, are explored. The experiments focused on chloride ingress and carbonation phenomena. The goal is to create a comprehensive data library, serving as a valuable resource for future research aimed at assessing the entire life cycle, including the “usage” and “end-of-life”/“recycling” stage.

3.1 From a prescription-based design to a durability-oriented one: a strategy to go beyond the "gate stage" for LCA and LCC analyses

Chapter 2 has highlighted that a fundamental challenge when using novel advanced construction materials stands in the need to go beyond the "gate" stage in order to perform a holistic sustainability assessment. This involves a thorough examination of multiple factors, encompassing usage scenarios, end-of-life considerations, and potential recycling phases. Thus, robust and reliable data are crucial for estimating durability, as the latter directly affects the maintenance frequency alongside with the production of post-use materials, whose management has emerged as a priority in numerous countries, especially within the European Union (European Commission, 2016). Nevertheless, most of the assessments for cement-based materials have so far excluded the usage and end-of-life phases from greenhouse gas (GHG) quantification, due to perceived low impact or uncertainties (Ochoa *et al.*, 2002; Junnila *et al.*, 2006). In contrast, the most recent literature highlights that the end-of-life phase can have a substantial impact on overall emissions due to scenarios including landfilling (which is common for processing concrete at the end of its life phase (Dodoo *et al.*, 2009) or recycling/reuse practices (Pade and Guimaraes, 2007; Wu et al., 2014)). Consequently, an appropriate structural design is essential to ensure efficient "usage" and "end-of-life" stages, especially under harsh environmental conditions. Two main approaches are then possible: the prescriptive method and the durability performance-oriented method. The first one, which involves identifying environmental factors and setting specific material and construction requirements, assumes that when fulfilling the specifications provided by the standard, the targeted service life is guaranteed. Due to this, it is named as the "deemed-to-satisfy" design method. Factors that may degrade concrete structures must be identified according to the specific exposure classes foreseen by the current standard framework. These exposure classes include various degradation mechanisms like carbonation, chloride ingress, freezing and thawing, chemical attacks. Durability specifications are then tailored to the identified exposure environment (and the corresponding severity classes). Parameters like concrete strength class, cement content, and water-to-cement ratio are then prescribed accordingly. Contrary to the prescriptive method, the durability performance-oriented approach verifies the service life of a structure based on its actual performance rather than assumed specifications. Degradation models are employed to predict material performance over the lifespan. Thus, since service life is defined as the duration before performance falls below a specified level or limit state; probabilistic models may be utilized to assess prediction reliability. This durability-oriented method is detailed in international standards such as ISO 16204 (ISO, 2012), the fib Model Code 2010 (fib, 2013), and fib Bulletin 34 (Schiessl *et al.*, 2006). Such approach becomes of a paramount importance especially when advanced cement-based materials are employed, since the prescriptive one may overlook long-term performance considerations, usually improved for these kind of materials in comparison to the most traditional ones. Moreover, such approach, goes beyond what is foreseen by the current standards framework according to which advanced cement-based materials automatically meet code specifications for durability. This is assumed because of their high cement content and low water-to-binder ratio, high compressive strength and tensile strain hardening behavior. Thus, the defined Durability Assessment-oriented Design (DAD) methodology, which integrates durability considerations into the design process, is herein synergistically integrated with LCA and LCC analyses. While the first strategy can help in achieving efficient “usage” and "end-of-life" stages, LCA and LCC, focusing on large scale applications, can then go beyond the “gate” stage, quantify the sustainability of the entire life cycle, until the “grave”, thus supporting the selection of specific structural materials or design layouts. Subsequent chapters of this research focus on the estimation of service life for structures exposed to either chlorides or carbonation. However, given that novel materials often lack sufficient durability data in this regard, considering their crucial importance within a durability-oriented approach integrated with sustainability estimations, the discussion also includes an overview of experimental set-ups for obtaining data in chloride-rich environments and in condition of carbonation.

3.2 Chloride induced corrosion

Concrete structures in chloride-rich and marine environments face significant challenges related to the ingress of chloride ion, which can lead to corrosion of embedded steel reinforcement, ultimately compromising durability and structural integrity. Quantifying chloride content within the concrete matrix and understanding chloride ingress mechanisms are crucial initial steps in addressing this degradation. The durability of concrete structures in marine environments has long been a principal concern due to the combined effects of chloride and sulphate ions found in seawater. These ions trigger various degradation mechanisms, including concrete cracking and reinforcement corrosion, compromising structural integrity. Factors such as micro-climate parameters (including wind direction and speed) and the presence of cracks significantly influence chloride content in concrete, particularly in maritime conditions (De Weerdt *et al.*, 2014; Santhanam and Otieno, 2016; Andersson *et al.*, 2019; Kušter Marić *et al.*, 2020). However, the complexity of marine environments is further compounded by the presence of sodium chloride and magnesium sulphate, leading to combined attacks by magnesium and sulphate ions, exacerbated by chloride presence. This complex chemistry highlights the vulnerability of structures exposed to a chloride rich environment, necessitating comprehensive strategies for predicting and extending concrete service life (Alexander *et al.*, 2013; Van den Heede *et al.*, 2016). In general, concrete structures in marine environments undergo various deterioration mechanisms based on their exposure zones. In the atmospheric zone, airborne chlorides can initiate chloride-induced corrosion of steel, with potential for carbonation-induced corrosion as well. However, chloride-induced corrosion typically prevails. Gaseous and water vapor diffusion, along with sorption during wetting and drying cycles by rain, contribute to the transport of aggressive substances. In the splash or tidal zone, concrete faces the most severe deterioration, with diffusion, sorption, and permeation playing significant roles. Mechanical wave action can cause physical damage such as abrasion and erosion, while drying cycles may lead to salt crystallization. In fully immersed zones, concrete saturation is complete, and further sorption is absent. However, permeation and diffusion remain critical factors, emphasizing impermeability as a top priority. Deterioration processes such as sulphate attack, leaching, and chloride-induced corrosion may occur (Santhanam and Otieno, 2016).

3.2.1 Chloride induced corrosion – initiation time

Chloride-induced reinforcement corrosion can be divided into two phases, with the initiation phase corresponding to the penetration of chloride within the matrix (Figure 3.1). In this scenario, rebar corrosion occurs only when the chloride content of the pore solution reaches a critical threshold, known as the critical chloride content. This threshold depends on various factors including the types of steel and concrete, as well as environmental condition (Angst *et al.*, 2009; Cao *et al.*, 2019).

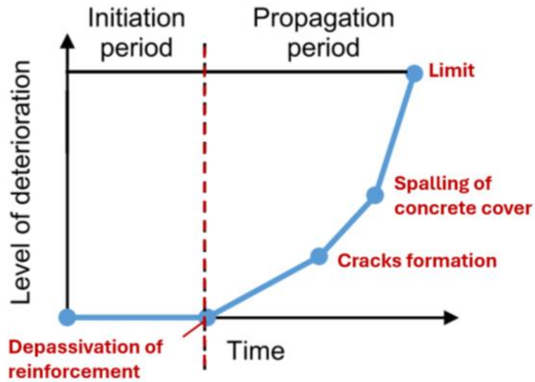

Figure 3.1: Schematic representation of initiation and propagation periods for concrete

The diffusion of chlorides can be described by employing Fick's second law that describes the rate of diffusion of a substance across a concentration gradient. More specifically, a general solution to Fick's laws is required to describe the relationship between time, depth, and concentration for service-life modeling, as depicted in Eq. 3.1.

$$C(x,t) = C_i + C_s \cdot \left(1 - erfc\left(\frac{x}{2\sqrt{D_a \cdot t}}\right)\right) \qquad \text{Eq. 3.1}$$

where, C(x, t) represents the chloride content at depth x and time t, C_i is the initial chloride content in concrete, C_s is the chloride content at the concrete surface, D_a is the apparent diffusion coefficient of chloride, and *erf* denotes the error function. However, some authors (Poulsen and Mejilbro, 2005) suggest an approximation of Eq 3.1 as follows, valid within the hypothesis that $0 \leq x < \sqrt{12 \cdot D_a \cdot t}$

$$C(x,t) = C_i + (C_s - C_i) \cdot \left(1 - \left(\frac{x}{\sqrt{12 \cdot D_a \cdot t}}\right)\right) \qquad \text{Eq. 3.2}$$

For service-life prediction, parameters such as, C_s, and D_a can be determined by measuring the chloride profile of existing structures with similar concrete types and exposure conditions. Alternatively, D_a can be calculated based on laboratory tests, such as rapid chloride migration method or diffusion tests below described. With respect to the diffusion coefficient, Shafikhani and Chidiac conducted a study, analyzing data from over 160 concrete mixtures (Shafikhani and Chidiac, 2019). They examined variables including water-to-cement ratio, types of supplementary cementitious materials, aggregate volume fraction, cement content, and maximum aggregate size to provide an overview of the range of achievable values. Generally, diffusion coefficients fell within the range of 10^{-11} m^2/s and 10^{-13} m^2/s, with optimal performance observed when employing Cem I with a lower water-to-binder ratio of 0.30.

3.2.2 Chloride induced corrosion: experimental set-up for non-steady migration test

A non-steady-state migration test can be carried out as an alternative to the other time-consuming non-steady experiments (namely diffusion test). It consists of a modification to the conventional migration cell (steady-state migration test) and is termed as rapid migration test. This method has been standardized by NordTest as NT Build 492 in 1999 (Nordtest, 1999). The test consists in applying an external electrical potential longitudinally across a concrete sample, inducing the migration of chloride ions from the catholyte solution into the sample. The test duration can be short, with results obtainable within 24 hours and up to 96 hours in total. Following these steps, the sample is longitudinally split. The depth of chloride penetration is measured by applying a 0.1 M silver nitrate solution to the sample, which allows to visualize the chloride penetration depth because of the whitish AgCl precipitation. Subsequently, a non-steady-state migration coefficient is computed using the equation below :

$$D_{NSSM} = \frac{0.0239 \cdot (273 + T) \cdot d}{(U - 2)} \cdot \left(x_d - 0.0238 \sqrt{\frac{(273 + T) \cdot d \cdot x_d}{U - 2}} \right) \qquad \text{Eq. 3.3}$$

Where D_{NSSM} is the non-steady-state migration coefficient (m^2/s), U is the applied voltage (V), T is the average value of the initial and final temperatures in the anolyte solution (°C), d is the thickness of the sample (mm), x_d is the average value of the measured penetration depths (mm) and t is the test duration (h). The non-steady migration test was conducted on concrete samples incorporating different types of superabsorbent polymers (SAPs), denoted as “C”, “SNF”, and “C+SNF” (a blend of the latter two). Type “C”, was produced by ChemStream bvba (Belgium). It was initially designed for the promotion of instant sealing of cracks with later enhancement of the self-healing potential of the concrete. It mainly consists of the monomer

NaAMPS (2-acrylamido-2-methyl-1-propanesulfonic acid sodium salt) and has been initially developed to meet the requirements of an internal curing promoter. It has two different types of crosslinkers: an alkali-stable crosslinker (0.15 mol% with respect to the NaAMPS monomer) and an alkali-unstable crosslinker (1 mol% with respect to the NaAMPS monomer). The mean particle size (d50) of 300 μm was used. It can absorb up to 11 g/g of mixing water in concrete in the first 10 minutes after contact with mixing water. Type "SNF", used for internal curing purpose, made by SNF Floerger (France) is a cross-linked acrylate copolymer produced through bulk polymerization and has a mean particle size (d50) of 360 μm. It can absorb up to 21 g/g of mixing water in concrete in the first 10 minutes after contact with water. The combination of both SAPs was foreseen to be used not only as internal curing agent for mitigation of shrinkage but also to enhance the self-sealing/healing of possible occurring cracks (Tenório Filho et al., 2021).

In addition to these SAPs-based mixes, experiments were performed on specimens from the corresponding reference mix design. All of the specimens were obtained from cores extracted from walls cast in Bruges (Belgium) as part of the iSAP project, which aimed to develop smart concrete mixtures with properties such as internal curing, self-sealing, and self-healing of cracks through the incorporation of SAPs(Tenório Filho *et al.*, 2021).

In total, five walls were cast: two reference walls (referred to as Ref1_wall and Ref2_wall) and three walls incorporating alternatively one of the different types of SAPs mentioned earlier (identified as C_wall, SNF_wall, and C+SNF_wall). The assessed mix designs are reported in Table 3.1 while Figure 3.2 and Figure 3.3 respectively show the walls cast in Bruges and the cores extraction procedure that took place in November 2021. To ensure an adequate number of specimens for both non-steady state migration tests and non-steady state diffusion tests (described in the subsequent paragraph), two cores (100 mm in diameter) were extracted from each wall. These cores were then sliced into 50 mm thick sections, with nine cylindrical samples obtained from each mix design (3 for the non-steady state migration test and 3 for the non-steady state diffusion one).

Table 3.1: Mix design of the assessed specimens.

	Ref1_wall [kg/m³]	Ref2_wall [kg/m³]	C_wall [kg/m³]	SNF_wall [kg/m³]	C+SNF_wall [kg/m³]
CEM III-B 42.5N	360	360	360	360	360
Limestone 2/20	1,116	1,054	1,078	1,078	1,078
Marine sand 0/4	736	695	702	702	702
Superplasticizer Sika ViscoFlow-26	2.42	0.95	2.42	2.42	2.42
Superplasticizer Tixo	1.56	-	1.56	1.56	1.56
Water	158.4	187.2	194.4	187,2	223.2
C_SAP	-	-	3.6	-	3.6 -
SNF_SAP	-	-	-	1.37	1.37 -

Figure 3.2: Walls built in Bruges with different types of SAPs (in the framework of iSAP Project) from where the cores have been extracted for durability experiments.

Figure 3.3: Cores extraction through core drill machinery.

Subsequently, three cylindrical samples per wall, coming from the same extracted core, were subjected to non-steady state migration test. Initially, the cylindrical specimens were immersed in a 4 g/l $Ca(OH)_2$ solution under vacuum to obtain full saturation. Then, following an immersion period of 18±2 hours, according to the procedure described in NT Build 492 (Nordtest, 1999), as exemplified in Figure 3.4, the specimens were secured within silicon rubber sleeves containing a 0.3 M NaOH solution (anolyte) at the top. The bottom surface of the samples within the sleeves was exposed to a 10% NaCl solution (catholyte). Subsequently, an external electrical potential was applied axially across each cylinder, inducing the migration of chloride ions into the specimens. Upon completion of the test, the specimens were removed from the sleeves and axially split. A 0.1 M silver nitrate solution was then sprayed onto the freshly split sections, as shown in Figure 3.5. The penetration depth was measured from the center to both edges at 10 mm intervals, for each series of 3 specimens belonging to the same mix design. The average chloride ingress value obtained was then used to calculate a non-steady state migration coefficient reported per mix design in Table 3.2. This coefficient was determined using the Equation 3.3. As it is possible to observe, all the obtained results fall within the same order of magnitude, around 10^{-12} m^2/s, with no significant differences observed between the reference mix and those containing SAPs. More specifically, while the SAP-based concrete types presented values similar to each other, the two reference mix designs exhibited slight variations. This discrepancy was also influenced by water content. As outlined by Chidiac, a higher water-to-cement ratio in the mix design can lead to increased porosity and permeability of the concrete matrix, consequently enhancing the ingress of chlorides and resulting in higher chloride diffusion coefficients (Chidiac and Shafikhani, 2020). However, since migration tests are less representative of realistic situations where no electric field occurs, diffusion tests have also been carried out to obtain more reliable durability parameters.

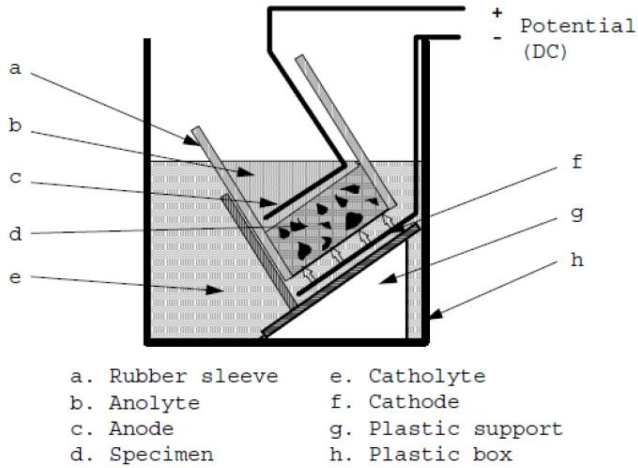

Figure 3.4: Schematic representation of the non-steady-state migration test setup.

Figure 3.5: On the left, the specimen is sprayed with a 0.1 M silver nitrate solution, while on the right, the border delineating the region affected by chlorides (appearing as light grey) is identified.

Table 3.2: Non-steady state migration coefficients obtained per series of specimens with indication of the standard deviation

	Non-steady state migration coefficient (D_{NSSM}) [m²/s]	Standard deviation [m²/s]
Ref1_wall	$3.7 \cdot 10^{-12}$	0.2
Ref2_wall	$6.3 \cdot 10^{-12}$	2.3
C_wall	$4.9 \cdot 10^{-12}$	0.9
SNF_wall	$5.5 \cdot 10^{-12}$	0.8
C+SNF_wall	$5.3 \cdot 10^{-12}$	1.1

3.2.3 Assessed mix designs and specimen preparation for non-steady state diffusion and carbonation tests

For the purpose of the non-steady state diffusion test, cylindrical specimens coming from the walls described in 3.2.2 were firstly tested. To such purpose, they have been immersed in a saturated Ca(OH)2 solution until reaching a constant mass. Subsequently, an epoxy coating was applied to all sides except the exposed surface. Following this, the samples were returned to the $Ca(OH)_2$ solution until mass stabilization. Additionally, specimens from beams cast with CEM I or, alternatively, CEM III + Crystalline Admixture (CA) were also examined. The purpose was to explore the potential durability enhancements achievable by utilizing more environmentally friendly solutions, given that CEM III incorporates materials with a reduced environmental impact (namely, supplementary cementitious materials such as blast furnace slag), and more durable alternatives, as CA is known to improve durability (Ravitheja *et al.*, 2019). The crystalline admixture used was supplied by Penetron, while the CEM III was provided by Buzzi Unicem, both partners of the SMARTINCS project. Figure 3.6 reports a schematic representation of the cross section of the beams besides a 3D view with indication of the reinforcement pattern. As can be observed, while 3 longitudinal Φ 12 reinforcing steel bars are present in tension zone, the shear reinforcement (Φ 6 steel bars) is placed with a distance ranging from 0.15 m up to 0.20 m to favour shear cracks creation during a subsequent induced crack phase in correspondence of the less reinforcement area. Figure 3.7 details the casting activities of the two beams while the specific mix designs are detailed in Table 3.3. Four beams were cast in total: two containing CEM I (named as CEM I_beam) and two containing CEM III + CA (named ad CEM

III+CA_beam). One beam for each type was used to carry out, alternatively, the non-steady state diffusion tests or the carbonation test, subsequently described in section 3.4.1. Beams were cured for 28 days in a room with a temperature of 20°C and a relative humidity >95%.

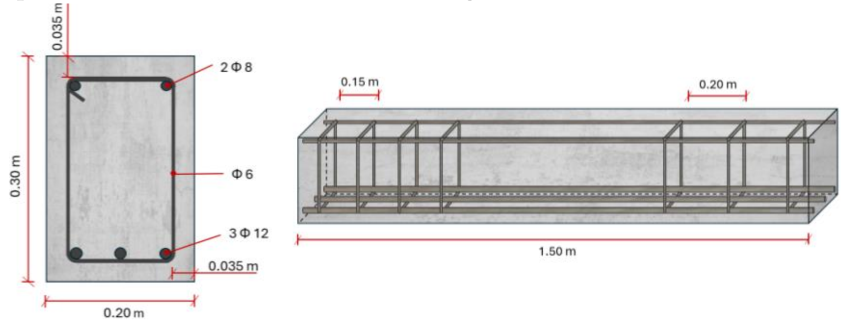

Figure 3.6: Cross section and 3D view of the beams with indication of the reinforcement details.

Figure 3.7: Formworks, reinforcing steel bars and CA used to cast the beams (left) casting procedures (middle) and beams right after casting procedures (right).

Table 3.3: Mix design for both Ref_beam and CEM III+CA_beam.

Components [kg/m³]	**CEM I_beam**	**CEM III+CA_beam**
CEM III/A 52.5 R or CEM I 52.5 N	337,6	337,6
Sand 0 – 4 mm	742,9	742,9
Gravel 2 - 8 mm	1031,1	1031,1
Limestone filler	58	58
Water	168,8	168,8
Superplasticizer	2	2
Crystalline admix.	-	3.37

Moreover, to test both chloride penetration and carbonation resistance, also in cracked state, the beams were subjected, after curing time, to bending under a three point bending test (3PBT). This was done to induce both flexural and shear cracks. The load was applied at midspan and subsequently at one third of the length from each edge. This loading scheme was chosen to obtain multiple cracks. At the location where the load was applied, to better distribute the latter, a neoprene pad was inserted underneath, followed by a metal plate on top. The beams were realized by employing B500C as reinforcing steel. Thus, since it was possible to estimate yielding of steel at 101 kN of load, increments of 10 kN were applied near the 90 kN load in steps. Loading was at 130 kN when observing a flexural crack opening of 0.06 mm. However, the subsequent loading (again, up to 130 kN) caused a widening of certain cracks previously induced up to 0.2 mm.

In addition to the beams, 30 cubes (150 mm x 150 mm) were cast separately, by using CEM III+CA and cured for 28 days in a room with a temperature of 20°C and a relative humidity >95%. These cubes were to be tested in compression at the age of 28 days, 3, 6, 9 and 12 months, with 6 cubes being tested per age. Results are reported in Table 3.4 demonstrating an increase of compressive strength with time, that can primarily be attributed to the hydration process. Also the cubes were then.

Table 3.4: Obtained compressive strength values for CEMIII+CA with indication of the standard deviation.

Age	Compressive strength [MPa]	Standard deviation [MPa]
28 days	55.11	2.76
3 mths	60.47	2.57
6 mths	60.93	3.14
9 mths	62.57	2.96
12 mths	63.35	3.01

3.2.4 Chloride induced corrosion: experimental set-up for non-steady state diffusion test

Specimens coming from the walls described in 3.2.2 besides two out of the four realized beams (one CEMI_beam and one CEMIII+CA_beam) were then submerged in a pool containing an aqueous NaCl solution with a concentration of 33 g/l at 20 °C. For the beams, the purpose was to check chlorides diffusion in cracked and uncracked zones. The selected NaCl concentration is in line with the seawater concentration reported in (Van Den Heede, 2014) with the aim of replicating a chloride diffusion as close as possible to the reality. Moreover, three electric pumps were installed to ensure continuous water circulation and prevent the precipitation of NaCl as in Figure 3.8.

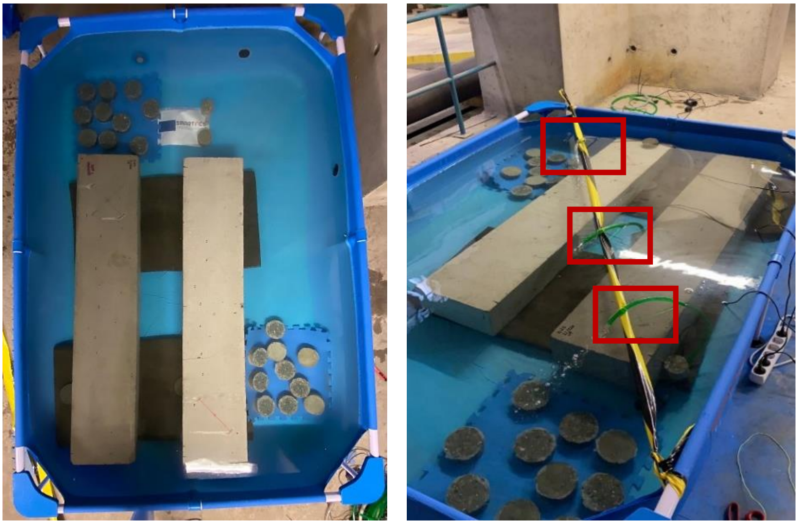

Figure 3.8: The beams are submerged into the pool (left), while the setup with three pumps, installed to prevent sodium chloride deposition is highlighted on the right.

The bulk diffusion test was developed and standardized by NT Build 443 (Nordtest, 1999), based on the immersion test APM 302 (Sorensen, 1994). In this method, cylindrical concrete samples are coated on all faces except one and submerged in a high-concentration (165 g/l) NaCl solution. Following a designated exposure period (minimum 35 days), the samples are removed from the solution, and a chloride profile is determined through profile grinding and subsequent chemical analysis of the ground powders. To obtain a chloride profile, material is systematically removed from a concrete sample in layers parallel to the surface exposed to the chloride solution. This removal process typically involves grinding with a diamond-coated drilling head, with layer thickness typically ranging from 0.5 to 2 mm. The collected powder from each layer is subsequently dried in an oven at 105 ± 5 °C, followed by chemical analysis to determine the chloride content. Several methods exist for this analysis, however, for the scope of this research, titration has been used. It allows for the derivation of both total chloride and free chloride content from the powders. More specifically, the total chloride content of a powder (herein taken into account) is determined through acid-soluble extraction, typically utilizing a nitric acid solution and involving potentiometric titration against silver nitrate. A detailed procedure for potentiometric titration has been elaborated by (Song, 2012). At the end, by fitting the data to Fick's second law, a non-steady-state chloride diffusion coefficient (D_{NSS}) can be derived. Details of the entire procedure are provided in 3.2.4.1. The diffusion profiles were measured after 6 months and 12 months of exposure.

3.2.4.1 Total chlorides profile

As said, diffusion was checked after 6 and 12 months of exposure. To obtain cylindrical specimens from the beams, cores (100 mm diameter) were drilled from each beam in correspondence of the cracked and uncracked zone, after having temporarily removed the beams from the NaCl solution. For what concerns the cracked specimens, the zones from which the cores were drilled were selected to ensure consistency in the crack width. While it was not always possible to replicate identical conditions, the average crack openings varied between 0.06 mm and 0.1 mm. Furthermore, at the 6-month mark, after having extracted the cores, the holes were coated with epoxy resin. Upon removal from the aqueous NaCl solutions, all the samples were stored for one week in an air-conditioned room (20 °C, 60% RH) to ensure they were dry. Thus, by employing an apparatus equipped with 10 mm diameter diamond drill, powder grinding was carried out from the surface in contact with the salt solution in an area of 60 x 20 mm. The first layer of 1 mm was discarded due to the convection zone, while subsequent 10 layers have been grinded with a depth of 2 mm per layer. In the case of cracked specimens extracted from the beams, the ground area was selected to fully include the crack width. A schematic exemplification is reported in Fig 3.9 while Figure 3.10 shows the collected grinded powders.

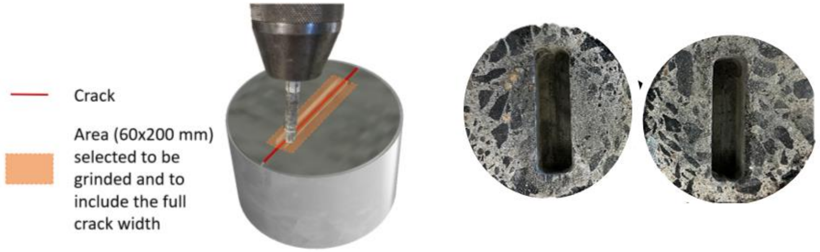

Figure 3.9: Grinded area in correspondence of a crack (left) and specimen after grinding procedure (right)

Figure 3.10: Collected grinded powders. The different colors of the powders are due to the different mix designs. In general, the employment of CEM III favoured lighter colors.

Acid-soluble extraction in a nitric acid solution followed by potentiometric titration against silver nitrate was employed to determine the total chloride concentration, referred to as the acid-soluble chloride concentration. Additionally, the water-soluble chloride concentration was determined by mixing the powder with deionized water and subsequently titrating the solution. The obtained powders were then dried at 105 °C until a constant mass and then 2 ± 0.001 g of each powder was weighed in a 150 ml glass beaker where they were mixed with 5 ml of 0.3 mol nitric acid solution and 40 mol of demineralized water. The obtained solution was then stirred and warmed up until boiling. After cooling, it was filtered and diluted with demineralized water to 100 ml. From these 100 ml, 10 ml were pipetted and analysed by using the 862 Compact Titrosampler from Metrohm®. Figure 3.11 shows the filtering powders of 10 layers coming from one specimen along with the employed Titrosampler. The station employed a titration solution of 0.01 mol/L silver nitrate, while the test solution consisted of 10 ml of the extract, 10 ml of demineralized water, and 40 ml of nitric acid (0.3 mol/L). From the resulting chloride profiles per sample, the surface concentration (C_s) and effective chloride diffusion coefficient (D_e) were estimated by fitting Equation 3.1 to the measured chloride contents using non-linear regression analysis (through SPSS Statistics 29® software), omitting the first point of the profile (coming from the first layer with a thickness of 1 mm). This was done to omit the convection zone close to the exposed surface mainly characterized by capillary absorption(Zhang *et al.*, 2023).

Figure 3.11: Filtering process (left) and Titrosampler (right)

The mean values and standard deviations of the diffusion coefficients and surface concentrations were calculated based on three samples from each series. Results are presented in Table 3.5 and Figure 3.12. Uncracked specimens extracted from the beam are labeled as CEMIII+CA_uncr and CEMI_uncr, depending on whether CEM III or CEM I was utilized. Additionally, specimens obtained from the walls are denoted as Ref1_wall and Ref2_wall (if sourced from the reference walls), while those extracted from walls with superabsorbent polymers are categorized as C_wall, SNF_wall, or C+SNF_wall, depending on the type of polymers integrated into the concrete matrix. The R^2 values reported in Table 3.5 represent the proportion of the variance in the dependent variable that is predictable from the independent variables within the regression analysis. It is, in short, a measure of how well the regression equation fits the data, indicating how well the independent variables explain the variability of the dependent variable. R^2 values close to 1, indicate a good fit of the regression model to the data. Conversely, values closer to 0, indicate that the independent variables do not explain much of the variability in the dependent variable, indicating a poor fit of the regression model. However, it is notable that the R^2 values obtained for CEMIII+CA_cr at 12 months indicate a poor fit. Additionally, it must be observed from both the chloride fitting profile illustrated in Figure 3.12 and the values presented in Table 3.5 that CEMIII+CA_uncr outperforms CEMI_uncr. This is in line with the fact that crystalline admixture plays a crucial role in reducing the chloride diffusion coefficient in concrete since it favours the formation of insoluble crystalline structures within the concrete pores, physically blocking the pathways for chloride ion penetration, self-sealing cracks. Additionally, the formation of crystals contributes to the densification of the concrete matrix, making it more compact and impermeable (Antón *et al.*, 2024). Moreover, the superiority of CEMIII+CA_uncr might be due to the higher CEM I_uncr specimens porosity since the chlorides profile of the latter aligns more closely with a pure penetration pattern.

However, regarding CEMI_uncr and CEMI_cr, the obtained values for the chlorides diffusion coefficient indicate a similar behavior between the cracked and uncracked states at the age of 6 months, with even worse performance observed for the uncracked state at 12 months. Despite having conducted the experiments across three series per type of specimens, these findings appear not in line with the expectations since the presence of cracks should increase the chlorides diffusion coefficient (actually in this case the chlorides undergo a process of absorption into the crack instead of diffusion). Further investigations are needed confirm the validity of the results and to explain the factors influencing these results and the underlying causes.

As it can be observed, a similar chloride profile is noticed for cracked specimens. However, due to the crack opening variation up to 110 μm of the tested specimens, the obtained result is in line with the literature. As a matter of fact, some studies (Djerbi *et al.*, 2008) highlight that the diffusion coefficient tends to stabilize when the crack width reaches approximately 80 μm or greater, independently of material effects (such as tortuosity and roughness).

It must be also observed that, with regard to the concrete containing SAPs, results appear to be of the same order of magnitude as those obtained through the migration test , apart from slight variations. This happens also for the corresponding reference mix design, even though, among each other, they present a slight difference that is mainly dictated by the different water contents. The outcomes are in line with the expectations since Ref2_wall, which has a higher w/c, presents worse performance than Ref1_wall at the age of 12 months. As outlined in the literature, a lower w/c ratio leads to a denser concrete matrix with fewer capillary pores, hindering the movement of chloride ions and slowing down their diffusion rate. The hydration process is also influenced by water content, with lower ratios resulting in a denser network of hydrated products (and consequently a denser microstructure), further impeding chloride ion movement (Li *et al.*, 2023).

Table 3.5: Obtained diffusion coefficients at the age of 6 and 12 months of exposure.

Type of mix	6 mth	12 mth
CEMIII+CA_uncr	D= 1.07 x 10^{-12} m^2/s C_s= 5.05 R^2= 0.99	D= 8.56 x 10^{-13} m^2/s C_s= 4.31 R^2= 0.99
CEMIII+CA_cr	D= 7.14 x 10^{-12} m^2/s C_s= 2.82 R^2= 0.95	D= 2.08 x 10^{-11} m^2/s C_s= 3.70 R^2= 0.49
CEMI_ref_uncr	D= 5.02 x 10^{-12} m^2/s C_s= 2.45 R^2= 0.96	D= 6.64 x 10^{-12} m^2/s C_s= 2.02 R^2= 0.92
CEMI_ref_cr	D= 5.08 x 10^{-12} m^2/s C_s= 2.87 R^2= 0.98	D= 5.83 x 10^{-12} m^2/s C_s= 2.45 R^2= 0.95
Ref1_wall	D= 1.32 x 10^{-12} m^2/s C_s= 3.46 R^2= 0.99	D= 9.95 x 10^{-13} m^2/s C_s= 3.40 R^2= 0.98
Ref2_wall	D= 8.25 x 10^{-13} m^2/s C_s= 2.71 R^2= 0.99	D= 1.13 x 10^{-12} m^2/s C_s= 2.62 R^2= 0.99
C_wall	D= 1.36 x 10^{-12} m^2/s C_s= 2.79 R^2= 0.97	D= 1.54 x 10^{-12} m^2/s C_s= 2.35 R^2= 0.95
SNF_wall	D= 9.64 x 10^{-13} m^2/s C_s= 3.89 R^2= 0.99	D= 9.31 x 10^{-13} m^2/s C_s= 3.49 R^2= 0.96
C+SNF_wall	D= 1.67 x 10^{-12} m^2/s C_s= 2.66 R^2= 0.99	D= 1.42 x 10^{-12} m^2/s C_s= 2.13 R^2= 0.98

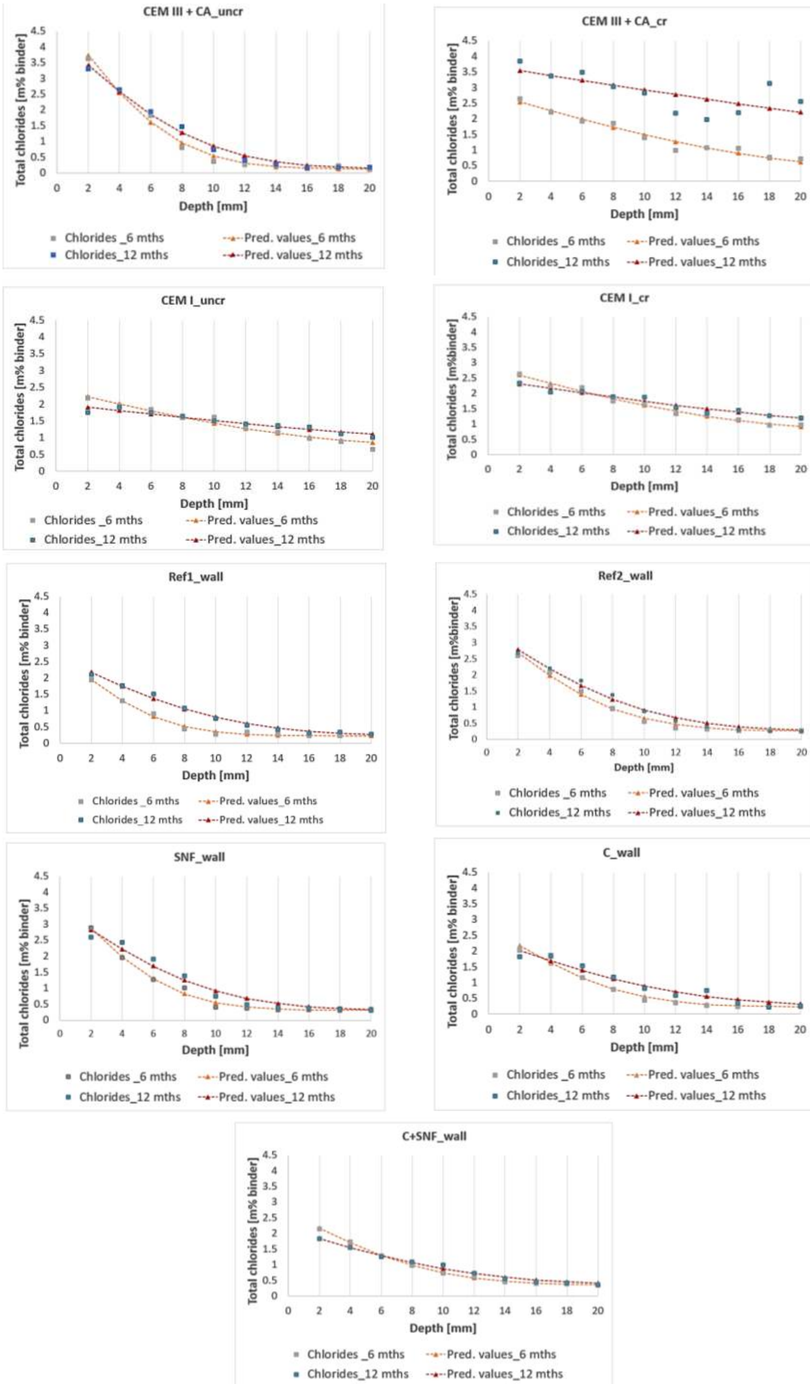

Figure 3.12: Obtained chloride profiles

3.3 The importance of chloride diffusion coefficient: a parametric investigation

As outlined so far, the diffusion coefficient plays a key role in assessing chloride penetration within concrete since it represents the rate at which chlorides migrate through the concrete matrix, being then a critical parameter for ensuring the durability and longevity of reinforced concrete infrastructure. In light of this, it was decided to conduct a parametric analysis to evaluate the values of the chloride diffusion coefficients obtained experimentally. This analysis aims to determine the initiation time and subsequently quantify the duration required for the corrosion process to begin under specific boundary conditions. For the purpose of comparison, the following boundary conditions have been considered, in line with the large case study described in 4.5: Ci, the initial chloride content of concrete equal to 0.20% by weight of cement according to EN 206 CEN, 2016); Cs chloride concentration at the surface, equal to 0.01% and Ccrit is the critical chloride concentration equal to 0.44% by weight of cement according to Alonso and Sanchez (Alonso and Sanchez, 2009) and based on field exposure tests. The initiation times reported in Table 3.6 can be then obtained. However, the considered value of the diffusion coefficient corresponds to the one obtained at 12 months of exposure, with the exception of CEMIII+CA_cr, where the value at 6 months was utilized. This adjustment was necessary due to the unacceptable R-squared value obtained at 12 months.

Table 3.6: Employed diffusion coefficients and calculated initiation time.

Type of mix	Diffusion coefficient	Obtained initiation time
CEMIII+CA_uncr	$D= 8.56 \times 10^{-13} m^2/s$	13.58 years
CEMIII+CA_cr	$D= 7.14 \times 10^{-12} m^2/s$	1.62 years
CEMI_uncr	$D= 6.64 \times 10^{-12} m^2/s$	1.75 years*
CEMI_cr	$D= 5.83 \times 10^{-12} m^2/s$	1.99 years
Ref1_wall	$D= 9.95 \times 10^{-13} m^2/s$	11.68 years
Ref2_wall	$D= 1.13 \times 10^{-12} m^2/s$	10.28 years
C_wall	$D= 1.54 \times 10^{-12} m^2/s$	7.54 years
SNF_wall	$D= 9.31 \times 10^{-13} m^2/s$	12.48 years
C+SNF_wall	$D= 1.42 \times 10^{-12} m^2/s$	8.18 years

*value here reported is unexpected and should be used with caution

The different values of the diffusion coefficient reported in Table 3.6 reflect substantial differences in permeability to chloride ions among the various concrete mixes. Calculated initiation times span from 1.62 years to 13.58 years, indicating significant disparities in corrosion resistance. Notably, "CEMIII+CA_uncr" and "Ref2_wall" demonstrate the longest initiation times, suggesting superior resistance to corrosion compared to other mixes. Conversely, "CEMIII+CA_cr" and "CEMI_cr" exhibit relatively shorter initiation times, potentially indicating lower corrosion resistance. However, as said in 3.2.4.1, further investigations are needed to better describe the performance of CEMI_uncr and CEMI_cr and better compare these results with those of concrete containing CEMIII and crystalline admixture.

3.3.1 Non-steady-state migration test vs non-steady diffusion tests: differences and challenges

According to what has been described so far, while migration tests are valuable for promptly assessing resistance of concrete against chloride penetration, it is acknowledged that the obtained migration coefficient should be related with caution with the diffusion coefficient of concrete (Van Belleghem, 2018). As a matter of fact, comparing results from different test methods can be challenging because they not only consider different transport mechanisms (migration versus diffusion) but also employ varying concentrations of chloride solutions. Additionally, the duration of each test affects the development of chloride binding. For instance, in a non-steady-state migration test, there is typically less chloride binding compared to other tests due to the short test duration. Given this, many researchers tried to investigate the relationships between migration and diffusion testing (Andrade *et al.*, 2000; Castellote *et al.*, 2001; Tang and Sørensen, 2001). Moreover, since the chloride diffusion coefficient is known to be concentration-dependent and time-dependent, this adds complexity to the comparison of methods. Indeed, it can change over time due to various factors that can influence ions transport. Among these, important factors are curing and aging processes (leading to alterations in the permeability), carbonation, hydration, environmental exposure and damage like cracking(Song *et al.*, 2013). Given this, a prolonged non-steady state diffusion test is generally preferred.

3.4 Carbonation-induced corrosion

Concerning the carbonation progress, one CEMI_beam along with one CEMIII +CA_beam have been exposed to open air under a shelter to be then checked after 6 months and 12 months of exposure.

Carbonation-induced corrosion in concrete arises from the reaction between atmospheric carbon dioxide (CO_2) and calcium hydroxide ($Ca(OH)_2$) present in the cement paste, to produce calcium carbonate and water, reducing the alkalinity of concrete (Park, 2008; Aguiar and Júnior, 2013):

$CO_2 + Ca(OH)_2 + \rightarrow CaCO_3 + H_2O$

Then, as carbonation progresses, the calcium hydroxide in the concrete is gradually consumed, reducing the pH of the concrete. Moreover, CO2 dissolved in water forms carbonic acid, further lowering the pH of the concrete:

$CO_2 + H_2O \rightarrow H_2CO_3$

Concrete typically forms a protective passive layer around the steel reinforcement, avoiding corrosion. However, the decrease in pH resulting from carbonation disrupts this passive layer, leaving the steel vulnerable to corrosion and the related formation of expansive products. As a matter of fact, the iron in the steel is subjected then to oxidation, resulting in the formation of iron oxide (rust) and causing the cross section reduction. The overall consequence of carbonation-induced corrosion is a deterioration in the structural integrity of the reinforced concrete. Cracks may develop due to the expansion of the corroding steel, leading to the spalling of the concrete cover and potentially compromising the structural stability of the reinforced concrete elements. With regard to the main contributors, dry-wet cycles, relative humidity, temperature, and CO_2 concentration, all of which are environmental variables, are of the utmost importance. Other factors influencing carbonation relate to the microstructural characteristics and materials of concrete, such as its porous nature (Neves *et al.*, 2013). Concrete with low permeability can impede CO_2 ingress, especially when designed with a low water-to-cement ratio, high cement content, and elevated compressive strength (Marques *et al.*, 2013). Furthermore, under completely dry or wet conditions, carbonation does not occur unless the relative humidity falls within the range of 40% to 80% (von Greve-Dierfeld *et al.*, 2020). Below 50% relative humidity, moisture levels are insufficient for reactions, while above 80%, excessive moisture in pores restricts CO_2 penetration, with the optimal relative humidity for the carbonation process identified as 65% (Roy *et al.*, 1996; Stewart *et al.*, 2012). However, for materials containing supplementary cementitious materials, the RH range at which carbonation is fastest may differ with a maximum carbonation progress already at 30% when slag and fly ash are present. Temperature plays a crucial role, as CO_2 penetration escalates with increasing temperatures due to faster chemical reactions and decrease of the solubility of portlandite and CO_2 in water. (Huang *et al.*, 2012; Talakokula *et al.*, 2016; von Greve-Dierfeld *et al.*, 2020). In view of this, recent studies highlighted that climate change-induced variations, such as a 2 °C temperature rise, could accelerate steel corrosion rates by 15% (Stewart *et al.*, 2012). During the carbonation process, three different zones can be identified, as discussed in various studies (Chang and Chen, 2006; Talukdar *et al.*, 2012b,a). The initial zone, situated near the surface exposed to air, is fully carbonated, with a constant carbonate content. Subsequently, a transition zone, often termed as the carbonation front, represents the segment of concrete material where the degree of carbonation gradually diminishes from its peak (at the interface with the initial zone) to zero. In the third zone, no carbonation is evident. Due to the fact that the process is primarily governed by carbon dioxide diffusion within concrete, a common approach for modeling carbonation employs the square root of time formula. The CO_2 diffusion model proposed in(fib, 2013) is based on the analytical solution of Fick's first law, expressed as:

$$x_c = W(t)\, k\, \sqrt{t} \qquad \text{Eq. 3.4}$$

where: x_c, is the carbonation front depth, t is the exposure time, W(t) is a function utilized to account for the time during which the concrete will remain wet, while k, measured in mm/$\sqrt{years}$, is the factor governing the speed of the process which depends on various factors including the characteristics of the concrete (e.g., water-to-cement ratio, type of cement and additives), relative humidity, and CO_2 concentration. Details are provided in (fib, 2013), from which, particularly for W(t) it is possible to obtain:

$$W(t) = \left(\frac{t_0}{t}\right)^w \qquad \text{Eq. 3.5}$$

where t_0 is the reference time in years equal to 0.0116, while w is an atmospheric factor defined as:

$$w = (p_{SR} \cdot T_w)^{b_w} \qquad \text{Eq. 3.6}$$

where p_{SR} represents the probability of raining on the surface of the assessed element while b_w is a regression exponent equal to 0.446 while the time of wetness T_w is defined as in Eq. 3.7:

$$T_w = \frac{days\ with\ more\ than\ 2.5\ mm\ of\ rain\ in\ one\ year}{365} \qquad \text{Eq. 3.7}$$

The value of w ranges between 0 and 1 depending on the location of the assessed structure/component.

3.4.1 Carbonation front – experimental outcomes

Cores with a diameter of 100 mm were drilled at both cracked and uncracked zones of each beam after 6 and 12 months of exposure to carbonation for both CEMI_beam and CEMIII+CA_beam, respectively. Every time, three specimens were extracted for each condition (cracked or uncracked). Each cylindrical specimen was then split into two halves (perpendicular to the crack, if present) to assess the carbonation profile using phenolphthalein spray. The results highlighted the absence of carbonation after both 6 months and 1 year (as it is possible to observe in Figure 3.13), even in areas with cracks. In order to understand the reasons behind this, temperature and relative humidity data were also collected during the exposure period, based on a weather station in Ghent, Belgium, where the beams have been exposed to open air. These data are reported in Table 3.7. As it is possible to observe, relatively low temperatures in conjunction with relative humidity higher than 80% for 7 out of 12 months contributed to the absence of carbonation after one year of exposure. This is further confirmed in the case of the CEM III+CA_beam (containing blast furnace slag) since some works (Drouet *et al.*, 2019) indicates an optimal RH around 30% when supplementary cementitious materials are present. In light of this, it was not possible to collect carbonation data for the specific case study.

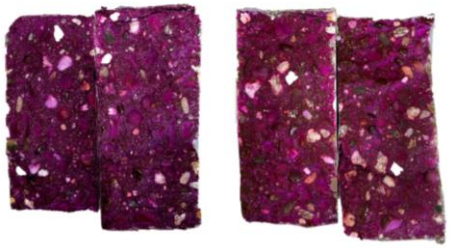

Figure 3.13: Example of carbonation after 6 and 12 months of exposure for CEMIII +CA.

Table 3.7: Temperature and RH data of the geographical area where the beams have been exposed to check carbonation profile.

	T min (°C)	T max (°C)	Avg. T (°C)	Avg. RH. (%)
Mar-22	-1.1	21.8	9.2	66.3
Apr-22	-0.3	22.5	11.4	66.8
May-22	3.6	29.1	16.4	67.2
Jun-22	7.4	34.5	19	67.2
Jul-22	11.1	39.7	21	63.6
Aug-22	11.9	33.8	22.3	64.2
Sep-22	6.4	29.4	15.8	80.9
Oct-22	3.6	24.1	14.6	84.7
Nov-22	1.9	17.2	9.2	91.8
Dec-22	-6.9	15.8	4.4	94.2
Jan-23	-2	15	6	90.9
Feb-23	-3.7	13.1	6.6	85.1
Mar-23	-0.8	18.8	8.3	82.8

3.5 Conclusions

This chapter has explored the experimental acquisition of durability parameters for advanced cement-based materials. A focus has been given to the experimental set-up relevant for concrete exposed to chloride attack and carbonation. The acquisition of these data allows to bridge the existing gap for novel materials where durability parameters may be lacking. This becomes particularly relevant given the crucial role of the latter within an innovative approach where they become essential for achieving better LCA and LCC outcomes but also fundamental within the Durability Assessment-oriented Design (DAD) workflow, which encompasses the performance over time. With DAD, usage and end-of-life stages can be adequately addressed, thereby overcoming a current limitation in the sustainability evaluation of advanced construction materials.

4 From laboratory-scale components to structural-scale realities: case studies and LCA/LCC implementation within the design phase

Despite its numerous advantages, concrete is prone to damage under specific environmental conditions, particularly in highly aggressive environments. This susceptibility leads to increased environmental and economic impacts due to the necessity for frequent maintenance activities to restore the original functionality. However, recent technological advancements offer a solution to these vulnerabilities through the utilization of advanced cement-based construction materials. This chapter focuses on the application of LCA and LCC methodologies to quantify the environmental impacts of both novel concrete constituents (such as additions able to provide self-healing properties) and structures constructed with these advanced materials. For the latter, Durability Assessment-oriented Design is investigated, within a holistic perspective, as part of LCA and LCC to estimate the enhanced efficiency of these materials when usage/end-of-life/recycling phases are also encompassed. Microcapsules, UHPC, recycled UHPC besides concrete containing SAPs/crystalline admixture and 3D printed vascular networks are the technological innovations herein presented.

Chapter 4

Part of this chapter was redrafted after:

[1] D. di Summa, M. Parpanesi, L. Ferrara, N. De Belie, A holistic life cycle design approach to enhance the sustainability of concrete structures, Structural Concrete 24 (2023) 7684–7704. https://doi.org/10.1002/suco.202300645.

[2] D. di Summa, J.R. Tenório Filho, Didier. Snoeck, Philip. Van den Heede, S. Van Vlierberghe, L. Ferrara, N. De Belie, Environmental and economic sustainability of crack mitigation in reinforced concrete with SuperAbsorbent polymers (SAPs), J Clean Prod 358 (2022). https://doi.org/10.1016/j.jclepro.2022.131998.

[3] N. Kannikachalam, D. di Summa, R.P. Borg, E. Cuenca, M. Parpanesi, N. De Belie, L. Ferrara, Assessment of Sustainability and Self-Healing Performances of Recycled Ultra-High-Performance Concrete, ACI Mater J 120 (2023). https://doi.org/10.14359/51737336.

[4] D. di Summa, L. Ferrara, N. De Belie, How to account for benefits of Self-Healing concrete in design? A LCA/LCC perspective, in: M. di Prisco, A. Meda, G.L. Balazs (Eds.), Proceedings of the 14th Fib PhD Symposium in Civil Engineering, 2022: pp. 689–696.

[5] D. di Summa, M. Parpanesi, N. De Belie, L. Ferrara, How to address sustainability and economic viability of advanced cementitious based materials by means of Life Cycle Assessment (LCA) and Life Cycle Cost (LCC) tools integrated into a holistic design-wise approach., in: ICSHM2022 Milano -8thInternational Conference on Self-Healing Materials, 2022: p. 105.

[6] D. di Summa, M. Parpanesi, L. Ferrara, N. De Belie, Life Cycle Assessment (LCA) and Life Cycle Cost (LCC) analysis as crucial part of a holistic approach to the design of structures with advanced cement based materials, in: 76th RILEM Annual Week and International Conference on Regeneration and Conservation of Structures (ICRCS 2022), 2022.

[7] D. di Summa, Y. Shields, V. Cappellesso, L. Ferrara, and N. De Belie, “The sustainability profile of a biomimetic 3D printed vascular network to restore the structural integrity of concrete,” in MATEC Web of Conferences, Apr. 2023, p. 06002. doi: 10.1051/matecconf/202337806002.

[8] D. di summa, A. Marcucci, M. Nicolo`, F. Martignoni, A. Carrassi, F. Liberato, N. De Belie, LCA assessment related to the evolution of the earthquake performance of a strategic structure, in: F. Biondini, D.M. Frangpol (Eds.), Proceedings of the eighth international symposium on life cycle civil engineering (IALCCE 2023), 2-6 JULY, 2023, Politecnico di Milano, Milan, Italy, Milano, 2023: pp. 1169–1176.

4.1 Software and data libraries employed for LCA and LCC

The LCA analyses herein presented have been carried out by employing SimaPRO software (version 9.1.1.1.) complemented by data sourced from the Ecoinvent library (version 3.6). Life Cycle Costing computation involved the consideration of a list of cost issues specific to the locations of the case studies. In instances where data were unavailable, as explained later, assumptions have been made by selecting the most representative construction market for the specific case. Objective of this chapter is to provide a comprehensive overview, ranging from the component scale for advanced cement based materials (e.g. microcapsules for self-healing concrete) to that of large structures (e.g. tunnel element walls casted with SAPs-based concrete or a UHPC water basin). Importantly, the focus on Life Cycle Costing was directed to large structures throughout their service life. This approach aligns with existing literature that emphasizes the necessity of including the performance of the materials in assessments based on exposure conditions, to encompass all the properties (strength, durability etc.) and to ensure valuable comparisons (Al-Obaidi *et al.*, 2022a).

4.2 Microcapsules

Microcapsules technology finds application in agriculture (encapsulating fertilizers), pharmaceuticals (drug delivery), healthcare (encapsulating actives), food (flavor enhancement) and construction. Microcapsules embedded and homogeneously distributed in a concrete matrix serve as a storage for healing agents to be released when cracks occur causing shells' rupture. To investigate the feasibility of microcapsules embedded in a concrete matrix, Wang et al. (Wang *et al.*, 2014) used microcapsules to encapsulate bacterial spores for the purpose of self-healing concrete. Microcapsules were added in the range between 3-5% by weight of cement. Specimens with microcapsules exhibited a higher healing ratio (48%–80%) as compared to those without bacteria (18%–50%) with a healed crack width four times larger than concrete without microcapsules. The efficacy and efficiency of this technology are influenced by factors like capsule diameter, shell size, and surface texture (Joseph *et al.*, 2010; Kanellopoulos *et al.*, 2017; Sidiq *et al.*, 2019). Pelletier et al. (2011) pioneered the fabrication of microcapsules for self-healing concrete, utilizing sodium silicate as the core material and polyurethane as the shell material. The research involved obtaining a surfactant solution, removing a portion, and adding shell material (methylene diisocyanate) to create a homogenized solution. Beglarigale et al (Beglarigale *et al.*, 2018) conducted experiments to determine the optimum shell to core material ratio in fabricated microcapsules obtaining, for the specific case of the study, a value of 0.67, with an average microcapsule diameter of 29 μm. However, despite the advancements in the specific field within the recent past, there are still key challenges to be overcome including product consistency and how it is embedded in cementitious systems. In this respect, membrane emulsification ensures minimal product variability while offering scalability and continuous processing. Simultaneously, it contributes to reduced energy and material consumption (Vladisavljevic, 2003; Holdich *et al.*, 2020). Thus, the investigation herein addressed was conducted employing stainless steel membranes with laser-drilled pores in Advanced Cross Flow (AXF) equipment, all supplied by Micropore Technologies, partner in the SMARTINCS consortium. Scope of this part of the study extends beyond merely quantifying the environmental burdens since it also aims to produce a commercial document, such as the Environmental Product Declaration (EPD), which can facilitate the market penetration of microcapsules as healing agents. Additionally, conducting an LCA at this scale provides valuable insights into which aspects of the production process/ which components can be refined or substituted to achieve more favorable environmental outcomes, thereby enhancing the overall sustainability and market appeal of the product.

4.2.1 Membrane emulsification - process details

Riordan et al. have provided a detailed overview of the entire membrane emulsification process in (Riordan *et al.*, 2023). These procedures were subsequently taken into consideration for all estimations forming the basis of the LCA analysis. Capsules are formed through an oil-in-water emulsion made up of a dispersed mixture of Sikagard-705L and isophorone diisocyanate in the oil phase. Sikagard-705L, a one-component, solvent-free alkoxysilane water repellent agent, and IPDI have been supplied by Rawlins Paints and Fisher Scientific, respectively. The aqueous phase consists of a polyvinyl alcohol solution using deionized water and polyvinyl alcohol grade 23-88 from Fisher Scientific. Shell formation involves 1,4-butanediol and dibutyltin dilaurate, both supplied by Fisher Scientific. All chemicals were employed without additional purification. One piece of AXF equipment, namely the AXF-1 with stainless steel membranes (10 μm pore diameter), was used for emulsion production. Moreover, flow rates have to be adjusted to maintain laminar flow, preventing excess shear and ensuring consistent product quality. Polyurethane shells are synthesized through interfacial polymerization of isophorone diisocyanate and 1,4-butanediol. Following emulsion formation, the product undergoes shell synthesis via interfacial polymerization of isophorone diisocyanate with 1,4-butanediol. The reaction is carried out for two hours, continuously stirring the capsule product at all times. The membrane proposed emulsification method is regarded as a good route for scaling up, because of its repeatability even though it could be influenced by environmental factors such as temperature. This is attributed to the necessity for a strictly controlled environment during the droplet formation phase to ensure identical formation and reaction conditions. Figure 4.1 provides a scheme of the membrane emulsification process while Figure 4.2 presents an optical microscope image of microcapsules.

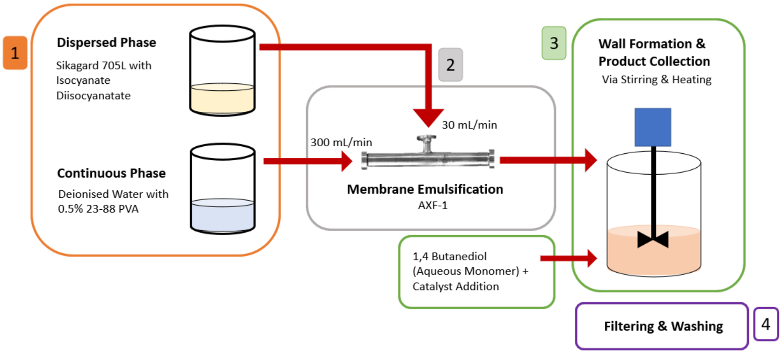

Figure 4. 1: Membrane emulsification process flow by employing AXF-1.

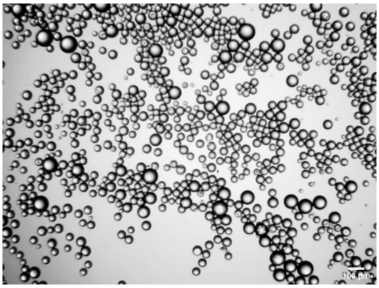

Figure 4.2: Optical microscope image of microcapsules created with microencapsulation.

4.2.2 Membrane emulsification: LCA system boundaries and data input

Life Cycle Inventory for microcapsules is herein presented. As previously discussed, a significant challenge in developing a Life Cycle Assessment for novel/advanced materials and their constituents lies in the scarcity of useful data (including both scientific literature and existing Environmental Product Declarations). In this case, in contrast to many commercially available products, where production processes are typically confidential, all data pertaining to microcapsules produced with membrane emulsification are accessible. Nonetheless, adjustments and assumptions were necessary, given the absence of most raw components, particularly chemicals, in the Ecoinvent library used for this research. Notably, the assessment of flows and energy consumptions presented herein is based on the industrial-scale production that has resulted from Riordan et al. research (2023). Table 4.1 details the inventory to be used based on membrane emulsification production process besides providing a breakdown of Ecoinvent library-available components used as substitutes for the original ones that are unavailable. For this specific purpose, reference have been made to available literature and patents, as in (United States Patent, 1989, 1996; Chiellini *et al.*, 2003; Gresta *et al.*, 2014; Temnikov *et al.*, 2018; Putro *et al.*, 2021; Zhu *et al.*, 2022; Cangzhou Weida Polyurethane Hi-Tech Co Ltd, 2024). Further details about the employed LCI are provided in Annex 1.

Table 4.1: Details of LCI input data for production of 1 kg of microcapsules through membrane emulsification. Due to the unavailability of certain input data within the employed Ecoinvent data library, assumptions have been made to find appropriate surrogate components.

Components based on production process detailed in (Riordan et al. 2023)	**Surrogate Ecoinvent components according to literature and patents**	**Quantity [g]**	
		Total	Waste
Water	-	• 10,000	-
Vinyl alcohol	• vinyl acetate • methanol	• 390.84 • 145.46	• 39.08 • 14.54
Alkoxysilane	• silicon powder • methanol	• 249.86 • 266.50	• 24.98 • 26.65

Components based on production process detailed in (Riordan et al. 2023)	Surrogate Ecoinvent components according to literature and patents	Quantity [g]	
		Total	Waste
Ethanol diamine	• Monoethanolamine • ammonia	• 25.44 • 7.09	-
Isophorone diisocyaante	• acetone • ammonia • methane • oxygen • hydrogen • phosgene	• 209.34 • 43.01 • 19.21 • 57.72 • 2.64 • 130.86	• 20.93 • 4.29 • 1.92 • 5.77 • 0.26 • 13.08
1,4 butanediol	• acetylene • formaldehyde • copper • hydrogen	• 31.44 • 36.26 • 7.66 • 2.65	-
Dibutyltin dilaurate	• coconut oil • ethanol • sodium hydroxide • tin	• 0.75 • 0.10 • 0.04 • 0.06	-
Acetone	• acetone	• 313.27	-

4.2.3 Membrane emulsification: LCA outputs

The analysis has been carried out by employing a cradle-to-gate system boundary, in between A1-A3 stages of Table 2.1 while results are presented through the EPD impact assessment method. The selection of this particular method is aimed at facilitating seamless comparisons with other commercially available concrete constituents. This is particularly relevant given the growing prevalence of Environmental Product Declarations as a means of quantifying sustainability in the construction industry. Table 4.3 lists the results obtained per each impact indicator while Figure 4.3 schematically represents the influence, per each indicator, of the main components. It is possible to observe that acetone, vinyl acetate and copper always represents the highest percentage per each impact indicator especially due to the high content of the first two. However this could be also linked to other causes. As a matter of fact, acetone can contribute to volatile organic compounds (VOC) emissions during the production and application of products that play a role in air quality and can contribute to the formation of ground-level ozone and other air pollutants (Liew *et al.*, 2022). With regard to vinyl acetate its production involves energy-intensive processes and the use of raw materials, contributing to environmental impacts (United States Environmental Protection Agency, 2000). Similarly, copper extraction can cause greenhouse gases emissions (Dong et al., 2020). The results obtained serve as a sign of potential adjustments that can be made to the production process in the future to attain more sustainable outcomes. The impacts of concrete containing microcapsules have also been evaluated. In this regard, the literature still appears limited, but some studies (Litina and Al-Tabbaa, 2020) suggest a usage percentage of 5.34% by weight of cement. For this purpose, the mix design reported in Table 4.2 was assumed to be used, while the impacts were assessed using the EPD methodology. Numerical value of these outcomes are reported in Table 4.3 while Figure 4.4 summarizes which factors influence more each impact indicator. Observing the data, it is evident how cement consistently exhibits the highest impact, whereas microcapsules contribute within a range of 13% to 38%. Similarly, transportation constitutes over 10% of the impact for 9 out of 10 indicators. These findings shed light on potential future enhancements achievable by engineering a different mix design. This approach would not only entail reducing transportation impacts through a more efficient supply chain but also exploring partial replacement of cement with supplementary cementitious materials. Moreover, the improvements previously discussed in the context of microcapsule production, could lead to better overall results also when evaluating the influence of concrete matrix with microcapsule addition.

Table 4.2: Assessed mix design

Components	**Quantities [kg/m^3]**
CEM I 52.5 N	337.6
Sand 0-4 mm	742.9
Gravel 2-8 mm	1031.1
Limestone filler	58
Water	168.8

Superplasticizer	2
Microcapsules	18.02

Table 4.3: Obtained results per each impact indicator. The assessed Functional Units corresponds to 1 kg of microcapsules 1 m3 of concrete containing 5.34% by weight of cement of microcapsules.

Impact category	**Unit**	**Total 1 kg of microcaps.**	**Total 1 m3 of concrete with microcaps.**
Acidification	kg SO2 eq	1.63E-02	1.34
Eutrophication	kg $PO4^{---}$ eq	5.29E-03	0.36
Global warming (GWP100a)	kg CO2 eq	3.03E+00	4.32E+02
Photochemical oxidation	kg NMVOC	1.29E-02	1.22
Abiotic depletion, elements	kg Sb eq	5.91E-05	4.64E-03
Abiotic depletion, fossil fuels	MJ	7.76E+01	3.64E+03
Water scarcity	m^3 eq	2.50E+00	1.67E+02
Ozone layer depletion (ODP)	kg CFC-11 eq	4.26E-07	3.14E-05

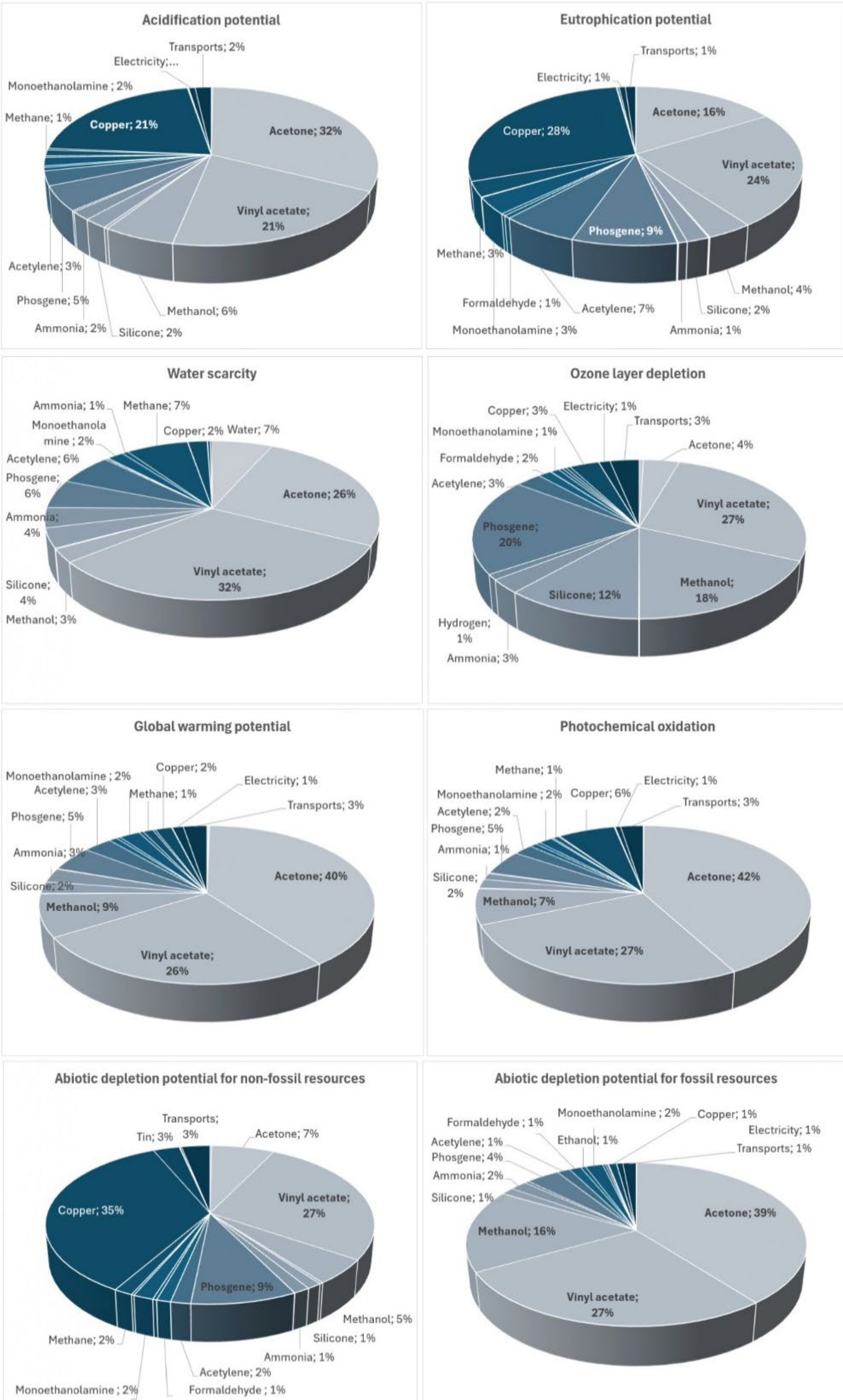

Figure 4.3: Indication of the influence of each component per each environmental impact indicator.

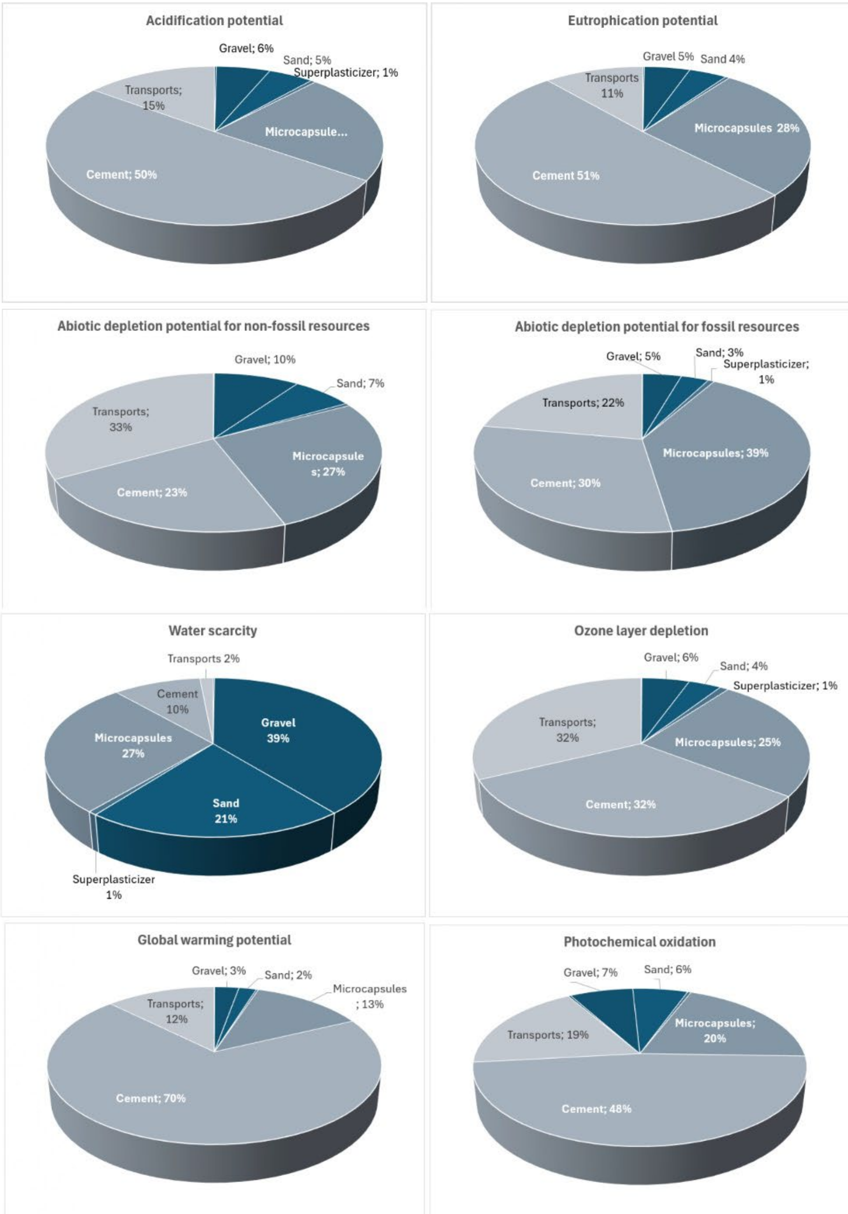

Figure 4.4: Indication of the influence of each component per environmental impact indicator for 1 m³ of concrete containing microcapsules.

4.3 Alumina nanofibers

The benefits derived from applying a nanotechnology approach in the field of construction materials development have captured the attention of both academia and industry in the recent past (Sobolev and Guitierrez, 2005). More specifically, within the realm of concrete, one of the most prevalent applications of nanotechnology has been the incorporation of nano-scale constituents. As an example, constituents like nano-silica contribute to improved mechanical properties, predominantly compressive strength, and bulk transport properties (Sobolev *et al.*, 2009; Sobolev, 2016). Moreover, the use of nano-sized reinforcement, including carbon nano-fibers, nano-tubes, and cellulose nano-fibers, has demonstrated their effectiveness in enhancing various functionalities, such as corrosion resistance, self-curing, self-sensing ability, and durability in cracked states (Vera-Agullo *et al.*, 2009; Zhao *et al.*, 2020). Recent developments involve the utilization of graphene nanoplatelets and graphene oxide, offering enhanced properties with lower loading compared to conventional nano-constituents (Alatawna et al., 2020;Li and Leung, 1992; Li et al., 1995a,b). Additionally, the effects of nano-constituents on material microstructure enable effective control of chemical reactions and processes responsible for material performance evolution over time and in aggressive scenarios (Muthu and Santhanam, 2018). In this framework, cement-based composites, characterized by a compact micro-structure and strain-hardening tensile behavior, offer a platform for effective development and implementation of durability-based material concepts and designs (Li and Leung, 1992; Li *et al.*, 1995b,a). Thus, other investigations already explored the role of specific nano-constituents, such as alumina nano-fibers, in enhancing the autogenous healing capacity of Ultra High Performance concrete mixes for applications in chemically aggressive environments (Ferrara *et al.*, 2019). The investigation highlighted how the inclusion of alumina nano-fibers, made possible through a customized preparation process, improves the capacity for redistributing stress in the cracked state. This improvement is evident in the increased number and narrower width of cracks observed during the pre-peak stable propagation phase. Additionally, the hydrophilic characteristics of the fibers promote delayed binder hydration reactions, leading to enhanced and quicker recovery in both crack sealing and mechanical properties. This effect persists even when concrete with such nano-fibers is exposed to highly aggressive conditions, such as geothermal water with elevated levels of chlorides and sulphates (Cuenca *et al.*, 2021a). As with the microcapsules, the scope of assessing alumina nanofibers or UHPC encompassing the latter, includes not only quantifying their environmental impacts but also producing a commercial document, such as an Environmental Product Declaration (EPD), to support their diffusion within the market. Furthermore, conducting a Life Cycle Assessment at this level offers valuable insights into refining the production process to improve environmental benefits, thus enhancing both the sustainability and marketability of the alumina nanofibers.

4.3.1 Alumina nanofiber and UHPC with alumina nanofibers: LCA system boundaries and data input

As said before, in this case the analysis was conducted using the Environmental Product Declaration methodology described in 2.1.3.5 . The chosen functional units for the assessment were 1 kg of alumina nanofibers and 1 m3 of Ultra-High Performance Concrete containing alumina nanofibers. For both, a cradle-to-gate system boundary (A1-A3 stages of Table 2.1) was adopted. In the case of alumina nanofibers production, the methodology assessed is in line with the manufacturing process employed by Nafen® alumina nanofibers. The concentrated alumina nanofiber dispersions are provided in a 10% concentration aqueous suspension and necessitate the utilization of specific chemical admixtures, such as polycarboxylate sodium salt, to facilitate dispersion and prevent gelatinization induced by the hydrophilic nature of alumina nanofibers. The production process is based on ultrasonic and disintegrator treatment technologies. This method, commonly employed in nano-manipulation processes, effectively generates nano-sized material slurries, dispersions, and emulsions through de-agglomeration and the mechanical effects of ultrasonic cavitation. Moreover, to effectively conduct the dispersion process, several stages are needed, including pre-treating of the fibers in water using the disintegrator machine and iterating disintegrator treatment cycles to achieve a stable semi-product. The obtained result is a product, whose main components per 1 kg are reported in Table 4.4, able to remain stable for a minimum of 3 months after production. Given the absence of more specific data, all components are assumed to be transported an average distance of 250 km to Tallinn, Estonia, where the producer is situated. Regarding the production process, a timeframe of 45 minutes has been allocated for the disintegrator and 1 hour for the ultrasonic process. Energy consumptions have been calculated based on the technical specifications provided in the data sheets of the machineries

(Desintegraator Tootmise OÜ, 2024; Inlab, 2024). Further details about the employed LCI are provided in Annex 1.

Table 4.4: Alumina nanofibers dispersion.

Aluminum oxide nanofibers (diameter 4-11 nm; length 100-900 nm)	110 g
Polycarboxylate superplasticizer	60 g
Distilled water	840 g

For what concerns the UHPC mix design containing alumina nanofibers, the one reported in (Cuenca *et al.*, 2021a), which exhibits an average compressive strength of 136 MPa, has been taken into consideration for the scope of this analysis. Details are reported in Table 4.5. The mixing protocol for electricity power consumption during the production process aligns with the procedures outlined in the same study.

Table 4.5: Assessed UHPC mix design.

Components	**kg/m³**
CEM I 52.5R	600
Blast furnace Slag	500
Water	200
Steel fibers (l=20 mm; d= 0.22 mm)	120
Sand	982
Superplisticizer	33
Crystalline admixture	4.8
Alumina nanofibers (0.25% by weight of cement)	1.5

4.3.2 Alumina nanofiber and UHPC with alumina nanofibers: LCA outputs

The outcomes of the sustainability analysis are reported in Table 4.6 and Table 4.7, while Figure 4.5 and Figure 4.6 illustrate the impact percentages of each component for alumina nanofibers and UHPC mix design, respectively. As observed, in the case of alumina nanofibers, electricity stands out as the most influential factor for all impact indicators, with influence indices reaching up to 96%, as seen in the case of acidification potential. This is due to an overall consumption of 9.91 kWh in total, mainly related to the disintegrator machinery. Conversely, the impact of aluminum oxide is minimal, except for ozone layer depletion and water scarcity, where it peaks at 13% and 32%, respectively. This can be mainly due to the production and refining processes of alumina oxide that involves the electrolytic refining of alumina (aluminum oxide) from bauxite ore, which requires significant energy consumption. This energy often comes from fossil fuel combustion, releasing greenhouse gases such as carbon dioxide (CO_2) and methane (CH_4) into the atmosphere. These gases contribute to global warming, indirectly affecting the ozone layer through changes in atmospheric dynamics (Sáez-Guinoa *et al.*, 2024). For what concerns the UHPC with alumina mix design, cement and steel fibers continue to be the major influencers, with peaks up to 53% for cement (global warming potential) and 45% for steel fibers in the case of eutrophication. Notably, the impact of alumina nanofibers never exceeds 2%. These findings offer insights into potential future enhancements in the production processes of both alumina nanofibers and UHPC with alumina nanofibers. Specifically, refining the production process for alumina nanofibers through a different and more sustainable energy mix source could yield improved outcomes. Similarly, in the case of UHPC, aside from incorporating more sustainable cement types like CEM III, reassessing the production chain could mitigate transportation impacts, particularly considering their influence, which reaches up to 31%.

Table 4.6: Obtained results per impact indicator. The assessed functional unit corresponds to 1 kg of alumina nanofibers.

Impact category	**Unit**	**Total**
Acidification	kg SO_2 eq	2,02E-02
Eutrophication	kg PO_4^{---} eq	1,52E-02
Global warming (GWP100a)	kg CO_2 eq	4,79E+00
Photochemical oxidation	kg NMVOC	1,03E-02
Abiotic depletion, elements	kg Sb eq	1,89E-05
Abiotic depletion, fossil fuels	MJ	5,34E+01
Water scarcity	m^3 eq	1,95E+00
Ozone layer depletion (ODP)	kg CFC-11 eq	6,19E-07

Table 4.7: Obtained results per impact indicator. The assessed functional unit corresponds to 1 m^3 of UHPC containing alumina nanofibers.

Impact category	**Unit**	**Total**
Acidification	kg SO_2 eq	3,05E+00
Eutrophication	kg PO_4^{---} eq	1,11E+00
Global warming (GWP100a)	kg CO_2 eq	9,87E+02
Photochemical oxidation	kg NMVOC	2,94E+00
Abiotic depletion, elements	kg Sb eq	1,48E-01
Abiotic depletion, fossil fuels	MJ	6,75E+03
Water scarcity	m^3 eq	2,20E+02
Ozone layer depletion (ODP)	kg CFC-11 eq	5,98E-05

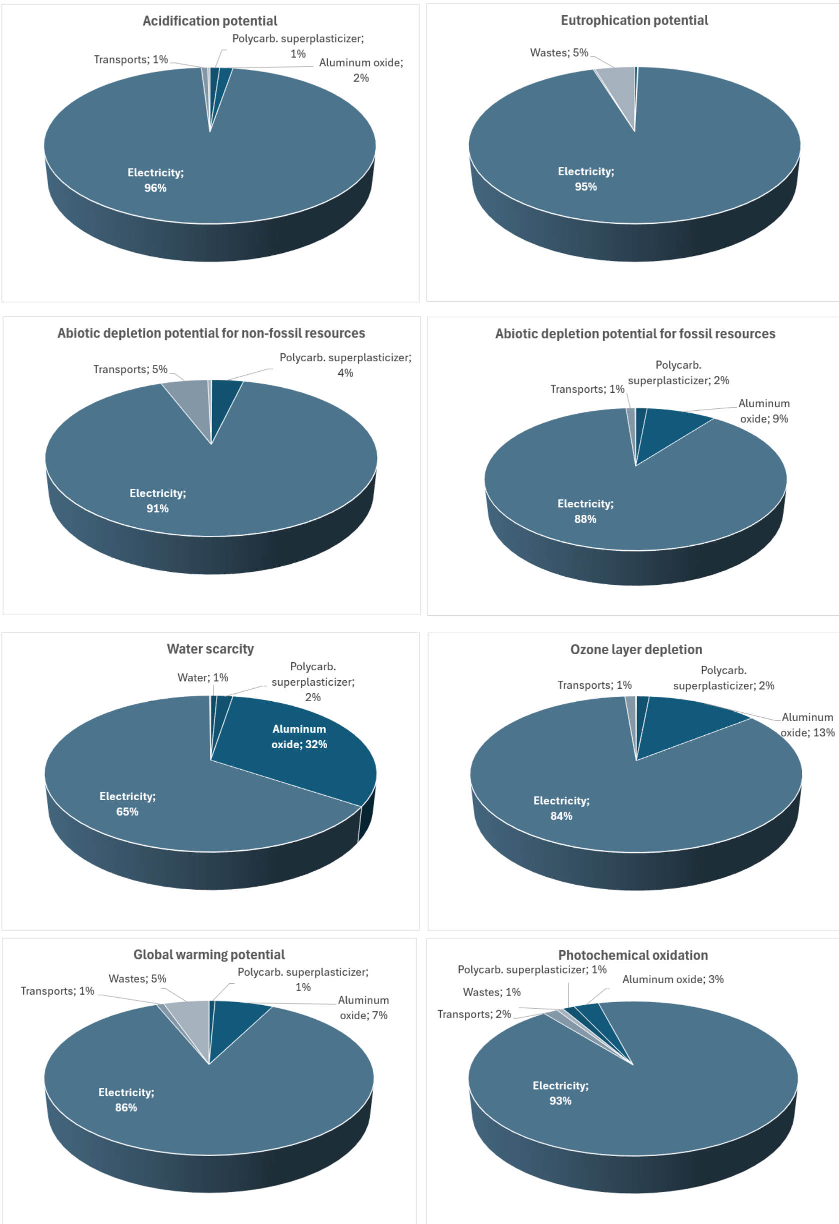

Figure 4.5: Indication of the influence of each component per environmental impact indicator. The assessed Functional Unit corresponds to 1 kg of alumina nanofibers.

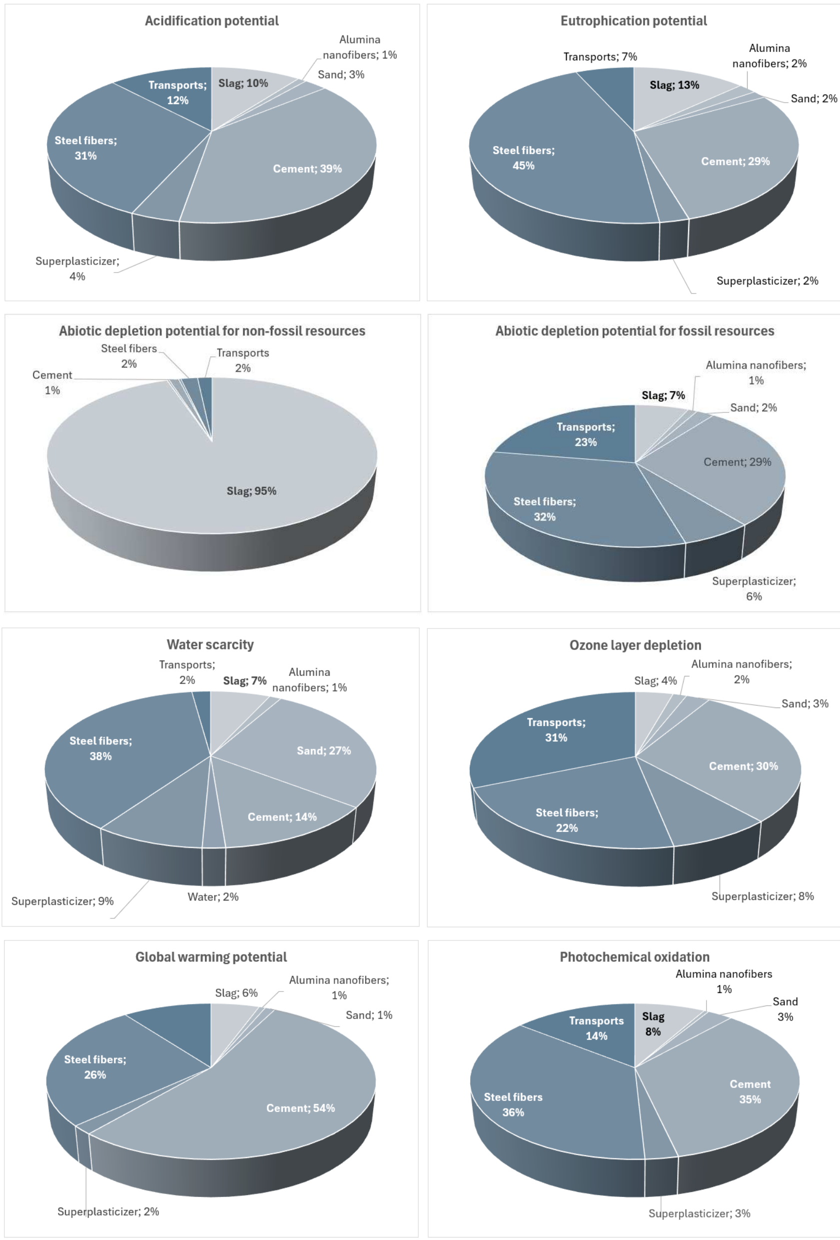

Figure 4.6: Indication of the influence of each component per environmental impact indicator. The assessed Functional Unit corresponds to 1 m³ of UHPC containing alumina nanofibers.

4.4 Vascular network

The potential advantage of using a vascular network embedded in concrete structural elements to inject healing agents upon crack occurrence, has been also investigated. This system takes inspiration from the human blood vascular system. Previous research on this topic has outlined the potential advantages of such solution due to the possibility to indefinitely replenish the healing agent (Li *et al.*, 2020b). Nevertheless, the replication of a vascular network such as the ones present in nature, poses a challenge in terms of fabrication process. Therefore, 3D printed hollow polymer tube networks have been recently investigated because of their fast production as well as the various geometries that can be provided. The idea behind the system is that, upon cracking of the material in which the network is embedded, the agent is injected (under pressure) into the system and is then released through the network to favour the drawing of the agent into the open crack voids through the capillary forces (Selvarajoo *et al.*, 2020; Shields *et al.*, 2021). To date, several self-healing technologies have been explored, but the literature is still quite scarce in terms of investigation of durability and sustainability performance of concrete with an embedded vascular network, when exposed to specific aggressive environmental scenarios (e.g. chloride or sulphate attack) (van Breugel, 2007; Li *et al.*, 2010; Tsangouri, 2019). In view of this, the ecological profile of a structural element, i.e. a typical reinforced concrete beam, provided with a 3D printed vascular network to restore its functionality and exposed to an XS3 environmental scenario (concrete exposed to seawater tidal, splash and spray zones) is herein investigated. This part of the research aims at representing a first attempt of transitioning from the conventional cubic meter scale to the one of a structural element. This shift enables a deeper exploration into the potential enhancements achievable in terms of holistic sustainability. The aim is to also introduce structural evaluations to assess reliable usage scenarios based on the structural performances and on the degradation of the employed materials according to the exposure scenarios. In this sense, LCA is conducted to quantify overall environmental sustainability to then identify which aspects can be adjusted to optimize the efficiency across the entire service life of the case study.

4.4.1 Description of the assessed structural element

Two concrete beams with dimensions of 0.15 m x 0.24 m x 1.27 m (W x H x L) with two 16 mm diameter reinforcement steel bars placed near the bottom, were assessed for the scope of this research. The concrete cover was designed equal to 45 mm as in accordance with a S4 structure (a structure with a service life of 50 years) and exposed to a XS3 environment. In order to assess the potential improvements coming from the employment of self-healing technologies in aggressive environments, the mix design detailed in Table 4.8, typically used for a XS3 environment has been employed. It foresees the use of CEM I 52.5 N cement with a water to cement ratio of 0.50 and limestone filler with a particle size <125 μm. Aggregates no larger than 8 mm were also chosen to easily pass between the branches of the 3D printed network and the mould. One beam, hereinafter referred as Ref_beam, was cast without any vascular network while a second one, named Vas_beam was built with an embedded 3D printed polylactic acid (PLA) vascular network. Four cubes from the mix design used in the demonstrator wall were cast with dimensions of 100 x 100 x 100 mm^3 and resulted in an average compressive strength of 58.9 MPa (standard deviation = 1.81 MPa) at 28 days in accordance with EN 12390-3. The used printer is a Carbon X1 type, provided by BambuLab, and the following print parameters were used: 40 mm/sec of printing speed; 0.25 mm of layer height and 30 °C as bed plate temperature. Moreover, the network itself, was a ductile porous network (developed by Shields et al., 2024) assembled in 200 mm long sections and characterized by the presence of 1 mm diameter pores spaced at 10 mm and filled with gelatin gel. The gelatin had to protect the pores during the casting procedures and to be then removed through a flush of warm water right after the demoulding procedures. In previous work on vascular networks, brittle networks have been used, that need to be fractured to release a healing agent in case of crack occurrence. This then requires the network to have weak tensile properties so that it cracks along with the concrete. These network types are the most extensively researched thus far in vascular self-healing concrete, and have been made with glass, ceramic materials, or 3D printed materials that impart brittle properties (Shields *et al.*, 2021). A drawback to brittle vasculature is that it requires extra care when handling and installing in a large-scale scenario, and self-consolidating concrete mixes are necessary to avoid vibrating the delicate networks, in turn adding more cost to the project. A ductile-porous network mitigates these constructability issues as it is not prone to damage during installation and casting, as well as involves a simpler manufacturing process. Figure 4.7 shows details of the geometry of the network. The network was placed in correspondence with the bending cracks formation area, within the cover zone and right below the reinforcement bars to which it was hooked by a metal wire. The employed healing agent was a polyurethane that can be used either as a one- or a two-component healing agent. Due to its properties, an expansive foaming reaction with a volume increase of up to 25–30 times occurs upon contact with moisture, favouring the crack filling.

Table 4.8: Mix design employed for the scope of this study.

Components	**Quantities [kg/m³]**
CEM I 52.5 N	337.6
Sand 0-4 mm	742.9
Gravel 2-8 mm	1031.1
Limestone filler	58
Water	168.8
Superplasticizer MasterGlenium 27 (BASF)	2

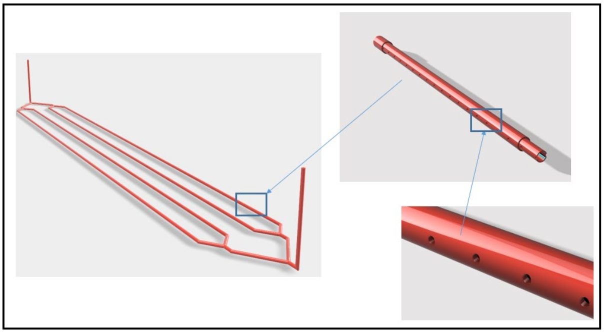

Figure 4.7: 3D model of the vascular network used for the scope of this study.

After casting the two types of beams, they were stored in a curing room with a temperature of 20°C and a relative humidity >95% to be then demoulded after one day. Figure 4.8 details the network assembled for the scope of this research while Table 4.9 provides information about the realization of the network, namely total number of pieces and printing time. These quantities will be used further on as part of the inventory for the Life Cycle Assessment analysis.

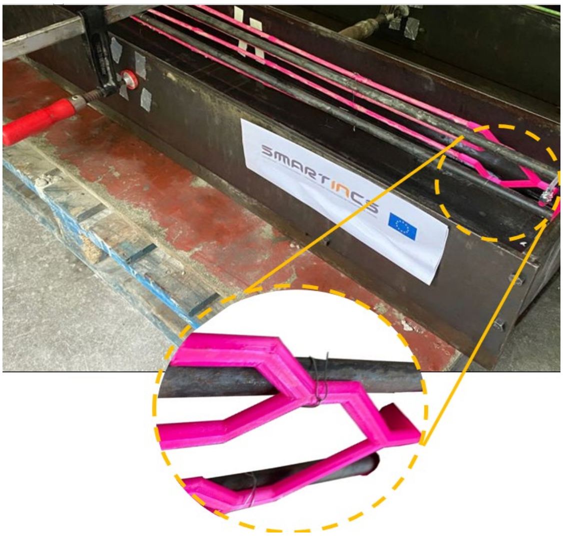

Figure 4.8: Assembled vascular network.

Table 4.9: Details of the needed network elements per beam. The components have been printed separately and manually assembled.

Vascular network element	**Quantities**	**Printing time**
Branched ends 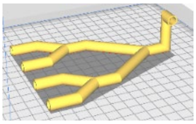	2	1 h and 27 minutes
Channels (200 mm of length) 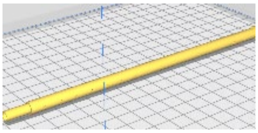	20	29 minutes

To check the chloride penetration in the cracked and healed state, the beams with and without vascular network were loaded at the age of 28 days in sequential three-point bending tests over a span of 400 mm, with the aim of producing three cracks equally distributed along the length of the beam. Loading was applied in displacement control at a rate of 0.001 mm/sec, with the crack width monitored using a crack mouth opening displacement (CMOD) clip gauge. The loading procedure was stopped once this reached a crack mouth opening of 0.5 mm. At three points along the corners of the beam 25 mm deep notches were made with a manual concrete saw-cutter to allow the crack to develop in the intended location. The beam with the vascular network was then healed with polyurethane (PU) that was pressurised up to 6 bar through the network. After 30 days, nine cores (100 mm of diameter) were extracted from the cracked and uncracked zone to be then immersed in an aqueous NaCl solution with a concentration of 33 g/L for three months after having coated the circumference with epoxy resin. Immediately after the removal from the solution, eight layers of concrete powders were collected parallel to the exposed surface by grinding material around the crack. The area of grinding was 18 mm wide with the crack in the middle and 50 mm in length along the crack. After having discarded the top layer of 1 mm, the 1st, 2nd and 3rd layer had a thickness of 2 mm, the 4th, 5th, 6th layer of 3 mm, the 7th was 4 mm and the last (8th) was 5 mm. The layers were defined based on the EN 12390-11 (2010). The determination of the total chloride concentration consisted of an extraction in a nitric acid solution followed by a potentiometric titration against silver nitrate. First, in accordance to [10] and [11], the powders were dried at 105 °C until constant mass and, after cooling down at room temperature, 2 g of each powder were weighed in a 50 ml glass beaker to be mixed with 5 ml of nitric acid (concentration: 0.3 mol/L) and 40 ml demineralized water. The obtained solutions were then heated on a plate until they just started to boil. Then, after being cooled down, they were filtered and diluted with deionized water in a 100 ml volumetric flask to take, later on, through a pipette, 10 ml for the determination of the chloride concentration per layer. For such purpose, a titration apparatus Metrohm (Salt Compact titrosampler by Metrohm Belgium) was used. The effective chloride profile was then determined for both the cracked and uncracked beams with and without the vascular network. Figure 4.9 shows the profiles used to determine the effective chloride diffusion coefficients (D_{app}). The values are reported in Table 4.10 for both Ref_beam and Vas_beam and indicate that the PU was not able to prevent the chloride ingress in this case, in contradiction to what was found for some types of PU in earlier research of our group (Van Belleghem et al., 2018), maybe due to the insufficient penetration of the healing agent. In this regard, further investigations will be needed in the future. Therefore, in the further analysis it will be considered that only where the PU fills the crack (as seen microscopically), it provides an effective sealing against chloride ingress.

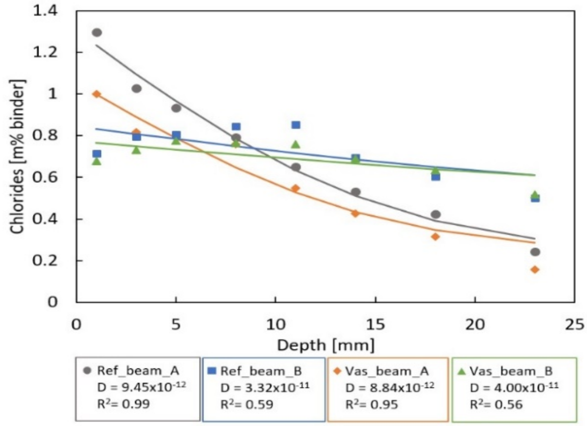

Figure 4.9: Chloride profiles for Ref_beam and Vas_beam for both uncracked (Ref_beam_A and Vas_beam_A) and cracked state (Ref_beam_B and Vas_beam_B).

Table 4.10: Obtained D_{app} [m²/s] and C_s [m% binder] values.

	Uncracked	**Cracked**
Ref_beam	D_{app} 9.45E-12 C_s 1.30	D_{app} 3.32E-11 C_s 0.84
Vas_beam	D_{app} 8.84E-12 C_s 1.12	D_{app} 4.00E-11 C_s 0.77

4.4.2 Concrete beam with vascular network: LCA system boundaries and data input

The LCA analysis was carried out by employing an extended cradle-to-gate system boundary and supposing a service life of 50 years in total. Similarly to our previous works (Kannikachalam *et al.*, 2022), the moment when the longitudinal bars lose 20% of their cross section area was assumed as serviceability limit state, considering the development of localized corrosion with the shape of a hemispherical pit. Exposure to a chloride concentration equal to 3.3% was considered, while the beams were supposed as initially cracked because of the loading conditions. Two different scenarios have been estimated for Ref_beam and Vas_beam, respectively. To predict the initiation time of the first one, the chloride diffusion coefficient equal to 3.32E-11 and the relative chlorides content at the surface (C_s) were adjusted and employed within the second Fick's law. More specifically, D_{app} has been considered constant within the time and equal to that reached after 5 years. Being D_{app} and C_s, time dependent parameters, have been adjusted according to Eq. 4.1 and Eq. 4.2 as in (Stipanovic Oslakovic *et al.*, 2010) where D_i and $C_{s,i}$ are the values obtained through the experimental results, t is the time assumed equal to 5 year (assumed as time reference as in (Stipanovic Oslakovic *et al.*, 2010; Van Belleghem, 2018a)since no significant variations are expected after that timeframe), while m and n are empirical coefficients assumed as 0.44 and 0.47 respectively, because of the similar exposure conditions in the case study and in the reference (Stipanovic Oslakovic *et al.*, 2010). With these assumptions, 1.63 x 10^{-11} m^2/s and 1.7 m% binder have been obtained for D_{app} and C_s respectively.

$$D(t)=D_i \cdot t^{-m} \qquad \text{Eq. 4.1}$$

$$C_s(t)=C_{s,} \cdot t^{n} \qquad \text{Eq. 4.2}$$

This leads to an estimated initiation time of 4.65 years by employing the second Fick' law. For the propagation of the corrosion, in accordance to the work of Van Belleghem (Van Belleghem, 2018a), a time of 7.5 years was calculated to develop a pit which reduces the cross section of the reinforcement bars with 20% (corresponding to a volume of the pit equal to 388 mm^3). Thus, at the age of 12.15 years the first maintenance activities are supposedly carried out for Ref_beam. Then, hypothesizing a reasonable structural loading scenario for a pedestrian bridge, with a load combination resulting in 22.10 kN/m, it has been verified that the acting bending moment exceeds the value of the one corresponding to the first cracks creation (M_{cr}) according to the Eurocode and calculated equal to 4.061 kNm. These calculations were made, considering 1.14 kN/m as weight of the beam, 0.38 kN/m as the load of a railing, 9 kN/m as crowd load and 11.58 kN/m as deck load (considering for both the crowd load and the deck load a tributary area of 2.5 m).

Moreover, once the maintenance activities are supposed to be executed, assuming a perfect adhesion of the repair layers to the concrete substrate, they have been assumed as immediately cracked as well. Due to this, initiation and propagation time have been assumed identical to the ones above mentioned. Thus, maintenance activities have been supposed to be carried out every 12.15 years, which means for a total of 4 times within 50 years of SL. A different scenario was figured out for Vas_beam since the injection of the PU was executed immediately at day one to prevent the ingress of the harmful substances from outside. Supposing a perfect sealing of the cracks up to 37 mm away from the vascular network towards the crack mouth, based on the spread of PU in the crack observed by microscope analysis (meaning a remaining crack depth of 8 mm) this thickness has been assumed as the new cover depth to calculate the initiation time for Vas_beam. This means that the chlorides are expected to penetrate quickly through the outer 8 mm of the crack and further diffuse slowly through the "uncracked" 37 mm of the cover. The uncracked D_{app} equal to 8.84 x 10^{-12} m^2/s which has been adjusted as well, together with Cs (resulting in 4.35 x 10^{-12} m^2/s and 2.3 m% binder), according to equations 4.1 and 4.2, have been used in this case. This leads, by employing the second Fick' law described in Eq. 3.2, to an initiation time of 35 years in total to which 7.6 years for the propagation must be added, resulting in 42 years in total to lose 20% of the cross section of the reinforcement bars. With regard to the maintenance activities, they consisted for both Ref_beam and Vas_beam in the removal of the concrete cover and of the damaged rebars with their consequent replacement. In this respect, it must be highlighted that while all of the concrete debris coming from the maintenance activities was considered to be treated as waste material, the steel scraps were accounted as recycled in respect to the current European regulations. The LCA was initially conducted assuming, for Vas_beam, the use of nylon to produce the vascular network and subsequently compared to PLA. This comparative analysis was feasible due to the similar mechanical characteristics of both materials, making them suitable as vascular network wall materials. Consequently, the outcomes are presented specifically for Vas_beam_N and Vas_beam_P, corresponding to the utilization of nylon and PLA, respectively. The software SimaPro with Ecoinvent 3.6 has been employed as data source for all of the raw components. Further details about the corresponding Ecoinvent inventories, including the one of the specific concrete mix design, are provided in Annex 1. Moreover, the environmental footprint has been calculated by employing the CML-IA impact method described in 4.4.3 .

4.4.3 Concrete beam with vascular network: LCA outputs

Due to the capacity of the PU to partially heal the cracks, different performance has been observed for Ref_beam and Vas_beam_N because of the different amount of maintenance activities to be carried out, namely four for the first one and only one for the second. Another difference is represented by the fact that for Vas_beam_N, besides the repair consisting of the removal and replacement of the damaged concrete layer and reinforcement bars, also the burdens referred to the vascular network itself and to the polyurethane (considered as injected under pressure) must be added. Figure 4.10 and Figure 4.11 present the details for the ten impact indicators of Vas_beam_N. As expected and outlined in previous research (Colangelo *et al.*, 2018), the highest impacts are due to the cement and reinforcement content that create, for example, 42% and 46 % of the Global Warming impact respectively for the case of Vas_beam_N as detailed in Figure 4.10.

For all of the other indicators the incidence of the reinforcement is always higher than 33% (up to 86% for the case of human toxicity potential) while the impact of cement ranges between 6 % (human toxicity potential) and 42 % (global warming potential). The influence of the vascular network is between 6% (human toxicity potential) and 20% (ozone layer depletion). Note that the category “other” includes also the treatment of the concrete debris and recycling of the steel scraps. As a matter of fact, a material that is recycled has a negative numerical impact value which, for the case of this study, exceeds the positive impacts related to all of the remaining components included in the “other” category (e.g. gravel, water, limestone etc). In general, as summarized by Figure 4.12, when exposed to the same environmental conditions, Vas_beam_N compared to Ref_beam, presents lower impacts for all of the ten indicators, sometimes reaching reductions higher than 40% as for human toxicity, fresh water aquatic ecotoxicity, marine aquatic ecotoxicity and terrestrial ecotoxicity.

However, vascular networks utilizing PLA were expected to exhibit lower environmental impacts compared to other polymeric filaments, due to its derivation from corn rather than fossil fuels. However, across various categories, its impacts were found to be similar or even greater than those of nylon, as explained in Figure 4.13. PLA, being a plant-based bioplastic, is manufactured from harvested corn or sugar cane. The production process involves extracting starch from raw materials, followed by drying and fermentation to produce lactic acid. Subsequently, the lactic acid undergoes polymerization, forming polylactic acid resin, a step that can be accomplished through ring-opening polymerization (Yang and Urban, 2013). The entirety of the PLA filament production process encompasses additional steps like drying and fermentation, absent in the production of other filaments. In contrast, the production of nylon involves fewer steps. Raw materials, such as adipic acid and hexamethylenediamine (derived from refined crude oil), undergo a condensation polymerization process to yield nylon (Tomasini and León-Santiesteban, 2015; Tonucci *et al.*, 2022; Ulkir, 2023).

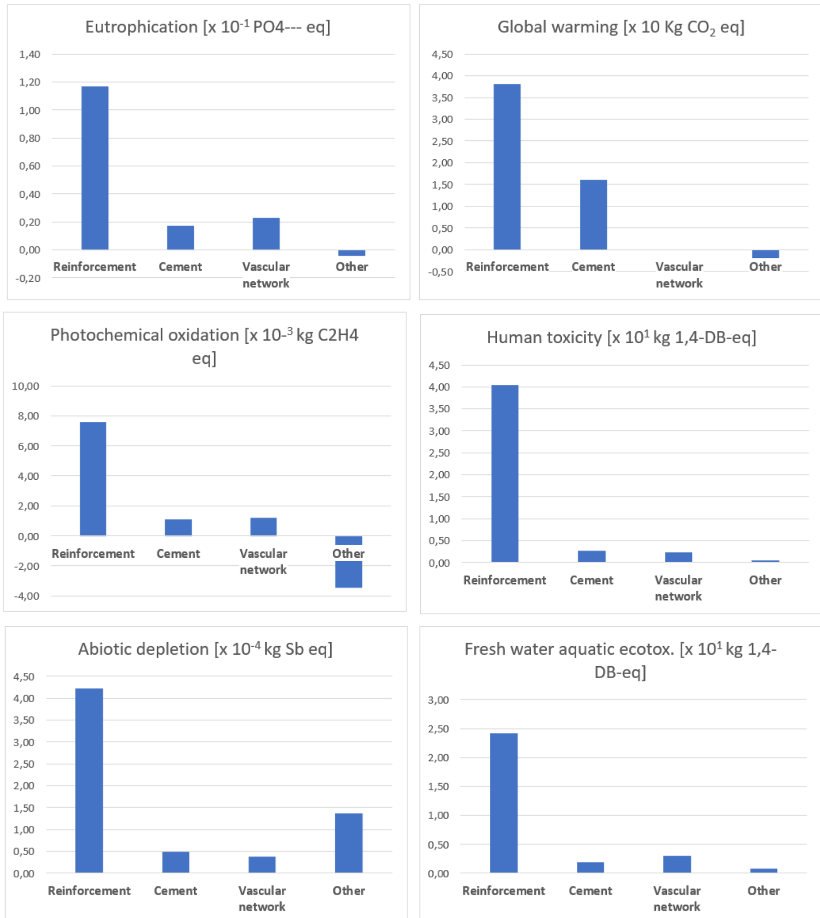

Figure 4.10: 6 out of 10 CML_IA impacts of Vas_beam_N. “Other” includes also the treatment of the concrete debris and recycling of the steel scraps, reason why it can be here displayed with a negative value.

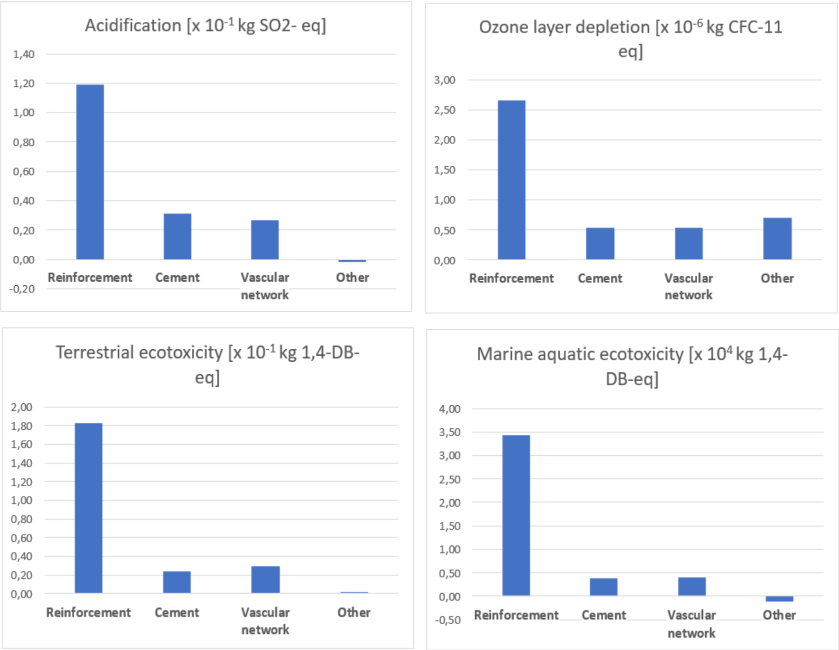

Figure 4.11: 4 out of 10 CML_IA impacts of Vas_beam_N. “Other” includes also the treatment of the concrete debris and recycling of the steel scraps, reason why it can be here displayed with a negative value.

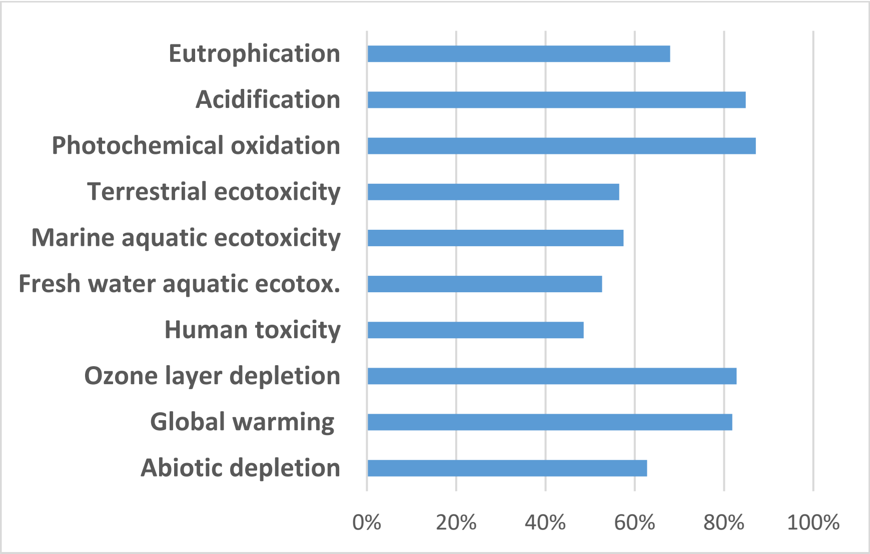

Figure 4.12: Impacts of Vas_beam_N relative to Ref_beam.

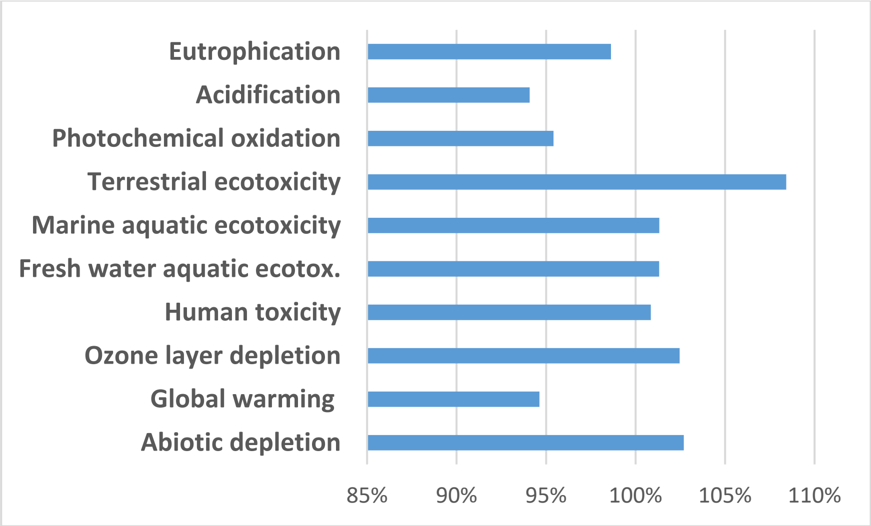

Figure 4.13: Impacts of Vas_beam_P relative to Vas_beam_N.

4.5 Concrete containing CEM III + Crystalline Admixture

Scope of this investigation is to address the effects that, in the event of an earthquake, certain aggressive degradation phenomena have on the structural and environmental performance of a construction. More specifically, the largest water treatment plant within Northern Europe, identified as a strategic structure, has been assessed. Aim of the conducted LCA analysis was to test the environmental behaviour of concrete containing crystalline additives and to evaluate the potential sustainability implications of using a more durable material for such type of structures. This aimed to also indirectly understand the implications for the local surrounding communities, in view of the social importance of a project like this. Moreover, to integrate structural evaluations as done for the case presented in 4.4, the moment when a specific damage affects the structural performance is taken into consideration as serviceability limit state in correspondence of which the maintenance activities have to be carried out to restore the normal functionality.

4.5.1 Description of the case study and degradation mechanisms

4.5.1.1 Description of the case study

The water treatment structure is located in Genoa, northern Italy, within the port area and aimed at serving a population of 250,000 inhabitants. It has been identified as a strategic structure in the case of an earthquake event, reason why a SL equal to 100 years has been taken into consideration for the following analysis. A frame structure, with beams which are sometimes eccentric in relation to the corresponding pillars, characterizes the ground level. The beams have a cross section equal to 0.70m x 0.70m or 0.70m x 1.00m, the pillars of 0.70m x 0.70m while the walls of the basins at the first floor have a thickness varying between 0.30m and 0.25m. Figure 4.14 shows an overview of the layout of the entire structure. To have a complete knowledge of the structure, the behaviour in the event of an earthquake has been assessed prior to estimating the durability of the construction within the SL. This was possible by carrying out a modal analysis in which the vibration response has been identified for each element of the structure. Figure 4.14 details a vibration example in which it is possible to highlight how the overall behaviour is not uniform. The analysis hereinafter presented is focused on the 26 pillars of the structure. The pillars are characterized by 24 Φ24 mm steel reinforcement bars equally located along the 4 sides. They are subjected to a biaxial compression and bending with an average axial force of 2,300 kN and the highest value of the acting bending moment (M_{Ed}) is equal to 1200 kNm (Carrassi, 2023). Figure 4.15 details the the M-N interaction diagrams due to the eccentric axial force. The structure being located at the seaside and being characterized by an XS1 exposure class, both the carbonation and the chlorides penetration phenomena have been taken into consideration. With regard to the concrete, two alternatives, employing ordinary reinforced concrete (ORC) or ORC containing crystalline admixture (1% by mass of cement) are considered. The latter was added to enhance not only the self-healing properties but also to reduce the permeability of the concrete, avoiding the ingress of harmful substances. Even though the pillars have been realized without the addition of the crystalline admixture (CA), hereinafter two cases are assessed. The first one, corresponding to the reality, with the pillars made with ORC (referred as P_ORC) and the second one, purely hypothetical, in which they are made with the addition of the crystalline admixture (referred as P_CA).

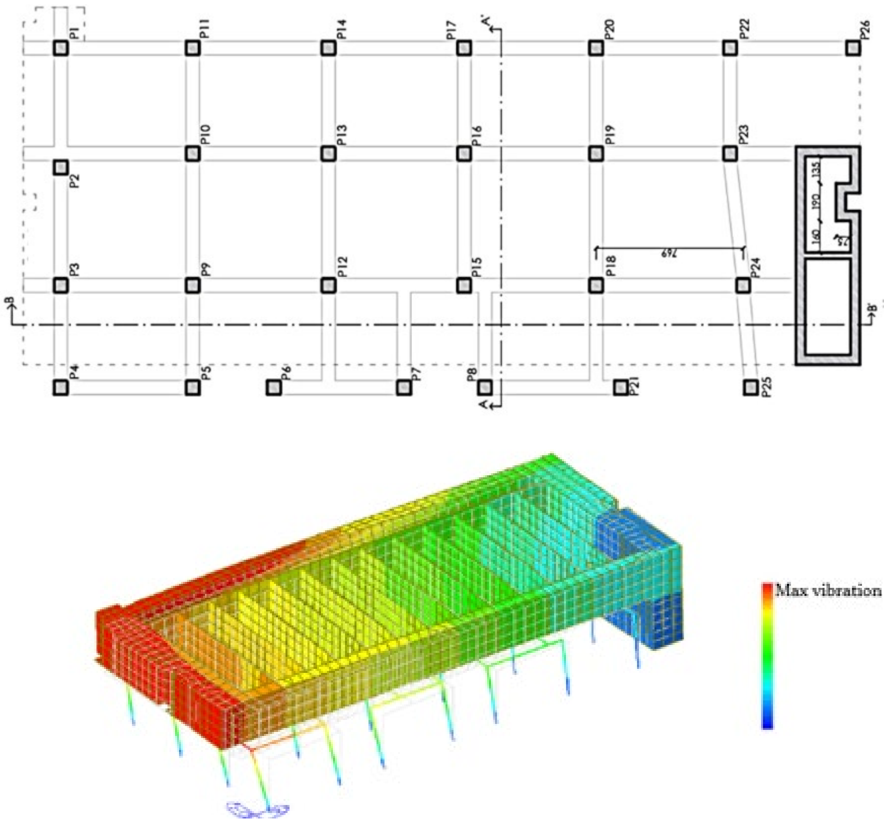

Figure 4.14: Layout of the structure (top) and the vibration response (bottom) in which the color red represents the parts more vulnerable to vibration.

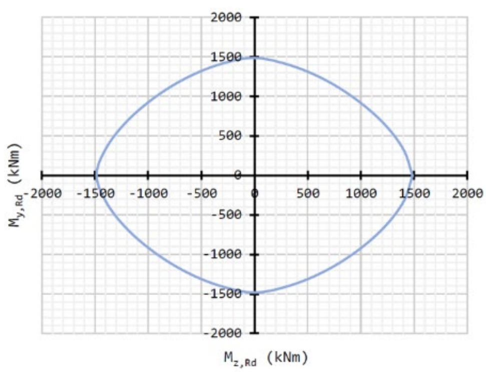

Figure 4.15: Biaxial interaction diagram due to an eccentric axial force.

4.5.1.2 Carbonation

To estimate the carbonation penetration, 12 cube specimens (150 mm x 150 mm) have been cast during the structure casting phases (March 2022). Half of the specimens were realized with the mix design of P_ORC while the remaining ones with the one of P_CA. With regard to the carbonation tests, after being exposed to open air at the worksite for 3, 6 and 9 months, as shown in Figure 4.16 each specimen was split into two halves and each half was then divided in two equal parts to have two perpendicular areas on which phenolphthalein was then sprayed. Table 4.11 indicates the average penetration depth achieved after 3, 6, 9 and 13 months respectively. To check whether there are relevant differences between the means of the two groups of data (the ones referred to P_ORC and those to P_CA), the statistical *t*-test has been used, obtaining a value equal to 0.012. Thus, considering that the latter is smaller than a significance level of the t-test equal to 0.05 (commonly used for these type of analyses) it is possible to conclude that P_CA outperforms P_ORC.

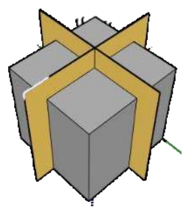

Figure 4.16: Example of the division of the specimen to spray the phenolphthalein.

Table 4.11: Carbonation depth (mm), average and standard deviation (SD) after 3, 6 9 and 13 months.

	P_ORC	P_CA	P_ORC	P_CA	P_ORC	P_CA	P_ORC	P_CA
	3 months		6 months		9 months		13 months	
Average	3.8	1.72	3.92	2.54	4.3	3.03	4.73	3.27
SD	0.60	0.35	0.33	0.53	0.75	0.25	0.86	0.43

Values presented in Table 4.11 have been then employed to predict the evolution of the carbonation over the SL of the structure through Equation

4.3 where x_c represents the depth of the carbonation, t the time expressed in years, W(t) a weather function used to consider the time in which the concrete is wet and k is the carbonation coefficient measured in mm/(years)$^{0.5}$. The latter depends on several factors such as water to cement ratio, relative humidity and CO_2 concentration. While W(t) has been assumed as equal to 1 due to the fact that the pillars are inside a prefabricated structure and, then, they are not wet, *k* has been determined by employing a non-linear regression analysis for Equation 4.3 and using the values reported in Table 4.11. The values obtained were 6.23 mm/(years)$^{0.5}$ for P_ORC and 3.53 mm/(years)$^{0.5}$ for P_CA. Thus, it was then possible to calculate the time needed for the carbonation process to reach the reinforcement bar surfaces located at a depth of 0.40 mm according to the standards prescriptions for structures exposed to a XS1 environment. This corresponded to 4.17 years for P_ORC and 128.1 years for P_ CA.

$$x_c = W(t)k\sqrt{t} \qquad \text{Eq. 4.3}$$

The result of P_CA being even higher than the accounted SL, the reduction of the diameter of the steel reinforcement bars have been estimated only for P_ORC by employing Equation 4.4 in which ϕ_0 represents the initial diameter of the reinforcement (mm), t the time (years), t_{in} is the time that the carbonation needs to reach the steel bars surface. Moreover, *j* is a constant equal to 0.0116 for the case of the steel and i_{corr} represents the power intensity in μA/cm^2 assumed as equal to 0.5 μA/cm^2 for the scope of this analysis according to (Bertolini and Pedeferri, 1996).

$$\phi(t) = \phi_0 - 2i_{corr}j\,(t-t_n) \qquad \text{Eq. 4.4}$$

By employing Eq. 4.4 it has been possible to estimate for P_ORC, a reduction of the cross section of each bar within a lifetime of 100 years, with a value equal to 5.60% at the time of 100 years. These results are reported in Figure 4.17 and Figure 4.18 which also contains the behaviour that the bars would have had in the case of P_CA. Then, following the model proposed by Maaddawy (2006) the time needed to form the first cracks because of the expansion products of the corrosion has been calculated. Such phenomenon is dictated by the thickness of the concrete cover, the diameter and the expansion volume of the steel bars, the elastic modulus of concrete and the thickness of the porous layer between concrete and steel. It was then estimated that the complete detachment of the concrete cover happens 11 years after the corrosion onset, in correspondence of the obtainment of 1 mm cracks, meaning after 52 years in total for P_ORC. Nevertheless, it must be specified that these results have to be considered as optimistic predictions since they are referring to a non-cracked state which is practically never achievable in the reality.

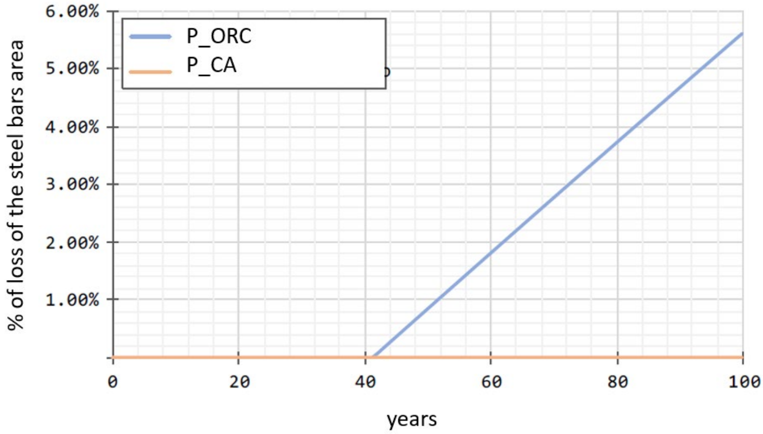

Figure 4.17: Loss of the cross section of the reinforcement bars in percentage.

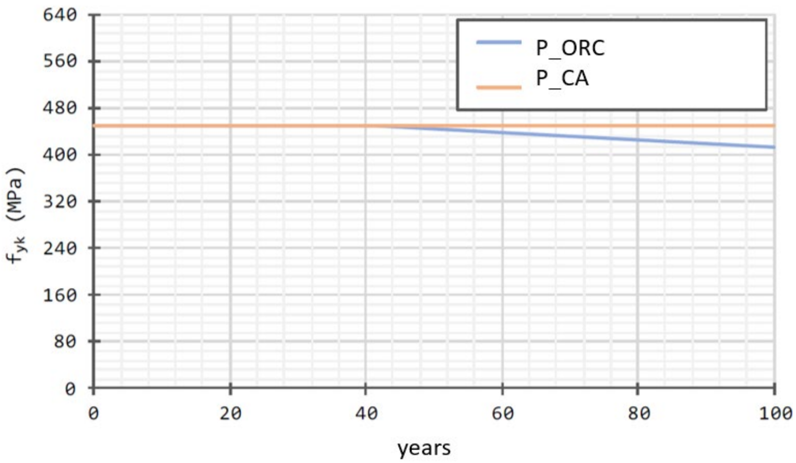

Figure 4.18: Decrease of steel tensile strength (F_{yk}).

4.5.1.3 Chlorides induced corrosion

As for the carbonation tests, 12 cubic specimens (150 mm x 150 mm) were realized during the casting procedures and were then split along two perpendicular areas to spray the 0.1-N $AgNO_3$ solution and check the chlorides penetration after 3, 6, 9 and 13 months of exposure to open air. Table 4.12 reports the value observed for the chloride penetration. A t-test has been performed also in this case and gave a value equal to 0.33 showing that the difference among the two series of data is not statistically relevant.

Table 4.12: Chlorides depth (mm), average and standard deviation after 3, 6, 9 and 13 months.

	P_ORC	P_CA	P_ORC	P_CA	P_ORC	P_CA	P_ORC	P_CA
	3 months		6 months		9 months		13 months	
Average	1.24	0.97	2.10	1.13	3.03	2.10	4.71	3.11
SD	0.45	0.34	0.81	0.22	0.57	0.64	0.46	0.37

The values presented in Table 4.12 have then been used to calculate the apparent chloride diffusion coefficient (D_{app}) which, as already highlighted before, is a key parameter to predict the penetration of the chlorides within a certain time. Thus, considering a critical chloride content equal to 0.11% by weight of concrete and a chloride content at surface equal to 0.17% by weight of concrete as in (Stipanovic Oslakovic et al., 2010), it has been possible to calculate a value of 9 x 10^{-13} m^2/s and 3.4 x 10^{-13} m^2/s for P_ORC and P_CA respectively by employing the second Fick's law described in Eq 3.2. Figure 4.19 and Figure 4.20 provide an overview of the chloride content for both P_ORC and P_CA at the age of 20, 40, 60, 100, 140 and 180 years for which both C_s and D_{app} have been assumed as constant over the time for the scope of these calculations. As it is possible to observe, the critical chloride content is reached, at the level of the reinforcement bars surface (namely 40 mm as the designed concrete cover) after 137 years for P_ORC and after more than 300 years for the case of P_CA. These years correspond to the corrosion initiation time. However, considering that these values are based on the results obtained from the experimental campaign conducted on the uncracked samples the influence of the cracks on the D_{app} value has also been checked. Click or tap here to enter text.A model studied by Wang et al., presented Eq. 4.5, has been employed (Wang *et al.*, 2016). There, W_{cr} represents the crack width, β_{cr} is a crack geometry factor (that the author suggests to be equal to 0.087), b_{cr} is the extending lengths of the crack on the bottom surface, h_{cr} is the extending lengths of the crack on the lateral surface, l_{cr} the average crack spacing, b the width of the beam where the crack appears, D_{cr} the diffusion coefficient inside the crack and D_o is the diffusion coefficient of the species in the homogeneous (uncracked) material solid (m^2/s). D_{cr} is calculated according to Eq. 4.6 depending on the crack width. Thus, considering a crack opening equal to 0.2 mm as suggested for the assumed environmental condition in the Eurocode, an initiation time equal to 82 years for P_ORC and 135 years for P_CA was then calculated. Both periods are much higher than the ones previously estimated for the carbonation.

$$D_{app} = \frac{4\beta_{cr} W_{cr} b_{cr} h_{cr}}{3bhl_{cr}} (D_{cr} - D_0) + D_0 \qquad \text{Eq. 4.5}$$

$$D\left(\frac{m^2}{s}\right) = \begin{cases} 2x10^{-11} W_{cr} - 4x10^{-10} & 30\mu m \leq W_{cr} \leq 50\mu m \\ 14x10^{-10} & W_{cr} \geq 50\mu m \end{cases} \qquad \text{Eq. 4.6}$$

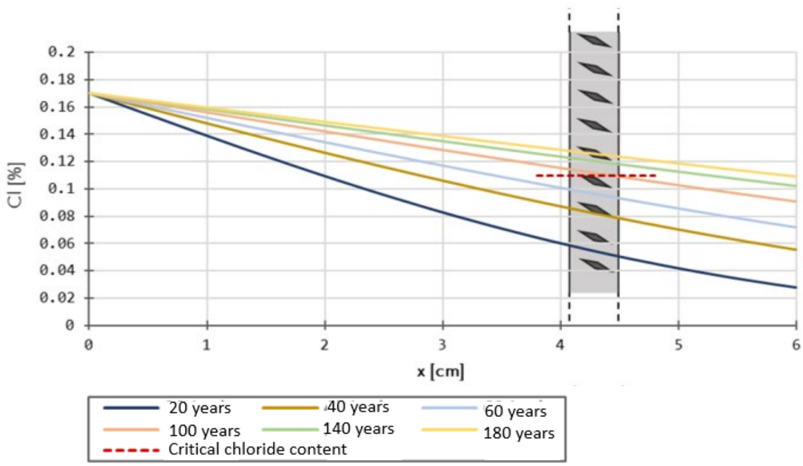

Figure 4.19: Calculated chloride content at different ages for different depths for P_ORC.

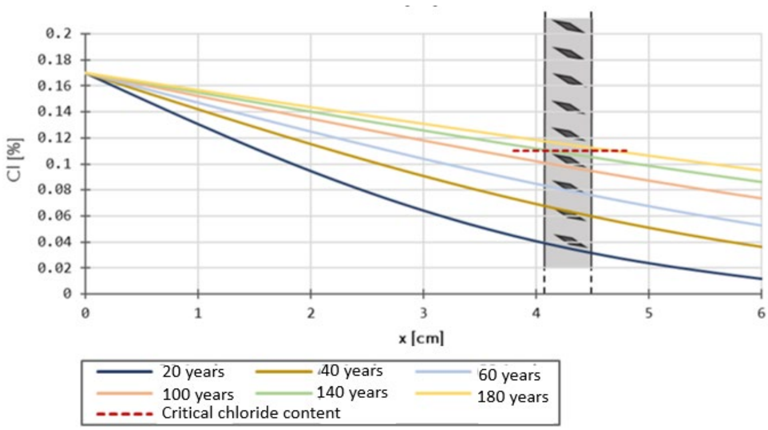

Figure 4.20: Calculated chloride content at different ages for different depths for P_CA.

4.5.1.4 LCA and LCC: system boundaries and data input

A cradle to grave system boundary has been employed to develop the LCA taking into consideration a SL of 100 years in total and supposing the need of one maintenance activity at 52 years only for the case of P_ORC columns. This is due to the carbonation that, based on the results of experiments, turned out to be the most severe degradation phenomenon for the case here assessed. The hypothesized maintenance activities consisted in the removal of the damaged concrete cover and reinforcement bars with the substitution of the latter and the casting of a new layer for the concrete cover after having applied a primer to favor its adhesion to the substrate. Moreover, ten impact indicators have been employed in total to describe the outcomes of the analysis according to the 10 CML IA impact method, aiming at quantifying the overall consequences on a local, regional and global scale.

4.5.1.5 LCA and LCC outputs

The LCA analysis highlighted a relevant reduction of the impacts of P_CA compared to P_ORC up to 40% as for HTP, FAETP and TETP. This is mainly due to the complete absence of the maintenance activities within the predefined SL for the case of P_CA. In this regard it must also be highlighted that all the steel scraps generated because of the maintenance activities of P_ORC are accounted as recycled, representing an environmental benefit, and for this reason are numerically counted with a negative value. If that were not the case, the reduction of the impacts of P_CA in comparison to

P_ORC would have been even higher. In general, cement has a relevant contribution to some impact indicators as 45 % for GWP for both P_ORC and P_CA. Such percentage value is even higher in the case of MAETP impacts of reinforcement, with a value equal to 98% for P_ORC. Moreover, the effect of reinforcement on the overall impacts is smaller in the case of P_CA due to the fact that no replacement of the steel bars is supposed for the latter. Figure 4.21 presents some results in this regard.

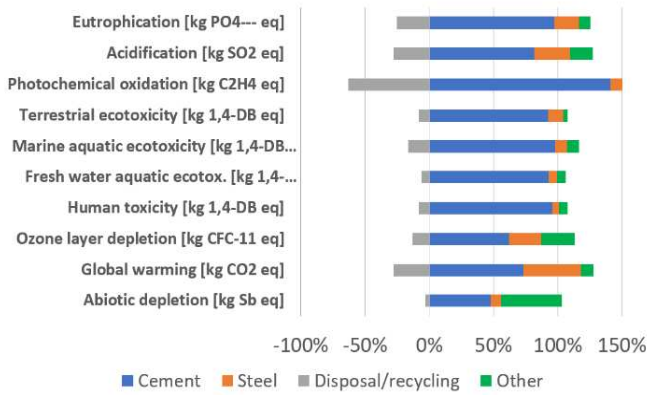

Figure 4.21: Impacts reduction of P_CA relative to P_ORC (top) and indication of the incidence of the main components on the overall impacts for P_ORC (bottom).

4.6 Use of SuperAbsorbent Polymers (SAPs) to enhance durability

As outlined in the introduction, concrete durability is a critical issue with environmental, economic and social impacts on society. The deterioration of concrete structures requires continuous maintenance and repairing activities, that generally imply the removal and the disposal of the damaged reinforcement and concrete, with the consequent need of new raw materials, energy and labour to restore the integrity and the pristine level of performance of the structure. Related expenditures also have to be taken into consideration. As said in chapter 2, recent researches have been developing innovative materials that can represent a solution in this respect, taking advantage of specific mechanisms that ensure the self-repair of cracks upon occurrence, hence improving structural durability (Liu et al., 2021; Plank et al., 2015; Craeye et al., 2011a; Feiteira et al., 2016; Gruyaert et al., 2016; Pelto et al., 2017). As example of that, SuperAbsorbent Polymers (SAPs), blended into the concrete matrix, represent an interesting technology. SAPs are a natural or synthetic water-insoluble 3D network of polymeric chains cross-linked by chemical or physical bonding. They possess the ability to take up a significant amount of fluids (up to 1500 times their own weight) (Mechtcherine, n.d.). The initial water uptake, followed by swelling, and the later gradual water release are of great interest in the development of more durable cementitious materials. Once in contact with the mixing water of the fresh cementitious matrix, SAPs absorb and retain a certain amount of it (depending on their absorption capacity), later on acting as water reservoirs for the system, able to keep high levels of internal relative humidity for a considerable time frame. Because of this feature, over the past two decades, SAPs have been used in cementitious materials for the purposes of internal curing to prevent shrinkage-cracking due to self-desiccation (Snoeck et al., 2015; Craeye et al., 2011b). Additionally, SAPs can promote the immediate sealing of cracks: upon cracking, the water that penetrates the cracks is generally absorbed by the SAPs that expand in volume, blocking the crack and preventing further entry of water and harmful substances (Snoeck *et al.*, 2012). Then, over time, the captured water is released again stimulating the hydration of unhydrated binder materials (when present) resulting in autogenous healing of the cracks (Snoeck *et al.*, 2014). Nevertheless, this kind of innovations usually face several barriers in their use, mainly due to the lack of information and to the possible higher initial investment cost. Hence, Life Cycle Assessment and Life Cycle Costing analyses are the tools to be adopted to lead design decisions throughout the entire design process. For a SAP-containing concrete, the use of 1 wt% by binder of SAP to favor the autogenous crack healing, together with 2 vol% of polypropylene microfibers, specifically employed to ensure a multiple cracking behavior in a concrete matrix based on Portland cement and including fly ash, silica sand, water and poly-carboxyl ether-based superplasticizer, was already investigated (Van den Heede *et al.*, 2018). The work, selecting as functional unit (FU) a slab (5 m large, 1 m wide and 0.17 m thick) with a service life of 100 years, highlighted that the investigated advanced cementitious composites allow to reduce around 60% the environmental impacts in comparison to Portland cement concrete solutions (Van den Heede *et al.*, 2018). Despite the literature which is continuously growing in this field, the above-cited work still represents the only one that applied LCA to assess environmental impacts related to the use of SAPs on a large-scale structure. Therefore, the aforesaid possible benefits have been further and deeper addressed from the environmental and the economical point of view. This was done developing also a Life Cycle

Costing analysis to assess the potential economic viability of these polymers, as "non-conventional" concrete constituents in a real structural service scenario. To this purpose, reference has been made to a case study consisting of two mock-up walls built in Bruges (Belgium), intended to replicate a tunnel segment element, also to demonstrate and foster the feasibility of employing these advanced materials on a large scale industrial basis. Moreover, to better understand the impact of different durability behaviors and to estimate reliable usage scenarios, the study integrates, within the sustainability assessment, the structural performance and their degradation over time due to exposure conditions.

4.6.1 SAPs-based concrete: case study

The case study consists of two earth-retaining walls intended to replicate tunnel segment elements. Both "walls" are 14 m long, 2.75 m high and have a 0.80 m deep cross section. One of them, henceforth indicated as Wall_Ref, was produced with concrete C35/45 and reinforced on either side with horizontal Φ16 mm steel bars spaced at 96 mm and vertical Φ12 mm reinforcement bars spaced at 140 mm. The second wall, denoted as Wall_SAP, was produced with concrete C30/37, containing the same amount of vertical Φ12 steel bars with a reduced quantity of longitudinal Φ16 mm bars spaced at 107 mm instead of 96 mm as done for Wall_Ref. The reinforcement of both walls was designed to allow a maximum crack width of 300 μm. In fact, given the difference in the strength class and considering that the internal curing promoted by the SAPs could counteract the shrinkage-deformation and hence mitigate the restrained shrinkage-cracking, both walls were designed expecting the same cracking pattern, even with a reduction in the reinforcement for Wall_SAP. Additionally, the walls were built on two foundation slabs casted at least three months prior to the walls and made with the same concrete of Wall_Ref. As it is possible to observe in Table 4.13, which details the two adopted mix designs, Wall_SAP contains a higher water-to-cement ratio since it includes both the effective mixing water and the entrained water in the SAPs. However, it is important to highlight that the entrained water in the SAPs is considered only for the purpose of internal curing, thus, it is also possible to affirm that both concrete mixtures have the same effective water-to-cement ratio. The walls were casted in the framework of the iSAP project, in which innovative superabsorbent polymers were used for the production of smart concrete mixtures, designed to possess the features of internal curing, self-sealing and self-healing of cracks. It was shown that the thereby developed innovative

SAPs added to the concrete mixture were even more efficient in crack mitigation than expected and no cracks were noticed over the complete monitoring period of 9 months (Tenório Filho *et al.*, 2021) differently from the reference structure where, as shown in Figure 4.22, several cracks were already observed. Previous laboratory experiments had further shown that this concrete mixture features the potential to reduce water permeability through cracks of up to 250 μm in width, and increase the resistance to salt-scaling under frost attack with a limited reduction in the compressive strength (Tenório Filho et al., 2020b;Tenório Filho et al., 2020a).

Table 4.13: Wall_Ref and Wall_SAP mix design per 1 m³

	Wall_Ref [kg]	Wall_SAP [kg]
CEM III-B 42.5N	359.78	359.82
Limestone 2/20	1,124.44	1,084.55
Marine sand 0/4	782.22	744.55
Superplasticizer Sika ViscoFlow-26	1.56	1.55
Superplasticizer Tixo	2.42	2.42
Water	144.44	137.45
Commercial SAP	-	1.36

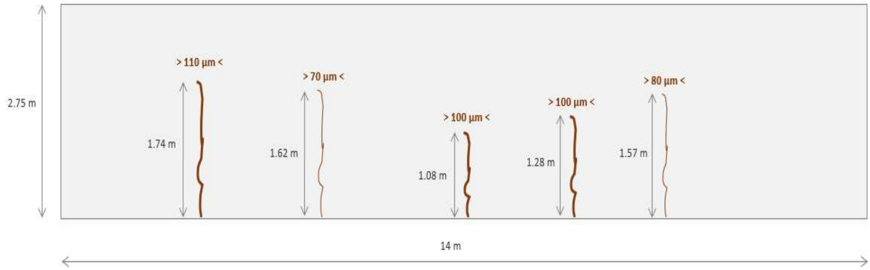

Figure 4.22: Cracking pattern of the reference wall at the age of 30 days. Adapted from (Tenório Filho *et al.*, 2021).

4.6.2 Assessed repairing techniques for the scope of LCA and LCC analyses

Nowadays, several methods are available to restore the functionality of damaged concrete structures, with a broad variety of materials and technologies to be used according to the occurred damage. However, it should be emphasized that the design phase of a given structure already takes into account the minimum “deemed to satisfy” requirements to ensure an adequate durability according to the boundary conditions. For instance, current codes and regulations, e.g. Eurocode 2 (Cen, 2005a), identify three measures to protect the steel reinforcement: limitation of the crack width, adequate concrete cover and appropriate concrete quality, achieved through minimum compressive strength and cement content, and maximum water-to-cement ratio. Additionally, EN 1504 (Cen, 2005b) defines the procedures and the characteristics of the products to repair the concrete structures. The standard is divided into ten parts, where the ninth describes eleven principles in total, defining for each one a specific prevention or repair activity. These range from hydrophobic impregnation to control the humidity, casting of new concrete layers to restore the damaged sections, substitution of reinforcement bars or post-tensioning of the existing ones to ensure the stability of the structure, up to the application of an electric potential to realize cathodic protection. Therefore, the commercially available materials that could be used for this purpose are various but, as easily understandable, each solution will result into different environmental impacts. This paper investigates the concrete cover replacement with the substitution of the damaged reinforcement bars as the main conventional technique to restore the functionality of Wall_Ref. This intervention would be needed from the moment when preferential penetration of chlorides or carbonation along the cracks will result into unacceptable damage to the reinforcement that would impair the structural stability. This choice is also supported by the work of Tilly and Jacobs (G.P. Tilly, 2007) who developed an international survey whose results were already used in similar LCA researches (Van den Heede *et al.*, 2018) highlighting that the concrete cover repairing technique had been used in 60% of the surveyed cases. Additionally, as these results could not be exhaustive, also polyurethane resin injection by pressure was assessed as repair technique for the purpose of this research, commonly applied in Belgium for repairing cracks occurring in tunnel elements.

4.6.2.1 Concrete cover and reinforcement substitution

According to the carbonation and chloride corrosion mechanisms, after the initiation time, the volumetric expansion of the corrosion products causes cracks along the concrete cover up to its spalling. Various experimental studies have been carried out to address the radial expansion of corroded reinforcement and its effects on concrete structures (Andrade et al., 1996; Liu et al., 1998; Clark et al., 1993;Al-Sulaimani et al., 1990; Rasheeduzzafar et al. 1992,Williamson et al., 2000). Generally, a common adopted technique to restore the functionality of a concrete structure, consists of the mechanical removal of the concrete cover, the substitution of the damaged reinforcement bars and the casting of a new concrete layer after a prior treatment with an epoxy-based product to ensure a better adhesion to the substrate. A key research focus, in view of the aforementioned discussion, is to determine when the reduced structural stability due to the reinforcement corrosion, will require the demolition of the concrete cover to replace the damaged bars for both Wall_Ref and Wall_SAP. The following sections better detail the approach here used, whose results are employed to define the 4 different scenarios in which the functional unit is assessed for the scope of this research. More specifically, while Scenario 1 and Scenario 2 assess a uniform corrosion propagation rate presented in 4.6.2.5, Scenario 3 and 4 take into account a more severe condition with a localized corrosion area as detailed in 4.6.2.6. Furthermore, Scenario 1 and 3 are limited to 50 years of SL, while Scenario 2 and 4 are aiming at 100 years.

4.6.2.2 Structural stability

Since the wall mock-ups can be regarded as earth-retaining walls, it is possible to calculate the lateral earth pressure using the Coulomb theory as in Eq. 4.6.

$$S = \frac{\gamma_t}{2} \times H^2 \times tg^2\left(\frac{90 - \varphi}{2}\right) \qquad \text{Eq. 4.6}$$

where, H is the height of the structure while γ_t and ϕ are the specific weight and the internal friction coefficient of a saline soil, assumed respectively equal to 18 kN/m³ and 35° according to the literature. As shown in Figure 4.23, a cantilever model was employed to design the structure and to calculate the bending moment action due to the soil thrust which has to be resisted through the moment resisting capacity of the wall base cross section.

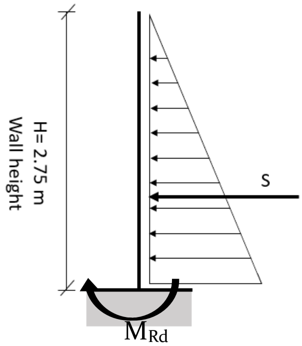

Figure 4.23: Model used for calculations.

Therefore, using Eq. 4.6, it is possible to calculate, for a 1 m long strip of the wall, a total earth thrust equal to 18.44 kN/m applied at H/3, which corresponds to a bending moment equal to 16.90 kNm/m. The latter, was then amplified by a coefficient γ_G of 1.35 as per EN 1990:2002, with a resultant bending moment design value (M_{Ed}) equal to 22.82 kNm/m. Eq. 4.7 was then adopted to estimate the resistant moment M_{Rd}, equal to 212.9 kNm. According to the cross section of the wall presented in Figure 4.24, a value of 391.3 N/mm² was used for the design yielding strength of steel f_{yd}, calculated from the characteristic yield stress f_{yk} of a B450C steel, while 791 mm² and 764 mm were used for the tension reinforcement bar area A_s and the effective depth d, respectively.

$$M_{rd} = 0.9 \cdot f_{yd} \cdot A_S \cdot d \qquad \text{Eq. 4.7}$$

The self-weight of the wall should also been taken into account for the M_{Rd} calculations. However, since for the considered 1 m long strip, it is equal to about 55 kN/m (less than 1% of the axial load capacity of the base cross section), it can be regarded as negligible for the scope of this research, not significantly affecting the final results. Therefore, since it must be always verified that $M_{Ed} < M_{Rd}$, it is easily possible to calculate that the A_s value must be higher than 8483 mm². This means that, as in one meter of the wall 7 Φ12 mm bars are located, assuming the same corrosion progress along the entire wall, each reinforcement bar cannot lose more than 89% of its cross-section. The reduced A_s values imply that the safety of the structure cannot be ensured any longer and specific repairing activities must be adopted to reinstate an acceptable A_s value.

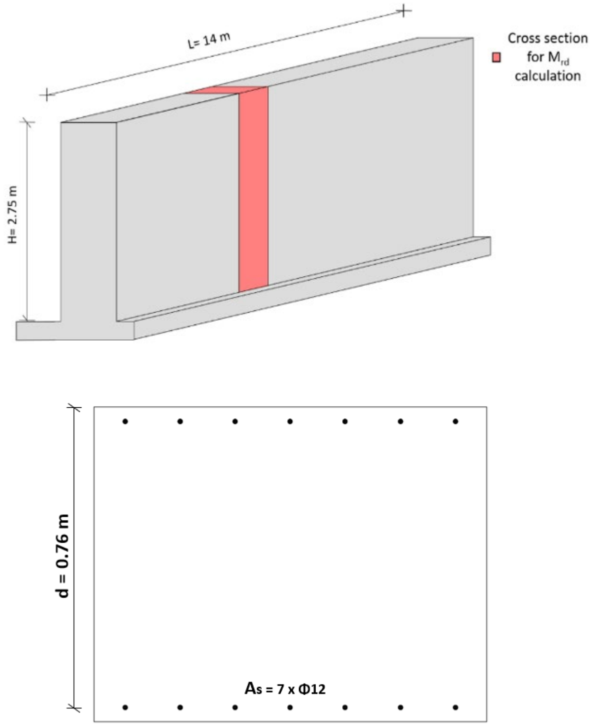

Figure 4.24: Three-dimensional view of the wall (top) and horizontal cross section (bottom) considered to calculate M_{Rd}

4.6.2.3 Corrosion initiation

Before calculating how long it would take the chloride-induced corrosion to affect the load bearing capacity of the structure, it is necessary to calculate the time the chloride ions will need to penetrate the concrete matrix and reach a critical concentration value at the cover depth, i.e. at the level of the most external surface of the reinforcement. To this purpose, the 2nd Fick law described in chapter 3 and presented again in Eq. 4.8 is generally employed.

$$x_{crit} = 2\sqrt{3(t-t_0)\cdot D_{app}}\cdot\left[1-\sqrt{\frac{(C_{crit}-C_I)}{C_s-C_i}}\right] \qquad \text{Eq. 4.8}$$

where x_{crit} is the critical chloride depth assumed equal to the concrete cover, C_i is the initial chloride content of concrete equal to 0.20% by weight of cement according to EN 206 (Cen, 2016a); C_s is the chloride concentration at the surface being 0.92% by weight of soil for the case of saline soil (Romagna, 2011) and C_{crit} is the critical chloride concentration equal to 0.44% by weight of cement according to Alonso and Sanchez. (Alonso and Sanchez, 2009a) and based on field exposure tests developed for the specific purpose. D_{app} is the apparent chloride diffusion coefficient whose values, as better detailed in 3.1.3, may range from 10^{-10} m²/s to 10^{-12} m²/s.

4.6.2.4 The incidence of D_{app} values for both LCA and LCC calculations

With regard to the D_{app} value, the currently available literature does not give any detail about the effect of SAP addition. A value of 10^{-10} m²/s is generally reported for the case of cracked concrete while for the uncracked one, containing CEM I, a value one order of magnitude smaller could be used, equal to 10^{-11} m²/s (Al-Obaidi et al., 2020a;Shafikhani and Chidiac, 2019a;Torres-Acosta et al., 2019a;Liu et al., 2015a). Additionally, since Wall_SAP contains CEM III/B, a theoretical correction factor of 0.2 according to (Coppola, 2007) allows to pass from 10^{-11} m²/s to the 10^{-12} m²/s order of magnitude). According to this, an initiation time of almost 0 was calculated for the cracked Wall_Ref (corresponding to the wall itself prior to any other maintenance activity) using 10^{-10} m²/s. In contrast, a D_{app} value equal to 10^{-12} m²/s has been used for Wall_Ref after having received the first maintenance activity and for Wall_SAP. This resulted into a corrosion initiation time of 13 years in total. This could be assumed, considering that no cracks were observed up to 9 months after casting for the Wall_SAP and no cracks are supposed for Wall_Ref after its restoration until when the chloride will reach the reinforcement surface causing the steel corrosion. These different initiation times clearly express the need to integrate the structural properties of a given structure into the LCA and LCC evaluations. As a matter of fact, different D_{app} values lead to clearly different initiation times, passing from around years when assuming a value of 10^{-10} m²/s, through 1 year when using 10^{-11} m²/s up to 13 years in total with 10^{-12} m²/s. Therefore, since a longer initiation period corresponds to a more delayed corrosion of the steel bars with a resulting different frequency of the maintenance activities, the more precise the structural considerations will be, the more accurate the LCA and LCC will be.

4.6.2.5 Corrosion propagation - rates from the literature

When water and oxygen are present on the surface of the reinforcement, the corrosion occurs with a rate, denoted as penetration rate and usually expressed in μm/y. Some authors (Bertolini et al., 2004a) distinguish among a negligible rate lower than 2 μm/year, a low rate between 2 and 5 μm/year, a moderate rate between 5 and 10 μm/year, an intermediate rate between 10 and 50 μm/year, a high rate between 50 and 100 μm/year and a very high rate above 100 μm/year. More specifically, for a concrete contaminated by chlorides and subjected to 80-90% of relative humidity (RH), the closest assumption to the case studies of this research, the corrosion rate can vary from 10 μm/year up to 50 μm/year (Bertolini et al., 2004a). Therefore, taking into account the most severe condition equal to 50 μm/year after the initiation period, it is possible to estimate a propagation time for a Φ12 mm rebar system as in Figure 4.25.

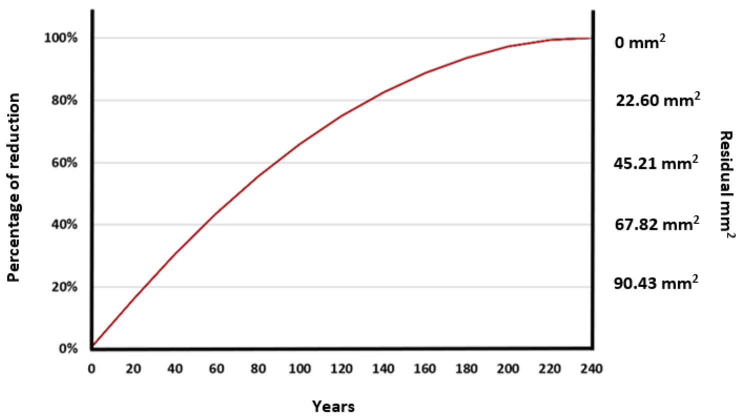

Figure 4.25: Percentage of cross area reduction for Φ12 bars, assuming 50 μm/year, according to (Bertolini et al., 2004a.

4.6.2.6 Corrosion propagation – hemispherical pit calculation

Differently from the previous type of corrosion, that basically considers a uniform deterioration of the steel reinforcement, it is possible to assume that chloride induced corrosion is restricted to a very localized damage. This means that the mass (and volume) loss of steel is concentrated in a small zone (pit corrosion) that increases as the corrosion propagates in time, generating a volumetric mass loss of the steel, as shown in Figure 4.26.

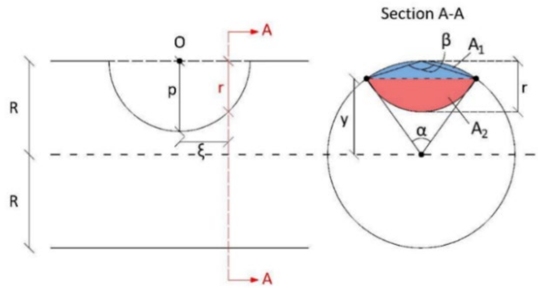

Figure 4.26: Schematic representation of the hemispherical pit model as detailed in (Van Belleghem, 2018)

However, this still represents a simplified approach since the corrosion itself also implies the build-up of expansive corrosion products at the rebar surface with a consequent concrete cover cracking which will favor the ingress of further chlorides, here not taken into account. The volume and the area of the pit are calculated as stated by Van Belleghem (Van Belleghem, 2018b), using the Eq. [4.9] and Eq.[4.10].

$$A_{pit} = A_1 + A_2 = \frac{R^2}{2} \cdot (\alpha - \sin\alpha) + \frac{r^2}{2} \cdot (\beta - \sin\beta) \qquad \text{Eq. 4.9}$$

$$V_{pit} = \int_{-p}^{p} A_{pit}\ (\xi) \cdot d\xi \qquad \text{Eq. 4.10}$$

Where:

$$r = \sqrt{p^2 - \xi^2} \qquad \text{Eq. 4.11}$$

$$y = \frac{2R^2 - r^2}{2R} \qquad \text{Eq. 4.12}$$

$$\alpha = 2 \cdot \cos^{-1}\left(\frac{y}{R}\right) = 2 \cdot \cos^{-1}\left(1 - \frac{r^2}{2R^2}\right) \qquad \text{Eq. 4.13}$$

$$\alpha = 2 \cdot \cos^{-1}\left(\frac{y}{R}\right) = 2 \cdot \cos^{-1}\left(1 - \frac{r^2}{2R^2}\right) \qquad \text{Eq. 4.14}$$

With reference to a Φ12 mm bar, it is thus possible to calculate the area and the volume of a progressing pit (from 1 mm up to 12 mm) as in Table 4.14, from which the time necessary to develop the loss of a specific volume can be estimated (in years). According to (Van Belleghem, 2018b), a loss of 13.36 mm^3 was estimated for a period of 20 weeks, and 0.58 mm^3 per week from 20 weeks onwards. These results are obtained from an experimental campaign based on a fly ash containing concrete, with a water-to-binder (W/B) ratio of 0.41 and a fly ash-to-binder ratio of 15% by mass. This mixture was designed to be a representative reference mixture for concrete in exposure class XS2, i.e. submerged reinforced concrete subject to corrosion initiated by chlorides. The specimens, with an approximate crack width of 300 μm, were exposed to a 33 g/L NaCl solution in order to simulate a chloride containing environment (sea water, typically) and adopting two exposure regimes. One of these consisted of a 3.5 day wet period followed by a 3.5 day dry period, for 26 weeks in total, while the second one was changed to a 1 day wet period followed by a 6 day dry period for a total of 44 weeks (Van Belleghem, 2018).

Table 4.14: Calculated area and volume of the hemispherical pit.

p (mm)	**V_{pit} (mm^3)**	**A_{loss} (mm^2)**	**A_{loss} (%)**	**Years to develop corrosion pit**
1	**2.03**	**1.52**	1	**0.4**
2	15.71	5.84	5	0.5
3	51.22	12.63	11	1.6
4	117.13	21.54	19	3.8
5	220.27	32.20	28	7.2
6	365.66	44.22	39	12
7	556.28	57.18	51	18.3
8	792.78	70.59	62	26.1
9	1073.01	83.88	74	35.3
10	1391.16	96.33	85	45.8
11	1735.81	106.87	95	57.2
12	2083.11	113.10	100	68.7

4.6.3 Crack filling by means of resin

Since cracks affect the overall durability of a concrete structure, a repair solution could be to fill them with chemical resins (epoxy, acrylic and polyurethane) acting as an offset and stopping the ingress of the external agents (SIKABrazil Marketing Catalog. Available online at http://bra.sika.com (September 2015)"). ACI 503R report identifies the resin injection as an efficient method for crack repair in buildings, bridges, dams and other types of concrete structures (American Concrete Institute, 1998) while several guidelines and methods of application are described in ACI 504R (ACI, 1997). Furthermore, thanks to their mechanical properties, the resins can be able to restore the structural integrity (Araújo, 2016;Magazine, Spring, available online at www.waterproofmag.com (August 2015) and, moreover, the polyurethane, expanding during the injection, guarantees strong adhesion to the concrete both in wet and dry cracks, ensuring the regain in impermeability. Therefore, one of the repairing techniques that this study analyzes, is the filling of the cracks by means of a pressure-injected polyurethane resin, since it is a commonly used method in Belgium and several countries worldwide. More specifically it was supposed to employ a commercial one-component polyurethane-based resin. As the technical specifications clarify, these kind of products are recommended to be injected at a pressure of 14 bar up to 200 bar. The product is pumped into the cracks by holes drilled at an angle of 45° distributed around the crack at a distance that, according to the specific situation, can vary from 150 mm up to 900 mm. A schematic representation of the procedure is reported in Figure 4.2727. Furthermore, according to what is stated in (G.P. Tilly, 2007) in which the concrete repair performances throughout the service life are assessed, it was assumed that around 90% of the cracks filling will fail in 25 years requiring further injections to restore the integrity of the structure.

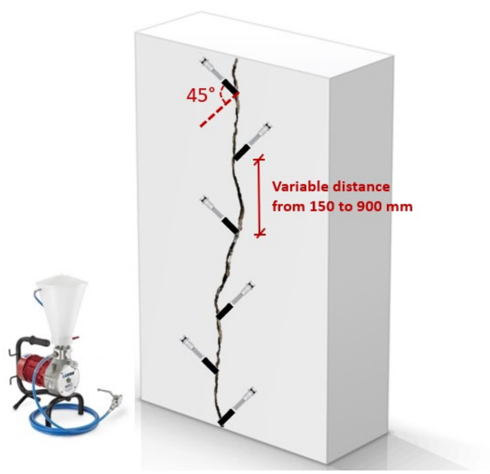

Figure 4.27: Schematic representation of polyurethane resin injection.

4.6.4 Concrete walls with SAPs: LCA system boundaries and data input

To the purpose of assessing and quantifying the environmental and cost benefits of the SAP-based concrete, an extended cradle to gate system boundary has been employed. The exclusion of the end-of-life phase is mainly dictated by the fact that these types of concrete mixes are still under development with a consequent lack of information regarding the disposal scenario or the recyclability option which is still subject of investigation (Snoeck *et al.*, 2022). In fact, the presence of SAPs could imply a specific disposal specification for the entire structure, that is still unknown at the time of writing. Therefore, the goal of highlighting the possible environmental benefits of these innovative materials, is pursued taking into account the impacts referring to the production and use stages that correspond to the A1-B7 stages indicated in EN 15804 (UNI, 2019a) as reported in Table 2.1

4.6.4.1 Data source

Also in this case, Ecoinvent was used as data source for collecting the LCIs for all raw materials both for traditional and SAP-containing concrete. This was not difficult for most of the common constituents like sand/gravel/cement/water, but needed further and dedicated investigation for data referring to commercial products such as SAPs, epoxy resin and superplasticizers. About the latter, the existing libraries contain data only for plasticizers based on sulfonated melamine formaldehyde while in the concrete matrix a polycarboxylate-based one, was also used. Therefore, a modelled version by Agustí-Juan et al. (Agustí-Juan *et al.*, 2017a) was used and reported in Table 4.15 in accordance to the Environmental Product Declaration (EPD) of the product (Concrete and Associations, 2019).

Table 4.15: LCI used for the polycarboxylate-based plasticizer.

Materials/fuels	**Amount**	**Unit**
Chemical, organic (GLO)| market for | APOS,U	0.167	kg
Formaldehyde (GLO) | market for | APOS,U	0.038	kg
Sodium hydroxide, without water, in 50% solution state (GLO) | market for | APOS,U	0.137	kg
Sulfuric acid (GLO) | market for | APOS,U	0.162	kg

Water, completely softened, from decarbonised water, at user (GLO)| market for | APOS,U	0.496	kg

The SAP was modeled as a commercially available synthetic polymer, made of acrylamide and sodium acrylate (Table 4.16). As the exact composition is confidential, some assumptions, based on the existing literature, had to be made to model its LCI. The employed SAP was considered as a 30% anionic synthetic polymer, made of acrylamide and sodium acrylate. This implies that 30 mol% of the monomers incorporated in the SAP are negatively charged while the remaining ones are divided into 60 mol% acrylamide and 10 mol% crosslinker (that, for the polymerization purpose, could be methylene bisacrylamide). Then, using 71.08 g/mol, 94.04 g/mol and 154.17 g/mol as molar masses for acrylamide, sodium acylate and crosslinker respectively, the mol-% were calculated into mass-%.

Table 4.16: SAP_acrylamide / sodium acrylate LCI.

Known outputs to technosphere	**Amount**	**Unit**
SAP_ acrylamide / sodium acrylate	1	kg
Known inputs from technosphere	**Amount**	**Unit**
Polyacrylamide {GLO}|market for|APOS,U	0.326	kg
Acrylate	0.494	kg
Ammonium persulfate (as modeled after Gontia & Janssen)	0.004	kg
Polyacrylamide {GLO}|market for|APOS,U (adopted as crosslinker)	0.178	kg
Electricity, medium voltage {BE}|market for|APOS,U *(for stirring)*	0.001	kWh
Electricity, medium voltage {BE}|market for|APOS,U *(for flushing)*	0.094	kWh
Electricity, medium voltage {BE}|market for|APOS,U *(for drying)*	4.138	kWh
Electricity, medium voltage {BE}|market for|APOS,U *(for grinding)*	0.016	kWh

Furthermore, as can be observed in Table 4.1616, due to the lack of data regarding the methylene bisacrylamide as crosslinker, polyacrylamide (the most similar one from a chemical point of view) was used for the specific purpose. This assumption is based on the fact that polyacrylamide is a polymer resulting from acrylamide polymerization while methylene bisacrylamide is chemically similar to the acrylamide monomer. Additionally, 2 kg of water were assumed as necessary during the polymerization phase while for the energy consumptions values the ones stated by Van Den Heede et al., for the synthetic acrylic acid + acrylamide based SAP, have been adopted (Van den Heede *et al.*, 2018). Here, the ones referred to the heating process, typically required to initiate the polymerization in case a thermal photo-initiator is used, were excluded since this was not the case.

With reference to the concrete manufacturing, as already done by Van den Heede et al., also the impacts referring to the production process at a ready-mix concrete plant have been incorporated. The existing Ecoinvent LCI for concrete mixing (reported as “Concrete, normal {CH}| unreinforced concrete production, with cement CEM II/A | APOS, U”) was used after a slight modification. In fact, removing the items “Gravel, round {CH}| market for gravel, round | APOS, U”, “Cement, alternative constituents 6-20% {CH}| market for | APOS, U” and “Tap water {CH}| market for | APOS, U” from the existing LCI, it was possible to obtain the specific inventory referring to the act of concrete mixing on an industrial scale. No inventory data were readily available in Ecoinvent 3.6 for the acrylate; for this reason, as shown in Table 4.17, the LCI adopted by Gontia and Janssen (Gontia and Janssen, 2016) for the sodium poly(acrylate), excluding the ammonium persulfate and sodium hydroxide, was used. The former is the initiator for the polymerization and does not play a role in the production of the acrylate monomer as such. With regard to consumption of electricity, the same value was assumed as for acrylamide, due to the fact that the production process requires approximately the same amount of energy.

Table 4.17: Acrylate LCI.

Known outputs to technosphere	**Amount**	**Unit**
Acrylate	1	kg
Known inputs from technosphere	**Amount**	**Unit**
Acrylic acid {GLO}| market for | APOS,U	0.782	kg

Known inputs from technosphere	**Amount**	**Unit**
Electricity, medium voltage {BE}| market for | APOS,U	7.830	MJ
Water, deionised, from tap water, at user {GLO}| market for |APOS,U	1.753	kg
Emissions to water	**Amount**	**Unit**
Water	1.953	kg

About the polyurethane resin injection, the EPD (FEICA - Association of the European Adhesive and Sealant Industry, 2015a) of a commercial product, already provides the CML_IA impacts values referred to the production process. These impacts, scaled on the basis of the quantity of the included product, were simply added to the ones referring to Wall_Resin construction itself. Anyway, since they were not exhaustive enough, it was necessary to estimate the impact of the whole injection process too. To do this, the use of a rotary hammer with a 850 W of power to drill the holes and an equipment for the injection by pressure with 750 W power to pump the product were considered. As the time needed to complete the process can vary according to the boundary conditions, a time of around 1 hour to drill all the holes and of 8 hours to fill the cracks was roughly estimated. Therefore 0,972 kWh and 6 kWh of the Ecoinvent data "Electricity, medium voltage {BE}| market for | Alloc Def, U" have been respectively used to estimate the act of drilling and the resin injection.Regarding the replacement of the damaged reinforcement bars with the concrete cover substitution, the concrete substrate is usually treated with specific epoxy adhesives to ensure a good adhesion of the new cover. For this scope, a commercial product was considered of which the associated impacts, starting from the preparation of a perfectly clean and solid substrate until its on-site installation, were deduced from its EPD (FEICA - Association of the European Adhesive and Sealant Industry, 2015b) and scaled on the basis of the quantity of the necessary product and added to the ones referring to Wall_Ref.

4.6.4.2 Description of the Functional Unit.

For the purpose of this research a functional unit (FU) corresponding to the wall itself was selected with a service life varying from 50 years up to 100 years according to four different scenarios. With regard to the reference structure, since several vertical cracks were already observed after 5 days;

and after 1 month the cracks ranged from 50 up to 110 µm width and varying from 870 mm up to 1,880 mm length (Tenório Filho *et al.*, 2021), the two above-mentioned repairing activities were taken into account to restore the structure functionality. The first technique implies the demolition and the reconstruction of the concrete cover with the substitution of the damaged bars with a pre-treatment of the concrete cover substrate prior to the casting of the new layer. When the uniform corrosion propagation rate is taken into account, the associated impacts and costs are below indicated with Wall_Ref_M1_50 and Wall_Ref_M1_100 referring to 50 and 100 years of SL according to the specific scenario. When the hemispherical pit model is taken into account, then the associated environmental burdens and overall costs are indicated with Wall_Ref_M2_50 and Wall_Ref_M2_100 for 50 and 100 years of SL respectively. The second refurbishment option for the reference structure, consists of the injection by pressure of a polyurethane resin into the cracks. This, according to what was stated before, allows to restore the M_{Rd} values to the original ones obtaining an extension in terms of service life as shown by way of example in Figure 4.28 for the case of Wall_SAP.

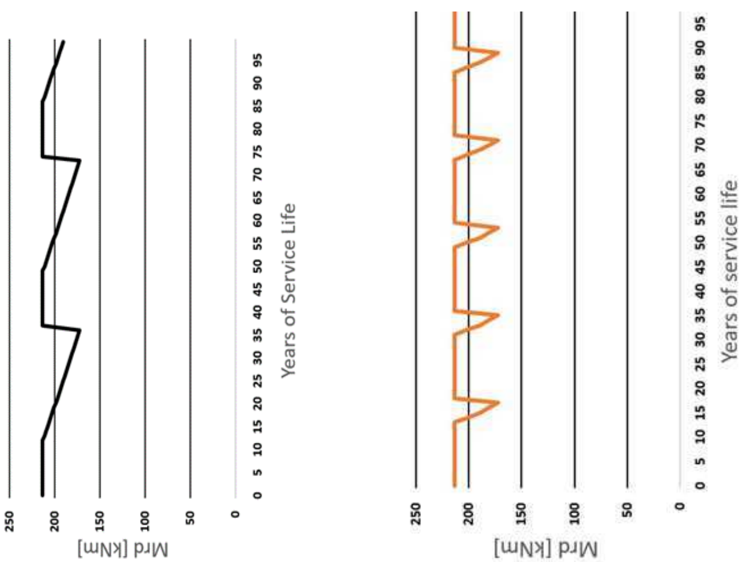

Figure 4.28: Representation of M_{Rd} as a function of time and its "upgrade" along the service life thanks to the retrofitting operations adopting the corrosion rate from the literature (left) and the hemispherical pit model (right) for the case of Wall_SAP. The increases in M_{Rd} correspond to the time when the repairing activities are carried out.

Thus, assuming that, as stated in 4.6.3 , it has been estimated that every 25 years it is necessary to reiterate the activity for 90% of the cracks already filled in the past. The impacts associated to this second option are described in what is below indicated with Wall_Resin 50 and Wall_Resin 100 depending on the considered timeframe. With regard to the SAPs-based structure, it is supposed to be subjected to the same corrosion propagation models as the reference wall, but, since no cracks were observed up to 9 months, just the concrete cover reconstruction with the replacement of the damaged bars are taken into account. The environmental footprint of the FU has been calculated using the CML-IA impact method.

4.6.5 LCA outputs

The different conditions in which the FU is assessed are below better described and discussed. Furthermore, in each scenario, which only takes into account the concrete cover reconstruction and the replacement of the damaged steel bars, the related environmental impacts are compared to the impacts of the scenarios with the epoxy resin injection. The latter scenarios include more specifically Wall_Resin_50 and Wall_Resin_100 depending on the considered timeframe of 50 years or 100 years respectively. With regard to the frequency of the resin injections, according to section 4.6.3, two reiterations were taken into account for Wall_Resin_50 while 4 were considered for Wall_Resin_100. The frequency of the maintenance activities are estimated as better detailed in subsequent sections and summarized in Table 4.18.

4.6.5.1 Scenario 1

The first scenario is limited to 50 years of service life. As described in 3.1.1, the structural stability is compromised when the tension bars lose 89% of their cross-section but it is reasonably considered that the maintenance works are carried out already when the bars lose 20% of its cross-section. This is in line with what is considered in studies like the one by Zhang et al.(Zhang *et al.*, 2021a) in which it is outlined that when the corrosion loss exceeds 15% it causes a critical concrete damage able to affect shear behavior of reinforced concrete beams. Also in (Noh *et al.*, 2018), assessing the case of a beam of which the reinforcement is subjected to different corrosion scenarios, it is stated that a 20% degree of corrosion causes significant reduction in terms of structural strength capacity. In this scenario, to calculate the frequency of these activities, the corrosion rate described in 4.6.2.5 and Figure 4.25 was used. For the case of the reference solution, in this scenario identified as Wall_Ref_M1_50, the first repairing activities are estimated to be developed after 25 years, including the initiation period which is almost instantaneous for the case of cracked concrete. Then, since the new concrete cover is supposed to be un-cracked, an initiation period of 13 years was added to the remaining time to lose again 20% of the cross section (which adds up to further 25 years). With regard to the SAPs-based structure, for this case indicated as Wall_SAP_M1_50, a calculated period of 13 years and 25 years were used for the initiation and propagation respectively. According to this, for scenario 1, only one repairing activity is taken into consideration for both Wall_Ref_M1_50 and Wall_SAP_M1_50. Figure 4.29, Figure 4.30 and Figure 4.31 show the obtained results where it is possible to see that the impacts reduction between Wall_SAP_M1_50 and Wall_Ref_M1_50 is generally limited and lower than 5% while the one between Wall_Resin 50 and Wall_Ref_M1_50 is more pronounced reaching 9% for the case of Photochemical oxidation. Additionally, except for the case of GWP, ODP and ADP, under scenario 1, the reinforcement content always causes higher impacts in comparison to the cement ones.

4.6.5.2 Scenario 2

The second scenario considers the same corrosion rate as before but extending the service life up to 100 years. The initiation and propagation times are the same as for Scenario 1 with a resulting reiteration for the maintenance activity of 3 and 2 times for the reference structure and the SAPs based one, represented by Wall_Ref_M1_100 and Wall_SAP_M1_100 respectively. As detailed Figure 4.29, Figure 4.30 and Figure 4.31, this scenario better highlights the environmental advantages of Wall_SAP_M1_100 in comparison to Wall_Ref_M1_100, reaching reductions higher than 10% for the case of HTP, FAETP, TETP and POCP while Wall_Resin 100 in comparison to Wall_Ref_M1_100 registers differences always higher than 15% except for EP. Also in this case, the reinforcement amount affects stronger the final results for most of the impact indicators in comparison to the cement content. What was observed with regard to the impacts associated to the cement and reinforcement content under scenario 1 is also confirmed in scenario 2.

4.6.5.3 Scenario 3

In the third scenario, the selected FU is analyzed in a timeframe of 50 years but using the corrosion model described in 4.6.2.6. As above, considering the necessity to carry out maintenance activities when the steel bars lose

20% of their cross-section, a corrosion pit depth equal to 4 mm according to the values reported in Table 4.14 was taken into account. Therefore, considering that the initiation periods will remain the same as for Scenario 1 and 2, assuming a propagation time equal to 3.8 years, in this scenario are taken into consideration 3 and 2 maintenance activities for the reference and the SAPs-based solution respectively, here indicated as Wall_Ref_M2_50 and Wall_SAP_M2_50 respectively. As shown in Figure 4.29, Figure 4.30 and Figure 4.31, since for Wall_Ref_M2_50 and Wall_SAP_M2_50 the number of the maintenance activities are the same as for Wall_Ref_M1_100 and Wall_SAP_M1_100, no relevant differences can be remarked in comparison to Scenario 2. Additionally, it must be noted that the incidence of the epoxy resin for all the ten impact indicators is almost neglectable with no relevant differences between Wall_Resin_50 and Wall_Resin_100. Thus, comparing Wall_Resin_50 to Wall_Ref_M2_50, the considerations are the same as for scenario 2 between Wall_Resin_100 and Wall_Ref_M1_100.

4.6.5.4 Scenario 4

The final scenario adopts the same hemispherical pit model as before within a service life of 100 years. This framework allows to better highlight the enhanced eco-performances of the SAP technology in comparison to conventional solution. Here, according to what was stated above, seven and five maintenance activities are taken into account for Wall_Ref_M2_100 and Wall_SAP_M2_100 respectively. The highest reductions are achieved for the case of FAETP (20%) with values higher than 15% also for MAETP, TETP, POCP and AP. Furthermore, comparing Wall_Resin_100 to Wall_Ref_M2_100, the reductions are always higher than 15% with values around 67% as in the case of HTP. It is worth noting that what primarily influences impacts deriving from both construction and maintenance activities is steel. This naturally brings advantages in terms of a solution more durable and able to ensure a fewer reinforcement replacement (as Wall_Ref_M2_100), especially when performance are assessed within a long timeframe.

Table 4.18: Summary of the maintenance activities.

	Nr. Of epoxy resin injections	**Corrosion model**	**Initiation time**	**Propagation time**	**Nr. Of maintenances**
Wall_Resin 50	**2**	-	-	-	-
Wall_Resin 100	**4**	-	-	-	-
Wall_Ref_M1_50	-	50 μm/year	0 (if cracked) or 13 years (if uncracked)	25 years	**1**
Wall_Ref_M1_100	-	50 μm/year	As above	25 years	**3**
Wall_Ref_M2_50	-	hemisph. pit model	As Above	3.8 years	**3**
Wall_Ref_M2_100	-	hemisph. pit model	As above	3.8 years	**7**
Wall_SAP_M1_50	-	50 μm/year	13 years	25 years	**1**
Wall_SAP_M1_100	-	50 μm/year	As above	25 years	**2**
Wall_SAP_M2_50	-	hemisph. pit model	As Above	3.8 years	**2**
Wall_SAP_M2_100	-	hemisph. pit model	As above	3.8 years	**5**

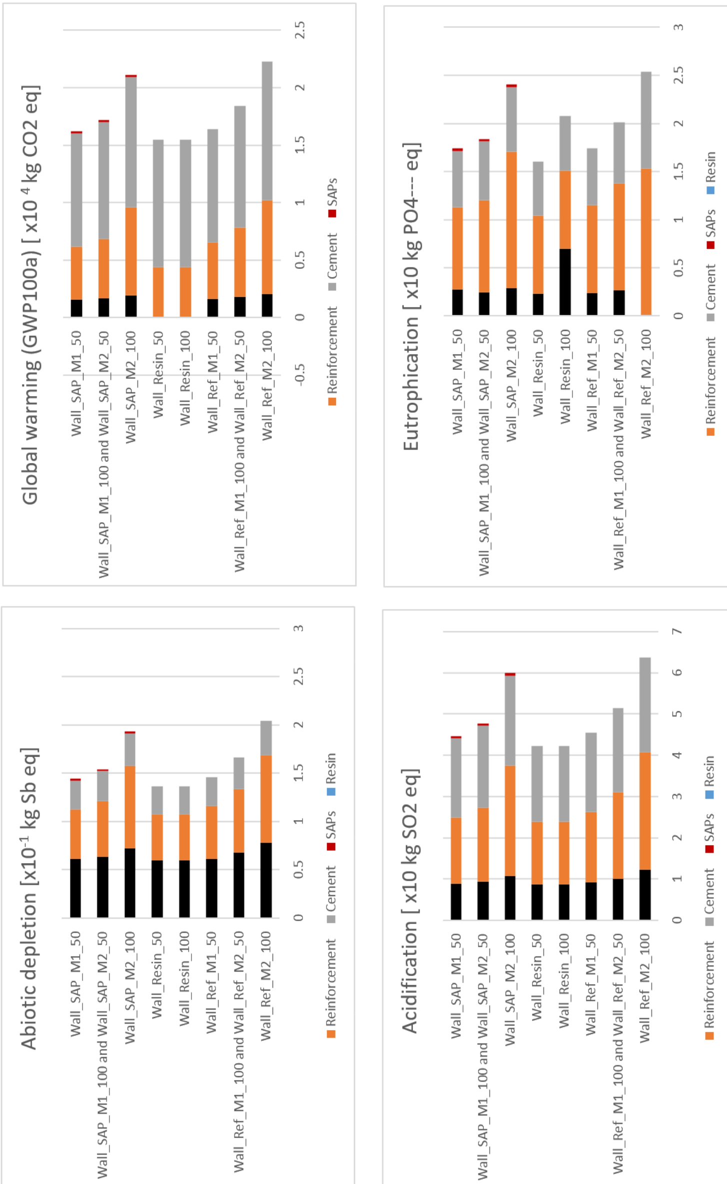

Figure 4.29: Environmental impacts for the different scenarios for 4 out of 10 CML impact categories with indication of SAP, cement and reinforcement contribution. The black color represents the environmental burdens due to the remaining components.

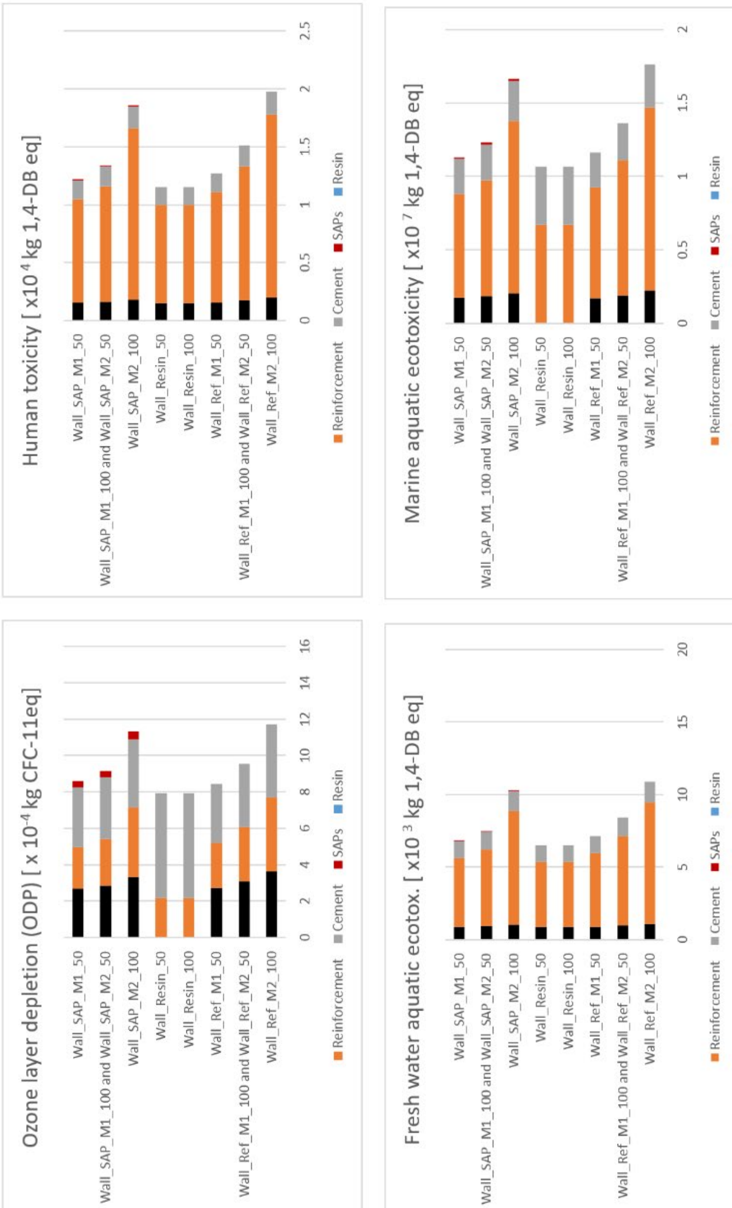

Figure 4.30: Environmental impacts for the different scenarios for 4 out of 10 CML impact categories with indication of SAP, cement and reinforcement contribution. The black color represents the environmental burdens due to the remaining components.

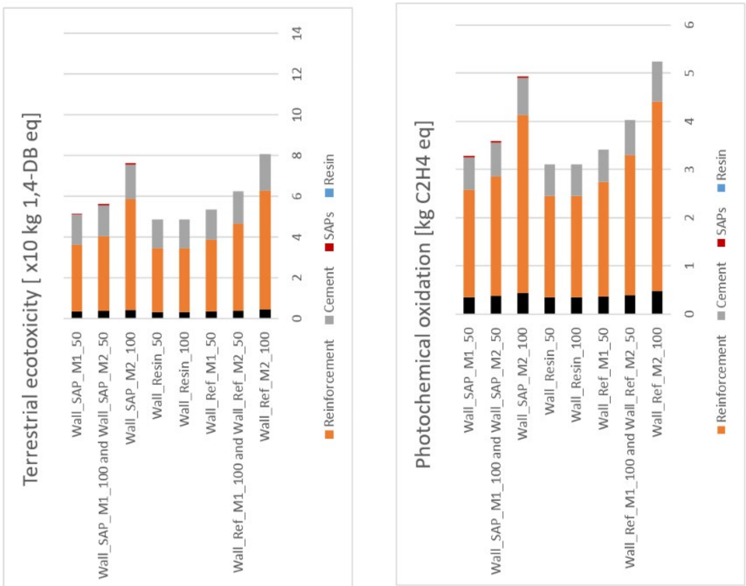

Figure 4.31: Environmental impacts for the different scenarios for 2 out of 10 CML impact categories with indication of SAP, cement and reinforcement contribution. The black color represents the environmental burdens due to the remaining components.

4.6.6 Life Cycle Costing for SAPs-based concrete

The European Community, already in 2008, defined the concept of Green Public Procurement (GPP) as a voluntary instrument used by the authorities to procure goods, services and works with reduced environmental impacts. Its use should lead the industry to develop green technologies and products. In this framework, the importance of the cost assessment is based on a product life-cycle. In relation to the civil sector this means that the construction price just represents one element of the entire estimation, since also the hidden costs related to the maintenance activities can be relevant. Therefore, the Life Cycle Cost (LCC) was here used to better state the potential of the investigated advanced concrete materials determining the potential cost-effectiveness throughout the entire service life. Since much information was lacking, part of this work consisted of a market survey to collect the necessary data. In fact, except for the cost of SAPs, already outlined by Snoeck (Snoeck, 2015), "casting of concrete C 35/45", "casting of concrete C30/37" and "supply and installation of rebars" rates were obtained from company perspectives. For the remaining ones, as no further bill of quantities (BoQ) were found for the Belgium construction market, after verifying that the above-mentioned rates were comparable to the Italian ones, they were obtained from the Italian construction costs list (Emilia-Romagna, Provveditorato interregionale alle Opere Pubbliche di Lombardia ed, 2019a). Additionally, since the maintenance activities will be developed in the future, it has been necessary to adopt the principle suggested by EN 16627:2015 (UNI, 2015) to calculate the value today for an economic transaction in the future by using a discount factor as in Eq. 2.3 presented in 2.4. The annual real discount rate is assumed equal to 3% as reported in chapter 2, according to the Commission Delegated Regulation n°244/2012 of 16 January 2012 (Commission Delegated Regulation, 2012). Therefore, all the rates referred to maintenance activities to be developed in the future have been actualized assuming a variable T value, up to 100 years.

Despite the added cost of the SAP, assessed at around 10 € per kg, due to the reduced amount of reinforcement, the Wall_SAP itself, without including any maintenance activity, costs around 7,860 € that is just 2.5% higher as compared to the Wall_REF itself (around 7,670 €). The economic convenience of Wall_SAP in comparison to Wall_Ref is confirmed also taking into account the repairing activities in the four scenarios as detailed in Table 4.27 to Table 4.30. Significant reductions can be observed in the case of Scenario 3 and 4 where it is possible to pass from 11,272.00 € and 12,084.00 € for Wall_Ref_M2_50 and Wall_Ref_M2_100 respectively up to 9,609.00 € and 10,408.00 € for the case of Wall_SAP_M2_50 and Wall_SAP_M2_100 with a reduction of around 14 % in both scenarios. Furthermore, as indicated in Table 4.21: Wall_Resin 50 construction costs. Rates marked with "*" are calculated according to the discount factor depending on when the maintenance activity will be carried out.Table 4.21 and Table 4.22, the maintenance activities by means of polyurethane resin injection brings the total amount up to 11,838.00 € and 12,725.00 € in a timeframe of 50 and 100 years, higher than costs for Wall_SAP assessed in the same timeframe under different boundary conditions. Therefore, as clearly shown in Figure 4.32 , the epoxy resin injection represents always the most expensive solution with an incidence of the maintenance activities assessed at around 30 % of the total costs for both Wall_Resin 50 and Wall_Resin 100. The same cost incidence can be observed also for Wall_Ref_M2_50 and Wall_Ref_M2_100 while in the same scenarios Wall_SAP_M2_50 and Wall_SAP_M2_100 maintenance activities generate a lower extra expense of 15% and 22% respectively. Figure 4.33 and Figure 4.34 show the costs trend in a timeframe of 50 and 100 years respectively, outlining for the FU always a continuous cost increasing from 20 years of service life onwards, except for Wall_SAP in scenario 1 and 2 whose costs increases starting from 30 years of SL.

Table 4.19: Wall_Ref construction costs. Note: here refurbishment works are not included.

Wall_Ref				
Work	**Rate per unit (€)**	**quantity**	**unit**	**Amount (€)**
Casting of concrete C 35/45	78.70	30.08	m^3	2,367.29
Supply and installation of rebars	0.95	1,933	kg	1,836.35
Formworks up to 4 m of height	35.95	77	m^2	2,768.15
sum				6,971.80
unexpected costs (10%)				697.18
TOTAL				**7,669.00**

Table 4.20: Wall_SAP construction costs. Note: here refurbishment works are not included.

Wall_SAP				
Work	**Rate per unit (€)**	**quantity**	**unit**	**Amount (€)**
Casting of concrete C 30/37	75.00	30.08	m^3	2,256.00
Supply and installation of rebars	0.95	1,800	kg	1,710.00
Formworks up to 4 m of height	35.95	77.00	m^2	2,768.15
Commercial SAP	10.00	40.9	kg	409.00
sum				7,143.15
unexpected costs (10%)				714.32
TOTAL				**7,857.00**

Table 4.21: Wall_Resin 50 construction costs. Rates marked with "*" are calculated according to the discount factor depending on when the maintenance activity will be carried out.

Wall_Resin 50				
Work	**Rate per unit (€)**	**quantity**	**unit**	**Amount (€)**
Casting of concrete C 35/45	78.70	30.08	m^3	2,367.30

Wall_Resin 50				
Work	**Rate per unit (€)**	**quantity**	**unit**	**Amount (€)**
Supply and installation of rebars	0.95	1,933	kg	1,836.35
Formworks up to 4 m of height	35.95	77	m²	2,768.15
Polyurethane resin injection by pressure	240.00	11.03	m	2,647.20
Extra polyurethane resin injection by pressure*	variable*	9.97	m	1,1142.81
sum				10,761.81
unexpected costs (10%)				1,076.18
TOTAL				**11,838.00**

Table 4.22: Wall_Resin 100 construction costs. Rates marked with "*" are calculated according to the discount factor depending on when the maintenance activity will be carried out.

Wall_Resin 100				
Work	**Rate per unit (€)**	**quantity**	**unit**	**Amount (€)**
Casting of concrete C 35/45	78.70	30.08	m³	2,367.30
Supply and installation of rebars	0.95	1,933	kg	1,836.35
Formworks up to 4 m of height	35.95	77	m²	2,768.15
Polyurethane resin injection by pressure	240.00	11.03	m	2,647.20
Extra polyurethane resin injection by pressure	variable*	28.91	m	1,949.31
sum				11,568.31
unexpected costs (10%)				1,156.31
TOTAL				**12,725.00**

Table 4.23: Wall_SAP with concrete cover reconstruction and steel rebars substitution, Scenario 1. Rates marked with "*" are calculated according to the discount factor depending on when the maintenance activity will be carried out.

Wall_SAP_M1_50				
Work	**Rate per unit (€)**	**quantity**	**unit**	**Amount (€)**
Casting of concrete C 30/37	75.00	30.08	m^3	2,256.00
Supply and installation of rebars	0.95	1,800	kg	1,710.00
Formworks	35.95	77.00	m^2	2,768.15
Commercial SAP	10.00	40.9	kg	409.00
Extra commercial SAP	variable*	1.56 in total	kg	5.07
Extra Formworks*	variable*	38.5 in total	m^2	450.14
Demolition of damaged concrete*	variable*	1.15 in total	m^3	28.05
Transport of waste material to landfill*	variable*	1.15 in total	m^3	17.80
Extra concrete casting*	variable*	1.15 in total	m^3	28.05
sum				7,672.26
unexpected costs (10%)				767.23
TOTAL				**8,439.00**

Table 4.24: Wall_SAP with concrete cover reconstruction and steel rebars substitution, Scenario 2. Rates marked with "*" are calculated according to the discount factor depending on when the maintenance activity will be carried out.

Wall_SAP_M1_100				
Work	**Rate per unit (€)**	**quantity**	**unit**	**Amount (€)**
Casting of concrete C 30/37	75.00	30.08	m^3	2,256.00
Supply and installation of rebars	0.95	1,800	kg	1,710.00
Formworks	35.95	77.00	m^2	2,768.15
Commercial SAP	10.00	40.9	kg	409.00

Extra commercial SAP	variable*	3.12 in total	kg	6.72
Extra Formworks*	variable*	77 in total	m²	596.53
Demolition of damaged concrete*	variable*	2.30 in total	m³	37.17
Transport of waste material to landfill*	variable*	2.30 in total	m³	23.59
Extra concrete casting*	variable*	2.30 in total	m³	37.17
sum				7,844.34
unexpected costs (10%)				784.43
TOTAL				**8,629.00**

Table 4.25: Wall_SAP with concrete cover reconstruction and steel rebars substitution, Scenario 3. Rates marked with "*" are calculated according to the discount factor depending on when the maintenance activity will be carried out.

Wall_SAP_M2_50				
Work	**Rate per unit (€)**	**quantity**	**unit**	**Amount (€)**
Casting of concrete C 30/37	75.00	30.08	m³	2,256.00
Supply and installation of rebars	0.95	1,800	kg	1,710.00
Formworks	35.95	77.00	m²	2,768.15
Commercial SAP	10.00	40.9	kg	409.00
Extra commercial SAP	variable*	3.12 in total	kg	6.72
Extra Formworks*	variable*	77 in total	m²	1,355.01
Demolition of damaged concrete*	variable*	2.30 in total	m³	84.43
Transport of waste material to landfill*	variable*	2.30 in total	m³	53.57
Extra concrete casting*	variable*	2.30 in total	m³	84.43
sum				8,735.89
unexpected costs (10%)				873.59
TOTAL				**9,609.00**

Table 4.26: Wall_SAP with concrete cover reconstruction and steel rebars substitution, Scenario 4. Rates marked with "*" are calculated according to the discount factor depending on when the maintenance activity will be carried out.

Wall_SAP_M2_100				
Work	**Rate per unit (€)**	**quantity**	**unit**	**Amount (€)**
Casting of concrete C 30/37	75.00	30.08	m^3	2,256.00
Supply and installation of rebars	0.95	1,800	kg	1,710.00
Formworks	35.95	77.00	m^2	2,768.15
Commercial SAP	10.00	40.9	kg	409.00
Extra commercial SAP	variable*	10.92 in total	kg	22.21
Extra Formworks*	variable*	269.50 in total	m^2	1,972.47
Demolition of damaged concrete*	variable*	8.05 in total	m^3	122.92
Transport of waste material to landfill*	variable*	8.05 in total	m^3	77.99
Extra concrete casting*	variable*	8.05 in total	m^3	122.92
sum				9,461,66
unexpected costs (10%)				946.17
TOTAL				**10,408.00**

Table 4.27: Wall_ref with concrete cover reconstruction and steel rebars substitution, Scenario 1. Rates marked with "*" are calculated according to the discount factor depending on when the maintenance activity will be carried out.

Wall_Ref_M1_50				
Work	**Rate per unit (€)**	**quantity**	**unit**	**Amount (€)**
Casting of concrete C 35/45	78.70	30.08	m^3	2,367.29
Supply and installation of rebars	0.95	1,933	kg	1,836.35
Extra rebars supply and installation*	variable*	244.2 in total	kg	110.80
Formworks	35.95	77	m^2	2,768.15

Extra Formworks*	variable*	38.5 in total	m^2	661,04
Demolition of damaged concrete*	variable*	1.15 in total	m^3	43,41
Transport of waste material to landfill*	variable*	1.15 in total	m^3	26.25
Extra concrete casting*	variable*	1.15 in total	m^3	43.41
			sum	7,856.72
unexpected costs (10%)				785,67
TOTAL				**8,642.00**

Table 4.28: Wall_Ref with concrete cover reconstruction and steel rebars substitution, Scenario 2. Rates marked with "*" are calculated according to the discount factor depending on when the maintenance activity will be carried out.

Wall_Ref_M1_100				
Work	**Rate per unit (€)**	**quantity**	**unit**	**Amount (€)**
Casting of concrete C 35/45	78.70	30.08	m^3	2,367.29
Supply and installation of rebars	0.95	1,933	kg	1,836.35
Extra rebars supply and installation*	variable*	732.6 in total	kg	158.55
Formworks	35.95	77	m^2	2,768.15
Extra Formworks*	variable*	115.5 in total	m^2	945.95
Transport of waste material to landfill*	variable*	3.45 in total	m^3	37.40
Demolition of damaged concrete*	variable*	3.45 in total	m^3	61.68
Extra concrete casting*	variable*	3.45 in total	m^3	61.68
sum				8,237.42
unexpected costs (10%)				823.74
TOTAL				**9,061.00**

Table 4.29: Wall_Ref with concrete cover reconstruction and steel rebars substitution, Scenario 3. Rates marked with "*" are calculated according to the discount factor depending on when the maintenance activity will be carried out.

Wall_Ref_M2_50				
Work	**Rate per unit (€)**	**quantity**	**unit**	**Amount (€)**
Casting of concrete C 35/45	78.70	30.08	m^3	2,367.29
Supply and installation of rebars	0.95	1,933	kg	1,836.35
Extra rebars supply and installation*	variable*	732.6 in total		410.33
Formworks	35.95	77	m^2	2,768.15
Extra Formworks*	variable*	115.5 in total	m^2	2,448.07
Demolition of damaged concrete*	variable*	3.45 in total	m^3	160.08
Transport of waste material to landfill*	variable*	3.45 in total	m^3	96.80
Extra concrete casting*	variable*	3.45 in total	m^3	160.08
sum				10,247.16
unexpected costs (10%)				1,024.72
TOTAL				**11,272.00**

Table 4.30: Wall_Ref with concrete cover reconstruction and steel rebars substitution, Scenario 4. Rates marked with "*" are calculated according to the discount factor depending on when the maintenance activity will be carried out.

Wall_Ref_M2_100				
Work	**Rate per unit (€)**	**quantity**	**unit**	**Amount (€)**
Casting of concrete C 35/45	78.70	30.08	m^3	2,367.29
Supply and installation of rebars	0.95	1,933	kg	1,836.35
Extra rebars supply and installation*	variable*	1,465.2 in total	kg	502.83
Formworks	35.95	77	m^2	2,768.15

Wall_Ref_M2_100				
Work	**Rate per unit (€)**	**quantity**	**unit**	**Amount (€)**
Extra Formworks*	variable*	192.5 in total	m²	2,999.93
Demolition of damaged concrete*	variable*	5.75 in total	m³	196.17
Transport of waste material to landfill*	variable*	5.75 in total	m³	118.62
Extra concrete casting*	variable*	5.75 in total	m³	196.17
sum				10,985.51
unexpected costs (10%)				1,098.55
TOTAL				**12,084.00**

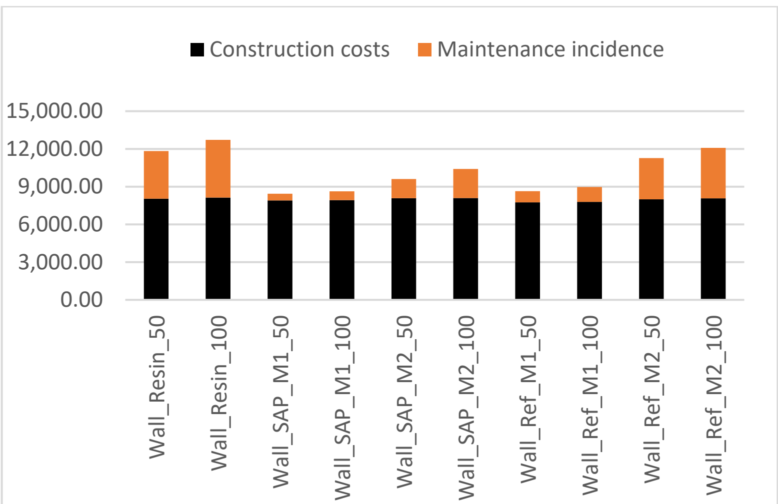

Figure 4.32: Overall costs summary including maintenance incidence (€).

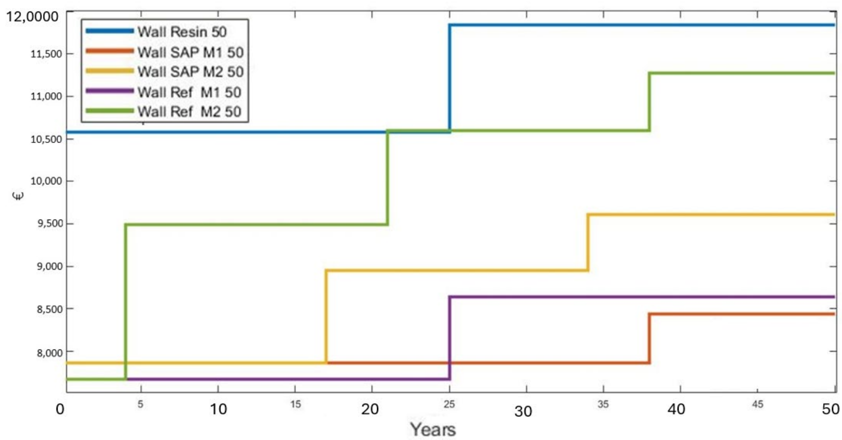

Figure 4.33: Costs trend within 50 years of service life.

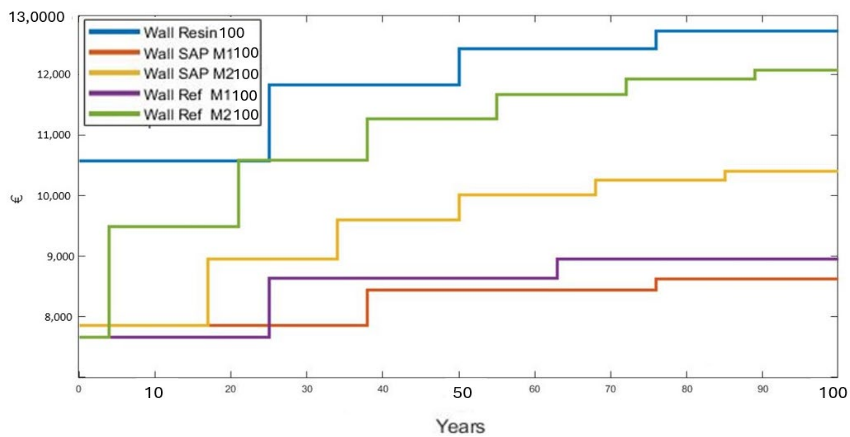

Figure 4.34: Costs trend within 100 years of service life.

4.7 Ultra-High Performance Concrete (UHPC)

Durability represents a design target requisite which in current design codes (Folić and Zenunović, 2010), is achieved through "deemed to satisfy" prescriptions, including maximum water to cement ratio, minimum cement content and minimum concrete cover to guarantee the target service life. Nonetheless, because of the random and sometimes one-of-a-kind characteristics of structural service scenarios, this approach has resulted so far into a continuous need of repairing activities which for ORC. Thus, the reiteration of the same design approach will lead to an exacerbation of the sustainability issues of concrete structures both in terms of environmental impact and cost implications throughout their entire service life. Because of this, UHPC has started attracting more interest due to its improved durability performance both in the uncracked and cracked state (Li et al., 2020a;Azmee and Shafiq, 2018a). This is due respectively to its low porosity and to the presence of micro-fibres (steel or polymeric) which provide the tensile strain hardening behaviour favoring the formation of small and tightly spaced cracks, tighter than what obtainable in ordinary reinforced concrete structures (Hung et al., 2019;Luo et al., 2019). However, its use has been so far somewhat limited by the lack of appropriate design codes (Azmee and Shafiq, 2018b) and the cost, although Al Obaidi et al. warned about how the cost assessment of UHPC, usually made on the basis on the material cost per unit volume, generates a misperception (Al-Obaidi *et al.*, 2022a). This is due to the fact that an estimation as such does not take into consideration the UHPC mechanical and durability properties which allow to conceive, design and build structures using less raw materials while guaranteeing the same structural performance and a longer SL in comparison to a reference ordinary reinforced concrete solution (Al-Obaidi *et al.*, 2022a). All the above converges towards the need to employ a design approach able to evaluate the evolution of the structural performance all along the structure service life encompassing the effects of material and structural degradation mechanisms. It is furthermore worth highlighting that for most of the advanced cementitious composites, because of the high cement content and low water to binder ratio, which endows with high compressive strength (generally higher than 100 MPa) and, as said, tensile strain hardening behaviour, deemed to satisfy code specifications for durability are automatically fulfilled.

In the aforesaid framework, this research investigates the use of a semi-probabilistic approach based on the evaluation over time of structural performance indicators (such as the resistant bending moment), shifting from a "deemed to satisfy" to a Durability Assessment-oriented Design (DAD) paradigm. Such design methodology, as described in 3.1, quantifies and schedules the maintenance activities upon the attainment of a limit state defined according to the structural service scenario . This conceptual framework is here applied to a real-size case study which is a water tank intended to be part of a cooling tower in a geothermal power plant. The structure is expected to contain geothermal water rich in chlorides and sulphate ions as in (Al-Obaidi et al., 2022a), as a condensate from the vapour extraction during the geothermal drilling functioning, and needs to be stored and cooled prior to be re-injected into the soil. LCA and LCC methodologies have been used to assess the potential environmental and economical convenience of UHPC in comparison to a conventional reinforced concrete solution. UHPC has been taken into consideration because its superior performance in aggressive environments, as well as its mechanical properties that offer opportunities for optimizing the design of structural element cross-sections. From this point of view, the scope of this research is to carry out a more comprehensive LCA and LCC assessment that, including the analysis of the structural performance throughout the service life, contributes to the validation of a new design approach able to exploit the superior performance of UHPC since the conceptual design phase and not merely in the design check stage. This is in line with the way paved in other studies that highlighted the possibility, for UHPC, to reduce the environmental burdens up to 50% when assessed on a structure scale (Shao *et al.*, 2023). This part of the study aims, then, at demonstrating how sustainability assessments can guide the structural design phase, ensuring higher durability performance and, consequently, better LCA and LCC outputs. The goal is to validate a holistic design approach that, representing an improvement of the design practice in extremely aggressive scenarios for innovative cementitious composites, is capable of favouring their spread to an as broad as possible market.

4.7.1 Description of the case study

The structure chosen as a benchmark case study in this research is a tank intended to serve as geothermal water collector, part of a cooling tower of a geothermal energy plant. Cooling towers work by condensing and transforming into "raining water" the vapour which is extracted from the subsoil, led to the same tower and then collected in basins. The case here assessed, replicates the layout of a geothermal power plant in Chiusdino

(Tuscany, Italy), owned and operated by Enel Green Power (already presented within the ReSHEALience project, funded by the European Union's Horizon 2020 research and innovation program under grant agreement No 760824). It has been re-designed using both Ordinary Reinforced Concrete (ORC) and UHPC. The geometry and cross sectional dimensions of the existing structure have been used for the ORC structure design, only taking care of the optimization of the reinforcement bars layout. With regard to the UHPC basin, it has been designed keeping the same geometry and optimizing the cross section in terms of the thickness of the walls and the layout of the reinforcement. Figure 4.35 shows the plan and a 3D sketch of the existing basin. Each wall is identified by a number since a structural analysis has been developed for each of them according to the specific loading conditions. The structure consists of perimeter walls and septa that divide it into individual tank cells. Wall 1 has a total height of 4.87 m, while Wall 3 and Wall 2 measure 3.00 m and Walls 4 vary in height from 3.00 mm to 4.87 m. The service scenario for this type of structures, which are built partially underground, includes the soil thrust, traffic overload and the pressure of the water, which is characterized, among the others, by an average content of chlorides equal to 10 g/L in line with (Al-Obaidi *et al.*, 2022a).

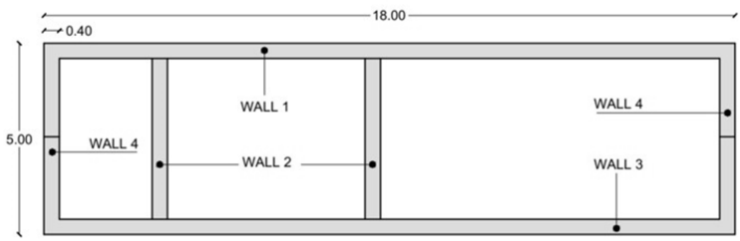

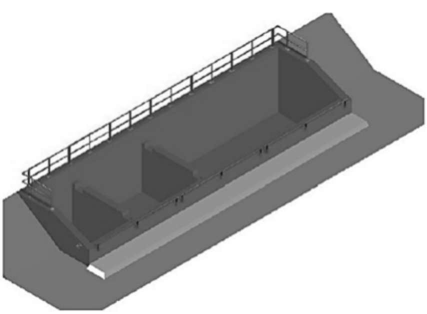

Figure 4.35: Layout (top) and 3D model (bottom) of the existing basin structure according to (Parpanesi, 2021).

4.7.1.1 Loading conditions and structural analysis

Since the structure is built partially underground and has to contain water, its walls have to be designed to withstand, as above mentioned, the soil thrust from outside and the water hydraulic pressure from inside. Two different kind of soils, the characteristics of which are reported in Table 4.31, have been hypothesized in the design according to (Parpanesi, 2021): a filling soil, that is only in contact with Wall 1 of Figure 4.35 and a compacted foundation soil which is in contact with Walls 4 and Wall 3. This is due to the morphology of the site where the basin is supposed to be located, in a zone with different altitudes that requires to import reclaimed soil alongside Wall 1. The water table is always considered at 2 m depth for the sake of simplicity and in line with the geotechnical reports in (Parpanesi, 2021).

Table 4.31: Characteristics of the soil.

		Filling soil	Foundation soil
Specific weight	γ_{sat} [kN/m³]	13	17
Internal friction angle	ϕ'_k [°]	20	33

The four walls have been designed to withstand the following combination of actions:

i) Wall 1 and Walls 4: the soil thrust, the water hydraulic pressure and the self-weight;

ii) Walls 2: the water hydraulic pressure and the self-weight;

iii) Wall 3 is subjected to the same actions as Wall 1, plus the machinery traffic overload for which an excavator, with the weight equal to 94 tons, according to the producer's technical sheet ("Caterpillar products," 2019), has been taken into consideration and has been assumed as the only variable action, all the other ones being permanent.

The structural analysis has been developed according to the following hypotheses:

i) each wall is modelled as a cantilever beam considering a unit (1m) width;

ii) soil pressure is estimated by means of the Rankine theory as per Eurocode 7 and through the parameters in Table 4.31;

iii) each wall is subjected to the worst loading conditions for both Ultimate Limit State (ULS) and Serviceability Limit State (SLS) in favour of safety, which correspond, for Walls 1, Wall 3 and Wall 4, to the empty basin (soil thrust and machinery variable overload) and for Wall 2 to the presence of water only in one of the tank compartments. Table 4.32 reports the design values of the bending moment (M_{Ed}) and axial force (N_{Ed}) which have been calculated as acting on each wall critical cross section according to the worst combination of actions. Figure 4.36 and Figure 4.37 report the design models used for Wall 1, Walls 2, Wall 3 and Wall 4 that differ from each other by the presence of the action of the soil and of the water.

Table 4.32: Design actions for each wall (worst combination).

	M_{Ed} [kNm]	N_{Ed} [kN]
Wall 1	84.26	49.90
Wall 2	58.50	30.51
Wall 3	68.83	30.51
Walls 4	63.60	49.90

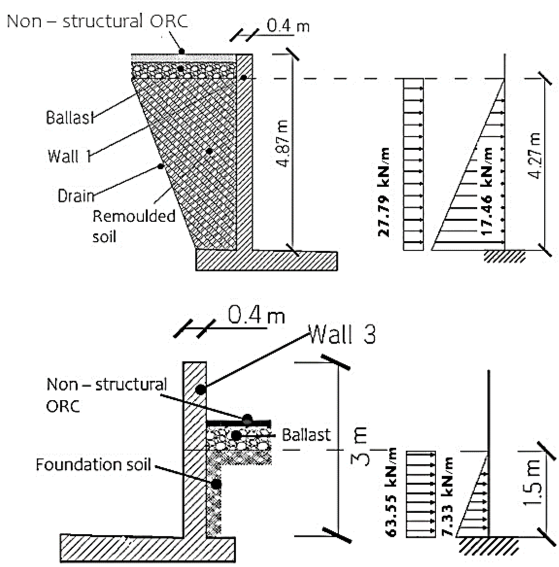

Figure 4.36: Representation of the structure and of the related structural design models for Wall 1 and Wall 3 (top part, left and right side respectively) and Wall 3 and Wall 4 (bottom part, left and right side respectively). While a triangular distribution has been assumed for the soil and for the water, a rectangular one has been employed for the other actions.

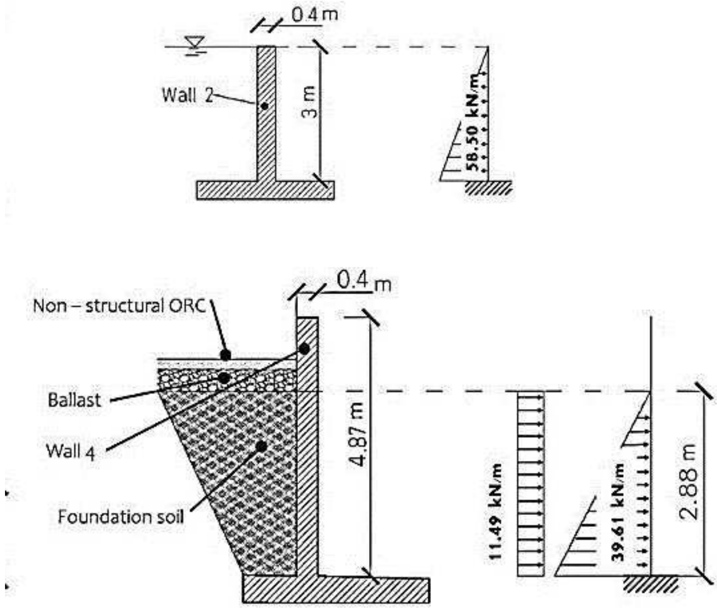

Figure 4.37: Representation of the structure and of the related structural design models for Wall 2 and Wall 4 While a triangular distribution has been assumed for the soil and for the water, a rectangular one has been employed for the other actions. An average loaded portion between Wall 1 and Wall 3 has been considered for Wall 4, due to the fact that its height passes from 4.87 m to 3 m.

4.7.1.2 Ordinary reinforced concrete basin design

The corresponding exposure classes have first been identified to define the prescriptions provided by the current standards (CEN, 2002): XS2 (corrosion induced by chlorides from seawater for a permanently submerged element) and XA3 (highly aggressive chemical environment). The XA3 exposure class is due to the presence of $S_2O_3^{2-}$, SO_3^{2-}, SO_4^{2-} and H_2S expected to have a concentration equal to 46 mg/L, 325 mg/L, 5.1 mg/L and 1.5 mg/L respectively as in (Al-Obaidi *et al.*, 2022a). The XA3 exposure class requires a minimum C35/45 strength class, with a maximum water to binder ratio equal to 0.45 and a minimum cement content equal to 350 kg/m^3. To fulfill these prescriptions, the mix design reported in Table 4.33 has been employed for the ordinary reinforced concrete structure herein assessed. Furthermore, the structural design considered the following values of the main mechanical material properties, computed according to (Cen, 2002): a characteristic compressive strength of 35 MPa, a mean concrete tensile strength of 3.20 MPa, and a Young modulus of 34 GPa.

Table 4.33**:** ORC mix design (in kg/m³).

	ORC
Cement I 42.5 R	370
Water	150
Aggregate 7/10	354
Aggregate 12/20	377
Natural Sand (0-2 mm)	1108
Superplasticizer	3

Moreover, the Eurocode provides not only minimum material composition requirements but also structural prescriptions such as minimum concrete cover, to ensure the protection of the steel against the corrosion, and a minimum reinforcement area, for exquisite structural performance purposes. While 40 mm had to be guaranteed as a minimum concrete cover due to the exposure classes above mentioned, the minimum vertical reinforcement (the main flexural reinforcement) area had to range between 0.002 Ac and 0.04 Ac, Ac being the cross sectional area of concrete. Similarly, the cross sectional area of the horizontal reinforcement (the transverse reinforcement) had to be higher than 25% of the vertical reinforcement area and 0.001 Ac, whichever larger. This lead then to design a 400 mm thick cross section for the ordinary reinforced concrete basin as the one reported in Figure 4.38. The design philosophy which governed the dimensioning has been structured to ensure a simple construction phase according to the following principles: i) reinforcement bars duplicated at both tension and compression side (longitudinal Φ 10 spaced at 125 mm and transversal Φ 10 spaced at 250 mm). For the sake of simplicity, the reinforcement at the compression zone has been then designed equal to the tensile one; ii) small diameters of the reinforcement bars to facilitate their handling.

With regard to the SLS, the stress limitation, crack control and deflection control have been taken into consideration. The design governing limit state is the crack width control (a maximum crack opening equal to w_k=0.2 mm has been enforced); deformation control, with a top edge deflection equal to 1/200 of the wall height, has been also enforced for the sake of integrity of the supported superstructure. Moreover, the mix design of Table 4.33 being characterized by an average tensile strength equal to 3.2 MPa, and the maximum tensile stress resulting from linear elastic calculations being equal to 5.2 MPa, cracked cross section assumptions have been made in the design calculations. The axial load to the wall self-weight was not able to keep the cross section within the decompression limit state or at least within the crack formation SLS. This obviously was reflected in the related assumptions on the values of durability parameters, including e.g., chloride diffusion coefficient and the cracked state representing preferential paths for the ingress of harmful substances from outside. The ordinary reinforced concrete structure is herein after referred as Basin_ORC.

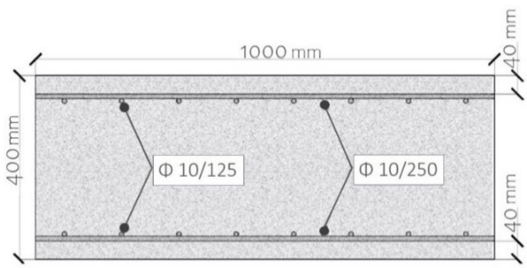

Figure 4.38: Cross section of the wall of Basin_ORC.

4.7.1.3 UHPC basin – mix designs properties and proposed structural solutions

With reference to the UHPC basin, two different mix designs, UHPC1 and UHPC2 (to check whether a different material composition leads to different environmental consequences), as reported in Table 4.34, have been chosen and two possible structural solutions have been proposed. The first one consists of cast in situ cantilever walls while, in the second case, the walls are made of, and designed as, precast UHPC slabs supported by ordinary reinforced concrete buttresses. Both UHPC structural solutions have been designed following fib Model Code 2010 provisions on ULS and SLS as initial stage, also considering that UHPC automatically fulfills the EN 206-1 “deemed to satisfy” composition prescriptions with reference to durability (Cen, 2016b;Cen, 2002). As a matter of fact, water to cement ratio (equal to 0.33 for both mixes), strength class (compressive strength higher than 100

MPa, ranging from 126.9 MPa to 147.6 MPa depending on the specific mix design, as in (Al-Obaidi et al., 2022a;Cuenca et al., 2022a)) and minimum cement content (600 kg/m³ or 700 kg/m³ for the cases here assessed) are already in line with the prescriptions for XS2 and XA3 exposure classes identified for the current case study (Fládr and Bílý, 2018). Besides these aspects, UHPC, in comparison to conventional concrete, allows to reduce the minimum concrete cover (down to 25 mm as assumed for the case study at issue) due to its high tensile capacity, ductility and enhanced durability (Al-Obaidi *et al.*, 2022b).

Table 4.34: UHPC1 and UHPC2 mix designs (in kg/m³).

	UHPC1	UHPC2
Cement 52.5 R	700	600
Silica Fume	400	-
Slag	-	500
Water	231	200
Natural Sand (0-2 mm)	817	982
Superplasticizer (ACE 442)	64	33
Steel fibers (l_f=22 mm, d_f=0.2 mm)	160	120
Crystalline admixture	5.6	4.8

4.7.1.4 UHPC basin – structural design

The first designed structural scheme includes reinforcing steel bars only on the tension side to reach consistent advantages in terms of walls thickness in comparison to Basin_ORC. This also in view of the fact that, differently than for ordinary reinforced concrete, it is here possible to avoid reinforcement in the compression zone since the properties of the material can already cope with the ductility requirement. This resulted into longitudinal Φ 14 mm steel bars spaced at 165 mm for Wall 1 and Wall 3 and at 200 mm for Wall 2 and Walls 4. Moreover, transversal Φ 8 mm bars every 1000 mm have been placed to purely favour the stability of the longitudinal reinforcement. The thickness of the walls varied case by case, being equal to 160 mm for Wall 1, 120 mm for Walls 2 and 130 mm for Wall 3 and Walls 4. Figure 4.39 reports a schematic representation of the cross section adopted for the cast in situ walls solution while Table 4.35 reports the safety factors for each wall according to this design.

For the solution with precast slabs, the latter were designed to have a width of 2 m with the supporting columns characterized by a 200 mm wide cross section, the depth of which reduces from 400 mm at the base to 200 mm at the top. Moreover, if on the one hand the supporting buttresses can be designed employing a cantilever beam structural model, on the other hand, the slabs have been designed with three fixed edges and one free edge and employing the yield line methodology. (Al Obaidi *et al.*, 2021). A similar model is also described by Timoshenko and Woinowsky (Timoshenko and Woinowsky-Krieger, 1959) but, due to the different loading conditions and to the possibility to have torsional moments in correspondence of the corners, the Wood-Armer (WA) method has been used. Although WA methodology has been conceived for ordinary reinforced concrete, the presence of the steel fibers in UHPC, allowed to assume a ductile behaviour. This is mainly due to the tensile constitutive law of the material and to its documented tensile strain hardening behaviour (characterized by a continued plastic deformation even after reaching peak tensile strength, with improved ductility and energy absorption before failure (Lo Monte and Ferrara, 2020)). Therefore, at the first stage, a thickness equal to 70 mm for Wall 1, 80 mm for Wall 3 and 50 mm for both Walls 2 and Walls 4 has been assumed. The highest WA bending moment in absolute terms, reported in Table 4.36, has then been considered, due to the uniformity of the slab. With regard to the buttresses, which are not only subjected to the external loads (e.g. soil, water) but also to the reaction forced transmitted to them by the supported slabs, a cantilever beam has been employed as a structural scheme. Table 4.37 reports the calculated bending moment acting on the buttresses where $M_{Ed,ext}$ is the calculated acting bending moment on the panels and $M_{Ed,reaction}$ refers to the reaction forces transferred from the latter in correspondence of the column (counted twice since two walls insist on one buttress). Figure 4.40 illustrates the cross section of the structure made with slabs and buttresses.

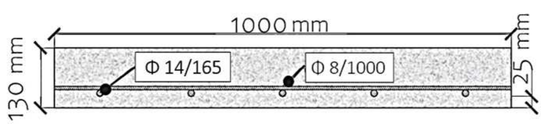

Figure 4.39: Uniform wall design for Wall 4 utilizing either UHPC1 or UHPC2.

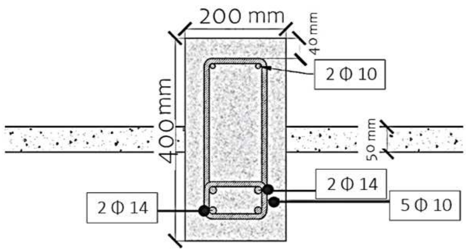

Figure 4.40: Slabs supported by buttresses. Design for Wall 4 utilizing either UHPC1 or UHPC2

Table 4.35: Safety factors (M_{Rd}/M_{Ed}) for the initial proposed design.

	M_{Rd}/M_{Ed}
Wall 1	1.04
Walls 2	1.03
Wall 3	1.09
Walls 4	1.05

Table 4.36: Wood-Armer bending moments in the panels.

	$M_{WA,\ ab,\ max}$ [kNm]
Wall 1	6.35
Walls 2	5.95
Wall 3	13.66
Walls 4	4.76

Table 4.37: Design bending moments acting on the buttresses and applied to the cantilever beam structural model.

	$M_{Ed,ext}$ [kNm]	$M_{Ed,reaction}$ [kNm]	$M_{Ed,tot}$ [kNm]
Wall 1	100.53	5.24	111.00
Walls 2	58.50	2.33	63.15
Wall 3	68.83	5.65	80.13
Walls 4	66.08	4.09	74.26

Both UHPC solutions have been verified at ULS and SLS. With regard to the ultimate limit state, the calculation of the resisting bending moment requires to explicit a constitutive law for both compression and tension. A stress block model (as for ordinary reinforced concrete) has been used in compression (considering a concrete class C100/120) while for tensile behaviour, reference was made to the research of Lo Monte and Ferrara (Lo Monte and Ferrara, 2020) and following the guidelines of the fib Model Code 2010 (fib, 2013), a simplified elastic perfectly plastic constitutive law was adopted, as identified from back analysis of the results of 4-point bending tests. Table 4.38 summarizes the main UHPC design parameters then employed for the scope of this research. For the case of Basin_2_UHPC1 and Basin_2_UHPC2, the ULS calculations carried out for the UHPC panels also considered a transient design situation which included the lifting and handling of the precast slabs. With regard to the SLS, the compression stress limitation below 0.6 f_{ck} or 0.45 f_{ck} depending on the combination of actions), crack width limits ($w_{k,lim}$= 0.2 mm according to (Cen, 2005c)) and deflection (l/200 as in (CEN, 2005c), where l is the loaded height of the wall) have been checked in line with what has been reported in (F. du béton and J.C. Walraven, 2012).

Table 4.38*:* Main UHPC design parameters.

f_{ck} characteristic compressive strength	100 [MPa]
f_{ct} tensile strength)	7.5 [MPa]
E (Young modulus)	41.7 [GPa]
εpeak (ultimate tensile strain)	0.005

4.7.2 Corrosion effects on overall durability

The corrosion and its effects on the overall durability of the assessed structures have been a key point of the study due to the environment rich in chlorides the tank walls are exposed to that can penetrate the concrete structure leading to the initiation and propagation of the corrosion. This is in line with the expectations since other researchers (Al-Obaidi *et al.*, 2020b) already outlined how a Cl^- concentration might reach values as high as 213 mg/l, considered critical for geothermal power plants similar to the one here assessed. Moreover, it is worth observing that, for the case here analyzed, the depassivation and the consequent corrosion start from the part of the walls in contact with the water, since the soil is assumed to have a negligible chloride content. On the other hand, the carbonate ions coming from the permeated rainwater can potentially reach the surface of the wall, but, in line with (Papadakis *et al.*, 1991), they are considered as unable of triggering a carbonation process since the structure is in contact with the soil and, then, the concrete can be hypothesized in saturated conditions. The ingress of chloride ions through the concrete matrix is governed by the process of diffusion that follows the second Fick' law. In this regard, a critical chloride concentration C_{crit}, of 0.44% by weight of cement (namely the concentration to be reached for the beginning of the propagation period) has been assumed, according to Alonso et al. (Alonso and Sanchez, 2009b). The latter was based on field exposure tests which defined a depassivation chloride threshold that can vary from 0.3 % up to 3.5%. Another key role in the 2nd Fick's law is played by D_{app}, the apparent chloride diffusion coefficient, whose values, as already detailed in other works (di Summa *et al.*, 2022b)(di Summa *et al.*, 2022a), might significantly affect the initiation time. A value of 10^{-11} m^2/s is generally used for the case of uncracked concrete containing CEM I (Al-Obaidi et al., 2020b;Shafikhani and Chidiac, 2019b;Torres-Acosta et al., 2019b;Liu et al., 2015b) although, considering the microcracking initial state already described in 2.2 and caused by shrinkage, it has been set one order of magnitude higher and equal to 10^{-10} m^2/s for Basin_ORC. A value of 5×10^{-13} m^2/s has been taken into consideration for the structures made with UHPC_1 and UHPC_2 because of the compact matrix with much lower porosity but also in compliance with international standards, including, e.g., the French National Annex of EC2 (Cen, 2005c) and the Swiss standard BFUP (Béton Fibrés Ultra Hautes Performance; "BFUHP Bétons Fibrés à Ultra Hautes Performances," 2022;Cuenca et al., 2022a;Cuenca et al., 2022b). Right after the initiation period, (whose value can vary case by case as detailed in 4.7.2.1 and 4.7.2.2) namely when at the level of the reinforcement the C_{crit} above mentioned is reached, the corrosion propagation stage starts and the steel bars start being corroded. As already done in similar studies, two different corrosion mechanisms have been assessed for the reinforcing bars within this research to have a more complete vision of what could happen in reality: a uniform one and a localized one. The uniform corrosion is considered to uniformly affect the surface of the steel bars with a speed which is mainly dependent on chloride content of the solution and relative humidity (RH). It has been assumed equal to 100 μm per year according to what has been reported by Bertolini in (Bertolini and Carsana, 2014) and for the case of concrete contaminated by chlorides with a RH higher than 90%. On the other hand, a hemispherical pit model was employed to describe a more aggressive phenomenon where mass and volume loss of steel are concentrated in a localized zone. This model assumes that the corrosion starts at a certain location of the reinforcement steel bar generating a pit damage with an hemispherical shape (Van Belleghem, 2018c;Val and Melchers, 1997). Thus, by employing equations 4.6 and 4.7 presented in 4.6.2.6, it has been possible to Click or tap here to enter text.compute a volume loss equal to 30.54 mm^3/year. Moreover, despite other studies (Harnisch and Raupach, 2015) outlined how the damage to steel bars could be shaped in needle-like pits in early stage of chloride induced corrosion, it was anyway described that the damage occurs in a localized area with a length no longer than twice the diameter of the bars. In view of this, the use of a model aimed at describing a perfect hemispherical pit, like the one above mentioned, is considered as the one closest to the reality. On the other hand, while the corrosion process of steel bars has been extensively studied and analysed, the corrosion of the steel fibres embedded into the concrete matrix is still debated, making the prediction of the degradation phenomena more difficult for UHPC. It is worth noting that Balouch et al. (Balouch *et al.*, 2010) concluded that, under alternated cycles of salt fog and drying, with a w/c ratio of 0.78, the fibres protected from the external environment by a maximum concrete cover thickness of 1 mm present corrosion spots on the surface. On the opposite, when the w/c drops to 0.5, a thickness of 0.02 mm is already sufficient to prevent such phenomenon. At the same time, the increased roughness, which is a corrosion effect, can improve the frictional interaction between the matrix and the fibres enhancing the tensile strength and toughness of the material. Other findings, as in (Alobaidi *et al.*, 2023) point out that the potential formation of healing particles in correspondence of the severely damaged fibre-concrete matrix interface, greatly improve the friction phase of the bond-slip behaviour, leading to a higher residual capacity in comparison to non-pre-slipped samples. Further works (Granju and Balouch, 2005), assessing the corrosion attack through the crack of the fibres caused by a NaCl marine environment (with a concentration of 35 g/l), observed that the fibres (0.8 mm of diameter) within a rim 2 to 3 mm wide from the external surface of the samples were severely corroded. Inside of this perimeter, the fibres presented a light corrosion without any reduction of their cross section. In line with this result, other experiments (Naidu Gopu and Joseph, 2022;Rivera-Corral et al., 2017;Jia et al., 2020;Fu et al., 2020;Murad et al., 2021) pointed out the rapid corrosion for the fibres located within 10 mm from the exposed surface regardless of the exposure period and testing an environment characterized by a chloride concentration up to 35 g/L of NaCl with an exposure time ranging from 67 days up to 5 years. In view of this, the worst case scenario has been taken into consideration for the LCA and LCC purpose, assuming that fibres are immediately corroded as soon as the critical chloride concentration of above is reached (0.44% by weight of cement).

4.7.2.1 Steel reinforcement corrosion in ordinary reinforced concrete basins

As from the models summarized above, the time to corrode a given percentage of steel reinforcement bars has been then calculated, with the aim of estimating the frequency of appropriate maintenance works to restore the functionality of the ORC structures. Both the initiation time and propagation rate (for uniform or hemispherical corrosion alternatively) have been computed according to what has been described in 4.7.2. As a matter of fact, due to the thickness of the walls of Basin_ORC, service conditions concerning deflections and stresses are negligible while crack opening is more impactful. Bossio et al. (Bossio *et al.*, 2017) addressed this problem linking the crack opening to corrosion propagation along and across a steel bar. Thus, it is assumed that once a loss of reinforcement area in the range 16-25% (on a single line of bars) is reached, the consequent expansion due to corrosion products is likely to result into a crack opening 0.5-1 mm wide. The latter is considered as able to disrupt the serviceability of the structure with the consequent need for major maintenance activities. Hence, for the scope of the analysis, in line with the estimations by (Zhang *et al.*, 2021b), which stated that a loss higher than 15% causes a critical concrete damage able to affect the structural capacity of reinforced concrete, a value of 20% of loss of the reinforcement bar has been deemed as critical. Therefore, the time needed to reach this value has been estimated for each wall of Basin_ORC, together with the variation over time of the resistant bending moment M_{Rd} at the critical cross section of the cantilever , in order to further check the structural capacity variation. Assuming a value equal to 40 mm as x_{crit} in the 2nd Fick' law detailed in 2.5, namely the concrete cover of Basin_ORC walls, and keeping the values above listed for C_{crit}, and D_{app}, an initiation time of 0.3 years has been calculated to depassivate the reinforcement steel bars surface. Consequently, 6 and 3 years are the estimated times to lose 20% of the cross section of the bars employing the uniform corrosion assumption (100 μm/year) and the hemispherical pit model respectively (30.5 mm^3/year) including the initiation period. In these calculations a key role is played by the D_{app} value. As stated before, due to the microcracking state of ordinary reinforced concrete basins, 10^{-10} m^2/s has been accounted, while a value simply one order of magnitude lower (namely 10^{-11} m^2/s, as typical for uncracked ORC) would have led to a completely different initiation time, namely 2 years instead of 0.3 years. Basin_ORC subjected to the uniform corrosion is hereinafter referred as Basin_ORC_U while the one affected by the hemispherical pit corrosion is indicated as Basin_ORC_H. Figure 4.41 reports an example of the evolution over time of Wall 1 resistant bending moments (M_{Rd}), according to both forms of corrosion. It can be observed that the threshold to compute the moment when the maintenance activities have to be carried out is related to a situation when the structural capacity is still ensured ($M_{Rd} > M_{Ed}$). Table 4.39 summarizes the time spans, calculated as above and needed for each of the walls of Basin_ORC_U and Basin_ORC_H to achieve a situation where the resistant bending moment decreases down to the value of the design bending moment due to the relevant combination of actions, highlighting an occurrence of the event anyway not too delayed in the life time of the assessed structure.

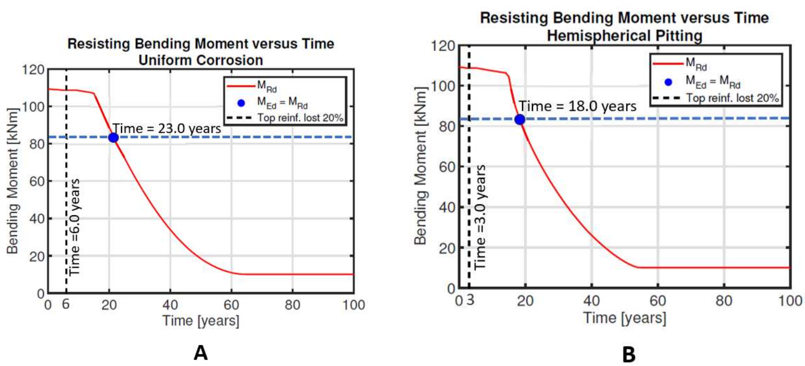

Figure 4.41: Wall 1 resisting bending moment within 100 years for Basin_ORC_U (A) and Basin_ORC_H (B).

Table 4.39: Time needed to have M_{Ed} equivalent to M_{Rd} for Basin_ORC_U and Basin_ORC_H.

	Basin_ORC_U	Basin_ORC_H
Wall 1	23 years	18 years
Wall 2	29 years	25 years
Wall 3	25 years	21 years
Wall 4	28 years	23 years

4.7.2.2 UHPC fibers and steel reinforcement corrosion

As stated in 2.5, the corrosion of the fibers which are uniformly distributed in the whole UHPC matrix is a topic that is still under investigation in the FRC and UHPC community. As a matter of fact, UHPC being a composite material, an overall integral degradation model must be employed to check its behaviour within the SL. For the scope of this research, the most severe condition has been taken into consideration, assuming immediate corrosion of the steel fibers once they are in contact with the chlorides and the critical chloride concentration (C_{crit}) is reached. This, because of their negligible size and not computing, then, a propagation period. According to this, the corrosion model assumed for the scope of this research defines a moving frontier of chlorides that have reached the critical threshold (the depth of which is estimated by means of 2nd Fick' law) and all the material within this frontier is disregarded in the calculations as usually done, e.g., for the design of timber structures in fire scenarios (CEN, 2004). This is a quite severe assumption and, however, it should be noted that in the case of UHPC, as an advantage in comparison to other materials, the tendency to have narrower crack widths can potentially delay the corrosion process. Furthermore, it is worth remarking that recent studies (Ferrara *et al.*, 2016; Cuenca *et al.*, 2021b; Al-Obaidi *et al.*, 2022a) have demonstrated the delay in terms of chlorides penetration due to the autogenous self-healing properties, also favoured by the presence of crystalline admixture even for quite high values of initial crack openings (up to 0.5 mm). The same self-healing capacity is able to compensate for early age cracking, e.g. due to restrained shrinkage**.** Thus, different and more realistic approaches are possible like the one by Davolio et al. (Davolio *et al.*, 2023) and by Al Obaidi et al. (Al-Obaidi *et al.*, 2022b) that assessed the flexural performance of UHPC slabs under simultaneous environmental and mechanical loading by implementing an experimentally calibrated constitutive law, evolving as a function of competing degradation and self-healing phenomena. The experiments were carried out by submerging thin beams (100 mm wide x 500 mm long x 30 mm thick) into geothermal water while keeping them under sustained loading through a dedicated testing rig; after having tested them up to failure at the end of prescribed exposure periods, the exposure-time affected constitutive law was obtained by using an inverse analysis procedure already employed in other studies (López *et al.*, 2016). Nonetheless, being aware that methods more conservative as the latter may need a proper modelling calibration to be extrapolated to the potentially much longer estimated service lives for UHPC (Cibelli *et al.*, 2022), for the sake of ordinary reinforced concrete vs UHPC comparison the most aggressive condition (moving chloride frontier and layer removal) has been taken into consideration for the analysis reported in the following. In addition, since the structural solution with UHPC uniform walls has been supposed to also include reinforcing steel bars, the potential corrosion of the latter has been assessed employing the same procedure as in 4.7.2.1 but using a D_{app} value of 10^{-13} m^2/s for UHPC. It was thus possible to estimate that these bars are never reached by the chlorides within the pre-determined service life period.

4.7.3 Durability Assessment-Based Design

In general, the approach proposed by the design codes is based on the idea that the concrete is a passive provider of protection rather than an active player in the degradation phenomena, without considering, then, the evolution over time of its performance and the resulting outcomes on the time evolution of the structural performance as well. Moreover, most of the current codes have been developed with reference to conventional ordinary reinforced concrete, with mechanical and durability characteristics that are completely different from those of UHPC. Thus, in line with the definition of the durability as the capacity to fulfill the performance requirements without unforeseen expenditure on maintenance and repair over the intended service life, as proposed by the fib Model Code 2010 (F. du béton and J.C. Walraven, 2012), the evolution along time of the material performance has been assessed according to what has been stated in 4.7.2.2 to calculate the serviceability and the ultimate structural performance. As a first step, following the structural consideration proposed in 4.7.1.3, the UHPC structures have been designed with the dimensions of the wall and of the slabs reported in the following Table 4.40. Moreover, no differentiation has been made in terms of the type of corrosion for the basins with uniform walls. This is due to the fact that the reinforcement bars are placed in correspondence of the tension side (ground side) where the chloride exposure is not significant. Thus, the only degradation mechanism is from a reduction of the cross section due to the progressive loss of the UHPC as per the model assumed. These walls are henceforth referred to as Basin_1_UHPC1 and Basin_1_UHPC2, depending on whether they are constructed with UHPC1 or UHPC2, respectively. Considering that the basin with precast UHPC slabs has the ORC columns, the structures subject to uniform corrosion of the columns were designated as Basin_2_UHPC1_U and Basin_2_UHPC2_U, depending on whether they are constructed with

UHPC1 or UHPC2, respectively. Similarly, the terminology Basin_2_UHPC1_H or Basin_2_UHPC2_H will be hereinafter used when the reinforcement is modeled as being subject to the same hemispherical pit corrosion mechanism as the ORC elements, and the UHPC elements are cast with UHPC1 or UHPC2 respectively.

Table 4.40: Time needed to have M_{Ed}=M_{Rd} for each wall of Basin_1_UHPC1, Basin_1_UHPC2,Basin_2_UHPC1_U,Basin_2_UHPC2_U, Basin_2_UHPC1_H and Basin_2_UHPC2_H without DAD assumptions on a maximum number of maintenance activities.

	Basin_1_UHPC1 and Basin_1_UHPC2		**Basin_2_UHPC1_U, Basin_2_UHPC2_U, Basin_2_UHPC1_H and Basin_2_UHPC2_H**	
	Thickness	**Time needed to have M_{Ed}=M_{Rd}**	**Thickness**	**Time needed to have M_{Ed}=M_{Rd}**
Wall 1	160 mm thick	1 year	70 mm thick	10 years
Walls 2	120 mm thick	1 year	50 mm thick	1 year
Wall 3	130 mm thick	2 years	80 mm thick	1 year
Wall 4	130 mm thick	1 year	50 mm thick	1 year

4.7.3.1 Durability Assessment-Based Design – rationale

It can be clearly observed, from the results summarized in Table 4.40 that the structural design performed as in section 4.7.2.2 without any consideration for the material degradation phenomena does not guarantee, at this stage and also considering the assumed reduction in reinforcement cover, adequate performance over the time. As a matter of fact, the calculated decrease of the resistant bending moment, because of corrosion degradation phenomena, resulted into an ultimate limit state achieved as early as after only one year (this being the time when the decreased M_{Rd} becomes equal to M_{Ed}). Figure 4.42 gives an example in this regard with reference to Basin_1_UHPC1_1 and Basin_1_UHPC2. The latter registered a M_{Rd} value, at time 0, of 104.9 kNm, 60.5 kNm, 75.1kNm and 69.8 kNm for Wall 1, Wall 2, Wall 3 and Wall 4 respectively. These values are respectively decreased up to 100.5 kNm, 58.5 kNm, 68.8 kNm and 66.1 kNm after mostly 1 year. Similarly, Basin_2_UHPC1_U, Basin_2_UHPC2_U, Basin_2_UHPC1_H and, Basin_2_UHPC2_H start from the values of M_{Rd} equal to 104.9 kNm, 60.5 kNm, 75.15 kNm and 68.8 kNm for Wall 1, Wall 2, Wall 3 and Wall 4 respectively that are then lowered up to 58.5 kNm, 58.5 kNm, 68.8 kNm and 66.1 kNm because of the corrosion process.

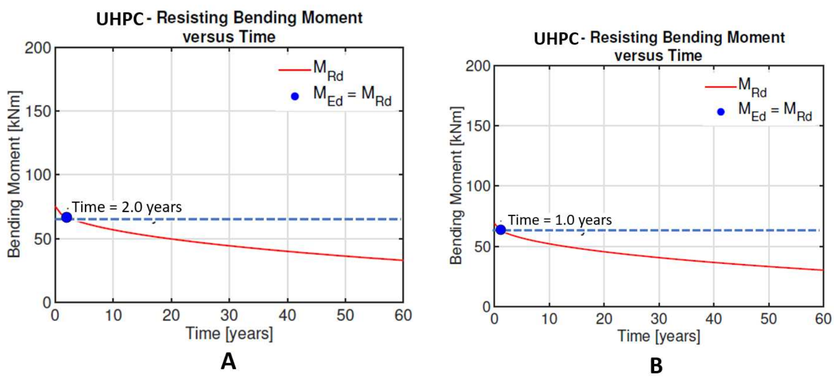

Figure 4.42: Resisting bending moment versus time for Wall 3 (A) and Wall 4 (B) of Basin_1_UHPC1 and Basin_1_UHPC_2

In view of this a DAD workflow (summarized in Figure 4.43) has been implemented to redesign the UHPC structure with the aim of achieving a performance such that the attainment of the ULS was delayed beyond the service life and with maximum one maintenance activity to be carried out within the 50 years of Service Life, due to the attainment of the relevant serviceability limit state.

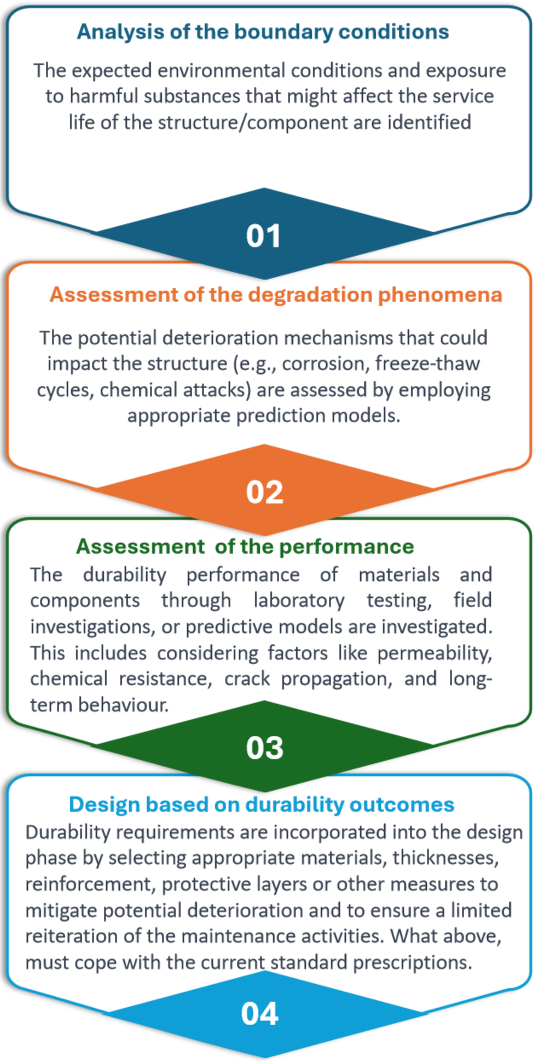

Figure 4.43 : Durability Assessment based Design workflow.

For the latter, differently than ordinary reinforced concrete structures where the crack opening limit state was evaluated, maintenance activities have been scheduled for UHPC when a deflection of l/200 is exceeded, the structure being more slender. This, also in view of the fact that, working in the strain hardening regime for UHPC and due to the characteristics of the material, crack opening always less than 0.2 mm is expected. With regard to Basin_1_UHPC1 and Basin_2_UHPC2, designing a thickness of 190 mm for

Wall 1, 150 mm for Wall 2 and Wall 3 and 160 mm for Wall 4, with longitudinal reinforcement bars of 14 mm, it was then possible to reach the goal above mentioned. As a matter of fact, the repairing activities are mainly dictated by Wall 4 since it reaches the deflection limit state at around 25 years of SL. In view of this, and even though it is estimated that the serviceability limit state is reached after 37, 31 and 92 years for Wall 1, Walls 2 and Wall 3 respectively, all of them are supposed to be maintained anyway at the age of 25 years for the sake of simplicity. With reference to Basin_2_UHPC1_U, Basin_2_UHPC2_U, Basin_2_UHPC1_H and Basin_2_UHPC2_H, increasing the thickness of the walls up to 100 mm it is possible to avoid any kind of maintenance activity for the UHPC elements in line with the aforesaid goal of the DAD approach. Table 4.41 indicates the improvements then obtained. Comparing Table 4.40 to Table 4.41 it is possible to highlight how a design purely based on durability prescription is not enough even for UHPC, as clarified by Table 4.40, since M_{Rd} reaches the M_{Ed} values after a short period. This, despite UHPC automatically satisfies the standards prescriptions, as stated so far. These outcomes also highlight how a design with a safety factor near to one, which is aimed at optimizing material usage, could anyway and potentially encounter certain durability concerns. Thus, an increase of the thickness up to the values of Table 4.41, besides ensuring a limited (for UHPC structures with uniform walls) or no (for other UHPC structures) amount of maintenance activities, also ensures a M_{Rd} always higher than M_{Ed}. Figure 4.44 shows, for the case of Wall 1, the bending moment versus time together with the tip deflection for Basin_UHPC1 as well as the resisting bending moment versus time for Basin_UHPC2_U and Basin_UHPC2_H.

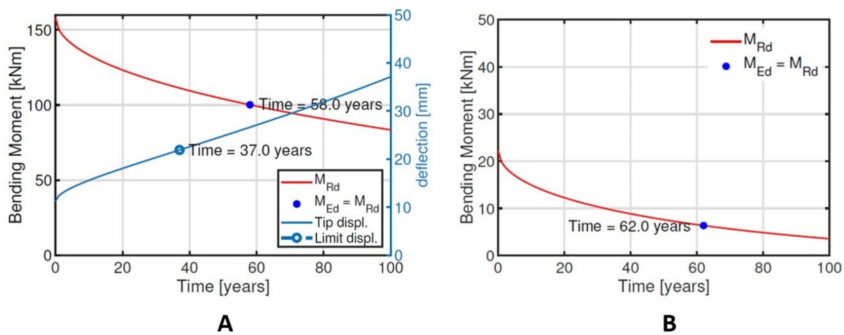

Figure 4.44: Bending moment and top deflection vs time for Wall 1 of Basin_1_UHPC1 and Basin_1_UHPC2 (A). Bending moment vs time for Basin_2_UHPC1_U, Basin_2_UHPC2_U, Basin_2_UHPC1_H and Basin_2_UHPC2_H (B).

Table 4.41: Time needed to have $M_{Ed}=M_{Rd}$ for each wall of Basin_1_UHPC1, Basin_1_UHPC2, Basin_2_UHPC1_U, Basin_2_UHPC2_U, Basin_2_UHPC1_H and Basin_2_UHPC2_H with DAD assumptions on a maximum number of maintenance activities.

	Basin_1_UHPC1 and Basin_1_UHPC2			**Basin_2_UHPC1_U, Basin_2_UHPC2_U, Basin_2_UHPC1_H and Basin_2_UHPC2_H**		
	Thickness	**Time needed to have $M_{Ed}=M_{Rd}$**	**Number of additional years in comparison the previous design**	**Thickness**	**Time needed to have $M_{Ed}=M_{Rd}$**	**Number of additional years in comparison the previous design**
Wall 1	190 mm thick	58 years	+ 57 years	100 mm thick	62 years	+ 52 years
Walls 2	160 mm thick	56 years	+ 55 years	100 mm thick	68 years	+ 67 years
Wall 3	160 mm thick	53 years	+ 51 years	100 mm thick	50 years	+ 49 years
Wall 4	160 mm thick	61 years	+ 60 years	100 mm thick	82 years	+ 81 years

4.7.4 UHPC geothermal water basin: the Influence of DAD on LCA and LCC outcomes

4.7.4.1 LCA and LCC – data input and system boundaries

The assumptions made in the previous sections represent the input for the sustainability analyses hereinafter described. More specifically, the latter have been carried out according to ISO 14040-14044 following the four main steps: i) definition of the goal and scope, ii) inventory analysis, iii) impact analysis and iv) interpretation (UNI, 2021a)(UNI, 2021b). Thus, since the main aim of the research is to identify the most convenient solution in terms of costs and environmental implications, the assessed Functional Units (FU) have been always the whole basins reported in Table 9, built employing the different materials and according to the different structural concepts as above, whereas the different degradation models, namely uniform and pitting corrosion, do enter into the assessment of the maintenance activities. A 50 year service life (SL) has been hypothesized, complying with code prescriptions (CEN, 2002). Moreover, an extended cradle-to-gate system boundary has been fixed including the use stage of the structures as well as the reiteration of the retrofitting activities whenever needed. Then, all the impacts and the costs starting from A1 phase (extraction of raw materials) up to D (reuse/recovery/recycling potential) of EN15805 standard (UNI, 2019b) have been accounted. The maintenance activities assessed for Basin_ORC_U and Basin_ORC_H consist of the removal of the concrete cover and of the corroded steel bars with the consequent substitution of the latter and the subsequent reconstruction of the cover layer by means of forms and cast-in-place concrete. The waterproofing of the ordinary reinforced concrete basin, as usually done in the current practice, has been considered as made of a bituminous emulsion applied by brushing in the amount of 1,500 g/m^2 without any pre-treatment of the concrete surface. The impacts associated with this layer have been estimated by means of the Environmental Product Declaration (EPD) developed for similar commercial products (European FEICA - Association of the and Industry, 2016). In this respect, it must be remarked that various repairing strategies are possible. However, the methodology usually employed for this type of structures is taken into consideration here, as confirmed by current practice for similar structures such as the one that this study aims to replicate in Italy. As stated above, the UHPC elements of Basin_1_UHPC1, Basin_1_UHPC2, Basin_2_UHPC1_U, Basin_2_UHPC2_U, Basin_2_UHPC1_H and Basin_2_UHPC2_H have been supposed not to require any steel replacement, also considering that in the case of Basin_1_UHPC1 and Basin_1_UHPC2, the reinforcement bars did not corrode within 50 years as detailed in 4.7.2. Therefore, as soon as the limit deflection is attained, the UHPC contaminated by chlorides is replaced by fresh UHPC with the same procedure described for the ordinary reinforced concrete elements. No waterproof layers are needed for UHPC elements since the waterproofing performance is ensured by the extremely reduced porosity of the UHPC, also thanks to the incorporation in its mix-design of the crystalline admixture, which served as porosity reducers, as well as self-healing stimulator, this having been well documented in the literature (de Souza Oliveira *et al.*, 2021) as well as by dedicated investigation performed also in the framework of the SMARTINCs project. Moreover, while the concrete is always supposed to be treated as a waste material, steel scraps (deriving from fibers and reinforcing bars) are supposedly recycled in compliance with the current EU protocols on construction and demolition waste(European Commission, 2016). Further details about the corresponding UHPC Life Cycle Inventory with data from Ecoinvent are provided in Annex 1. The LCA analysis has been developed using the CML-IA impact method released by the Center of Environmental Science (CML) of Leiden University in 2013. LCC has been performed employing the prices reported in the Italian construction costs list (Emilia-Romagna, Provveditorato interregionale alle Opere Pubbliche di Lombardia ed, 2019b, Regione Toscana, 2021) or, alternatively, carrying out a market survey to collect the missing ones. Costs of the activities to be developed in the future have been estimated by means of an interest rate calculated as in (Caruso *et al.*, 2020a). Table 4.42 provides a brief overview of the concrete and steel quantities accounted for the scope of this research while Table 4.43 lists the main construction rates employed for the cost estimation.

Table 4.42**:** total m³ of concrete and tons of steel accounted for the scope of this research.

	m³ of ORC	**m³ of UHDC**
Basin_ORC_U	207.40 (including maintenance activities)	-
Basin_ORC_H	304.39 (including maintenance activities)	-
Basin_1_UHPC1 and Basin_1_UHPC2	31.27 (including maintenance activities)	-
Basin_2_UHPC1_U and Basin_2_UHPC2_U	19.76	38.52 (due to the buttresses and their maintenance activities)
Basin_2_UHPC1_H and Basin_2_UHPC2_H	19.76	72.31 (due to the buttresses and their maintenance activities)

	Tons of steel (reinforcing bars)	Tons of steel (fibres)
Basin_ORC_U	36.09 (including maintenance activities)	-
Basin_ORC_H	20.01 (including maintenance activities)	-
Basin_1_UHPC1 and Basin_1_UHPC2	3.16 (including maintenance activities)	5
Basin_2_UHPC1_U and Basin_2_UHPC2_U	2.89 (due to the buttresses and their maintenance activities)	3.17
Basin_2_UHPC1_H and Basin_2_UHPC2_H	3.81 (due to the buttresses and their maintenance activities)	3.17

Table 4.43: Main construction rates employed for this investigation.

Work	**Rate per unit (€)**	**unit**
Excavation works	5.79	m^3
Excavation works (depth 1.5 m – 3 m)	6.86	m^3
Excavation works (depth higher than 3 m)	12.33	m^3
Formworks	23.94	m^2
Formwork fees for heights from 4.51 m to 18 m	1.54	m^2
Casting of concrete C 12/15	103.01	m^3
Casting of concrete C 35/45	158.66	m^3
Casting of UHPC	430.00	m^3
Supply and installation of rebars	2.23	kg
Demolition of concrete	423.96	m^2
Backfilling and soil compacting	29.99	m^3

4.7.5 LCA and LCC outputs

The boundaries above described led to highlight the potential advantages, both in terms of environmental burdens and overall costs, of UHPC in comparison to ordinary reinforced concrete when used to build structures exposed to an aggressive environment. To better analyze the outcomes, each impact indicator has been broken down into 5 items: cement, steel, others and disposal/recycling. Noteworthy that steel includes both reinforcing bars and steel fibers while the item disposal/recycling includes at the same time the treatment of concrete debris as waste materials as well as the recycling of the steel scraps. As detailed in Figure 4.45 and Figure 4.46, most of the environmental impact indicators registered a reduction higher than 60% in the case of Basin_1_UHPC1 and Basin_1_UHPC2 when compared to the reference Basin_ORC_H. The only indicator that was observed having a limited advantage is the Photochemical Oxidation with values of reduction not higher than 34%. On the opposite, the Fresh Water Aquatic Ecotoxicity was estimated having the highest reduction with a value of 74% in comparison to the reference for Basin_1_UHPC1. Similarly, the lowest reduction can be observed for the Photochemical Oxidation as well when Basin_2_UHPC1_H and Basin 2_UHPC2_H are compared to Basin_ORC_H or when Basin_2_UHPC1_U and Basin_2_UHPC2_U are compared to Basin_ORC_U. Moreover, for the case of the latter UHPC structures, the highest reduction has been observed for Basin_2_UHPC2_U with impact reductions as high as 76% for Human Toxicity and Fresh Water Aquatic Ecotoxicity. An exception to all of the values above reported is represented by the Abiotic Depletion for Basin_1_UHPC2, Basin_2_UHPC2_H and Basin_2_UHPC2_U which has been noted performing even worse when compared to the corresponding reference. This is due to the presence in the UHPC mix design of the blast furnace slag that, being a by-product of steel production process, accounts for around 83% of the overall impact value. In this respect it must be highlighted that this result strongly depends on the allocation methodology employed within the Ecoinvent data library used to account the impacts of the material. Since such allocation could redistribute the environmental burdens based on the physical weight or on the economic worth, future refinements of the iron process as well as a variation of the economic value within the market could lead to a complete different situation in the future. On the contrary, all the basins made with UHPC1 registered important improvements for the same impact indicator, that is a result in contrast with similar researches (Kannikachalam *et al.*, 2023). This is due to an update of the Life Cycle Inventory (LCI) that allowed to pass from the data of the activated silica to ones of silica fume, the latter having been here employed as the most proper inventory for the specific mix design of UHPC1. In addition to this, it is worth to note that negative values in Figure 4.45 and Figure 4.46 are due to the recycling process of steel scraps.

In general, the influence of the cement on the overall impact is in between 10% and 25% except for Photochemical Oxidation, Eutrophication and Global warming where it is possible to observe values up to 63% as in Basin_ORC_U. There are no relevant differences between the influence of cement of ordinary reinforced concrete and UHPC structures. This also in view of the optimized design here employed. As matter of fact, just considering the cement content (370 kg/m^3 and 700 kg/m^3 for ORC and for UHPC2 respectively) and ignoring the influence of the repairing activities and of other elements (e.g. the buttresses), the reduced thickness of the walls, from 0.40 m to 0.1 m, favours a reduction of the total quantity per each square meter of the structure. It is indeed possible to calculate that one square meter of the wall contains 140 kg and 70 kg for the basin made with ORC and UHPC2 respectively. On the other hand, for the steel a discrepancy between ordinary reinforced concrete and UHPC basins is registered, with percentage of influence always lower for the latter. As an example, steel is cause of 97% of marine Aquatic Ecotoxicity for Basin_ORC_U while its influence for UHPC structures is in the range 50 % - 70%. This is a direct consequence of two factors, namely the reduced maintenance activities for UHPC basins and the recycling of the steel scraps. As a matter of fact, the environmental benefits of the recycling treatment, which involves large quantities of steel for ordinary reinforced concrete basins, are accounted with negative numerical values. This reduces the total numerical value of the indicators, increasing then the incidence referred to the steel provision.

The cost assessment, as in Figure 4.47, highlights the same aforesaid advantages with consistent reductions higher than 42% and 46% when Basin_1_UHPC1 or Basin_1_UHPC2 and Basin_2_UHPC2_H are compared to Basin_ORC_H. It is therefore possible to observe that the most convenient solution is the one with UHPC precast slabs due to the lack of maintenance activities within the SL. Despite the different assessed cost per cubic meter of ordinary concrete and UHPC (around 160 and 430 euros respectively for the scope of this research), it is here possible to observe that cement and steel count for approximately the same percentage. This aligns with the observation that, unlike ordinary reinforced concrete where the reinforcement costs are not considered on a cubic meter scale, UHPC already includes the cost of the fibers. To better analyze the data, the overall costs have been split into both the construction and the maintenance phases. Moreover, they have been broken down into concrete and steel (reinforcing bars and fibres) contributions besides the one referred to the activities to be carried out to ensure a perfect execution of the works, excluding the casting of concrete and the steel provision/assembling, grouped into the item others. As possible to observe in Figure 4.47, for the ordinary reinforced concrete basins, while concrete generates 17% and 13% of the costs in the construction and the maintenance stages respectively, and the steel 16% and 9% within the same phases, UHPC registers similar values. More specifically, 16% and 19% in the construction, for the concrete, and 15% and 19% during the maintenance for the steel. In general, UHPC is found to be always the most economically convenient solution independently on the type of design and corrosion here assessed.

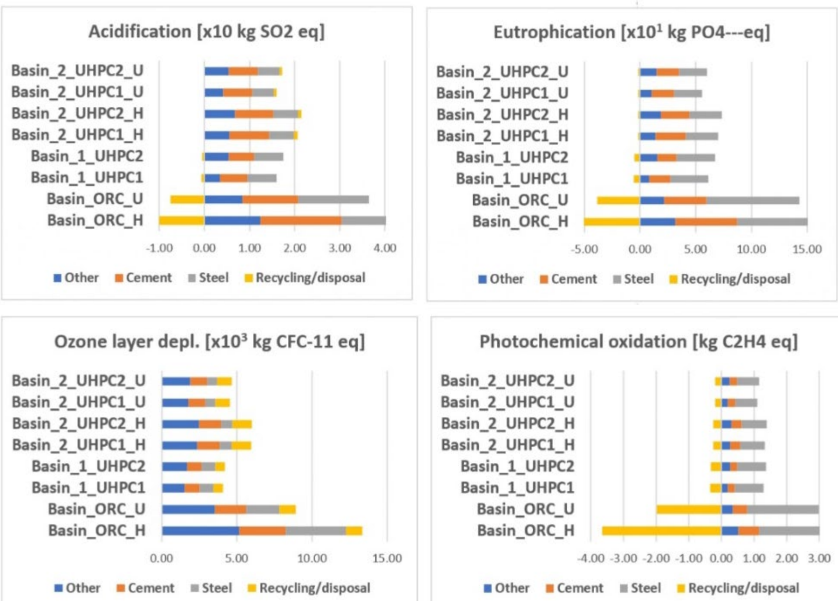

Figure 4.45: Comparison of environmental burdens for 4 out of 10 ten CML-IA impact indicators. “Steel” is intended as inclusive of the reinforcement bars for ORC basins and of the steel fibers for the UHPC ones. “Other” includes all the components of the mix design, except for the cement, including the relative transport burdens and the energy consumed during the construction and the maintenance phase.

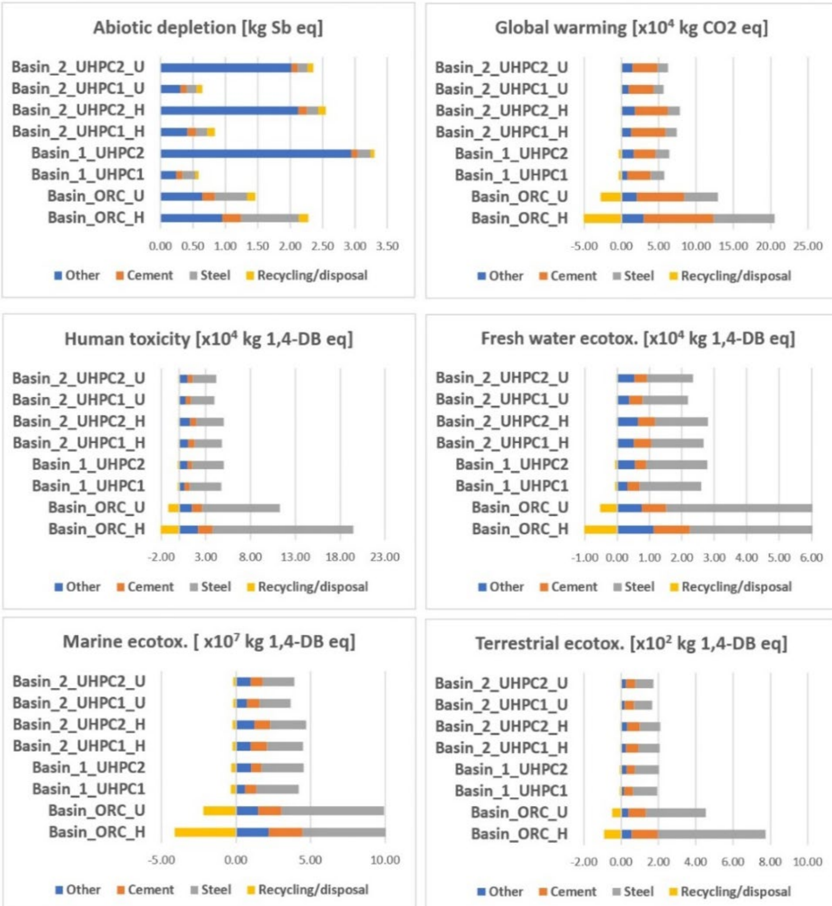

Figure 4.46: Comparison of environmental burdens for 6 out of 10 ten CML-IA impact indicators. “Steel” is intended as inclusive of the reinforcement bars for ORC basins and of the steel fibers for the UHPC ones. “Other” includes all the components of the mix design, except for the cement, including the relative transport burdens and the energy consumed during the construction and the maintenance phase.

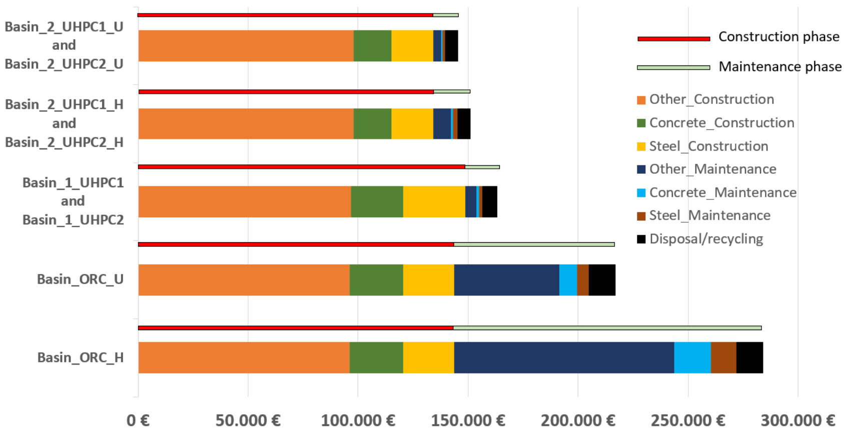

Figure 4.47: Comparison of overall costs within 50 years of SL. Other_C, Concrete_C and Steel_C are referring to the construction phase while Others_M, Concrete_M and Steel_M are related to the maintenance phases. “Steel” does include fibers for UHPC. “Others” includes all the activities to be carried out to ensure a perfect execution of the works, excluding the casting of concrete and the steel provision and assembling.

4.8 Recycled-UHPC (R-UHPC)

The existing literature regarding the use of recycled aggregates for ordinary reinforced concrete is quite extensive. Thomas et al., investigated the strength and the durability of concrete containing recycled aggregates, and highlighted the possibility to use a replacement ratio of natural by recycled aggregates of 25% without significant effects on the strength class (Thomas *et al.*, 2018). The authors also found that when higher replacement ratios are used a decrease in the compressive strength and modulus of elasticity has to be expected. Other studies like the one by Sabău and Remolina Duran defined a recommended ratio not higher than 30% of recycled aggregates, after having performed tests at 7, 14 and 28 days to guarantee a final compressive strength of 34 MPa (Sabău and Remolina Duran, 2022). Similarly, Singh et al. compared the compressive and flexural strength at the age of 28 days of concrete specimens with replacement of 15% and 30% of virgin aggregates highlighting that a replacement up to 30% is acceptable and possible to be utilized in construction practice (Singh *et al.*, 2022).

However, with regard to UHPC, other studies (Borg *et al.*, 2021), investigated both mechanical and durability performance after replacement of virgin aggregates up to 100%, showcasing potential enhancements are evident, attributed to the favorable impact of the delayed hydraulic activity within the cement/binder paste layer surrounding the recycled aggregate particles.The need to analyze the use of recycled aggregates for UHPC arises from a more general growing sustainability requirement in the construction sector. It involves an a-priori assessment of the life cycle phases of materials, which should, therefore, facilitate a recycling process at the end of their life cycle in favour of overall sustainability. However, high-strength concrete types such as UHPC are known for being extra durable. This means they can last longer, but it also means there might not be as much of these materials available for recycling. Nevertheless, structures built by employing these type of materials might not meet the needs within a long lifetime. So, there is a need to change how structure, infrastructures or cities in general are designed. Instead of just adding onto existing structures, we should replace them when they are no longer useful. To do this, the materials and structures must be designed to be recyclable from the start. Modern building codes are starting to include this idea, making it easier to reuse materials and reduce waste. As an example, the fib Model Code 2010, comprehensively address the use of cement-based construction materials and end-of-life options for disassembly at the design stage, aiming to facilitate reuse and/or recycling of original components and materials for new applications in a manner that minimizes environmental and social impacts.

Goal of this part of the study is to understand, by comparing R-UHPC to UHPC, how recycling practices (often associated with inherent environmental and cost implications) might lead to higher advantages (herein quantified) than solutions that solely use virgin raw materials.

4.8.1 R-UHPC geothermal water basin: LCA and LCC system boundaries and data input

To better quantify both the environmental and costs benefits resulting from the use of recycled aggregates for UHPC, LCA and LCC analysis have been here performed for the specific purpose assessing the use of R-UHPC for the same water basin structure above described. An extended cradle-to-gate system boundary has been used, including until the B7 stage reported in EN15804 standard (UNI, 2019b). Thus, the usage phase, along with the needed maintenance activities throughout the entire service life (SL) have been accounted. The functional unit here assessed is a water basin structure aimed to contain geothermal water as usual in geothermal electricity power plants in Italy (Al-Obaidi *et al.*, 2020b) and designed to ensure 50 years of serviceability. A basin structure characterized by three different structural concepts and two different concrete mix designs (with virgin and recycled aggregates alternatively), have been investigated. Moreover, each basin is supposed to be built in substitution of an identical old one which, because at the end of its SL, has to be demolished. The basin layout is assumed as the same of Figure 4.35. One basin is supposed to be made with traditional ordinary reinforced concrete whose structural design led to consider uniform walls with a thickness of 40 cm and it is herein after referred as Basin_Ref. The second assessed case, indicated as Basin_Ref_R, has the same structural characteristics as the latter but is made with ORC containing 30% of recycled aggregates. The second assessed basin structure in this study is supposed to be made of UHPC with uniform walls of thickness varying from 16 cm up to 19 cm according to the specific loading conditions (which vary depending on whether it is an internal or external wall) and is below indicated as Basin_UHPC. The latter, when assumed to be built with 100% of recycled aggregates, is indicated as Basin_UHPC_R. The third assessed basin is made with UHPC slabs with a thickness of 10 cm supported by PC buttresses. Also in this case it has been evaluated by considering both virgin aggregates , Basin_UHPC2, and 100% of recycled aggregates, reported as Basin_UHPC2_R. The buttresses are designed with a cross section at the bottom of 20 cm x 40 cm which becomes smaller at the top (20 cm x 20 cm) and are arranged every 2 meters. The cross section of the six different structures, according to (Parpanesi, 2021), are the same of the UHPC structure presented in 4.7 and reported in Figure 4.38 (Basin_Ref/Ref_R), Figure 4.399 (Basin_UHPC/UHPC_R) and Figure 4.40 Basin_UHPC2/UHPC2_R. Table 4.44 and Table 4.45 indicate the 4 different mix designs here employed according to (Serna *et al.*, 2019) and (Borg *et al.*, 2021).

Table 4.44: Mix design for the structures made with UHPC.

Components [kg/m³]	**Basin_UHPC** **Basin_UHPC2**	**Basin_UHPC_R** **Basin_UHPC2_R**
Cement 52.R	700	700
Silica fume	400	400
Superplasticizer	64	64
Water	231	231
Natural aggregate 1 – 1.5 mm	286	-

Natural aggregate 0.6 – 1 mm	409	-
Natural aggregate 0.2 - 0.35 mm	122	-
Recycled aggregate 0 - 2 mm	-	817
Steel fibers	160	160
Crystalline admixture	5.6	5.6

Table 4.45: Mix design for the structures made with Ordinary Reinforced Concrete.

Components [kg/m³]	**Basin Ref**	**Basin Ref_R**
Cement I 42.5	350	350
Water	207	207
Aggregate 7/12	600	-
Aggregate 4/7	300	-
Recycled aggregates blended of 4/7 and 7/12	-	900
Natural sand	950	950
Limestone filler	60	60
Superplasticizer	2	2

As discussed above, the scenario taken into account for the analysis of this research, hypothesizes the existence of an old basin structure that has to be demolished. Therefore, when a structure without recycled aggregates has to be built (Basin_Ref, Basin_UHPC and Basin_UHPC2), the old one is considered as demolished and then disposed, except for the steel which, in line with current regulations (Ministero dell'ambiente, 2018), is assumed to be recycled after having been separated from the concrete in a recycling plant. On the other hand, when the new structure is made with recycled aggregates (Basin_Ref_R, Basin_UHPC_R and Basin_UHPC2_R), the old one has been considered as entirely recycled. To this purpose, an in-situ recycling technology, aimed to obtain the recycled 0-2 mm fraction, investigated in the framework of C2CA project has been taken into account for the specific purpose. More specifically, after having considered the demolition of the structure, an autogenous milling, consisting in a process in which the size of the supplied concrete is reduced in a tumbling mill purely by the interaction of the pieces or by the interaction of the latter with the mill shell, has been foreseen. Thus the Advanced Dry Recovery technology reported by Lofti etl a., 2015, has been hypothesized to remove the fines and light contaminants with an adjustable cut-point of between 1 and 4 mm for mineral particles. As detailed in (Lotfi *et al.*, 2015, 2017; Lotfi and Rem, 2016), this machinery uses kinetic energy to break the bonds formed because of moisture and fine particles and after having broken up the material into a jet, the fine particles are separated from the coarse particles. Furthermore, ADR separation has the effect that the aggregate is concentrated into a coarse aggregate product while the fine fraction also includes the cement paste with contaminants such as wood, plastics and foams. Further details regarding the Ecoinvent data used to create the LCI of the UHPC recycling phase are provided in Annex 1. As stated before, the assessed scenario for the scope of this research excludes the end-of-life stage of the basin structures but includes their ordinary maintenance over time to ensure acceptable serviceability conditions. Therefore, it has been necessary to estimate the frequency of these activities according to the environmental conditions the structures are exposed to. For all of them, the corrosion caused by the chlorides has been regarded as the main degradation mechanism, due to an assumed chloride concentration, for the case of geothermal water, equal to 10 g/L. Moreover, for this specific case it has been considered that the corrosion starts from the inner part of the structure which is designed to be the compressed one, reason why the chlorides eventually reach first the reinforcement bars that bear a small amount of tension. This, also in view of the fact that the soil piled against the basin has a negligible chloride content. To predict the initiation time for Basin_Ref and Basin_Ref_2, in order to estimate the chlorides penetration into the concrete matrix to reach the reinforcement bars surface, the second Fick' law previously described has been used. x_{crit}, the critical chloride depth, has been assumed equal to the concrete cover; Ci, the initial chloride content of concrete, equal to 0.20% by weight of cement according to EN 206 (CEN, 2016); Cs, the chloride concentration at the surface, has been assumed equal to 1%. C_{crit} is the critical chloride concentration equal to 0.44% by weight of cement according to (Alonso and Sanchez, 2009b) and based on field exposure tests developed for the specific purpose. D_{app} is the diffusion coefficient that, as explained in 4.6.2.4, for the case of CEM I ordinary concrete, is in the order of 10^{-11} m^2/s. Then, the shrinkage verification has been performed according to the standard EC2§3.1.4 (Cen, 2005c) and allowed to obtain a value for the tensile stress, to which the walls are subjected to, equal to $\sigma_{t,c,s} \infty$ 5.2 MPa. Since this value is much greater than the one that can be borne by the walls, equal to 3.2 MPa, the related micro-cracking initial state caused by shrinkage, representing a privileged path for chlorides penetration, led to increase D_{app} valueby an order of magnitude. Thus, D_{app} has been set to 10^{-10} m^2/s with a result of 0.3 years for the initiation time. With regard to the corrosion propagation, a uniform corrosion has been considered for the scope of this research as indicated in (Bertolini *et al.*, 2004) where several rates are reported according to the specific boundary conditions that, for this case study, correspond to environment with high values of relative humidity alongside with important chlorides concentration. In view of this, a value equal to 100 μm/year has been estimated. With regard to the frequency of the maintenance activities, it has been assumed that a crack opening in the range of 0.5-1 mm should be present on the structure which corresponds to a loss of reinforcement (on a single line of bars) in the range of 16-25 [%] according to (Bossio *et al.*, 2017). Hence, as already done in 4.6.6, an average limiting value for loss of reinforcement has been set to 20 [%]. This resulted into a maintenance activity every 6 years that, within a timeframe of 50 years, means 8 maintenance activities in total.With regard to the UHPC structures, it must be stressed that the steel fibers, uniformly distributed into the cement matrix, due to their negligible size, have been considered as immediately corroded as soon as the chlorides reach the fibers as in 4.7.

To estimate the progress of chlorides into UHPC matrix the Fick' law has been used. With regard to the D_{app} coefficient, accordingly to what has been reported in international standards such as the French National Annex of EC2 and the Swiss standard BFUP (Alonso *et al.*, 2018), it has been assumed equal to 10^{-13} m^2/s. This has also been confirmed by dedicated studies performed on the parent mix employed in this study (Borg *et al.*, 2021) as well as on similar mixes investigated in the framework of the same project ReSHEALience (Cuenca *et al.*, 2022c). Additionally, since for the case of UHPC it has been considered that the material presents a ductile behavior, its reduced thickness, in comparison to the ORC solution, has required to consider the deflection limit state as the predominant one to be checked. In view of this, it has been scheduled that the maintenance activities must be developed when a deflection of l/200 is reached, meaning that for the case of Basin_UHPC and Basin_UHPC_R, it can be forecast when the chlorides affect 20% of the total thickness according to (Parpanesi, 2021). With regard to Basin_UHPC2 and Basin_UHPC2_R, the calculated deflection does not exceed 10 mm during the whole service life of the structure, reason why no maintenance activities are foreseen for slabs while the ORC buttresses follow the same frequency of the maintenance activities as for Basin_Ref and Basin_Ref_R. Table 4.46 reports the total maintenance activities for each structural solution as well as the supposed refurbishment works that have been taken into account for the LCA and LCC calculations.

Table 4.46: Type and number of maintenance activities for each structure

	Number of maintenance activities	**Type of foreseen maintenance activity**
Basin_Ref and Basin_Ref_R	8 in total, one every 6 years	Removal and disposal of damaged concrete cover and corroded reinforcement. Placement of new steel bars and realization of a new PC concrete cover after having pre-treated the substrate with hydrojet and an epoxy product to favor the adhesion of the new concrete cover to the substrate.
Basin _UHPC and Basin_UHPC_R	1 in total, one after 25 years since one wall already reaches the serviceability condition	Removal and disposal of damaged concrete cover and steel scraps. Placement of new steel bars and realization of a new UHPC concrete cover after having pre-treated the substrate with hydrojet and an epoxy layer to favor the adhesion of the new concrete cover to substrate.
Basin _UHPC2 and Basin_UHPC2_R	0 for the slab/ 8 in total for the buttresses (1 every 6 years)	Same as for Basin_Ref and Basin_Ref_R, for ORC buttresses and UHPC walls, respectively

4.8.2 R-UHPC geothermal water basin: LCA and LCC outputs

The environmental footprint of the assessed FU has been calculated using Ecoinvent as data source for the Life Cycle Inventories for most of the raw materials. Nevertheless, some constituents needed further investigations like the superplasticizer which has been modelled according to Agustí-Juan et al. (Agustí-Juan *et al.*, 2017b). Moreover, to also include the contribution of the demolition activities of the concrete cover, it has been considered a jackhammer of 1.700 W was used for a variable time depending on whether it was ORC or UHPC. With regard to the product to be used for the new concrete layer substrate, an epoxy adhesive has been considered whose associated impacts, starting from the preparation of the substrate, have been deduced from its EPD (FEICA - Association of the European Adhesive and Sealant Industry, 2015c) and scaled up according to the quantity of the product really needed. The same procedure has been followed for the crystalline admixture taking into account what has been reported in the referred EPD (EPD, 2020; Caruso *et al.*, 2022). Other assumptions were needed like for the ADR energy consumption where, in the case of UHPC structures, it has been roughly supposed to be 2.5 times higher than for the ORC structures. Similarly, data here used which will require more refinements in future studies, are the production of steel fibers which, here, has been considered as the same of the reinforcement steel bars. Also in this study, the CML-IA impact method described in chapter 2 has been employed. The obtained results are reported in Figure 4.48. It is possible to observe that for each impact indicator, the reinforcement, which for the case of UHPC includes also the steel fibers, has a huge influence. Due to this, the environmental burdens associated to ORC structures (namely Basin_Ref and Basin_Ref_R) are always higher than the others, except for ADP, AP and POCP indicators. This is definitely referred to the total accounted steel amount which, due to the reiterated maintenance activities (8 times in a timeframe of 50 years) is always higher than for the UHPC solutions, despite the presence of steel fibers but characterized by less maintenance activities. The graphs also shows the incidence of the disposal/recycling phase of the old basin structure which has to be demolished to build the new one. In this regard, some negative values are also displayed when the structure is disposed, due to the fact that, as stated above, the steel has been accounted anyway as separated and sent to the recycling plant where it is sorted and sent to foundries where it is melted down by a furnace. The existence of the negative impact values above mentioned is then explained by the fact that the extraction of virgin raw materials is avoided to produce new steel elements. This also better explains why the recycling process of the steel generates benefits that outweigh the disadvantages of the disposal of the concrete. It is also possible to outline that Basin_UHPC2_R is the solution that, among the ones here assessed, performs better in terms of environmental burdens. This is due not only to the reduced thickness (which supposes the use of less raw materials) but also to the absence of maintenance activities (except for the ORC buttresses).

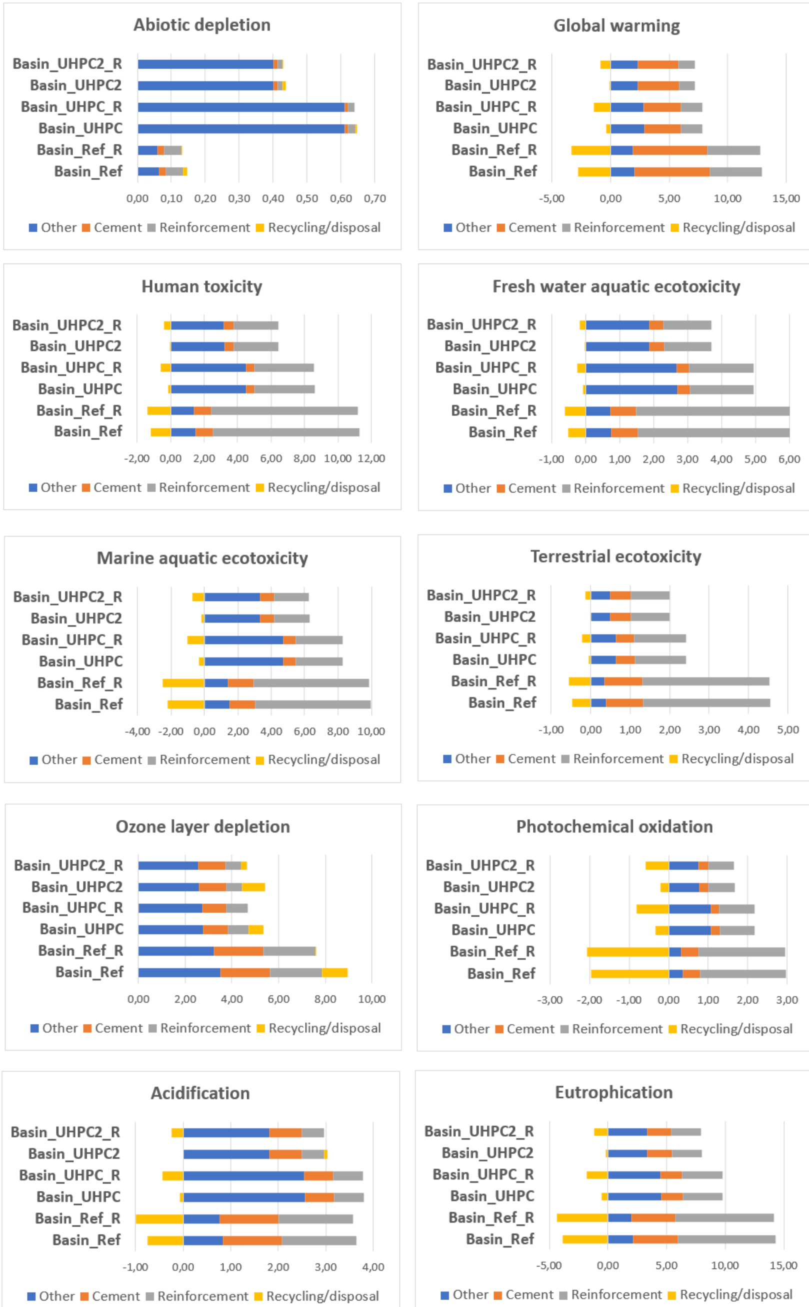

Figure 4.48: Environmental impacts for the different scenarios for the CML impact categories with indication of cement, reinforcement and recycling/disposal phase contributions.

The results here obtained highlight not only the importance, in the case of a recycling process, to use an on-site technology (otherwise the transportation of the materials might affect both the environmental impact and the related expenses), but also the relevance of using higher amounts of recycled aggregates for UHPC structures in comparison to ORC ones. As here outlined, thanks to the possibility to reach ratios up to 100%, in comparison to 30% for the case of ORC, R-UHPC is a more convenient solution when exposed to the environmental conditions such as the one here assessed.

LCC was also employed to compare the economic viability of each technological solution. Since all the basins are supposed to be built in Italy, the prices have been deducted from (Emilia-Romagna, Provveditorato interregionale alle Opere Pubbliche di Lombardia ed, 2019b; Regione Toscana, 2021)where are reported all the cost data to be used to fill the Bill of Quantities (BoQ) in the construction sector. Additional assumptions had to be made for the case of this study like the production cost of recycled aggregates according to (Hu *et al.*, 2012). For the maintenance activities to be developed in the future,it has been used the same discount factor as in 4.6.6. Results are reported in Figure 4.49 where it is possible to observe how Basin_UHPC2 and Basin_UHPC2_R allow to obtain a reduction in terms of overall expenses around 33 % in comparison to Basin_Ref and Basin_Ref_R respectively. Additionally, no relevant differences can be observed for each of the three different structural solutions between the mix containing virgin aggregates and the one with recycled ones. This is mainly due to the extra-costs referred to the recycling process which, in the future, might be reduced thanks to an optimization of the entire process.

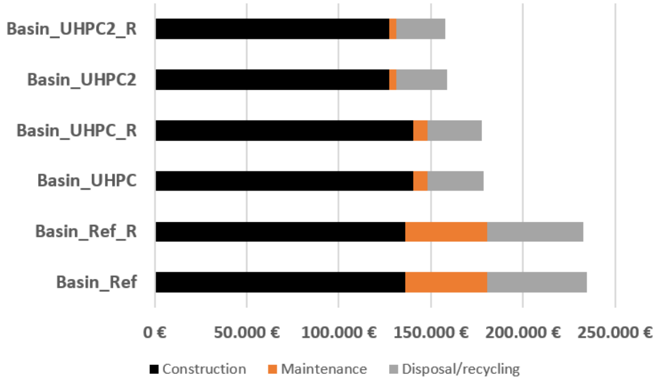

Figure 4.49*:* Costs comparison among the different assessed solutions.

These outcomes are in line with the results presented in 4.5 and 4.7, but also with other researches that, assessing the economic impacts of water basin structures similar to the one here proposed, pointed out a cost advantage of UHPC of around 22% with comparison to the reference made up of ordinary reinforced concrete (Caruso *et al.*, 2020b). This was noticed, even when employing different boundary conditions such as a different waterproofing solutions (bituminous coating layer) or a recycling process of the concrete debris at the end of life stage. The results presented so far, definitely highlight that the higher cement content and the higher price per unit volume of UHPC can be overcome by employing a tailored Durability Assessment-Based Design approach which at the same time allows to optimize the structural dimensions, and hence the consumption of materials, and the assess the evolution of the material and structural performance over the time, which results into a thorough and holistic evaluation of the improved sustainability performance. Figure 4.50 summarizes these aspects making a comparison among the highest reduction values observed in 4.5, 4.7 and 4.8.

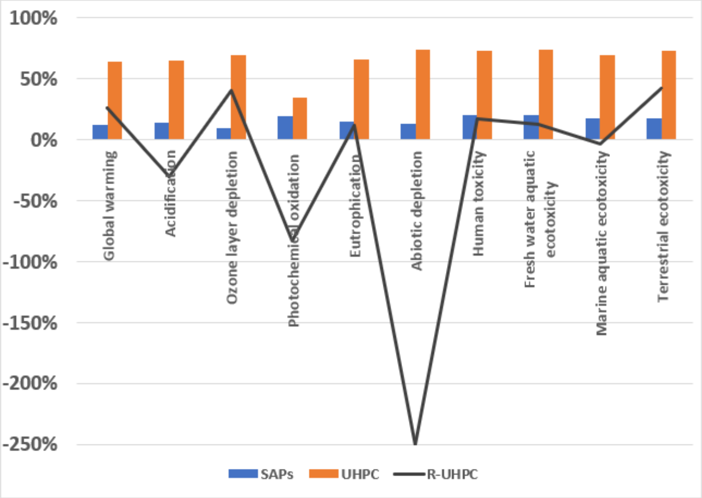

Figure 4.50: Highest reduction values, expressed in percentage, for concrete containing SuperAbsorbent Polymers (section 4.6), UHPC (section 4.7) and R-UHPC (section 4.8) in comparison to a reference solution. All of the studies are developed within an extended cradle-to-gate system boundary excluding the end-of-life stage. Negative reductions for R-UHPC are due to the recycling process whose benefits are accounted with a negative numerical value.

4.9 Conclusions on the main outcomes

In an era defined by an increasing emphasis on sustainability challenges and opportunities, the construction industry stands at the forefront of transformative innovation. This chapter navigates the complex landscape of advanced construction materials and their employment on a large scale. Each investigation, rooted in LCA and LCC considerations, unravels the intricate link among environmental impacts, economic feasibility, and structural resilience. The following key outcomes can be remarked.

<u>Microcapsules</u>: the analysis applied a cradle-to-gate system boundary, presenting results using the EPD 2018 impact assessment method. High content percentages drive the consistent contribution of acetone, vinyl acetate, and copper, key components of the membrane emulsification production process, to the highest influence across various impact indicators. Considerations on other factors, such as volatile organic compounds emissions from acetone, energy-intensive processes for vinyl acetate production, and copper extraction emissions, suggests potential refinement of the production stream to achieve more sustainable outcomes.

<u>Alumina nanofibers</u>: LCA results (by employing a cradle-to-gate system boundary and EPD 2018 as impact assessment method) for 1 kg of alumina nanofibers dispersion (10% concentration aqueous suspension) reveal electricity as the most influential factor, reaching up to 96% across impact indicators, notably in acidification potential. Aluminum oxide has minimal impact, except for ozone layer depletion and water scarcity. Literature review outlined how adding this type of nanofibers to concrete improves flexural strength and deformation capacity. Moreover, their surface, containing free hydroxyl groups, facilitates the hydration of cement particles, while due to the size of the oxide nanofibers they reinforce the layered CSH structure, leading to reduced shrinkage deformation and providing a nano-structural toughening effect. Thus, 1 m^3 of UHPC with alumina nanofibers has been assessed as well. The analysis of 1 m^3 (carried out by employing a cradle-to-gate system boundary and EPD 2018 as impact assessment method) shows cement and steel fibers as major influencers. Also in this case, the findings provide insights into potential improvements, suggesting refinement of the production process for alumina nanofibers and reevaluation of the UHPC production chain. Specifically, attention could be directed towards minimizing transport distances to mitigate their environmental impacts.

Concrete beam with vascular network: this part of the study outlined the potential advantages of employing a vascular network (either made of nylon or PLA) embedded into a concrete beam exposed to an aggressive environmental scenario rich in chlorides. Reductions up to 50% have been observed when the beam containing the vascular network has been compared to a more conventional solution. Future research endeavours could not only investigate alternative and refined production processes for PLA to potentially uncover additional advantages but could also include the end of life stage, not taken into account for the scope of this analysis. This is particularly crucial considering that PLA is a nature-based material, and comprehending its disposal in comparison to fossil-fuel resources (as nylon is) could lead to different outcomes, given its inherent lower environmental impact. Moreover, the durability characteristics employed to carry out the LCA analysis are strongly dependent on the healing agent which has been chosen for the injection (polyurethane), meaning that different and more performant products, able to better penetrate the cracks, could favour the achievement of better results when the structure is exposed in a chloride scenario, due to the potential extension of the initiation corrosion time. Additionally, better results could also be achieved in the future combining the potential advantages of the vascular network with the ones coming from the use of recycled concrete as aggregate and as partial replacement of cement

Concrete walls with SAPs: this part of the study has been developed taking into account a variable service life ranging from 50 up to 100 years with the assessed FU subjected to different maintenance activities to restore its functionality and to different scenarios related to the reinforcement corrosion progress, meant as the main degradation mechanism. One of the key focus points was to properly estimate the frequency of these repair activities according to the structural properties of the walls and to the durability parameters of a concrete structure exposed to a chloride environment. To this purpose, structural design approaches have been combined with equations governing the assessed degradation mechanisms, which have also allowed to highlight the importance, in the material and structural design phase, to target specific durability performance requirements, e.g. in terms of chloride diffusion coefficient values, which govern the corrosion initiation time. The adopted cradle-to-gate system boundary outlines that innovative materials like SAP containing concrete can lead to an impact reduction in comparison to the traditional ones, for all ten CML-IA impact categories. With reference to the four investigated scenarios, differing by service life and degradation scenario, the environmental and economic advantages of SAP-containing concrete have been clearly highlighted. The maintenance activities are not only responsible for most of the overall costs, summing up to more than 30% in some of the investigated scenarios, but since they imply the use of more reinforcement and cement as well, this inevitably causes higher impacts. As a matter of fact if, on the one hand, both the overall employed steel and cement quantities strongly affect all the ten impact indicators, on the other hand the influence of the SAP content is almost negligible. Additionally, the developed cost analysis also highlights the additional benefits of the concrete containing SAPs, with a significant reduction in terms of overall life-cycle costs in comparison to the conventional solution. Therefore, the use of SAPs is, among the investigated ones, the most convenient solution with reference to 50 and 100 years of service life and according to the adopted system boundary. The environmental and economic advantages are more significantly evident in longer time frames like 100 years, mainly due to the incidence of the frequency of the maintenance activities.

<u>UHPC basins and inclusion of Durability Assessment-based Design principles:</u> this part of the investigation has examined the incorporation of durability parameters into structural design workflows through the utilization of Durability Assessment-based Design (DAD) methodology, focusing on structures made with UHPC compared to ones made with ordinary reinforced concrete. The outcomes highlight how design approaches like the DAD herein proposed, can harness environmental, cost and structural benefits from the onset, contributing to a more sustainable built environment and mitigating, consequently, the social injustices before mentioned. This also implies the need to integrate the existing developments with a Social Life Cycle Assessment to establish a truly omni-comprehensive design approach that encompasses all relevant implications across various scales. However, the main findings can be summarized as follows.

- the current durability design approach for Ordinary Reinforced Concrete structures, which primarily relies on “deemed to satisfy prescriptions” on minimum cement content, concrete cover, strength class, and maximum water/cement ratios can cause potential issues. As an example, the initial microcracking in ordinary reinforced concrete can lead to an increased chloride diffusion coefficient, fostering an early chloride penetration and a likewise early onset of the reinforcement corrosion, thereby resulting into earlier and more frequent maintenance;

- the DAD methodology proposed here allows for tailored scheduling of maintenance activities, optimizing structural design accordingly. It also offers advantages in terms of cost and environmental impact, especially for innovative cementitious materials like UHPC, which inherently perform better and whose benefits, since the deemed to satisfy prescriptions of current design codes are automatically satisfied, would and could hardly be appreciated otherwise;
- UHPC, while having higher costs and cement content per cubic meter compared to ordinary reinforced concrete, demonstrates better overall environmental and cost performance when considering structural applications. This, due to both the reduced volume of materials required to build the structure, for the same target performance, and the reduced maintenance frequency. This is respectively allowed and promoted by enhanced mechanical and durability performance;
- slabs built with UHPC containing slag show significant environmental reductions in Human Toxicity and Freshwater Aquatic Ecotoxicity but poorer performance in Abiotic Depletion when compared to the reference;
- uniform walls made with UHPC containing silica fume registered similar reduction values to the slabs built with UHPC (and containing slag) for both the economic and environmental performance when compared to the reference, but with consistent improvements for the Abiotic Depletion. This is mainly due to the substitution of slag with silica fume and to the allocation of the environmental burdens associated to these type of by-products in the library Ecoinvent;
- the importance of employing quantitative tools like Life Cycle Assessment (LCA) to evaluate the influence of supplementary cementitious materials on overall sustainability and aid decision-making becomes clear.

<u>R-UHPC water basin</u>: the results highlight the influence of reinforcement and disposal/recycling phase on environmental burdens. The basin built with UHPC slabs and 100% of recycled aggregates emerges as the most environmentally favorable solution, emphasizing reduced thickness and maintenance activities as key factors..

<u>CEM III + CA</u>: this part focuses on quantifying the sustainability of a structure defined as strategic for the urban metropolitan area, comparing an ordinary technological solution to a self-healing one. To this purpose, the

seismic resistance has also been checked after the appearance of a consistent degradation at the age of 52 years, because of the carbonation. One of the first observations that can be made is that the use of crystalline admixture results in better durability parameters and hence longer predicted SL. In addition to this, the structural analysis demonstrated that the degradation mechanisms may affect the structural response but, for the case studied here, having been basically designed as non-dissipative, there is no significant problem though a reduction of the safety factor does actually occur.

To conclude, together, these studies contribute not only to the evolving discourse on sustainable construction practices but also offer valuable insights into the potential paths for shaping a future where the built environment harmonizes seamlessly with a holistic sustainable stewardship.

From laboratory-scale components to structural-scale realities: case studies and LCA/LCC implementation within the design phase

5 Driving the innovation: commercialization strategies and Key Exploitable Results (KERs)

It is not merely sufficient to analyze the impacts (environmental, social, and economic) of new construction materials within the construction sector landscape for them to gain market traction. It is also essential to develop specific marketing strategies to penetrate the market. In light of this, this chapter first explores the feasibility of effectively communicating, with clarity and impact, the results obtained so far. Additionally, it identifies the Key Exploitable Results (KERs) of the current research, proposing a business unit and offering insights into how the presented outcomes can be made profitable. As affirmed by the European Commissioner for Innovation, Research, Culture, Education and Youth Mariya Gabriel, in between 2019 and 2023, the results coming from Horizon projects must “flourish into innovations that contribute to our society and economy, and to a sustainable future!” (European commission, 2024).

5.1 Introduction

As shown in the previous chapters, LCA and LCC, besides their established role for quantifying environmental and economic implications, it is essential to recognize that they can contribute significantly to steering decision-making processes, especially in sectors where sustainability considerations are paramount. Thus, in the context of the construction market, where the demand for sustainable and environmentally conscious products is increasing, LCA and LCC play a pivotal role. However, they can also help in promoting the commercialization of innovative products if effective communication of holistic sustainability features is given to the interested stakeholders. This chapter firstly aims at providing an illustrative example of how sustainability can be communicated more effectively to stakeholders to not only meet environmental and economic targets but also to effectively market and position these products in a competitive industry landscape. This can be done through indexes as the ones subsequently presented that can serve as a comprehensive metric to encompass most of material performance, spanning aspects such as durability and mechanical strength. Scope is to exemplify the complexity of individual impact indicators and parameters, that may be difficult to grasp, by proving only one numerical value. Moreover, these indexes can assign varying weight to each encompassed parameter, according to specific needs. Additionally, the key exploitable results serve as a blueprint for other endeavors aiming to utilize holistic sustainability analyses for commercialization purposes. For such purpose, they are also herein discussed and presented.

5.2 Thoroughgoing sustainability indices to support the development of a forward-looking market for innovative construction materials

Managing challenges and opportunities related to sustainability requires policy makers and stakeholders to make balanced decisions based on scientific information, which is why reliable evaluation tools are needed to avoid making, in crucial stages of the decision making process, wrong assumptions which can result into unintended consequences. This key concept, tackled in the framework of the construction sector, takes on even higher significance due to the consequences in terms of sustainability implications that can be generated at every scale. As a matter of fact, the buildings within the European Union are responsible for 36% of greenhouse gas emissions (Committee on Industry, 2023), primarily originating from the construction, utilization, restoration, and dismantling phases. Moreover, a study by the Global Commission on the Economy and Climate (a partnership of seven economic and policy research institutes based in Colombia, Ethiopia, Indonesia, Norway, South Korea, Sweden and the United Kingdom), estimates that investing in sustainable infrastructure could lead to $26 trillion in economic benefits by 2030 (The Global Commission on the Economy and the climate, 2018). This is in line with what was foreseen in the World Green Building Council's study on green building practices that revealed how investing in green materials and practices can yield operational cost savings of up to 20% (Dodge Data & Analytics, 2018) However, the economic potential of sustainable construction materials is further highlighted by the projected market growth pointed out in a report by Oxford Economics. There, it was estimated that the global construction market will be worth $15.5 trillion by 2030 (Oxford Economics, 2021). In view of this, the potential economic value and growth due to the adoption of innovative and more sustainable materials become more apparent. It must be also emphasized that today's consumers are more environmentally conscious than ever, often making purchasing decisions based on the sustainability credentials of a product. Thus, some governments have already started acting to encourage substantial changes not only limited to the construction industry. As an example, all signatory nations of the Paris Agreement, operating within the United Nations Framework Convention on Climate Change, must formulate and implement strategies for diminishing their greenhouse gas emissions (Edenhofer *et al.*, 2014) with the goal of attaining carbon neutrality by 2050. However, this endeavor is notably intricate, especially considering that the global population is expected to increase up to ten billions by 2050, reason why one of the key challenges lies in reconciling the surge in requirements for structures and infrastructure due to population growth with the imperative of sustainability. To such purpose, concerted efforts must be made to enhance carbon removal and decrease carbon emissions. Hence, the cement and concrete sector (cement production itself is responsible for 5–7% of CO_2 emissions caused by human activity) faces mounting demands to reduce greenhouse gas emissions, alongside diminishing depletion of natural resources (Damtoft *et al.*, 2008). As an example, the calcination process accounts for a substantial 60% of the overall energy consumption within the cement production. Therefore, shifting towards renewable energy sources could yield significant benefits and alternative fuels (biogas, plastics, wood waste) could be used, but they require careful consideration to avoid clinker quality changes. A solid enhancement of the sustainability of construction materials such as concrete, involves more than just focusing on the reduction of the environmental impacts during the production stages of its basic components as most of the current approaches have done so far, surely meritoriously but also limiting the perspective to the very onset of the whole process (Hasanbeigi *et al.*, 2012; Gartner and Hirao, 2015; de Brito and Kurda, 2021).

While strategies like decreasing CO_2 emissions, energy usage, and raw material consumption are efficient in pursuing sustainability on one side, on the other hand, their long-term effectiveness also depends on the durability and structural performance of the material. In line with this, the development of innovative cementitious materials has to encompass a plural set of solutions, including the use of alternative constituents and innovative admixtures, as hereinafter reported. As an example, reducing Portland cement and replacing it with low-embodied carbon materials, such as supplementary cementitious materials (SCMs), can lessen the environmental impact at the level of the concrete material mass or volume unit. SCMs exploit aluminosilicate phases to balance the reduction of calcium silicates in Portland cement clinker, improving concrete properties and contributing to a more efficient management of industrial waste and by-products. A further demonstration could be the employment of calcium sulfoaluminate (CSA) cements that are able to reduce energy and CO_2 emissions, ensuring very high early age strength, low shrinkage and high resistance to sulfate attack but with uncertain resistance to carbonation and chlorides (Coppola *et al.*, 2018; Zhang *et al.*, 2018) Innovations like this could be used in combination with other strategies, like carbon capture technologies which are promising but still expensive (Warsi *et al.*, 2020).

Self-healing concrete is another remarkable innovative concept, which relies on the capacity of the material to autonomously repair cracks, through tailored additions in the concrete composition as well as changes in the design of the structural elements (e.g. employment of steel fibers to reduce cracks width favouring the self-healing). Through mineral or polymeric healing agents that are mixed in, either or not protected by (micro)capsules, or that are injected through a vascular network, crack healing by mineral deposition or polymerization is promoted under certain boundary conditions (De Belie *et al.*, 2018; Cappellesso *et al.*, 2023). This technology enhances concrete's longevity, reduces maintenance, and contributes to the possibility of “implementing” a more resilient and cost-effective building and infrastructure portfolio (di Summa *et al.*, 2022a,c; Kannikachalam *et al.*, 2023). Another opportunity that is raising interest among the stakeholders is the Ultra High Performance Concrete (UHPC). It is characterized by compressive strengths exceeding 150 MPa, a one-of-a-kind deflection and even tensile strain hardening performance and superior resistance to wear, chemicals, and extreme conditions, as compared to conventional, even high performance concrete. UHPC(Azmee and Shafiq, 2018; Al-Obaidi *et al.*, 2020; Li *et al.*, 2020; Kannikachalam *et al.*, 2023) is then an ideal candidate for various applications ranging from transportation infrastructure, including bridges and tunnels, to architectural marvels that demand both aesthetics and resilience. Despite its higher unit production cost, its mechanical performance allows for “daring” optimization of structure dimensions and its higher durability, resulting in extended lifespan and reduced maintenance needs, make it a compelling choice for creating lasting, sustainable structures of the future(Caruso *et al.*, 2020; di Summa *et al.*, 2022b; Kannikachalam *et al.*, 2023).

In the framework described above, standards are vital for integrating innovative sustainable materials into the design and construction practice, and accounting for their enhanced performance. Regardless of the progress in concrete technology, including developments in the field of cement aggregates, fillers, and chemical admixtures, existing design standards predominantly focus on traditional concrete compositions. These standards often fail to account for “innovative” or non-conventional constituents, but also for advanced technologies, such as self-healing. As an example, the use of alternative binders and even alternative supplementary cementitious materials, faces limitations due to the necessity of incorporating the binder into existing standard classification (e.g. EN 197-1:2011 (CEN, 2011) for cement and EN 206:2013+A1:2016(CEN, 2016) for concrete). In contrast, ASTM standard C150-20 prescribes Portland cement specifications, while ASTM C1157-20 and ASTM C1600-19 provide performance-based guidelines for hydraulic cements, allowing broader binder compositions (ASTM, 2021a,b, 2023). However, the shift towards performance-based standards in the concept and design of cementitious materials and structural applications is an urgent imperative to steer the practice towards a more sustainable use of materials and resources. This must be accomplished in synergy with an efficient assessment of the sustainability signature of materials and structures. In line with this scope, this work investigates the consistency of two indices to be used for such purpose, defined as material index (TS,M-index) and structural index (TS,S-index) combining a sustainability quantification (not solely limited to the CO_2 emissions), with cost efficiency, durability, and mechanical performance. The goal is to provide a rationale and objective tool for selecting the best material to be used based on holistic sustainability criteria.

5.2.1 Advancements in sustainability indices for cement-based materials

As before stated, to face the challenge of sustainability means to discretize a complex topic. Not only CO_2 emissions can be used to quantify environmental performance, but different other factors must be taken into account to gauge sustainability. Some of these encompass energy use (referring to the energy consumed throughout a material's or structure's lifecycle), depletion of natural resources, alternative greenhouse gas discharge (CH_4 and N_2O also contribute to the greenhouse effect (Jain, 1993)), water consumption, ozone layer depletion and other factors including acidification, eutrophication, and soil erosion (Pennington *et al.*, 2004). When evaluated together, they are able to provide a broader perspective on environmental consequences of a given activity. Gartner and Hirao better emphasized these aspects, pointing out the complexity of sustainability for the concrete construction sector, also due to the diverse array of involved components (such as binders, aggregates, admixtures, electricity consumption, type of electricity production)(Gartner and Hirao, 2015). Various indices have been proposed in the literature, condensing multiple sustainability aspects into a single value to gauge a product's overall sustainability and encompassing environmental, social, and economic aspects. A first attempt was made by Damineli et al. (Damineli *et al.*, 2010) who assessed concrete sustainability in relation to the total quantity of used binder or CO_2 emitted to achieve 1 MPa of strength. A couple of indicators were then proposed. The first one, defined as the binder intensity (b_i) consisted of what was reported in Eq. 5.1, where b is the total binder consumption (expressed in kg/m^3) and p is a performance parameter (such as the compressive strength expressed in MPa) that can be varied depending on the specific application. The second proposal, presented in Eq. 5.2 and defined as the CO_2 intensity (c_i), besides including the same p in the denominator, takes into consideration the total CO_2 emissions (kg/m^3) generated by the production and transportation of needed raw materials. In general, all the encompassed data have been chosen because of their presence in many national inventory databases (Josa *et al.*, 2007) and since they are easy to obtain for market and policy practitioners. Moreover, the authors took advantage of a previous study (Popovics, 1990) in which the estimation of the compressive strength of a specific mix design was related to the cement content instead of referring just to the water-to-cement ratio as in other proposals (Zhu *et al.*, 2021).

$$b_i = \frac{b}{p} \qquad \text{Eq. 5.1}$$

$$c_i = \frac{c}{p} \qquad \text{Eq. 5.2}$$

Other studies (Gettu *et al.*, 2018) further elaborated the aforesaid concepts, by proposing the Apathy Indexes (A-indexes) defined as the ratio between the carbon dioxide emissions per cubic meter of material (calculated through a LCA analysis), and a parameter F related to the carbonation or chlorides penetration front. This represented a first attempt to correlate such evaluation tools to durability parameters able to describe the performance of the material when exposed to XC and XS classes as defined by the Eurocode (CEN, 2002). Nevertheless, despite the advantage of including some data related to the performance throughout the service life, this proposal lacks consideration of the mechanical performance of the material. In line with this assumption, Müller (Müller *et al.*, 2014) developed a more comprehensive proposal, the so-called Building Material Sustainability Potential (BMSP) including, besides the durability characteristics, the mechanical performance as well. The index was intended to be used by concrete technologists during the planning process to choose the most appropriate mix design as a function of the intended application. The author starts from the key concept that minimizing the environmental footprint stemming from concrete production, regardless of its potential ramifications on material efficacy and lifespan, falls short. This inadequacy is underscored by the fact that concrete structures typically last between 50 and 100 years (Alexander and Beushausen, 2019). As a matter of fact, the pursuit of enhanced sustainability in building structures necessitates a dual strategy: diminishing the environmental repercussions entwined with construction, maintenance, and operation, while concurrently bolstering the structures' endurance and peak technical performance. This relation is summarized in their BMSP proposal as presented in Eq. 5.3. The result is expressed in $\frac{years\ x\ MPa}{kgCO_2}$ and takes into account the compressive strength as mechanical performance and the kg CO_2 per cubic meter of the material as environmental impact. Service life is expressed in years and determined by making reference to the target reliability index βt which refers to the reliability level necessary to ensure adequate safety, serviceability, or durability based on structural requirements. Its employment is also reported in ISO 2394 (ISO, 2015) and Model Code 2010 (fib, 2013) where it is related to the cost of safety measures and the consequences of failure.

$$BMSP = \frac{Service\ life \times Performance}{Environmental\ Impact} \qquad \text{Eq. 5.3}$$

According to Eq. 5.3, there are three possibilities for achieving sustainable concrete use. The first approach involves optimizing concrete composition to minimize environmental impact while upholding or enhancing performance and longevity. The second focuses on enhancing concrete performance without increasing environmental impact or reducing service life. The third centers on extending the service life of the building material and structure without compromising environmental impact and performance. Dan Georgescu et al. (Georgescu *et al.*, 2022) recently worked on a further simplification of the BMSP index by assuming the factors in the nominator (service life and performance) as constant. The authors worked on a comparison between two mix designs able to ensure the same performance and service life. This was assumed as possible simply by following the standard prescriptions by the Eurocode (Cen, 2005)and EN 206 (European committee for standardization, 2001). Thus, the difference is solely made by the denominator where the environmental burdens associated with the specific mix design can vary according to the different constituents, even though structural and durability characteristics in the nominator remain the same. Later, in line with an approach able to involve a blend of these strategies and with the aim to not overlook key aspects such as energy and natural resources consumption, Coppola et al. (Coppola *et al.*, 2019) introduced the Empathetic Added Sustainability Index (EASI). The scope of the proposed index, formulated as in Eq.5.4, was to go beyond evaluating solely the environmental impact of mortar and concrete, proposing the incorporation of durability aspects and the necessary engineering properties tailored to specific applications. This is translated into the multiplication of the performance at the nominator (encompassing properties such as compressive/tensile/bond strength and shrinkage as suggested by the authors), by the durability performance (depending on the specific environmental exposure condition). For the latter the authors foresee the possibility to encompass various parameters such as carbonation rate (usually expressed in mm/year) for exposure to air, chlorides diffusion coefficient (in m^2/s) for structures exposed to seawater and deicing salts, chemical attack and freeze-thaw resistance (for which the unit of measure can vary depending on the specific method of assessment, but mass loss expressed in percentage could be an example). The denominator takes into account three factors in total, namely Gross Energy Requirement (GER), Global Warming Potential (GWP) and Natural Raw Materials Consumption (NRMC) respectively. Moreover, all the factors are supposed to be normalized respect to a reference solution (e.g. OPCC). The aim is to obtain a value around the unit (justifying the presence of 3 at the nominator) with the consequence that values greater than 1 imply an improved sustainability with respect to the reference.

$$EASI = \frac{3 \times \prod_1^n performance \times \prod_1^n durability}{\sum_1^n environmental\ impact} \qquad \text{Eq. 5.4}$$

Subsequently, Coffetti et al. (Coffetti *et al.*, 2022) improved the latter by proposing a modified EASI index (M-EASI) expressed as in Eq. 5.5, making it suitable for concrete and mortars with negative carbon footprint by employing CO_2-capturing cements or CO_2-sequestrating aggregates by adding the mathematical Euler's constant e to both numerator and denominator. Also in this case all the factors are normalized to those of a reference solution with the scope of having a final value around the unit. The acronyms GER, GWP and NRMC included in Eq.5.5 stand for the same environmental parameters above described.

$$M - EASI = \frac{3e \times \prod_1^n performance \times \prod_1^n durability}{e^{GER} + e^{GWP} + e^{NRMC}} \qquad \text{Eq. 5.5}$$

What has been presented above represents the summary of concerted efforts to ensure that the construction industry aligns with the principles of sustainability. Nevertheless, there is a noticeable dearth of consideration for final costs and social consequences in the current approaches, despite them being fundamental pillars of sustainability. Herein lies the challenge: current approaches often overlook or inadequately quantify the long-term economic viability of sustainable concrete solutions and neglect the potential social ramifications of construction projects. Furthermore, it's important to note that these indices exclusively pertain to the properties of materials and do not take into account their utilization in structural applications. This lack of consideration for the practical use in structural contexts is a notable limitation. This could also represent a constraint to the potential employment of such tools within the existing rating and scoring systems that have gained prominence in the construction industry. Notable among these are LEED (Leadership in Energy and Environmental Design) (Dobiáš and Macek, 2014)and BREEAM (Building Research Establishment Environmental Assessment Method) (O'Malley *et al.*, 2014) which are generally focused on complex entities as whole building structures. In view of this, the following section presents the proposed thoroughgoing sustainability indices which are not solely limited to the material scale, covering a wide spectrum of factors ranging from mechanical performance, durability up to environmental and cost sustainability. The aim is to fill the existing gap above observed, providing a universal tool to be employed at different scales and under various environmental conditions.

5.3 Thoroughgoing material and structural index: proposal

Two distinct types of indices, defined as Thoroughgoing Sustainability Indices, are here put forward and assessed for their significance. The first one, defined as material index (TS,M-index), is focused on the material scale with the aim of gauging the sustainability when different types of mix designs are employed. This entails encompassing data such as LCA outcomes per cubic meter, unit costs, and mechanical performance. With regard to the LCA outcomes, it must be highlighted that, for the scope of this proposal, not only the GWP is tackled. A broader series of environmental implications, as the ones provided by the so-called CML-IA impact indicators, are employed. These indicators, varying from global warming potential to eutrophication or human toxicity, are able to provide a detailed overview not limited to a global scale (like when just the GWP is addressed) but also inclusive of regional and local perspectives (Guinee, 2002; Lamnatou and Chemisana, 2015). This is a way to indirectly include social implications as well. As an example, within areas highly contaminated because of the pollution, not only health risk is increased but the quality of life and healthcare burdens are affected as well, creating ghettoized zones (Human Rights Council United Nations, 2022; Renzetti *et al.*, 2022). Moreover, as before detailed, while previous attempts already proposed an inclusion of the mechanical performance of the material, the addition of the costs certainly represents an innovation in line with the need to address the costs challenges for a sustainable development (Nasereddin and Price, 2021). This approach will ensure that sustainable practices are not just environmentally friendly but also practical and economically viable for individuals, businesses, and society as a whole. The TS,M-index is reported in Eq. 5.6 and is characterized by the presence of the mechanical parameter in the numerator (selecting the one most suitable to characterize the material in the most common application), with the 10 CML-IA impact categories and costs in the denominator. All the parameters reported in the denominator are referred to one cubic meter of the material. In order to favor an easier use of the index, leading to a value close to one, and to allow the combination of parameters with different units, both numerator and denominator are intended as normalized to those of a reference that can vary case by case (e.g. OPCC in this study). Moreover, in the denominator, since 10 impact indicators have been taken into account to weigh in the same way the costs performance, it has been multiplied by 10. This can lead to a value of the denominator around 20. Thus, for the same purpose of achieving a value around the unit, the numerator has been multiplied by 20.

$$\text{TS,M-index}=\frac{20 \cdot mechanical\ parameter}{\sum_{1}^{10} CML\ impacts+10 \cdot costs} \qquad \text{Eq. 5.6}$$

The second index is defined as structural index (TS,S-index) and has been formulated with the scope of switching from the scale of the material unit volume (more suitable for producers) to that of a structure or of its elementary components. It has the aim of identifying the best material to be employed. For this purpose, not solely the mechanical characteristics are included, as many as relevant to the intended application, but also the durability performance indicators in order to describe the interaction of the material with the environment to which it is exposed, thus encompassing the degradation phenomena that can occur (including e.g., carbonation, chlorides attack, sulphate attack, freeze and thaw degradation). Also in this case, both numerator and denominator are normalized with respect to a reference solution (e.g. Ordinary Reinforced Concrete for the case of this study) to get a value around the unit. CML impacts and costs are related to the structure or to its components and not anymore on a cubic meter scale as for the TS,M-index. The TS,S-index is reported in Eq. 5.7 and is aiming at representing a practical and informed tool for making well-considered choices when selecting materials for large-scale applications.

$$\mathrm{TS,S-index} = \frac{\frac{\sum_1^n \text{durability parameters}}{n} + \frac{\sum_1^r \text{mechanical parameters}}{r}}{\sum_1^{10} CML\ impacts + 10 \cdot costs} \cdot 10 \quad \text{Eq. 5.7}$$

To summarize, when the calculated values of the TS,M-index or of the TS,S-index result higher than one, the assessed material is deemed to have a "holistic sustainability signature" more pronounced than the reference. On the contrary, if lower than one, it has to be regarded as less sustainable.

5.3.1 Thoroughgoing material and structural indices: application on case studies

The research herein reported has primarily focused on three distinct mix designs: an Ordinary Portland Cement Concrete (OPCC), a Ultra High Performance Concrete (UHPC), and what has been herein called Eco-UHPC. For the latter, CEM I, commonly employed so far in the formulation of this category of cementitious composites, has been replaced by CEM III with the primary aim of enhancing the sustainability signature at the material level. CEM III contains supplementary cementitious materials classified as by-products, such as blast furnace slag (Lo Monte and Ferrara, 2020; di Summa *et al.*, 2022c). Moreover, Eco-UHPC diverges from UHPC in its composition also due to the inclusion of polypropylene fibers, to mitigate the risk of spalling in the case of exposure to high temperatures. These fibers create a network that, when the matrix is subjected to temperatures exceeding 450ºC, has beneficial effects in mitigating explosive spalling to which UHPC is known to be sensitive. Table 5.1 provides an overview of the mix designs under evaluation. Additionally, the study has delved into the assessment of a specific structural application, i.e. of precast roof panels designed and supposedly manufactured employing the aforesaid concrete reported in Table 5.1; the structural characteristics of the panel replicate those of a product designed by RDC and produced by PREFFOR in Valencia, Spain. The collaboration with RDC originates from a research secondment, from March to June 2015, organized as part of the investigation project presented within this manuscript.

Table 5.1**:** Detail of the different mix designs assessed within this study

Components	**Eco-UHPC**	**UHPC**	**OPCC**
	kg/m^3		
Silica sand 0-0.5 mm	300	302	-

Silica sand 1-1.2 mm	700	600	-
Limestone sand 1-2 mm	-	-	211
Limestone sand 2-4 mm	-	-	897
Basalt aggregate 2- 5 mm	150	-	-
CEM 52.5 R type I + pozzolanic additions	0	1125	370
CEM III/A 42,5 N/SRC + pozzolanic additions	1000	-	-
Polypropylene SikaFiber M12	1	-	-
Water	152	160	150
Polycarboxylate Superplasticizer	28	30	3
Steel microfibres L=13 mm, d=0.2 mm	100	120	-
Aggregate 4/7	-	-	-
Aggregate 7/10	-	-	354
Aggregate 12/20	-	-	377

These panels, designed as simple supported beams over a 4.55 m span, have a width equal to 2.24 m, with a thickness depending on the performance of the specific mix design, aiming for a flexural capacity of the panel cross-section, equal to 2.45 kNm/m width. Specifically, the panels built with UHPC and Eco-UHPC, hereafter referred to as UHPC_panel and Eco-UHPC_panel respectively, have a total thickness of 35 mm, also complying with the requirements set by the producer on the acoustic performance of the element. In contrast, the panel made with Ordinary Portland Cement Concrete, denoted as the ORC_panel (with ORC standing for Ordinary Reinforced Concrete), is engineered with a thickness of 80 mm. While UHPC_panel and Eco-UHPC_panel achieve the aforesaid flexural capacity without the need for additional reinforcement besides the steel fibres, in the ORC_panel a primary flexural reinforcement consisting of ϕ 16 mm steel bars spaced at 250 mm intervals is needed, along with transverse ϕ 6 mm bars spaced at 1-meter intervals used to keep the longitudinal bars in place. Moreover, all panels are designed to withstand an XS1 exposure class, involving exposure to airborne salt but not direct contact with seawater, necessitating a 30 mm concrete cover for the reinforcement in the ORC_panel according to the current standards(Cen, 2005). Figure 5.1 details a 3D model of the ORC_panel.

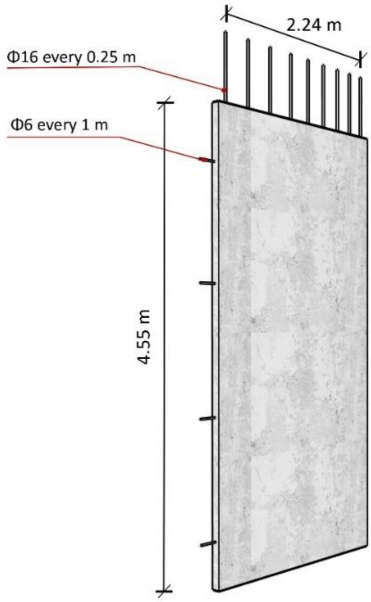

Figure 5.1: 3D model of ORC_panel.

5.3.1.1 LCA and LCC – system boundaries and outcomes of the assessed case studies

Environmental impact assessment is essential for the application of the proposed method. The sustainability assessment framework here discussed, centers on the 10-CML environmental impact categories, a methodology established by the Centre of Environmental Science at Leiden University (CML). This methodology operates as a midpoint approach, aiming to gauge environmental impacts at an intermediate stage. As a matter of fact, LCA analyses are made up of three key stages: inventory, midpoint assessment, and endpoint assessment. The CML methodology is positioned between the inventory and endpoint stages, focusing on characterizing environmental impacts associated with emissions or substances. It provides insights into environmental effects before reaching final human health or ecosystem outcomes. Again, as outlined in chapter 2, the methodology employs the following indicators:

(i) Global Warming Potential (GWP): this indicator measures the contribution to climate change in terms of CO_2-equivalent emissions;

(ii) Acidification Potential (AP): assesses the potential for acid rain formation and is expressed in sulfur dioxide (SO_2) or nitrogen oxides (NOx) equivalents;

(iii) Eutrophication (EP): evaluates the potential for nutrient enrichment in aquatic ecosystems and is reported in kg PO_4^{3-}-eq;

(iv) Ozone Layer Depletion (ODP): evaluates the potential for depletion of the ozone layer and is expressed in terms of CFC-11 equivalents and is measured in kg CFC-11-eq;

(v) Photochemical Oxidation (POCP): assesses the potential to create ground-level ozone, a key component of smog; and is reported in kg C_2H_4-eq;

(vi) Human Toxicity Potential (HTP):reported in kg 1.4-DCB eq., measures the potential for adverse human health effects due to exposure to toxic substances;

(vii) Freshwater Ecotoxicity Potential (FETP): evaluates, in terms of kg 1.4-DCB eq., the potential harm to aquatic ecosystems in freshwater bodies;

(viii) Terrestrial Ecotoxicity Potential (TETP): assesses the potential harm to terrestrial ecosystems, including soil and vegetation and is quantified in kg 1.4-DCB eq.;

(ix) Marine Aquatic Ecotoxicity Potential (METP): measures in kg 1.4-DCB eq. the potential harm to marine ecosystems;

(x) Abiotic Depletion (ADP): assesses the depletion of non-renewable resources, such as minerals and fossil fuels and is expressed in kg Sb eq.

The selection of the CML-IA methodology for the specific scope of this study is due to its ability to provide a comprehensive understanding of environmental consequences, which can have far-reaching implications for society (Vallance *et al.*, 2011; Amrutha and Geetha, 2020). This becomes especially relevant when considering vulnerable or marginalized populations and the potential for social disparities which can result as a consequence. As an example, to illustrate the societal impact of each of these indicators, the following considerations can be made:

(xi) GWP can lead to heat-related illnesses and deaths due to rising global temperatures;

(xii) AP can damage crops, potentially leading to reduced yields and increased food prices;

(xiii) EP can harm tourism and recreational industries due to algal blooms;
(xiv) ODP may increase the incidence of skin cancer;
(xv) POCP can exacerbate respiratory conditions such as asthma;
(xvi) HTP can result in occupational illnesses among workers;
(xvii) FETP can harm local fisheries, impacting livelihoods;
(xviii) TETP can affect the health of farmworkers and nearby residents;
(xix) METP can disrupt fishing industries and cause economic hardships in coastal communities;
(xx) ADP can lead to job losses in mining communities, with consequent economic instability (Amrutha and Geetha, 2020).

Each of these impacts has been calculated following ISO 14040 (UNI, 2021a) and ISO 14044 (UNI, 2021b)standards, using a cradle-to-gate system boundary for TS,M-index, extended until the A4 transport stage (from producer to worksite) defined in EN15804 (UNI, 2019) for TS,S index. Ecoinvent 3.6 has been used as the main data source for most of the raw materials, except for both type of cements, the admixture and the steel fibers for which the specific Environmental Product Declaration (EPD) of the manufacturer have been employed (IECA Instituto Espanol del cemento y sus aplicaciones, 2014; start2see Pty Ltd, 2016; Concrete and Associations, 2019; Instytut Techniki Budowlanej, 2021). The distances have been accounted according to the supply-chain of the company where concrete and panels are produced. More specifically, transport distances of 22 km have been accounted for sand and silica; 500 km for the basalt, 33 km for cement; 1,850 km for the pozzolanic additions; 32 km for polypropylene fibers and the superplasticizer, 1,500 km for the steel fibers. All the transports have been assumed as done by lorries, Euro 6 type.

With regard to the mixing process, a mixer similar to the one owned by the company has been taken into consideration with a capacity of 750 liters and an energy consumption of 22 kW in total, entirely drawn from the national grid. When assessing the breakdown of impacts associated with the sum of all CML-IA impacts for each mix design, certain crucial aspects stand out. In the case of the Eco-UHPC mix design, as it can be observed in Table 5.2 and Figure 5.2, the primary contributors to the overall impacts are the transportation of components (from the seller to where concrete is produced), accounting for approximately 27%. This can be attributed to the transportation of pozzolanic additions and steel fibers, covering distances of 1.850 km and 1.500 km, respectively. Additionally, CEM III constitutes a significant portion, totaling 17.6%. Comparatively, UHPC exhibits a similar pattern as shown in Table 5.3 and **Error! Reference source not found.**,

with a notable emphasis on the transportation of components, accounting for around 30% of the overall impacts. Cement, on the other hand, accounts for approximately 26% of the environmental burdens. This highlights the significance of embracing more sustainable alternatives to CEM I, like CEM III in contemporary practices, as well as the importance of employing appropriate allocation methods.
As a matter of fact, blast furnace slag, which is a component of CEM III, is considered a by-product according to current European regulations and carries a varying impact depending on the chosen allocation method, whether by mass or economic value. In stark contrast, the scenario shifts significantly when examining OPCC as clarified in Table 5.4 and Figure 5.4. Here, cement emerges as the predominant factor, contributing to a substantial 45% of the environmental impact, while the transportation of components is relatively minimal at 4%, owing to the absence of steel microfibers and pozzolanic additions in comparison to the previous mix designs. In this respect, it is worth remarking that the supply chain for the constituents of OPCC is notably widespread and consolidated. Thus, in order to promote and spread the use eco-friendly alternatives in construction, a similar level of efficiency is essential, particularly when dealing with advanced construction materials. Additionally, it is important to consider that this type of comparison does not account for the environmental burdens associated with the steel reinforcing bars for OPCC, while steel fibers are accounted in UHPC. Thus, when 1 m^3 is assessed as Functional Unit, OPCC appears to have a better environmental performance. Both UHPC and Eco-UHPC exhibit an increase in environmental ramifications of at least 120%, with peaks in abiotic depletion exceeding 400%, as shown in Figure 5.5. However, this highlights the potential for significant improvements in the environmental performance of UHPC and Eco-UHPC through a strategic reevaluation of raw material supply chains. At the same time, it is essential to acknowledge that comparing different materials solely on a cubic meter scale can be misleading: to gain a comprehensive understanding of their environmental sustainability when scaled up for specific uses and it's then necessary to transit from laboratory-scale assessments to real-world structural applications.

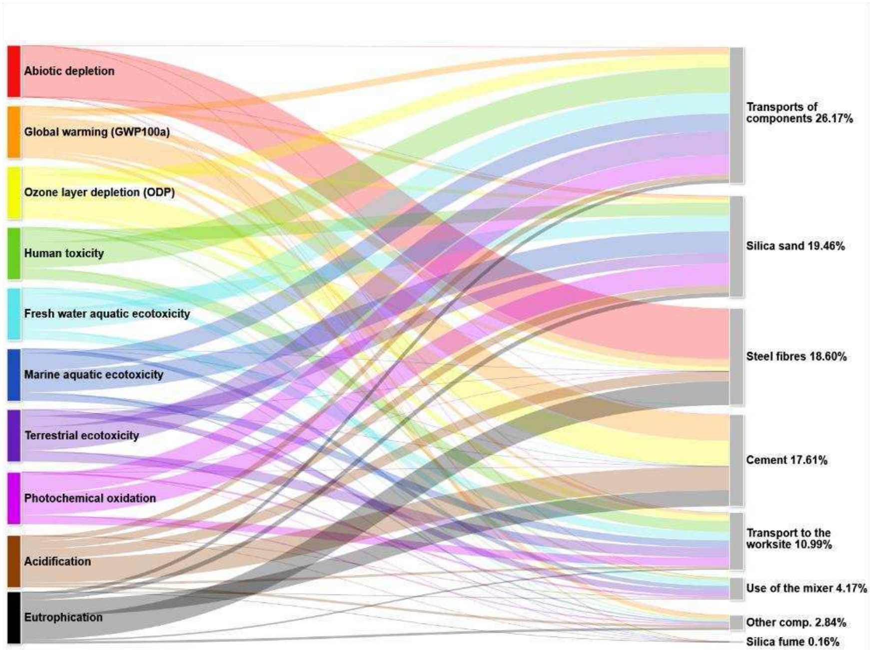

Figure 5.2: Percentage influence of the main Eco-UHPC components and processes on the sum of all CML-IA impacts.

Table 5.2: Breakdown of impacts by main components and processes. Results are referred to 1 m^3 of Eco-UHPC. “Other components” include: aggregates, basalt, water, superplasticizer and polypropylene fibers. “Transport of components” accounts for the transport from the supplier to the concrete plant. Transport of the final mix from the concrete plant to the worksite is included in the column “Transport to the worksite”.

	Abiotic depletion	Global warming
Cement	0.03	50.23%
Steel microfibres	98.25%	14.98%
Silica sand	0.21%	6.85%
Pozzolanic additions	0.00%	0.07%
Other components	0.02%	8.23%
Use of the mixer	0.02%	0.51%
Transports of components	1.03%	13.48%
Transport to the worksite	0.43%	5.66%

	Ozone layer depletion	Human toxicity	Fresh water aquatic ecotoxicity	Marine aquatic ecotoxicity	Terrestrial ecotoxicity	Photoch. oxidation	Acidific.	Eutrophic.
Cement	49.22%	0.00%	0.00%	0.00%	0.00%	0.00%	45.60%	31.05%
Steel microfibres	7.99%	0.00%	0.00%	0.00%	0.00%	0.00%	19.16%	45.57%
Silica sand	6.57%	24.32%	30.01%	41.51%	21.24%	40.97%	14.38%	8.53%
Pozzolanic additions	0.11%	0.28%	0.27%	0.24%	0.25%	0.25%	0.10%	0.08%
Other components	0.49%	1.44%	2.30%	2.60%	1.91%	2.15%	4.70%	4.56%
Use of the mixer	0.75%	3.92%	10.87%	8.17%	11.89%	3.41%	1.30%	0.89%
Transports of components	24.56%	49.32%	39.82%	33.43%	45.57%	37.48%	10.39%	6.56%
Transport to the worksite	10.32%	20.72%	16.73%	14.05%	19.14%	15.75%	4.36%	2.76%

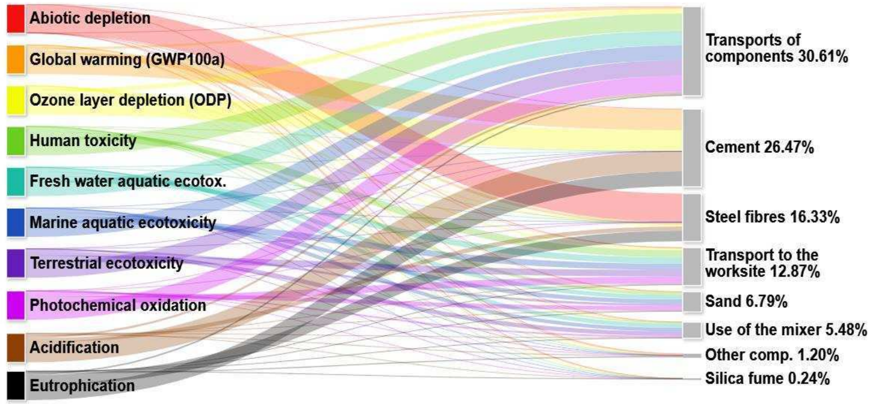

Figure 5.3: Percentage influence of the main UHPC components and processes on the sum of all CML-IA impacts.

Table 5.3: Breakdown of impacts by main components and processes. Results are referred to 1 m³ of UHPC. "Other components" include: aggregates, basalt, water and superplasticizer. "Transport of components" accounts for the transports from the supplier to the concrete plant. Transport of the final mix from the concrete plant to the worksite is included in the column "Transport to the worksite".

	Cement	Steel microfibres	Silica sand	Pozzolanic additions	Other components	Use of the mixer	Transports of components	Transport to the worksite
Abiotic depletion	0.03%	98.41%	0.12%	0.00%	0.01%	0.02%	0.98%	0.41%
Global warming	73.34%	9.23%	0.90%	0.05%	4.93%	0.31%	7.91%	3.33%
Ozone layer depletion	71.98%	5.09%	1.22%	0.08%	0.01%	0.48%	14.89%	6.26%

Eutrophic.	Acidific.	Photoch. oxidation	Terrestrial ecotoxicity	Marine aquatic ecotoxicity	Fresh water aquatic ecotoxicity	Human toxicity	
50.75%	68.60%	0.00%	0.00%	0.00%	0.00%	0.00%	**Cement**
36.22%	14.38%	0.00%	0.00%	0.00%	0.00%	0.00%	**Steel microfibres**
1.90%	2.35%	14.32%	7.72%	14.81%	14.43%	10.15%	**Silica sand**
0.07%	0.09%	0.45%	0.36%	0.43%	0.42%	0.42%	**Pozzolanic additions**
3.28%	3.05%	0.08%	0.27%	0.17%	0.15%	0.06%	**Other components**
0.71%	0.97%	5.36%	14.82%	12.94%	14.26%	4.96%	**Use of the mixer**
4.97%	7.43%	56.17%	54.09%	50.44%	49.80%	59.43%	**Transports of components**
2.09%	3.12%	23.61%	22.74%	21.21%	20.94%	24.98%	**Transport to the worksite**

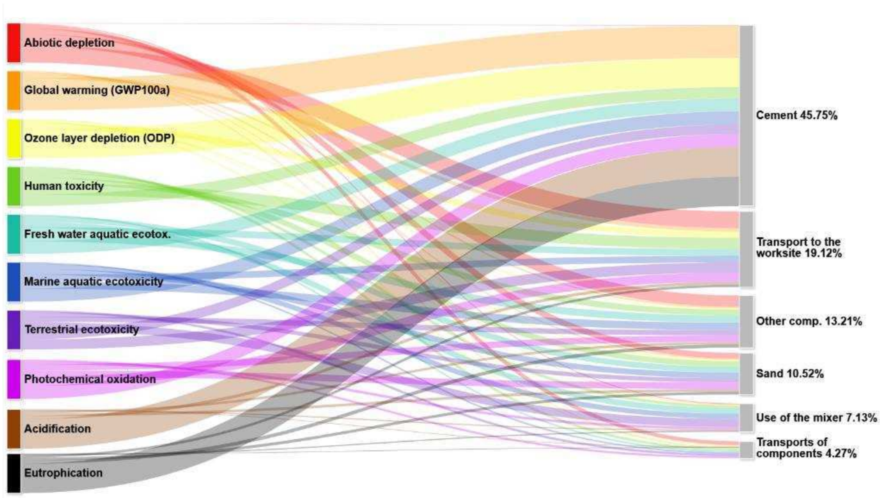

Figure 5.4: Percentage influence of the main OPCC components and processes on the sum of all CML-IA impacts

Table 5.4: Breakdown of impacts by main components and processes. Results are referred to 1 m³ of OPCC. “Other components” include: aggregates, basalt, water and superplasticizer. “Transport of components” accounts for the transports from the supplier to the concrete plant. Transport of the final mix from the concrete plant to the worksite is included in the column “Transport to the worksite”.

	Abiotic depletion	Global warming	Ozone layer depletion
Cement	1.33%	87.55%	78.87%
Limestone sand	15.06%	3.10%	3.84%
Other components	29.36%	4.13%	2.94%
Use of the mixer	1.76%	0.88%	1.23%
Transports of components	9.59%	2.11%	3.63%
Transports to the worksite	42.91%	9.45%	16.27%

	Human toxicity	Fresh water aquatic ecotoxicity	Marine aquatic ecotoxicity	Terrestrial ecotoxicity	Photoch. oxidation	Acidific.	Eutrophic.
Cement	41.97%	49.88%	51.67%	33.42%	50.05%	86.95%	88.36%
Limestone sand	20.18%	22.13%	22.45%	14.71%	25.43%	7.79%	8.27%
Other components	21.79%	27.76%	29.22%	18.71%	24.62%	7.05%	10.26%
Use of the mixer	8.03%	17.80%	15.97%	22.98%	7.75%	2.63%	2.51%
Transports of components	9.13%	5.90%	5.91%	7.96%	7.71%	1.90%	1.67%
Transports to the worksite	40.87%	26.41%	26.45%	35.64%	34.50%	8.52%	7.46%

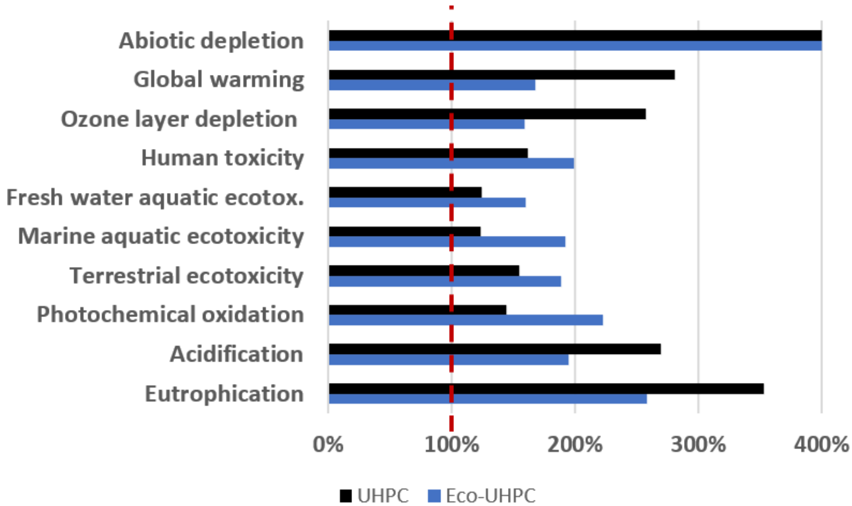

Figure 5.5: Impacts of 1 m³ of Eco-UHPC and UHPC relative to 1 m³ of OPCC.

When the assessment is made at the level of the structural element, i.e. the roof panel in this case study, a different pattern is observed. Starting with the UHPC_panel, it outperforms the Eco-UHPC_panel and ORC_panel in 5 out of 10 CML-IA impact indicators. Notably, when focusing on Abiotic Depletion, the ORC-panel records the lowest value, showcasing reductions of up to 97% when compared to Eco-UHPC_panel and UHPC_panel, respectively. In contrast, the UHPC_panel, along with the ORC_panel, exhibits less favorable performance in terms of Global Warming Potential, where the Eco-UHPC_panel highlights a reduction of up to 40% when compared to UHPC_panel.

Similarly, the Eco-UHPC_panel demonstrates noteworthy reductions, consistently surpassing 30%, when compared to the other two alternatives in Ozone Layer depletion. With regard to Human Toxicity, Freshwater Aquatic Ecotoxicity, Marine Aquatic Ecotoxicity, Terrestrial Ecotoxicity, and Photochemical Oxidation, the UHPC_panel presents the lowest environmental impact, achieving reductions of approximately 55% when compared to the ORC_panel. However, a different scenario emerges in the case of Acidification and Eutrophication, where the Eco-UHPC_panel and ORC_panel excel respectively. More specifically the first reaches reductions up to 25% when compared to the UHPC_Panel while the second one presents improvements of 30% in comparison to the UHPC_panel. These outcomes are summarized in Figure 5.6 where the Eco-UHPC_panel and UHPC_panel are both compared to the ORC_panel.

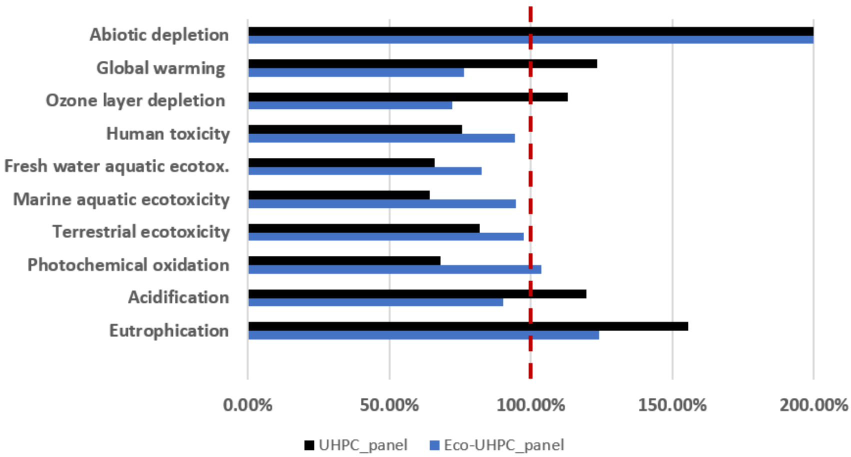

Figure 5.6: Impacts of the Eco-UHPC _panel and UHPC_panel relative to the ORC_panel.

To better understand the relevant differences among the three different investigated panel solutions, a more in depth study aimed at identifying the components that have the most significant influence on each environmental impact category has been carried out.

Figure 5.7 and Figure 5.8 detail the breakdown per each impact category. With regard to Abiotic Depletion, steel fibers have a pivotal importance, driving nearly 100% of the impact for the Eco-UHPC_panel and UHPC_panel. This highlights the pressing need to refine their production processes to be less harmful for the environment. These potential improvements can be also enhanced by a revision of the entire supply chain, to obtain, as an example, reduced distances for the transportation of the fibers within the countries. In contrast, ORC_panel charts a different course, with the transport to the worksite as primary influencer, accounting for approximately 43%. This difference between the three panel typologies is also due to the fact that as a consequence of the reduced thickness, the weight of UHPC and Eco-UHPC panels is almost half of ORC_panel (implying fewer emissions since transports are estimated in tons per kilometer, typical unit of measure of freight transport). At the same time, it highlights the critical importance of efficient logistics in minimizing environmental impact.

Focusing the attention on the concern of Global Warming, cement emerges as a central player, contributing approximately 50% of the impact for the Eco-UHPC_panel. Similarly, cement can be observed to be the main contributor to a wide spectrum of environmental impacts for the ORC_panel: Ozone Layer Depletion, Human Toxicity, Freshwater Aquatic Ecotoxicity, Marine Aquatic Ecotoxicity, Photochemical Oxidation, Acidification, and Eutrophication. All of these are predominantly driven by cement, with percentages ranging from 29% to 81%. This could be linked to several factors such as the release of pollutants during cement production, such as sulfur dioxide, for what concerns the ozone layer depletion, Human toxicity, photochemical oxidation and acidification, with consequent risk of acid rains and soil acidification. Similarly, its overall influence on freshwater ecotoxicity, marine aquatic ecotoxicity and eutrophication can be explained with the runoff of contaminants into freshwater sources and marine environments that can cause excessive nutrient levels.. This once more remarks the profound influence of the type of cement employed in the specific mix design. In the case of Ozone Layer Depletion (ODP), its influence remains significant, accounting for up to 72% of the impact, for both Eco-UHPC_panel and UHPC_panel.

Delving into Human Toxicity, it becomes evident that the transportation of components from the producer to the concrete plant plays a pivotal role, representing up to 59% of the impact for both UHPC panels. A similar scenario unfolds when considering Freshwater Aquatic Ecotoxicity. Furthermore, Marine Aquatic Ecotoxicity sees a notable impact from silica sand, accounting for approximately 42% for the Eco-UHPC_panel. The transportation of components continues to exert a significant influence on both UHPC panels in the case of Terrestrial Ecotoxicity. As for the ORC_panel, it is primarily affected by the transport from the concrete plant to the worksite. Photochemical Oxidation registers silica sand and the transport of components as main responsible for the impacts of Eco_UHPC and UHPC respectively, while cement plays a leading role in driving the Acidification for both UHPC panels. Finally, Eutrophication primarily finds its roots in steel fibers and cement for Eco_UHPC and UHPC panels, respectively.

As for the Life Cycle Costing (LCC), an analysis of the construction market in Spain, where the manufacturer of the panel has its headquarter, has been carried out. Therefore, by employing a cradle-to-gate system boundary for both the mix-design and the panels, a cost of 111 € per cubic meter of OPCC (mainly dictated by cement that accounts for overall 60% of the final price) has been first estimated. Then, a cost of 753 € and 689 € has been factored for 1 m3 of Eco-UHPC and UHPC respectively, where the main cost components are linked to the fibers that account for 44% and 52% respectively. The difference between Eco-UHPC and UHPC is mainly caused by the presence of basalt in the Eco-UHPC, that accounts for overall 20% of the price. A different situation is pictured for the panels since a production cost equal to 363 € was estimated for the ORC_panel while 241 € and 264 € have been appraised for the UHPC_panel and Eco-UHPC panel respectively. Also in this case steel fibers contribute for 40% and 52% of the price for Eco-UHPC_panel and UHPC_panel respectively, while 75% of the cost must be attributed to the reinforcement in the case of the ORC_panel. The cost difference between the UHPC and ORC panels can be explained by the significantly lower volume of the Eco-UHPC_panel and UHPC_panel (0.35 m3 for UHPC versus 0.80 m3 for the ORC_panel) but also to the fact that, while UHPC (whose unit cost per volume already includes the fibres) can be employed for structural elements as it is, reinforcing steel bars must be taken into account for the ORC_panel. This aspect gains further significance when considering that Eco-UHPC panels include 35 kg of steel fibres while ORC_panels contain 85 kg of steel reinforcement bars, the cost of which (3.30 euro per kg) must be added in the final expenses assessment.

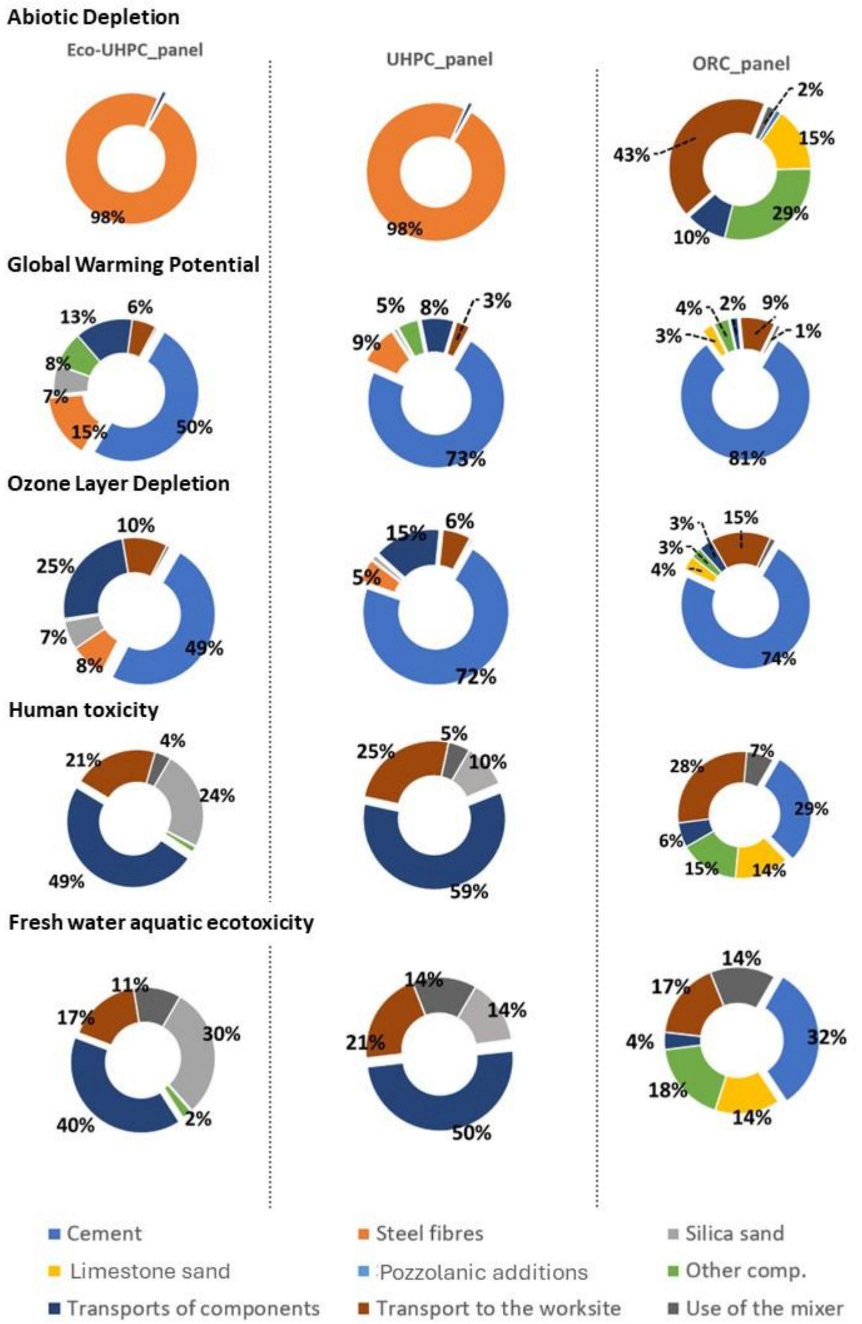

Figure 5.7: Percentage influence of the main components and processes of Eco-UHPC_panel, UHPC_panel and ORC_panel for 5 out of 10 CML-IA impact indicators.

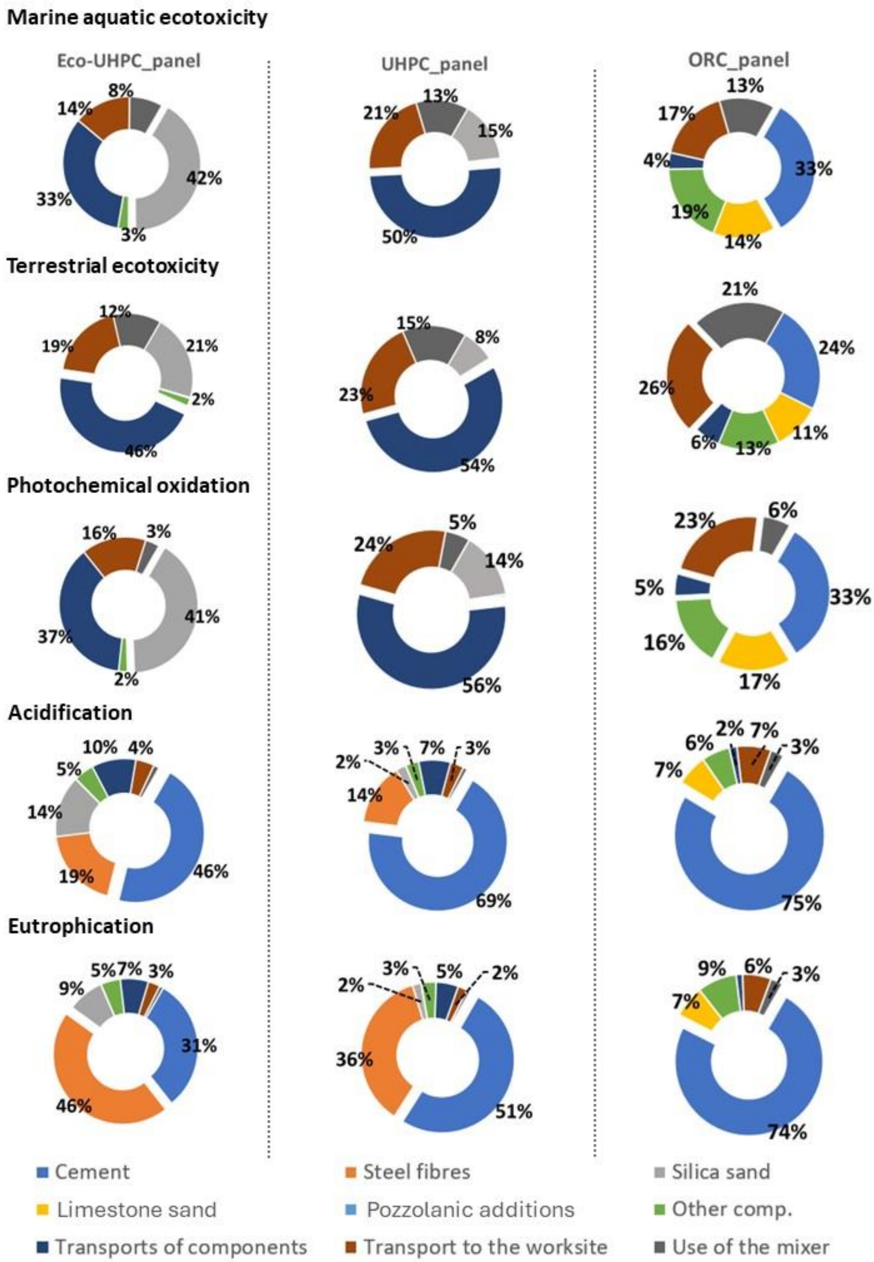

Figure 5.8: Percentage influence of the main components and processes of Eco-UHPC_panel, UHPC_panel and ORC_panel for 5 out of 10 CML-IA impact indicators.

5.3.1.2 Thoroughgoing material and structural indices – results and discussion

The coherence of both indices formulated in section 3 has been finally assessed according to the specific case studies. Regarding the TS,M-index, the parameters referring to 1 m^3 of Eco-UHPC and UHPC have been normalized to those of 1 m^3 of OPCC. Similarly, for what concerns the Eco-UHPC_panel and UHPC_panel in the case of TS,S-index, their parameters have been normalized to those of the ORC_panel. This has been done with the scope of having a final value around the unit as stated in section 5.3. The LCA and LCC outcomes analyzed in section 5.3.1.1 have been employed for the scope of both indices. Additionally, 40 N/mm^2 and 150 N/mm^2 have been taken as the compressive strength of OPCC and UHPC or Eco-UHPC respectively for the scope of the TS,M index. Thus, by implementing these values in Formula 6, a TS,M-index equal to 0.41 and to 0.44 has been calculated for UHPC and Eco-UHPC respectively, indicating a reduced benefit for employing the UHPC alternatives in comparison to OPCC when the cubic meter scale is taken into consideration. This can be attributed to the parameters in Eq. 5.6. Specifically, the environmental ramifications associated with 1 m^3 of UHPC and Eco-UHPC are, as detailed in the previous paragraph, mostly higher than those of 1 m^3 of OPCC, while the final cost is substantially increased for both UHPC mix designs when compared to the reference. However, it is worth emphasizing that UHPC can be employed without the need for steel reinforcement bars, unlike ORC. Therefore, an analysis, solely limited to the cubic meter scale, does not account for these distinctions.

A different scenario emerges when considering the structural index for the panels above described and exposed to a chloride-rich environment, as assumed in this research. Here, the chloride diffusion coefficient (D_{app}) has been employed since it is a key parameter in designing long-lasting concrete structures, making it essential for structural integrity, safety, and sustainability, especially in environments prone to chloride exposure. As a matter of fact, chlorides (often from deicing salt or seawater) can penetrate the concrete matrix, initiating steel reinforcement corrosion, weakening structures, and shortening their service life with direct effects on the overall environmental and cost sustainability as outlined in (Caruso *et al.*, 2022; di Summa *et al.*, 2022b,c). Thus, D_{app} values of 10^{-11} m/s^2 and 10^{-13} m/s^2 have been used for ORC_panels and Eco-UHPC_panel or UHPC_panel, respectively, based on previous investigations(Alonso and Sanchez, 2009; Liu *et al.*, 2015;

Cuenca *et al.*, 2022; di Summa *et al.*, 2022c). Furthermore, not only the compressive strength but also tensile strength has been considered as a key structural parameter, in the sight, e.g., of having the cracking moment as a representative structural performance parameter in limit state design for an aggressive scenario as the one herein analysed. While the same values as above have been kept for compressive strength, tensile strength values of 3.5 N/mm² and 10 N/mm² have been used respectively for ORC_panels and UHPC/Eco-UHPC panels. Eq. 5.8 provides a clearer understanding of how Formula 7 has been adapted for the purpose of this study.

$$\mathrm{TS,S-index} = \frac{-\mathrm{Log(Dapp)} + \frac{\text{compressive strength} + \text{tensile strength}}{2}}{\sum_{1}^{10} CML\ impacts + 10 \cdot costs} \cdot 10 \qquad \text{Eq. 5.8}$$

As it is possible to observe, the negative logarithm of D_{app} has been employed for the scope of this study, due to the fact that lower values of the chlorides diffusion coefficient imply better performance in terms of resistance against chloride penetration. This leads to a situation that is entirely distinct from the cubic meter scale analysis. More specifically, by implementing all the values before mentioned besides the LCA and LCC outcomes detailed in paragraph 5.3.1.1, the TS,S-index results equal to 1.36 for UHPC_panel and 1.53 for Eco-UHPC, indicating a significantly improved overall sustainability, with some further improvement when Eco-UHPC mix design is employed for the specific purpose. Table 5.5 summarizes the outcome of both indices besides reporting the relevant parameters here taken into consideration.

Table 5.5: Used parameters and obtained results for material index (TS,M-index) and structural index (TS,S-index).

Parameters taken into account	**TS,M-index**	**TS,S-index**
Compressive strength	40 MPa (OPCC), 150 MPa (Eco-UHPC and UHPC)	40 MPa (ORC_panel), 150 MPa (Eco-UHPC and UHPC_panel)
Tensile strength	-	3.5 MPa (ORC_panel), 10 MPa (Eco-UHPC_panel and UHPC_panel)
Cost	111 €/m³ (OPCC), 753 €/m³ (Eco-UHPC) 689 €/m³ (UHPC)	363€ (ORC_panel) 264€ (Eco-UHPC_panel) 241€ (UHPC_panel)

Parameters taken into account	TS,M-index	TS,S-index
D_{app}	-	10^{-11} m/s² (ORC_panel) 10^{-13} m/s² (Eco-UHPC_panel and UHPC_panel)
Outcome	**0.41** for **UHPC** and **0.44** for **Eco-UHPC**	**1.36** for **UHPC_panel** and **1.53** for **Eco-UHPC_panel**

It is worth remarking that the proposed indices should be regarded as an adaptable open protocol. This adaptability is crucial as it allows for adjustments on a case-by-case basis, considering both the specific boundary conditions and the specific purpose for which these tools will be employed. As an example, one option could be represented by the integration of a weighting system for the ten CML impact indicators at the denominator for both TS,M and TS,S indices. This enhancement involves multiplying the results of each impact category by weighting factors. As outlined by ISO 14044 (UNI, 2021b), the processes of weighting is an optional phase in the LCA assessment. However, it must be highlighted that any weighting scheme is fundamentally influenced by value choices, entwined with policy and cultural preferences. Thus, it is challenging achieving a consensus on weighting mechanisms, not only in the realm of LCA but also in many multicriteria approaches. Moreover, for what concerns the CML-IA methodology, a comprehensive literature review revealed a notable gap in this regard with an absence of a universally recognized weighting scheme. A recent investigation, as outlined in a technical report commissioned for the European community (Sala *et al.*, 2018), has scrutinized weighting approaches for prioritizing and aggregating results across 16 environmental impact categories within the life cycle-based Environmental Footprint (EF) methodology. Consequently, given the imperfect correspondence between the 10 CML impact indicators and the EF ones, to use the same weighting factors (expressed in percentage), both sets of indicators have been subdivided into nine subgroups. This approach facilitated the calculation of specific weights assigned to each group of EF indicators, and the same weights were applied to the corresponding CML sets. This ensured a methodologically coherent and comparable framework. Further details of the groups and the specific weights can be found in **Error! Reference source not found.**

Table 5.6: Groups subdivision and weight for both CML-IA and EF indicators according to (Sala et al., 2018)

Subgroups	CML-IA indicators	EF indicators	Assigned weight
Resource depletion	Abiotic depletion	- Resource use, mineral and metals - Resource use, fossil - Land use - Water use	32.32%
Climate change	Global warming potential	Climate change	21.06%
Ozone depletion	Ozone layer depletion	Ozone depletion	6.31%
Human toxicity and Human health	Human toxicity	- Human toxicity, cancer effect - Human toxicity, non cancer effects - Particulate matter - Ionizing radiation, human health	17.94%
Acidification	Acidification	Acidification	6.20%
Eutrophication and aquatic ecosystem impact	- Eutrophication - Fresh-water aquatic eco-toxicity - Marine ecotoxicity	- Eutrophication, freshwater - Eutrophication, marine - Ecotoxicity, freshwater	7.68%
Terrestrial ecosystem impact	Terrestrial ecotoxicity	Eutrophication terrestrial	3.71%
Air quality and smog formation	Photochemical oxidation	Photochemical ozone formation	4.78%

By applying these weighting factors alongside with parameters of Table 5.5 TS,S-index, it has been possible to get a final value of 3.07 and 3.21 for UHPC_panel and Eco_UHPC_panel respectively, highlighting the improvements when Eco-UHPC mix design is employed for the panels. This, despite the highest influence assigned to the abiotic depletion which registered increased value for both Eco-UHPC_panel and UHPC_panel compared to ORC_panel. Then, to further illustrate the flexibility of the indices, another variation of TS,S-index has been assessed by incrementing the integrated structural characteristics. The improved version is presented in Eq.5.9 . This adaptation involves the inclusion of crack opening at the nominator (normalized with respect to the reference solution), alongside the weights scheme for the sustainability indices previously detailed. Crack opening has -1 as exponent since a lower opening corresponds to a better performance. The adjustment is intended to refine the accuracy the index, offering a more comprehensive understanding of the structural integrity besides sustainability of the panels. Thus, under the SLS wind load of 0.65 kN/m calculated from the factored ultimate moment capacity, a crack opening (w_k) equal to 0.01 mm has been estimated for UHPC_panel and Eco-UHPC_panel and 0.17 mm for ORC_panel (both below the lowest limit of 0.2 mm allowed by the Eurocode (Cen, 2002)). These values led to calculate 6.37 and 6.66 as TS,S-index for UHPC_panel and Eco_UHPC panels respectively, showing improvements in comparison to ORC_panel.

$$\mathrm{TS,S-index} = \frac{-\mathrm{Log(Dapp)} + \frac{\text{compressive strength}+\text{tensile strength}+(\textit{crack opening})^{-1}}{3}}{\sum_{1}^{10} \textit{weighted CML impacts} + 10 \cdot \textit{costs}} \cdot 10 \quad \text{Eq.5.9}$$

As said, what has been herein proposed, must be intended as a first attempt of an open protocol to be adjusted according to the needs. As an example, a complete different version of TS,S-index could incorporate, in the numerator, a parameter equal to the design resistant bending moment divided by the thickness of the panel, instead of other structural design parameters as before done. This parameter must be normalized to a reference as well. In this case the index appears, in its general form, as in Eq.5.10. More specifically, in the case of an environment rich in chlorides, by assuming the negative logarithm for the chlorides diffusion coefficient and taking advantage of the LCA and LCC outcomes above reported, it is possible to obtain Eq. 5.11. Hence, a final value of 2.47 and 2.45 for UHPC_panel and Eco-UHPC_panel can be calculated respectively, confirming one more time the enhanced convenience in employing the Eco_UHPC mix design to manufacture such panels and contributing to validate the reliability and robustness of the methodology here proposed, even with a change in the parameters within the numerator.

$$\text{TS, S–index} = \frac{\frac{\sum_1^n \text{durability parameters}}{n} + \frac{\sum_1^r \frac{\text{designed structural performance}}{\text{relevant dimension of the structural element}}}{r}}{\sum_1^{10} weighted\ CML\ impacts + 10 \cdot costs} \cdot 10 \quad \text{Eq.5.10}$$

$$\text{TS, S–index} = \frac{-\text{Log(Dapp)} + \frac{\text{resistant bending moment}}{\text{thickness of the panel}}}{\sum_1^{10} weighted\ CML\ impacts + 10 \cdot costs} \cdot 10 \quad \text{Eq.5.11}$$

5.4 Key Exploitable Results of this research (KERs)

This research is focused on the assessment of environmental and costs benefits of advanced construction materials to make adequate choices during the design phase. Due to this, the obtained results represent an important cornerstone also to favour the commercialization of these innovative composites, helping to shape an efficient market strategy able to intercept the needs of the customers. Life Cycle Costing has a key role in this regard, demonstrating that the use of a novel material is not only feasible, but also more convenient. In this perspective, it is worth defining the Key Exploitable Results (KERs) deriving from this investigation.

A KER can be defined as a significant outcome that holds substantial potential for exploitation or applications such as commercialization, policy development, further research etc. Considering the work presented in the previous chapters, the key exploitable results reported in Table 5.7 and Table 5.8 can be addressed. For each of them, a brief description is provided, besides the targeted users and the Technology Readiness Levels (TRL). TRL is a systematic measure utilized to evaluate the maturity of a specific technology, spanning from its laboratory conceptualization to its full-scale deployment in practical applications. TRL is employed in research and development projects across various sectors and its scale spans across nine levels, each representing distinct stages of technological advancement: from initial observation and concept formulation (TRL 1 and 2) to final deployment and successful mission operations (TRL 8 and 9). TRL assessments offer a standardized framework for assessing technological progress, aiding decision-making, prioritizing investments, and facilitating the transition of technologies from development to implementation. Guidelines for practitioners on how to effectively utilize the KERs are also presented in Table 5.7 and Table 5.8.

Table 5.7: Key Exploitable Result 1

KER-1	Database of durability parameters for service life prediction.
Type	List of all the parameters used, according to the different exposure conditions, for the scope of LCA and LCC analyses.
Current TRL	5 - validation in relevant environment (data have been used already for real-life structures).
Brief description	Durability parameters play a crucial role in estimating the service life of a product or system, making them essential for effective maintenance planning and sustainability analyses. By collecting and analyzing these parameters, it is possible to assess the expected lifespan of a product or system. Moreover, by understanding the durability parameters, the failures, the downtimes and the costs of the maintenance activities can be taken into account for the sustainability analyses purpose. The parameters are then indispensable to evaluate environmental impacts, resource consumption and waste generation over time and costs. In summary, they provide valuable insights that enable proactive maintenance planning and informed decision-making, ultimately enhancing the efficiency, reliability and environmental performance of products and systems.
Targeted users	The KER-1 caters to two primary user groups. The first group consists of material developers, such as the one studied in the framework of the SMARTINCS project (Self-Healing concrete). They could be interested in exploring and analyzing the properties of the materials they are developing, making the customers aware about suitability, durability and performance of their products. The second group includes individuals or organizations seeking to demonstrate the sustainability credentials of the materials they employ, especially when

	participating in public tenders or competitive processes. By utilizing the database they can gather concrete data and evidence to showcase the eco-friendliness, energy efficiency and overall sustainability of their chosen materials, adding value to their work and improving their chances of success in tenders. This will allow them to be aligned with the increasing demand for sustainable practices across various industries.
Innovation compared with the current state of the art	The novelty of the materials under study brings about a significant challenge: the absence of an existing database with relevant information for the service life estimation. This uniqueness makes this KER-1 crucial for the development of LCA and LCC analyses, which are still relatively limited in the field of advanced construction materials. The lack of pre-existing data necessitates careful and thorough data collection, characterization and evaluation to accurately assess the environmental impact, economic viability and overall sustainability of these materials. By overcoming this challenge and generating comprehensive data, the way for more robust LCA and LCC analyses, enabling better-informed decision-making and promoting the adoption of sustainable materials in various applications, is paved.
Range of use or limitations for this KER	Only for advanced materials like the ones here presented and when subjected to different environmental conditions. The final users must be able to choose the specific data according to the boundary conditions of the case study of their interest.
Practitioners Guideline	Data must be employed for the specific service life prediction that can differ case by case, according to the specific boundary conditions. It is not possible to give a “general” guideline but the targeted users must be able to make an efficient use of the data according to the specific case study.

Table 5.8: Key Exploitable Result 2

KER-2	Database of costs and environmental impacts derived from LCA and LCC analyses.
Type	List of all the LCA and LCC databases obtained so far, according to the different assessed technologies.
Current TRL	5 - validation in relevant environment (data have been used already for real-life structures).
Brief description	The data collected for LCA and LCC analyses plays a vital role in conducting reliable assessments, especially when considering the upscaling of laboratory-produced materials to industrial production. The importance of these data lies in its ability to provide an accurate representation of the environmental and economic impacts associated with the materials at an industrial scale. By gathering and analyzing the data collected so far, it becomes possible to build a robust and comprehensive library of product information. This expanded database allows for more accurate predictions and assessments of the environmental performance, resource consumption and economic viability of these materials when produced on a larger scale. Having reliable and up-to-date data is crucial for stakeholders, including researchers, industry professionals, and policymakers, as it enables them to make informed decisions regarding the development, adoption, and commercialization of these novel materials. Additionally, the availability of such data supports transparency, credibility, and comparability in sustainability evaluations and facilitates the transition towards more sustainable industrial practices.
Targeted users	The KER-2 appeals to two primary user groups: material developers, particularly those involved in studying materials such as the ones assessed in the SMARTINCS framework and individuals or organizations aiming to demonstrate the sustainability

	of their product/material, especially in the context of public tenders. Additionally, the specific KER is also valuable for those operating in the development of Environmental Product Declarations (EPDs). Users can gather data and evidence to showcase the eco-friendliness and sustainability of their materials. This enhances the value of their work, increases their chances of success in tenders and facilitates the creation of comprehensive EPDs, contributing to transparent and sustainable practices in various industries.
Innovation compared with the current state of the art	The novelty of the materials poses a significant challenge in developing LCA and LCC analyses due to the lack of an existing database. This uniqueness not only highlights the novelty the KER-2 but also makes it distinct within the field. Consequently, this presents an opportunity to delve deeper into their environmental performance and economic viability, paving the way for the development of comprehensive Environmental Product Declarations (EPDs). As EPDs are currently absent for self-healing concrete, these databases can contribute to filling this gap and provide valuable information for stakeholders seeking to evaluate the sustainability aspects of these materials.
Range of use or limitations for this KER	Only advanced construction materials studied and developed within the SMARTINCS project. They can also be re-adapted for similar technologies but further considerations are then needed.
Practitioners Guideline	Data must be employed for the LCA and LCC specifically developed for one of the products studied within the framework of Smartincs. It is not possible to give a “general” guideline but the targeted user must be able to make an efficient use of the data according to the specific case study.

5.4.1 Intellectual Property Rights (IPR) strategy

An open policy is considered the best Intellectual Property Rights (IPR) strategy to be assumed: all the outlined results must be shared and communicated as much as possible. Doing this, it will be easier to convince and to penetrate a market that is still too much dependent on traditional solutions.

5.4.2 Potential business unit and market attractiveness: how to search results for the identified needs

A consultancy service could be a potential business unit that could leverage the defined Key Exploitable Results. It would focus on delivering expert support and specialized services to customers engaged in researching, developing, and implementing innovative construction materials. This consultancy service would also offer advice and assistance in areas such as material selection, testing and evaluation, regulatory compliance, sustainability considerations, and market analysis. Scope is to help clients to navigate the complexities of developing and introducing novel construction materials, ultimately supporting them in achieving their goals of innovation, performance improvement, and market success. As an example, the consultancy service could help in developing a proper business plan, predicting the payback time of an investment due to the use of advanced construction materials. Construction companies interested in investing part of their annual budget in innovation as well as producers of components/materials for which it is compulsory to provide an Environmental Product Declaration (EPD) are the potential clients to be reached with the identified business unit. Furthermore, while continuous dissemination efforts are essential to engage companies interested in economic consulting services, it's crucial to note that those seeking Environmental Product Declarations (EPDs) are obliged by current regulations to obtain such documentation. Therefore, to engage them, it will be just sufficient to offer not only a service which nobody else could develop (due to the lack of data, as the ones related to the self-healing components) but also offering competitive pricing aligned with market standards. However, it must be emphasized that the economic consulting service will require a prior study regarding the framework in which it will be offered (i.e. there will be, for sure, less information regarding countries out of Europe since SMARTINCS studies were mainly developed in EU zones). Below there is a PEST analysis which better analyzes the context in which the strategic business unit could be developed.

Table 5.9: PEST analysis for the identified business unit.

POLITICAL	ECONOMIC	SOCIAL	TECHNOLOGICAL
The political aspects, especially due to the implications related to the COP26 agreement, will, for sure, favor the growth of this business unit. This, thanks to the fact that the sustainability will become a crucial aspect, even for the construction sector, implying that not only more sustainable material will be needed but also the involved companies will be forced to allocate part of their budgets in this regard for the upcoming years.	COP26 agreement will affect not only the political choices but, consequently, also the market ones. This is also due to the increasing awareness regarding the sustainability implications. This will generate a rising need to provide sustainability certificates (EPDs) for materials/components (not only the self-healing ones) but also to properly shape the investment plans for the upcoming years. The consequence will be a continuous growing need for the provided business unit.	As stated before, the dissemination activities will be needed not only to spread information about the self-healing technologies but also to consequently create the demand for their use. This will allow to shape a socio-environment characterized by an increasing awareness regarding the sustainability issue where the business unit here assessed will be crucial.	The technological improvements will continuously increase the effectiveness of the self-healing technologies making them more accessible for the users and helping, at the same time, to spread their use in the field of the construction sector. On the other hand, the spread of open source software for LCA and LCC analysis might be a threat for the business unit here presented.

5.4.3 Competitive position: analysis

Due to the increasing awareness with regard to the sustainability issues, this could be offered to whoever will be interested in bringing innovative solutions in his daily business, but it will be also crucial to achieve specific sustainability goals. This highlights how large could be the customer portfolio in view of the fact that the regulations will, for sure, require new and higher sustainability standards. In this regard, consulting firms as well as universities interested in creating a spin-off to offer consultancy services could be the ones mainly suitable to exploit the result of this research. This, to create a business where part of the income could be also invested for the research purpose. At the moment, referring to the TRL as a method to measure the technology readiness level, the consultancy service could be considered as in a prototype stage since it only requires a constant updating of the databases. The main needed financial resources will be the ones for a constant research to better elaborate the results (i.e. sustainability and economic databases) while the budget to be spent for the software must be also foreseen (suitable for both the environmental ones and the economic ones). In this regard, at an initial stage, it will be useful to participate to several research calls whose funds will be used only for the research purpose. Hence, upon the starting of the consulting service, allocating a portion of the revenue for research purposes will become feasible. This integration of ongoing research with the provision of consulting services is essential for navigating through the challenging phase known as "the valley of death." This phase is characterized by numerous obstacles, including financial constraints, technological challenges, market uncertainties, and scalability issues, which startups or projects commonly encounter. A team made up of people able to use specific software for the LCA, but also confident with the cost estimation phase, will be then needed. Furthermore, to successfully penetrate the market, the support of all SMARTINCS partners producing self-healing materials is imperative. Their comprehensive component data, including production processes essential for environmental and cost estimations, is indispensable for offering a unique service that sets us apart from competitors.

5.4.4 Commercialization roadmap for the identified business unit

In view of what has been mentioned above, the most proper way to develop the business unit here described could be to create a spin off as part of a university (potentially, one university part of the SMARTINCS consortium). This will allow to continuously combine research innovation with a consultancy service which will be, then, always able to deal with the innovation in the field of the construction sector. Below is reported a timeline of the main milestones, combined with the valley of death scheme.

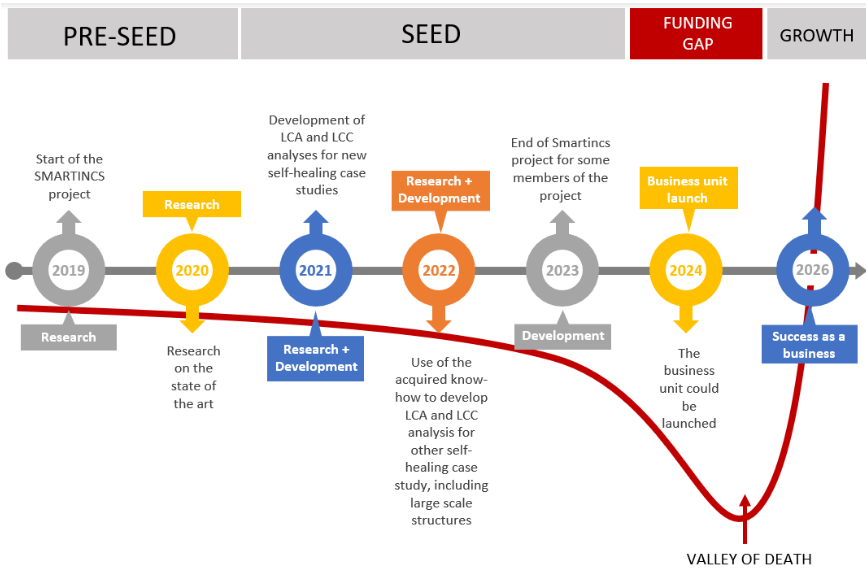

Figure 5.9: Commercialization roadmap for the identified business unit, according the timeline of the SMARTINCS project.

5.5 Social expectations

This work started by referencing a United Nations report that vividly outlines the issue of worldwide social inequities because of polluted environments. Such report, clearly delineates the gravity of the situation, prompting the construction stakeholders to question the role of civil engineering in modern society and whether it can contribute to shape a better future. This implies that future challenges will need to be addressed from a holistic perspective in which also social implications play a crucial role. As a matter of fact, the construction industry wields significant influence over communities, capable of yielding both positive and negative impacts. However, unlike environmental and financial value, which rely on measurable metrics, social value pertains to the overall improvement of communities. Consequently, construction endeavors must be purposeful and deliberate, aiming to enhance various aspects of community life in both the short and long term. An example of the social value of civil engineering includes the enhancement of local infrastructure, which addresses disparities in property quality across urban areas. Economic benefits ensue from improved infrastructure, fostering community pride and stimulating local economies through increased business activity and housing initiatives catering to diverse needs and income levels. Moreover, a well-developed construction sector can offer employment opportunities, contributing to socioeconomic stability. Addressing the affordable housing crisis, construction contributes to societal well-being, improving health and quality of life for vulnerable populations. In this framework, the penetration within the construction market of the materials assessed in this research (aided by a synergistic collaboration between sustainability assessment and structural design) can also promote the development of local industries, such as recycled material production. Additionally, by using sustainable and durable construction materials, communities can reduce property/infrastructure damage and protect the safety and well-being of people. To conclude, the scope of this work is also focused on shaping an eco-resilient construction sector maximizing the social value of the projects in which advanced construction materials can be employed.

5.6 Conclusions

This chapter has presented a robust framework for communicating and exploiting the sustainability of advanced cement-based construction materials to interested stakeholders. Through the examination of two distinct sustainability indices, the study highlights the necessity for comprehensive assessments that take into account a wide range of parameters in a real-world scenarios The proposed indices offer adaptable protocols that can be tailored to specific needs and boundary conditions, thereby providing a flexible framework for sustainability evaluations. These indices are validated by their consistency with existing analyses and their potential utility as an eco-label scoring system, enabling stakeholders to identify better-performing options within the sustainability context. An effective communication of the intrinsic sustainability properties can contribute to promote the commercialization of advanced construction materials, advocating for the development of an eco-resilient construction sector aligned with sustainability goals. Moreover, another significant aspect of this research is its potential to serve as the cornerstone for a profitable consulting service. By adopting an open Intellectual Property Rights (IPR) strategy, the findings generated in this study can be leveraged to offer expert guidance and support to various stakeholders involved in the construction industry. This consulting service could provide valuable insights into the implementation of innovative construction materials.

Driving the innovation: commercialization strategies and Key Exploitable Results (KERs)

6 Conclusions and future perspectives

Advanced cement-based materials offer enhanced mechanical and durability performance while also contributing to overall sustainability. These materials represent a promising solution for fostering resilience in the concrete sector from a holistic sustainability perspective. This work has highlighted the potential of integrating innovative materials to not only enhance durability but also improve mechanical and sustainability performance. By incorporating life cycle assessment (LCA) and life cycle costing (LCC) into a performance-oriented design methodology, this research showcases the optimization of resource utilization, reduction of environmental impacts, and bolstering of long-term resilience in concrete structures compared to conventional solutions. As the construction market continues to introduce novel and more durable materials, the approach outlined here provides a robust framework for effectively evaluating and leveraging their benefits, thereby shaping the future of the entire supply chain.

6.1 Outcomes, challenges and future perspectives

This work presents a holistic approach focused on enhancing sustainability within the construction sector by integrating, within the sustainability assessment, a structural design based on durability performance. For this scope, cement-based materials with enhanced mechanical performance, durability, and overall sustainability characteristics (in short, advanced cement-based materials) are assessed. Despite their advantages, these types of materials are not widespread within the market, primarily due to misconceptions such as their initial higher cost per cubic meter. However, this is an incomplete perspective that fails in considering the long-term benefits they offer also in terms of environmental and social implications. Thus, tailored market strategies must be formulated for their commercialization. First, to better penetrate the market, thorough research and development is crucial to ensure the materials meet industry standards and address the need for increased durability and efficiency when compared to more traditional solutions. Materials labeled as more environmentally friendly can attract a broader audience concerned about their ecological footprint. Similarly, considerations for social sustainability can enhance the reputation and credibility of companies promoting them while emphasizing cost sustainability, through highlighting long-term savings, can further incentivize adoption among budget-conscious stakeholders. Through the integration of these aspects into marketing strategies and product development, advanced construction materials not only differentiate themselves from other alternatives, but also positively contribute to environmental and social goals, thus enhancing market potential.

In this context, the requirement for robust assessment tools to gauge sustainability is of the utmost importance. Moreover, traditional construction materials and design methods wield substantial environmental/social/cost ramifications across the whole life cycle. Understanding these ramifications is crucial for identifying areas where improvements can be made effectively. As an example, current design approach, mainly prescribing requirements such as minimum cement content, concrete cover, strength class, and maximum water/cement ratios, does not consider concrete as an active player against harsh environment. However, this poses inherent risks since, for instance in an environment rich in chlorides, initial microcracking could promote premature chloride penetration and subsequent early onset of corrosion phenomena. Thus, methodologies such as Life Cycle Assessment (LCA) and Life Cycle Costing

(LCC) emerge then as pivotal, and are able to facilitate informed decision-making among stakeholders especially when the advantages of advanced construction materials must be addressed. However, most of the available sustainability assessments for novel cement-based materials, sometimes overlook the "usage" and "end-of-life" phases due to data gaps, particularly concerning durability aspects. The latter are also crucial for scheduling maintenance activities and understanding post-use material management. In this respect, Chapter 3 of this work aims at overcoming this current limitation. Through specific experiments (to be chosen according to the exposure conditions) and subsequent data analysis, these parameters can be obtained and encompassed within a performance-oriented design approach able to evaluate the performance of the material with time, optimizing the reiteration of the maintenance and, more generally, utilization and end-of-life phases. Such approach, can be termed as Durability Assessment-oriented Design (DAD) methodology. To clearly highlight the advantages of the latter from a LCA and LCC perspective, ranging from the microscale up to the structural level, chapter 4 presents a series of case studies. From microcapsules to superabsorbent polymers embedded in concrete structures, each conducted investigation aims at offering insights into environmental impacts, economic feasibility, and structural resilience. More specifically, what has been observed is:

i) microcapsules to be added in the concrete mix design for self-healing purposes: the analysis revealed that acetone, vinyl acetate, and copper, key components in the membrane emulsification production process, significantly influenced most of the impact indicators. This part of the analysis was focused exclusively on assessing the environmental burdens arising from the production process of these components. The objective was to gain insights into potential improvements that could facilitate greater penetration of these components into the market through the elaboration of an Environmental Product Declaration (EPD) document;

ii) 10% alumina nanofibers dispersion: the LCA conducted using a cradle-to-gate system boundary, shows, for 1 kg of alumina nanofibers dispersion, electricity as the predominant influencing factor, accounting for up to 96% of most of the impact indicators. Furthermore, the analysis of 1 m^3 of UHPC with inclusion of alumina nanofibers, highlights cement and steel fibers as the primary contributors to environmental impacts. Obtained results highlight the need for refining not only the entire production process (minimizing transports distances) but also reassessing the UHPC mix design, favouring the inclusion of alternatives to cement (e.g. supplementary cementitious materials) and virgin aggregates (e.g. recycled aggregates). As before, scope of this part of the assessment was to produce and EPD for commercialization purposes for both 1 kg of alumina nanofiber dispersion and 1 m^3 of UHPC with alumina nanofibers (0.25% by weight of cement);

iii) <u>3D printed nylon/PLA vascular networks embedded into the concrete matrix to inject a healing agent upon crack occurrence</u>: integrating a 3D printed vascular network, consisting of either nylon or PLA, injected with polyurethane to restore structural integrity, into concrete structures exposed to chloride-rich environments, offered significant advantages compared to conventional solutions, such as ordinary reinforced concrete. Reductions of up to 50% have been observed by employing an extended cradle-to-gate system boundary, accounting then for the maintenance activities. However, future research endeavors could prioritize exploring alternative and more efficient production processes for PLA, which remains demanding from an environmental standpoint due to the numerous steps involved in the process. Additionally, a need to investigate different types of healing agents has been outlined, as utilizing more advanced products capable of better crack penetration could lead to enhanced durability results;

iv) <u>concrete containing CEM III + Crystalline Admixture (CA):</u> the incorporation of a crystalline admixture leads to improved durability parameters and consequently extends the predicted service life of a structure against carbonation, identified as main degradation phenomenon for the specific case study within 100 years of service life. By employing an extended cradle-to-gate system boundary, reductions up to 40% have been observed in terms of environmental ramifications;

v) <u>concrete with Superabsorbent Polymers (SAPs)</u>: this segment of the study considered a variable service life ranging from 50 to 100 years, by employing an extended cradle-to-gate system boundary. With a focus on four distinct scenarios varying by service life and type of corrosion propagation (uniform or localized in the form of an hemispherical pit), the environmental and economic benefits of SAP-based concrete are clearly outlined. Reductions up to 67% for certain environmental impact indicators have been observed in comparison to a more conventional structural technology (ordinary reinforced concrete). Similarly, economic assessment registered improvements up to 22% within a timeframe of 100 years of SL. This is due to the reduced maintenance activities of SAP-based concrete, responsible for a significant portion of overall costs (up to 30%) for ordinary solutions;

vi) Ultra-High Performance Concrete (UHPC): despite its higher costs and cement content per cubic meter compared to ordinary reinforced concrete, UHPC exhibits superior environmental and cost performance in structural applications. This is attributable to the reduced volume of materials needed for achieving the same performance targets, along with decreased maintenance frequency, facilitated by its enhanced mechanical and durability properties in harsh environment. This part of the analysis delineated benefits of up to 63% in terms of environmental reductions and 46% in economic assessment compared to a more traditional solution;

vii) Recycled-UHPC (R-UHPC): the findings underscore the impact of reinforcement and the disposal/recycling phase on environmental burdens. The structure constructed with UHPC and incorporating 100% recycled aggregates, a proportion not possible to be reached with traditional mix designs where the replacement level is constrained to a maximum of 30%, stands out as the most advantageous choice. Through an extended cradle-to-grave system boundary, reductions of 50% and 33% have been identified in environmental impact and cost comparison, respectively, against a conventional solution. Once again, the outcomes emphasize the significance of reduced thickness and minimized maintenance activities as critical factors contributing to its environmental favorability.

However, communicating these results to stakeholders involved may pose a challenge. This is not only because of the complexity of the outcomes of an LCA analysis, which encompasses numerous indicators, but also because stakeholders are often primarily concerned with economic aspects. To address this challenge, attempts have been made to summarize all of the potential advantages deriving from the employment of a specific material (durability, mechanical performance, environmental and cost implications) into a single indicator with a value around the unit. The aim is to broadly and effectively communicate the above mentioned outcomes. Chapter 5 introduces a robust framework by proposing sustainability indices characterized by adaptable protocols for real-world scenarios, empowering stakeholders to identify and prioritize better-performing options. Two indices are proposed in total, applicable either on a materials scale or at a structural level. While the denominator comprises environmental and cost outcomes, the nominator of each index includes all the other relevant performance characteristics of the assessed material/structural element (e.g. compressive strength, tensile strength, chlorides diffusion coefficient etc.). Each encompassed parameter can be weighted according to specific perceptions (for instance, a single impact indicator may carry higher importance than others based on the perceptions of local communities. Scope is to effectively streamline a complex topic, as the sustainability, into a single numerical value.

This research is motivated by the recognition that novel cement-based materials are expected to continually emerge within the market, providing innovative solutions to address evolving needs. In response to this ongoing evolution, it becomes crucial to establish methodological frameworks, such as the one proposed by this work, to comprehensively assess the sustainability of these novel and improved materials. This investigation contributes to this endeavor by presenting a framework that synergistically integrates LCA and LCC methodologies with a durability assessment-oriented design to get efficient construction/usage/end-of-life phases when these materials are scaled up to the structural level. In this respect it must be highlighted that structural design codes should continue to further prioritize durability to ensure longevity, safety and economic viability, especially when high-performance materials are encompassed. At the same time, it is important to acknowledge that deepening of the understanding of these materials and their benefits must continue. This effort is necessary to consistently evaluate their performance, ensuring reliable outcomes to support the decision-making process. Scope is to pave the way for a more conscious civil sector and construction practices, in alignment with global sustainability goals and aspirations.

ANNEX 1

Data taken from Ecoinvent library for microcapsules LCI

Inputs from technosphere: materials/fuels
Water, deionized {Europe without Switzerland}| market for water, deionized | APOS,U
Acetone, liquid {GLO}| market for | APOS,U
Methanol {GLO}| market for | APOS,U
Hydrogen fluoride {RER}| hydrogen fluoride production | APOS,U
Silicone product {RER}| market for silicone product | APOS,U
Ammonia, liquid {RoW}| market for, APOS,U
Hydrogen, gaseous {GLO}| market for hydrogen, gaseous | APOS,U
Phosgene, liquid {RER}| market for | APOS,U
Acetylene {RER}| market for acetylene | APOS,U
Formaldehyde {RER}| market for formaldehyde | APOS,U
Ethanol, without water, in 99.7% solution state, from ethylene {RoW}| ethylene hydration| APOS,U
Monoethanolamine {GLO}| market for | APOS,U
Ammonia, liquid {RoW}| market for | APOS,U
Methane, 96% by volume {RoW}| market for methane, 96% by volume | APOS,U
Oxygen, via cryogenic air separation, production mix, at plant, gaseous EU-27 S
Copper {GLO}| market for | APOS, U

Tin {GLO}| market for | APOS, U
Sodium hydroxide, without water, in 50% solution state {GLO}| market for | APOS,U
Coconut oil, crude {GLO}| market for| APOS,U
Transport, freight, lorry 16-32 metric ton, euro5 {RER}|market for transport, freight, lorry 16-32 metric ton, EURO5| APOS,U
Electricity, medium voltage {GB}| market for | APOS,U
Emission to air
Methane
Final waste flows
Chemical waste, unspecified

Data taken from Ecoinvent library for alumina nanofibers LCI

Inputs from technosphere: materials/fuels
Water, deionized {Europe without Switzerland}| market for water, deionized | APOS,U
Polycarboxylate superplasticizer as detailed in 4.6
Alumina refining and primary aluminum production
Electricity, medium voltage {Europe without Switzerland}| market group for | APOS,U
Transport, freight, lorry 16-32 metric ton, euro5 {RER}|market for transport, freight, lorry 16-32 metric ton, EURO5| APOS,U
Outputs to technosphere: waste treatment

Waste polypropylene {EE}| market for waste polypropylene | APOS,IU

Data taken from Ecoinvent library for LCI of the nylon vascular network 3D printing process

Inputs from technosphere: materials/fuels
Nylon 6-6 {RoW}|market for nylon 6-6 | APOS,U
Electricity, low voltage, production BE, at grid/BE U

Data taken from Ecoinvent library for LCI of the PLA vascular network 3D printing process

Inputs from technosphere: materials/fuels
Tap water {CH}| market for | APOS,U
Natural gas, high pressure {BE}| import from DE| APOS, U
Heat, central or small-scale, natural gas {Europe without Switzerland}|market for heat, central or small scale, natural gas | APOS, U
Heat, central or small scale, other than natural gas {BE}| heat and power co-generation, biogas, gas engine| APOS,U
Maize grain {GLO}| market for | APOS,U
Chemical factory, organics {RER}| construction | APOS, U
Electricity, low voltage, production BE, at grid/BE U
Electricity, medium voltage {BE}| market for | APOS, U
Emission to air
NMVOC, non-methane volatile organic compounds, unspecified
Outputs to technosphere: waste treatment
Wastewater from maize starch production {GLO}| market for| APOS, u

Hazardous waste, for incineration {Europe without Switzerland}|market for hazardous waste, for incineration | APOS< U
Waste plastic, mixture {Europe without Switzerland}| treatment of waste plastic, mixture, municipal incineration| APOS, U

Data taken from Ecoinvent library for the LCI of the mix design considered to build the vascular beam

Inputs from technosphere: materials/fuels
Limestne, crusched, for mill {CH}| market for limestone, crushed, for mill |APOS,U
Tap water {CH}| market for | APOS,U
Gravel, round {CH}|market for gravel, round | APOS,U
Sand {CH}| market for sand | APOS,U
Polycarboxylate superplasticizer as detailed in 4.6
Reinforcing steel {GLO}| market for | APOS, U
Transport, freight, lorry 16-32 metric ton, euro5 {RER}| market for transport, freight, lorry 16-32 metric ton, EURO5| APOS,U

Data taken from Ecoinvent library for UHPC mix design

Inputs from technosphere: materials/fuels
Activated silica {CH}|market for | APOS,U
Gravel, round {CH}|market for gravel, round | APOS,U
Tap water {Europe without Switzerland}|market for | APOS,U
Polycarboxylate superplasticizer as detailed in 4.6
Reinforcing steel {GLO}| market for | APOS, U

Transport, freight, lorry 16-32 metric ton, euro5 {RER}|market for transport, freight, lorry 16-32 metric ton, EURO5| APOS,U

Data taken from Ecoinvent library for recycling process of UHPC

Inputs from technosphere: materials/fuels
Diesel {Europe without Switzerland}| market for | APOS,U
Transport, freight, lorry 16-32 metric ton, euro5 {RER}|market for transport, freight, lorry 16-32 metric ton, EURO5| APOS,U
Outputs to technosphere: waste treatment
Steel and iron (waste treatment) {GLO}| recycling of steel and iron| APOS,U
Waste plastic, mixture {RoW}| treatment of waste plastic, mixture, municipal incineration | APOS,U
Aluminium (waste treatment) {GLO}| recycling of aluminium | APOS,U
Waste building wood, chrome preserved {RoW}| treatment of, municipal incineration | APOS,U

References

Abreu, G.B. de, Costa, S.M.M., Gumieri, A.G., Calixto, J.M.F., França, F.C., Silva, C. & Quinõnes, A.D. (2017). Mechanical properties and microstructure of high performance concrete containing stabilized nano-silica. Matéria (Rio de Janeiro), 22.

ACI 503R-93, Use of Epoxy Compounds with Concrete (Reapproved 1998) American Concrete Institute. (n.d.). .

Aguiar, J.B. & Júnior, C. (2013). Carbonation of surface protected concrete. Construction and Building Materials, 49, 478–483.

Agustí-Juan, I., Müller, F., Hack, N., Wangler, T. & Habert, G. (2017a). Potential benefits of digital fabrication for complex structures: Environmental assessment of a robotically fabricated concrete wall. Journal of Cleaner Production, 154, 330–340.

Alatawna, A., Birenboim, M., Nadiv, R., Buzaglo, M., Peretz-Damari, S., Peled, A., Regev, O. & Sripada, R. (2020). The effect of compatibility and dimensionality of carbon nanofillers on cement composites. Construction and Building Materials, 232, 117141.

Alexander, M. & Beushausen, H. (2019). Durability, service life prediction, and modelling for reinforced concrete structures – review and critique. Cement and Concrete Research, 122, 17–29.

Alexander, M., Bertron, A. & Belie, N. De. (2013). Performance of Cement-Based Materials in Aggressive Aqueous Environments. RILEM State-of-the-Art Reports 10.

Al-Obaidi, S., Bamonte, P., Ferrara, L., Luchini, M. & Mazzantini, I. (2020). Durability-based design of structures made with ultra-high-performance/ultra-high-durability concrete in extremely aggressive scenarios: Application to a geothermal water basin case study. Infrastructures, 5, 1–44.

Al-Obaidi, S., Bamonte, P., Animato, F., Monte, F. Lo, Mazzantini, I., Luchini, M., Scalari, S. & Ferrara, L. (2021). Innovative design concept of cooling water tanks/basins in geothermal power plants using ultra-high-performance fiber-reinforced concrete with enhanced durability. Sustainability (Switzerland), 13.

Al-Obaidi, S., Davolio, M., Monte, F. Lo, Costanzi, F., Luchini, M., Bamonte, P. & Ferrara, L. (2022a). Structural validation of geothermal water basins constructed with durability enhanced ultra high performance fiber reinforced concrete (Ultra High Durability Concrete). Case Studies in Construction Materials, 17, e01202.

Al-Obaidi, S., Dicembre, S., Davolio, M., Galdo, M. Del, Monte, F. Lo & Ferrara, L. (2022b). Flexural performance of Ultra High Performance Concrete slabs under simultaneous environmental and mechanical loading. In: fib Symposium. Pp. 113–120.

Al-Obaidi, S., Davolio, M., Monte, F. Lo, Costanzi, F., Luchini, M., Bamonte, P. & Ferrara, L. (2022c). Structural validation of geothermal water basins constructed with durability enhanced ultra high performance fiber reinforced concrete (Ultra High Durability Concrete). Case Studies in Construction Materials, 17, e01202.

Al-Obaidi, S., He, S., Schlangen, E., & Ferrara, L. (2023). Effect of matrix self-healing on the bond-slip behavior of micro steel fibers in ultra-high-performance concrete. Materials and Structures, 56(9), 161. https://doi.org/10.1617/s11527-023-02250-5

Alonso, M.C. & Sanchez, M. (2009). Analysis of the variability of chloride threshold values in the literature. Materials and Corrosion, 60, 631–637.

Alonso, M.C., Gimenez, M., Menendez, E., Serna, P., Valcuende, M., Soto, J., Suesta, C., Fort, L., Camacho, E., Scalari, S., Borg, R.P. & Deegan, P. (2018). D3.2 – Definition of key durability parameters for each scenario.

Amrutha, V.N. & Geetha, S.N. (2020). A systematic review on green human resource management: Implications for social sustainability. Journal of Cleaner Production, 247, 119131.

Andersson, R., Stripple, H., Gustafsson, T. & Ljungkrantz, C. (2019). Carbonation as a method to improve climate performance for cement based material. Cement and Concrete Research, 124, 105819.

Andrade, C., Castellote, M., Alonso, C. & González, C. (2000). Non-steady-state chloride diffusion coefficients obtained from migration and natural diffusion tests. Part I: Comparison between several methods of calculation. Materials and Structures, 33, 21–28.

Antón, C., Gurdián, H., Vera, G. de & Climent, M.-Á. (2024). Effect of a Crystalline Admixture on the Permeability Properties of Concrete and the Resistance to Corrosion of Embedded Steel. Applied Sciences, 14, 1731.

Araújo, D. de A. (2016). Cracks Repair in Reinforced Concrete Structures Case Study–Reinforced Concrete Tunnel Repair Master dissertation in Civil Engineering.

ASTM. (2021a). ASTM C1157/C1157M-20a Standard Performance Specification for Hydraulic Cement.

ASTM. (2021b). ASTM C150/C150M-20 Standard Specification for Portland Cement.

ASTM. (2023). ASTM C1600/C1600M-19 Standard Specification for Rapid Hardening Hydraulic Cement.

Azmee, N.M. & Shafiq, N. (2018). Ultra-high performance concrete: From fundamental to applications. Case Studies in Construction Materials, 9, e00197.

Balouch, S.U., Forth, J.P. & Granju, J.-L. (2010). Surface corrosion of steel fibre reinforced concrete. Cement and Concrete Research, 40, 410–414.

Bartolini, L. & Carsana, M. (2014). Materiali da costruzione. Citta` Studi.

Beglarigale, A., Seki, Y., Demir, N.Y. & Yazıcı, H. (2018). Sodium silicate/polyurethane microcapsules used for self-healing in cementitious materials: Monomer optimization, characterization, and fracture behavior. Construction and Building Materials, 162, 57–64.

Belie, N. De, Gruyaert, E., Al-Tabbaa, A., Antonaci, P., Baera, C., Bajare, D., Darquennes, A., Davies, R., Ferrara, L., Jefferson, T., Litina, C., Miljevic, B., Otlewska, A., Ranogajec, J., Roig-Flores, M., Paine, K., Lukowski, P., Serna, P., Tulliani, J.-M.M., Vucetic, S., Wang, J. & Jonkers, H.M. (2018). A Review of Self-Healing Concrete for Damage Management of Structures. Advanced Materials Interfaces, 5, 1–28.

Belleghem, B. Van, Kessler, S., Heede, P. Van den, Tittelboom, K. Van & Belie, N. De. (2018). Chloride induced reinforcement corrosion behavior in self-healing concrete with encapsulated polyurethane. Cement and Concrete Research, 113, 130–139.

Belleghem, B. Van. (2018). Effect of Capsule-Based Self-Healing on Chloride Induced Corrosionof Reinforced Concrete.

Belleghem, Van, Heede, P. Van den, Tittelboom, K. Van & Belie, N. De. (2017). Quantification of the service life extension and environmental benefit of Chloride Exposed Self-Healing Concrete. Materials, 10.

Benetto, E., Rousseaux, P. & Blondin, J. (2004). Life cycle assessment of coal by-products based electric power production scenarios. Fuel, 83, 957–970.

Bertolini, L. & Pedeferri, P. (1996). Tecnologia dei materiali. Leganti e calcestruzzo. Torino: Citta studi edizioni.

BFUHP Bétons Fibrés à Ultra Hautes Performances [Internet document] . (2022). URL http://www.bfuhp.fr/. Accessed 27/07/2022.

Bicalho, T., Sauer, I., Rambaud, A. & Altukhova, Y. (2017). LCA data quality: A management science perspective. Journal of Cleaner Production, 156, 888–898.

Bonamente, E. & Cotana, F. (2015). Carbon and Energy Footprints of Prefabricated Industrial Buildings: A Systematic Life Cycle Assessment Analysis. Energies, 8, 12685–12701.

Borg, R.P., Cuenca, E., Garofalo, R., Schillani, F., Nasner, M.L. & Ferrara, L. (2021). Performance Assessment of Ultra-High Durability Concrete Produced From Recycled Ultra-High Durability Concrete. Frontiers in Built Environment, 7, 1–20.

Bossio, A., Lignola, G.P., Fabbrocino, F., Monetta, T., Prota, A., Bellucci, F. & Manfredi, G. (2017). Nondestructive assessment of corrosion of reinforcing bars through surface concrete cracks. Structural Concrete, 18, 104–117.

Breugel, K. van. (2007). IS THERE A MARKET FOR SELF-HEALING CEMENT-BASED MATERIALS_.pdf. In: roceedings of the First International Conference on Self Healing Materials. Noordwijk aan Zee, The Netherlands.

Brito, J. de & Kurda, R. (2021). The past and future of sustainable concrete: A critical review and new strategies on cement-based materials. Journal of Cleaner Production, 281, 123558.

C. Andrade, C. Alonso, J. Rodriguez, et al. Cover cracking and amount of rebar corrosion: importance of the current applied accelerated tests C. Sjostrom (Ed.), Durability of Building Materials and Components, 7, E&FN Spon, London (1996), pp. 263-273. (n.d.). .

Cangzhou Weida Polyurethane Hi-Tech Co Ltd. (2024). Synthesis method of dibutyltin dilaurate [Internet document] URL Synthesis method of dibutyltin dilaurate. Accessed 18/01/2024.

Cappellesso, V., Summa, D. di, Pourhaji, P., Prabhu Kannikachalam, N., Dabral, K., Ferrara, L., Cruz Alonso, M., Camacho, E., Gruyaert, E. & Belie, N. De. (2023). A review of the efficiency of self-healing concrete technologies for durable and sustainable concrete under realistic conditions. International Materials Reviews, 1–48.

Carrassi, A. (2023). Life Cycle Assessment and Corrosion Effects on Structural Behaviour: A Case Study of The New Water Treatment Plant in Genoa.

Caruso, M., Pascale, C., Camacho, E., Scalari, S., Animato, F., Alonso, M.C., Gimenez, M. & Ferrara, L. (2020). Life cycle assessment on the use of ultra high performance fibre reinforced concretes with enhanced durability for structures in extremely aggressive environments: Case study analyses. RILEM Bookseries.

Caruso, M., Pascale, C., Camacho, E., Scalari, S., Animato, F., Alonso, M.C., Gimenez, M. & Ferrara, L. (2020a). Life cycle assessment on the use of ultra high performance fibre reinforced concretes with enhanced durability for structures in extremely aggressive environments: Case study analyses. RILEM Bookseries.

Caruso, M., Pinho, R., Bianchi, F., Cavalieri, F. & Lemmo, M.T. (2020a). A Life Cycle Framework for the Identification of Optimal Building Renovation Strategies Considering Economic and Environmental Impacts. Sustainability, 12, 10221.

Caruso, M.C., Luchini, M., Montomoli, S., Camacho, E., Nteze, E., Sideri, S., Gastaldo, E. & Tretjakov, A. (2020b). Reshealience D7.1 - Life Cycle Sustainability Assessment: LCA LCC and SLCA.

Caruso, M.C., Pascale, C., Camacho, E. & Ferrara, L. (2022). Comparative environmental and social life cycle assessments of off-shore aquaculture rafts made in ultra-high performance concrete (UHPC). International Journal of Life Cycle Assessment, 27, 281–300.

Caruso, M.C., Pascale, C., Camacho, E., Scalari, S., Animato, F., Alonso, M.C., Gimenez, M. & Ferrara, L. (2020b). Life cycle assessment on the use of ultra high performance fibre reinforced concretes with enhanced durability for structures in extremely aggressive environments: Case study analyses. RILEM Bookseries.

Castellote, M., Andrade, C. & Alonso, C. (2001). Measurement of the steady and non-steady-state chloride diffusion coefficients in a migration test by means of monitoring the conductivity in the anolyte chamber. Comparison with natural diffusion tests. Cement and Concrete Research, 31, 1411–1420.

Caterpillar products [Internet document] . (2019). URL https://www.cat.com/en_US/products/new/equipment/excavators/large-excavators/104201.html. Accessed 07/02/2023.

Cen. (2002). EN 1990:2002, Eurocode - Basis of structural design.

CEN. (2004). EN 1995-1-1:2004 Eurocode 5: Design of timber structures - Part 1-1: General - Common rules and rules for buildings.

Cen. (2005a). EN 1992-2:2005, Eurocode 2 - Design of concrete structures - Concrete bridges - Design and detailing rules.

Cen. (2005b). EN 1504, Products and systems for the protection and repair of concrete structures - Definitions, requirements, quality control and evaluation of conformity, parts 1-10.

Cen. (2005c). EN 1992-2:2005, Eurocode 2 - Design of concrete structures - Concrete bridges - Design and detailing rules.

CEN. (2011). UNI EN 197-1:2011. CEN.

CEN. (2016). EN 206:2013+A1:2016 .

Cen. (2016a). UNI EN 206:2016, Concrete - Specification, performance, production and conformity.

Chalioris, Kosmidou & Karayannis. (2019). Cyclic Response of Steel Fiber Reinforced Concrete Slender Beams; an Experimental Study. Materials, 12, 1398.

Chang, C.-F. & Chen, J.-W. (2006). The experimental investigation of concrete carbonation depth. Cement and Concrete Research, 36, 1760–1767.

Chen, C., Habert, G., Bouzidi, Y. & Jullien, A. (2010). Environmental impact of cement production: detail of the different processes and cement plant variability evaluation. Journal of Cleaner Production, 18, 478–485.

Chidiac, S.E. & Shafikhani, M. (2020). Electrical resistivity model for quantifying concrete chloride diffusion coefficient. Cement and Concrete Composites, 113, 103707.

Chiellini, E., Corti, A., D'Antone, S. & Solaro, R. (2003). Biodegradation of poly (vinyl alcohol) based materials. Progress in Polymer Science, 28, 963–1014.

Cibelli, A., Luzio, G. Di & Ferrara, L. (2022). Numerical modelling via a coupled discrete approach of the autogenous healing for Fibre-Reinforced Cementitious Composites (FRCCs). In: Computational Modelling of Concrete and Concrete Structures. Pp. 86–95. London: CRC Press.

Climate Change 2007, the physical science basis . Contribution of Working Group I to the Fourth Assessment Report of the IPCC . (2007). .

Coffetti, D., Crotti, E., Gazzaniga, G., Carrara, M., Pastore, T. & Coppola, L. (2022). Pathways towards sustainable concrete. Cement and Concrete Research, 154, 106718.

Colangelo, F., Forcina, A., Farina, I. & Petrillo, A. (2018). Life Cycle Assessment (LCA) of different kinds of concrete containing waste for sustainable construction. Buildings, 8.

Colangelo, F., Petrillo, A., Cioffi, R., Borrelli, C. & Forcina, A. (2018b). Life cycle assessment of recycled concretes: A case study in southern Italy. Science of the Total Environment, 615, 1506–1517.

Commission Delegated Regulation. (2012). Commission Delegated Regulation (EU), 2012 No 244/2012 of 16 January 2012 supplementing Directive 2010/31/EU of the European Parliament and of the Council on the energy performance of buildings by establishing a comparative methodology framework.

Committee on Industry, R. and E. (2023). REPORT on the proposal for a directive of the European Parliament and of the Council on the energy performance of buildings (recast).

Concrete, E.F. of C. & Associations, A. (2019). ENVIRONMENTAL PRODUCT DECLARATION - Concrete admixtures – Plasticisers and Superplasticisers.

Coppola, L. (2007). Concretum. McGraw-Hill Education.

Coppola, L., Coffetti, D., Crotti, E. & Pastore, T. (2018). CSA-based Portland-free binders to manufacture sustainable concretes for jointless slabs on ground. Construction and Building Materials, 187, 691–698.

Coppola, L., Coffetti, D., Crotti, E., Gazzaniga, G. & Pastore, T. (2019). An Empathetic Added Sustainability Index (EASI) for cementitious based construction materials. Journal of Cleaner Production, 220, 475–482.

Craeye, B., Geirnaert, M. & Schutter, G.D. (2011a). Super absorbing polymers as an internal curing agent for mitigation of early-age cracking of high-performance concrete bridge decks. Construction and Building Materials, 25, 1–13.

Cuenca, E., Criado, M., Giménez, M., Alonso, M.C. & Ferrara, L. (2022). Effects of Alumina Nanofibers and Cellulose Nanocrystals on Durability and Self-Healing Capacity of Ultrahigh-Performance Fiber-Reinforced Concretes. Journal of Materials in Civil Engineering, 34.

Cuenca, E., D'Ambrosio, L., Lizunov, D., Tretjakov, A., Volobujeva, O. & Ferrara, L. (2021a). Mechanical properties and self-healing capacity of Ultra High Performance Fibre Reinforced Concrete with alumina nano-fibres: Tailoring Ultra High Durability Concrete for aggressive exposure scenarios. Cement and Concrete Composites, 118, 103956.

Cuenca, E., Mezzena, A. & Ferrara, L. (2021b). Synergy between crystalline admixtures and nano-constituents in enhancing autogenous healing capacity of cementitious composites under cracking and healing cycles in aggressive waters. Construction and Building Materials, 266, 121447.

Cuenca, E., Monte, F. Lo, Moro, M., Schiona, A. & Ferrara, L. (2021b). Effects of Autogenous and Stimulated Self-Healing on Durability and Mechanical Performance of UHPFRC: Validation of Tailored Test Method through Multi-Performance Healing-Induced Recovery Indices. Sustainability, 13, 11386.

Damineli, B.L., Kemeid, F.M., Aguiar, P.S. & John, V.M. (2010). Measuring the eco-efficiency of cement use. Cement and Concrete Composites, 32, 555–562.

Damtoft, J.S., Lukasik, J., Herfort, D., Sorrentino, D. & Gartner, E.M. (2008). Sustainable development and climate change initiatives. Cement and Concrete Research, 38, 115–127.

Davolio, M., Al-Obaidi, S., Altomare, M.Y., Monte, F. Lo & Ferrara, L. (2023). A methodology to assess the evolution of mechanical performance of UHPC as affected by autogenous healing under sustained loadings and aggressive exposure conditions. Cement and Concrete Composites, 139, 105058.

Desintegraator Tootmise OÜ. (2024). DISINTEGRATORS DESI-16 AND DESI-16C [Internet document] URL https://www.desi.ee/products/disintegrators/desi16-16c. Accessed 03/02/2024.

Desmyter, J. & Martin, Y. (2001). The environmental impact of building materials and buildings. WTCB Bulletin.

Dimov, D., Amit, I., Gorrie, O., Barnes, M.D., Townsend, N.J., Neves, A.I.S., Withers, F., Russo, S. & Craciun, M.F. (2018). Ultrahigh Performance Nanoengineered Graphene–Concrete Composites for Multifunctional Applications. Advanced Functional Materials, 28.

Djerbi, A., Bonnet, S., Khelidj, A. & Baroghel-bouny, V. (2008). Influence of traversing crack on chloride diffusion into concrete. Cement and Concrete Research, 38, 877–883.

Dobiáš, J. & Macek, D. (2014). Leadership in Energy and Environmental Design (LEED) and its Impact on Building Operational Expenditures. Procedia Engineering, 85, 132–139.

Dodge Data & Analytics. (2018). World Green Building Trends 2018 SmartMarket Report. Bedford.

Dodoo, A., Gustavsson, L. & Sathre, R. (2009). Carbon implications of end-of-life management of building materials. Resources, Conservation and Recycling, 53, 276–286.

Dong, D., Oers, L. van, Tukker, A. & Voet, E. van der. (2020). Assessing the future environmental impacts of copper production in China: Implications of the energy transition. Journal of Cleaner Production, 274, 122825.

Drouet, E., Poyet, S., Bescop, P. Le, Torrenti, J.-M. & Bourbon, X. (2019). Carbonation of hardened cement pastes: Influence of temperature. Cement and Concrete Research, 115, 445–459.

Dsilva, J., Zarmukhambetova, S. & Locke, J. (2023). Assessment of building materials in the construction sector: A case study using life cycle assessment approach to achieve the circular economy. Heliyon, 9, e20404.

Edenhofer, O., Pichs-Madruga, R., Sokona, Y., Minx, J.C., Farahani, E., Kadner, S., Seyboth, K., Adler, A., Baum, I., Brunner, S., Eickemeier, P., Kriemann, B., Savolainen, J., Schlömer, S., Stechow, C. von & Zwickel, T. (2014). Climate Change 2014 Mitigation of Climate Change Working Group III Contribution to the Fifth Assessment Report of the Intergovernmental Panel on Climate Change. New york.

Emilia-Romagna, Provveditorato interregionale alle Opere Pubbliche di Lombardia ed, C.D.M. (2019a). PREZZARIO REGIONALE delle opere pubbliche.

EPD. (2020). Environmental Product Declaration Penetron Products.

European Commission, The European Construction Sector, Eur. Union, 2016, p. 16. http://ec.europa.eu/growth/sectors/construction/. [Internet document] . (n.d.). .

European Commission. (2016). EU Construction & Demolition Waste Management Protocol.

European Commission. (2024). European Platform on LCA | EPLCA [Internet document] URL https://eplca.jrc.ec.europa.eu/lifecycleassessment.html. Accessed 14/01/2024.

European commission. (2024). Research and Innovation [Internet document] URL https://ec.europa.eu/newsroom/informatics/newsletter-archives/26146. Accessed 10/03/2024.

EUROPEAN COMMITTEE FOR STANDARDIZATION. (2001). NBN EN 206-1: Concrete - Part 1: Specification, performance, production and conformity. Belgium-Brussels.

European FEICA - Association of the & Industry, A. and S. (2016). ENVIRONMENTAL PRODUCT DECLARATION as per ISO 14025 and EN 15804. Dispersion-based products.

European Parliament and Council of the European Union. (2008). Directive 2008/98/EC of the European Parliament and of the Council [Internet document] URL https://eur-lex.europa.eu/legal-content/EN/TXT/?uri=celex%3A32008L0098. Accessed 22/12/2023.

European Parliament and Council of the European Union. (2014). Directive 2014/25/EU of the European Parliament and of the council of 26 February 2014 on public procurement and repealing Directive 2004/18/EC (Text with EEA relevance)

[Internet document] URL https://eur-lex.europa.eu/legal-content/EN/TXT/?uri=celex%3A32014L0025. Accessed 21/12/2023.

F. du béton and J.C. Walraven. (2012). Model Code 2010: Volume 1. Bulletin (fib Fédération internationale du béton).International Federation for Structural Concrete (fib).

FEICA - Association of the European Adhesive and Sealant Industry. (2015a). ENVIRONMENTAL PRODUCT DECLARATION - Reactive resins based on polyurethane or SMP, filled or aqueous, solvent-free.

FEICA - Association of the European Adhesive and Sealant Industry. (2015b). ENVIRONMENTAL PRODUCT DECLARATION - Reactive resins based on epoxy resin, filled and/or aqueous with low content of filler.

Feiteira, J., Gruyaert, E. & Belie, N. De. (2016). Self-healing of moving cracks in concrete by means of encapsulated polymer precursors. Construction and Building Materials, 102, 671–678.

Ferrara, L., Bamonte, P., Suesta Falcó, C., Animato, F., Pascale, C., Tretjakov, A., Camacho Torregrosa, E., Deegan, P., Sideri, S., Gastaldo Brac, E.M., Serna, P., Mechtcherine, V., Cruz Alonso, M., Peled, A. & Borg, R.P. (2019). An Overview on H2020 Project "ReSHEALience." Pp. 184–191.

Ferrara, L., Krelani, V. & Moretti, F. (2016). Autogenous healing on the recovery of mechanical performance of High Performance Fibre Reinforced Cementitious Composites (HPFRCCs): Part 2 e Correlation between healing of mechanical performance and crack sealing. Cement and Concrete Composites, 73, 299–315.

fib. (2013). fib Model Code for Concrete Structures 2010. Weinheim, Germany: Wiley-VCH Verlag GmbH & Co. KGaA.

Fládr, J. & Bílý, P. (2018). Specimen size effect on compressive and flexural strength of high-strength fibre-reinforced concrete containing coarse aggregate. Composites Part B: Engineering, 138, 77–86.

Flores-Vivian, I., Pradoto, R.G.K., Moini, M., Kozhukhova, M., Potapov, V. & Sobolev, K. (2017). The effect of SiO2 nanoparticles derived from hydrothermal solutions on the performance of portland cement based materials. Frontiers of Structural and Civil Engineering, 11, 436–445.

Folić, R. & Zenunović, D. (2010). Durability problem of RC structures in Tuzla industrial zone - Two case studies. Engineering Structures, 32, 1846–1860.

Frangopol, D.M., Lin, K.-Y. & Estes, A.C. (1997). Life-Cycle Cost Design of Deteriorating Structures. Journal of Structural Engineering, 123, 1390–1401.

Frischknecht, R. & Jungbluth, N. (2007). Overview and Methodology.

Fu, C., Zhou, K., Ling, Y., Jin, X., Fang, D. & Zhou, J. (2020). Chloride transport behavior in bending-shear section of reinforced concrete beam under combined effect of load and environment. Construction and Building Materials, 257.

G.J. Al-Sulaimani, M. Kaleemullah, L.A. Basunbul, et al. Influence of corrosion and cracking on bond behaviour and strength of reinforced concrete members ACI Struct. J., 87 (2) (1990), pp. 220-231. (n.d.). .

G.P. Tilly, J.J. (2007). Concrete Repairs, Performance in Service and Current Practice. Bracknell.

Gartner, E. & Hirao, H. (2015). A review of alternative approaches to the reduction of CO2 emissions associated with the manufacture of the binder phase in concrete. Cement and Concrete Research, 78, 126–142.

Georgescu, D., Vacareanu, R., Aldea, A., Apostu, A., Arion, C. & Girboveanu, A. (2022). Assessment of the Sustainability of Concrete by Ensuring Performance during Structure Service Life. Sustainability, 14, 617.

Gettu, R., Pillai, R.G., Santhanam, M., Basavaraj, A.S., Rathnarajan, S. & Dhanya, B.S. (2018). Sustainability-based decision support framework for choosing concrete mixture proportions. Materials and Structures, 51, 165.

Goedkoop, M. & Spriensma, R. (2001). Goedkoop M, Spriensma R (2001). The Eco-indicator 99. A damage oriented method for life cycle impact assessment, Methodology report, Third Edition. Amersfoort: PRé Consultants bv.

Gontia, P. & Janssen, M. (2016). Life cycle assessment of bio-based sodium polyacrylate production from pulp mill side streams: Case study of thermo-mechanical and sulfite pulp mills. Journal of Cleaner Production, 131, 475–484.

Granju, J.-L. & Balouch, S.U. (2005). Corrosion of steel fibre reinforced concrete from the cracks. Cement and Concrete Research, 35, 572–577.

Gresta, F., Luca, A.I. De, Strano, A., Falcone, G., Santonoceto, C., Anastasi, U. & Gulisano, G. (2014). Economic and environmental sustainability analysis of guar (Cyamopsis tetragonoloba L.) farming process in a Mediterranean area: two case studies. Italian Journal of Agronomy, 9, 20.

Greve-Dierfeld, S. von, Lothenbach, B., Vollpracht, A., Wu, B., Huet, B., Andrade, C., Medina, C., Thiel, C., Gruyaert, E., Vanoutrive, H., Saéz del Bosque, I.F., Ignjatovic, I., Elsen, J., Provis, J.L., Scrivener, K., Thienel, K.-C., Sideris, K., Zajac, M., Alderete, N., Cizer, Ö., Heede, P. Van den, Hooton, R.D., Kamali-Bernard, S., Bernal, S.A., Zhao, Z., Shi, Z. & Belie, N. De. (2020). Understanding the carbonation of concrete with supplementary cementitious materials: a critical review by RILEM TC 281-CCC. Materials and Structures, 53, 136.

Gruyaert, E., Debbaut, B., Snoeck, D., Díaz, P., Arizo, A., Tziviloglou, E., Schlangen, E. & Belie, N. De. (2016). Self-healing mortar with pH-sensitive superabsorbent polymers: Testing of the sealing efficiency by water flow tests. Smart Materials and Structures, 25.

Guinee, J.B. (2002). Handbook on Life Cycle Assessment.

Hache, E., Simoën, M., Seck, G.S., Bonnet, C., Jabberi, A. & Carcanague, S. (2020). The impact of future power generation on cement demand: An international and regional assessment based on climate scenarios. International Economics, 163, 114–133.

Harnisch, J. & Raupach, M. (2015). The residual cross section factor as a key parameter for the static evaluation of corroding reinforced concrete structures. Materials and Corrosion, 66, 829–838.

Hasanbeigi, A., Price, L. & Lin, E. (2012). Emerging energy-efficiency and CO2 emission-reduction technologies for cement and concrete production: A technical review. Renewable and Sustainable Energy Reviews, 16, 6220–6238.

Heede, P. Van den & Belie, N. De. (2012). Environmental impact and life cycle assessment (LCA) of traditional and "green" concretes: Literature review and theoretical calculations. Cement and Concrete Composites, 34, 431–442.

Heede, P. Van den, Belie, N. De, Pittau, F., Habert, G. & Mignon, A. (2019a). Life cycle assessment of self-healing engineered cementitious composite (SH-ECC) used for the rehabilitation of bridges. In: Life-Cycle Analysis and Assessment in Civil Engineering: Towards an Integrated Vision - Proceedings of the 6th International Symposium on Life-Cycle Civil Engineering, IALCCE 2018. Pp. 2269–2275.

Heede, P. Van den, Belleghem, B. Van, Keersmaecker, M. De, Adriaens, A. & Belie, N. De. (2016). Sustainability Effects of Including Concrete Cracking and Healing in Service Life Prediction for Marine Environments. Pp. 1281–1290.

Heede, P. Van den, Mignon, A., Habert, G. & Belie, N. De. (2018). Cradle-to-gate life cycle assessment of self-healing engineered cementitious composite with in-house developed (semi-)synthetic superabsorbent polymers. Cement and Concrete Composites, 94, 166–180.

Heede, P. Van Den. (2014). Durability and Sustainability of Concrete with High Volumes of Fly Ash.

Holdich, R., Dragosavac, M., Williams, B. & Trotter, S. (2020). High throughput membrane emulsification using a single-pass annular flow crossflow membrane. AIChE Journal, 66.

Hu, M., Maio, F. Di, Lin, X. & Roekel, E. Van. (2012). Fates of end-of-life concrete and their economic implications. Proceedings of the 27th international conference on solid waste technology and management., 1–9.

Huang, N.M., Chang, J.J. & Liang, M.T. (2012). Effect of plastering on the carbonation of a 35-year-old reinforced concrete building. Construction and Building Materials, 29, 206–214.

Huijbregts, M.A.J., Breedveld, L., Huppes, G., Koning, A. de, Oers, L. van & Suh, S. (2003). Normalisation figures for environmental life-cycle assessment. Journal of Cleaner Production, 11, 737–748.

Human Rights Council United Nations. (2022). Report of the Special Rapporteur on the issue of human rights obligations relating to the enjoyment of a safe, clean, healthy and sustainable environment.

Hung, C.-C., Lee, H.-S. & Chan, S.N. (2019). Tension-stiffening effect in steel-reinforced UHPC composites: Constitutive model and effects of steel fibers, loading patterns, and rebar sizes. Composites Part B: Engineering, 158, 269–278.

IECA Instituto Espanol del cemento y sus aplicaciones. (2014). Declaración Ambiental de Producto CEMENTO CEM III.

Industrial Waste Treatment Handbook. (2006). . Elsevier.

Inlab. (2024). Ultrasonic laboratory unit [Internet document] URL https://en.utinlab.ru/articles/ultrasonic-laboratory-unit-ultrasonic-dispersant-ultrasonic-emulsifier. Accessed 03/02/2024.

Instytut Techniki Budowlanej (ITB). (2021). Environmental Product Declaration Type III ITB No. 215/2021 Dramix® Steel fibres for Concrete Reinforcement.

ISO. (2012). ISO 16204:2012 Durability Service life design of concrete structures.

J.S. Williamson, L.A. Clark Pressure required to cause cover cracking of concrete due to reinforcement corrosion Mag. Concr. Res., 52 (6) (2000), pp. 455-467. (n.d.). .

Jacob-Lopes, E., Zepka, L.Q. & Deprá, M.C. (2021). Assistant's tools toward life cycle assessment. In: Sustainability Metrics and Indicators of Environmental Impact. Pp. 77–90. Elsevier.

Jain, P.C. (1993). Greenhouse effect and climate change: scientific basis and overview. Renewable Energy, 3, 403–420.

Jia, D., Guo, Q., Mao, J., Lv, J. & Yang, Z. (2020). Durability of glass fibre-reinforced polymer (GFRP) bars embedded in concrete under various environments. I: Experiments and analysis. Composite Structures, 234.

Jolliet, O., Margni, M., Charles, R., Humbert, S., Payet, J., Rebitzer, G. & Rosenbaum, R. (2003). IMPACT 2002+: A New Life Cycle Impact Assessment Methodology. International Journal of Life Cycle Assessment, 8, 324–330.

Josa, A., Aguado, A., Cardim, A. & Byars, E. (2007). Comparative analysis of the life cycle impact assessment of available cement inventories in the EU. Cement and Concrete Research, 37, 781–788.

Joseph, C., Jefferson, A.D., Isaacs, B., Lark, R. & Gardner, D. (2010). Experimental investigation of adhesive-based self-healing of cementitious materials. Magazine of Concrete Research, 62, 831–843.

Junnila, S., Horvath, A. & Guggemos, A.A. (2006). Life-Cycle Assessment of Office Buildings in Europe and the United States. Journal of Infrastructure Systems, 12, 10–17.

Kanellopoulos, A., Giannaros, P., Palmer, D., Kerr, A. & Al-Tabbaa, A. (2017). Polymeric microcapsules with switchable mechanical properties for self-healing concrete: synthesis, characterisation and proof of concept. Smart Materials and Structures, 26, 045025.

Kannikachalam, N., Summa, D. di, Borg, R.P., Cuenca, E., Parpanesi, M., Belie, N. De & Ferrara, L. (2023). Assessment of Sustainability and Self-Healing Performances of Recycled Ultra-High-Performance Concrete. ACI Materials Journal, 120.

Kline, J. & Kline, C. (2015). Cement and <inline-formula> <tex-math notation="TeX">$\hbox{CO}_{2}$</tex-math></inline-formula>: What is Happening. IEEE Transactions on Industry Applications, 51, 1289–1294.

Kurda, R., Silvestre, J.D. & Brito, J. de. (2018). Life cycle assessment of concrete made with high volume of recycled concrete aggregates and fly ash. Resources, Conservation and Recycling, 139, 407–417.

Kušter Marić, M., Ožbolt, J. & Balabanić, G. (2020). Reinforced concrete bridge exposed to extreme maritime environmental conditions and mechanical damage: Measurements and numerical simulation. Engineering Structures, 205, 110078.

L.A. Clark, M. Saifullah, Effect of corrosion on reinforcement bond strength, in: M. Forde (Ed.), Proceedings of 5th International Conference on Structural Faults and Repairs, Edinburgh: Engineering Technical Press, vol. 3, 1993, pp. 113–119. (n.d.). .

Lamnatou, Chr. & Chemisana, D. (2015). Evaluation of photovoltaic-green and other roofing systems by means of ReCiPe and multiple life cycle–based environmental indicators. Building and Environment, 93, 376–384.

Li, G., Zhou, Q., Wang, W., Lu, C., Chen, C., Guo, Z. & Lu, C. (2023). Chloride diffusion along the interface between concrete matrix and repair materials under flexural loading. Construction and Building Materials, 372, 130829.

Li, J., Wu, Z., Shi, C., Yuan, Q. & Zhang, Z. (2020). Durability of ultra-high performance concrete – A review. Construction and Building Materials, 255, 119296.

Li, M., Ranade, R., Kan, L. & Li, V.C. (2010). On Improving the Infrastructure Service Life Using ECC to Mitigate Rebar Corrosion. 2nd International Symp. on Service Life Design for Infrastructure, 773–781.

Li, V.C. & Leung, C.K.Y. (1992). Steady-State and Multiple Cracking of Short Random Fiber Composites. Journal of Engineering Mechanics, 118, 2246–2264.

Li, V.C., Mishra, D.K. & Wu, H.-C. (1995a). Matrix design for pseudo-strain-hardening fibre reinforced cementitious composites. Materials and Structures, 28, 586–595.

Li, Z., Souza, L.R.D., Litina, C., Markaki, A.E. & Al-Tabbaa, A. (2020b). A novel biomimetic design of a 3D vascular structure for self-healing in cementitious materials using Murray's law. Materials and Design, 190.

Liew, F.E., Nogle, R., Abdalla, T., Rasor, B.J., Canter, C., Jensen, R.O., Wang, L., Strutz, J., Chirania, P., Tissera, S. De, Mueller, A.P., Ruan, Z., Gao, A., Tran, L., Engle, N.L., Bromley, J.C., Daniell, J., Conrado, R., Tschaplinski, T.J., Giannone, R.J., Hettich, R.L., Karim, A.S., Simpson, S.D., Brown, S.D., Leang, C., Jewett, M.C. & Köpke, M. (2022). Carbon-negative production of acetone and isopropanol by gas fermentation at industrial pilot scale. Nature Biotechnology, 40, 335–344.

Litina, C. & Al-Tabbaa, A. (2020). First generation microcapsule-based self-healing cementitious construction repair materials. Construction and Building Materials, 255, 119389.

Liu, J., Farzadnia, N., Khayat, K.H. & Shi, C. (2021). Effects of SAP characteristics on internal curing of UHPC matrix. Construction and Building Materials, 280.

Liu, Y., Presuel-Moreno, F.J. & Paredes, M.A. (2015). Determination of chloride diffusion coefficients in concrete by electrical resistivity method. ACI Materials Journal, 112, 631–640.

López, J.Á., Serna, P., Navarro-Gregori, J. & Coll, H. (2016). A simplified five-point inverse analysis method to determine the tensile properties of UHPFRC from unnotched four-point bending tests. Composites Part B: Engineering, 91, 189–204.

Lotfi, S. & Rem, P. (2016). Recycling of End of Life Concrete Fines into Hardened Cement and Clean Sand. Journal of Environmental Protection, 07, 934–950.

Lotfi, S., Eggimann, M., Wagner, E., Mróz, R. & Deja, J. (2015). Performance of recycled aggregate concrete based on a new concrete recycling technology. Construction and Building Materials, 95, 243–256.

Lotfi, S., Rem, P., Deja, J. & Mróz, R. (2017). An experimental study on the relation between input variables and output quality of a new concrete recycling process. Construction and Building Materials, 137, 128–140.

Luca Bertolini, Bernhard Elsener, Pietro Pedeferri, R.P.P. (2004). Corrosion of steel in concrete.

Luo, J., Shao, X., Fan, W., Cao, J. & Deng, S. (2019). Flexural cracking behavior and crack width predictions of composite (steel + UHPC) lightweight deck system. Engineering Structures, 194, 120–137.

Maddalena, R., Roberts, J.J. & Hamilton, A. (2018). Can Portland cement be replaced by low-carbon alternative materials? A study on the thermal properties and carbon emissions of innovative cements. Journal of Cleaner Production, 186, 933–942.

Makul, N. (2020). Modern sustainable cement and concrete composites: Review of current status, challenges and guidelines. Sustainable Materials and Technologies, 25, e00155.

Marques, P.F., Chastre, C. & Nunes, Â. (2013). Carbonation service life modelling of RC structures for concrete with Portland and blended cements. Cement and Concrete Composites, 37, 171–184.

McDonough, W. & Braungart, M. (2002). Cradle to Cradle: Remaking the Way We Make Things. North Point Press.

McLellan, B.C., Williams, R.P., Lay, J., Riessen, A. Van & Corder, G.D. (2011). Costs and carbon emissions for geopolymer pastes in comparison to ordinary portland cement. Journal of Cleaner Production, 19, 1080–1090.

Mechtcherine, V. and H.W.R. (n.d.). Application of Super Absorbent Polymers (SAP) in Concrete Construction, in State-of-the-Art Report Prepared by Technical Committee 225-SAP. 2012, RILEM. p. 165.

Meyer, C. (2009). The greening of the concrete industry. Cement and Concrete Composites, 31, 601–605.

Miller, S.A., John, V.M., Pacca, S.A. & Horvath, A. (2018). Carbon dioxide reduction potential in the global cement industry by 2050. Cement and Concrete Research, 114, 115–124.

Monte, F. Lo & Ferrara, L. (2020). Tensile behaviour identification in Ultra-High Performance Fibre Reinforced Cementitious Composites: indirect tension tests and back analysis of flexural test results. Materials and Structures, 53, 145.

Müller, H.S., Breiner, R., Moffatt, J.S. & Haist, M. (2014). Design and Properties of Sustainable Concrete. Procedia Engineering, 95, 290–304.

Murad, Y., Tarawneh, A., Arar, F., Al-Zu'bi, A., Al-Ghwairi, A., Al-Jaafreh, A. & Tarawneh, M. (2021). Flexural strength prediction for concrete beams reinforced with FRP bars using gene expression programming. Structures, 33, 3163–3172.

Muthu, M. & Santhanam, M. (2018). Effect of reduced graphene oxide, alumina and silica nanoparticles on the deterioration characteristics of Portland cement paste exposed to acidic environment. Cement and Concrete Composites, 91, 118–137.

Naidu Gopu, G. & Joseph, S.A. (2022). Corrosion Behavior of Fiber-Reinforced Concrete—A Review. Fibers, 10, 38.

Nasereddin, M. & Price, A. (2021). Addressing the capital cost barrier to sustainable construction. Developments in the Built Environment, 7, 100049.

Nath, P., Sarker, P.K. & Biswas, W.K. (2018). Effect of fly ash on the service life, carbon footprint and embodied energy of high strength concrete in the marine environment. Energy and Buildings, 158, 1694–1702.

Neves, R., Branco, F. & Brito, J. de. (2013). Field assessment of the relationship between natural and accelerated concrete carbonation resistance. Cement and Concrete Composites, 41, 9–15.

Noh, H.M., Idris, N., Noor, N. & Sarpin, N. (2018). Structural Effects of Reinforced Concrete Beam Due to Corrosion, 01024, 1–9.

Nordtest. (1999). Concrete, mortar and cement-based repair materials: Chloride migration coefficient from non-steady-state migration experiments (NT BUILD 492).

O'Malley, C., Piroozfar, P.A.E., Farr, E.R.P. & Gates, J. (2014). Evaluating the Efficacy of BREEAM Code for Sustainable Homes (CSH): A Cross-sectional Study. Energy Procedia, 62, 210–219.

Ochoa, L., Hendrickson, C. & Matthews, H.S. (2002). Economic Input-output Life-cycle Assessment of U.S. Residential Buildings. Journal of Infrastructure Systems, 8, 132–138.

Oh, D.Y., Noguchi, T., Kitagaki, R. & Park, W.J. (2014). CO2 emission reduction by reuse of building material waste in the Japanese cement industry. Renewable and Sustainable Energy Reviews, 38, 796–810.

Ottosen, L.M., Jensen, L.B., Astrup, T., McAloone, T.C., Ryberg, M., Thuesen, C., Christiansen, S., Pedersen, A.J. & Odgaard, M.H. (2021). Implementation stage for circular economy in the Danish building and construction sector. Detritus, 26–30.

Ouellet-Plamondon, C. & Habert, G. (2015). Life cycle assessment (LCA) of alkali-activated cements and concretes. Handbook of Alkali-Activated Cements, Mortars and Concretes.

Oxford Economics. (2021). Future of Construction A Global Forecast for Construction to 2030.

Pade, C. & Guimaraes, M. (2007). The CO2 uptake of concrete in a 100 year perspective. Cement and Concrete Research, 37, 1348–1356.

Papadakis, V.G., Vayenas, C.G. & Fardis, M.N. (1991). Physical and chemical characteristics affecting the durability of concrete. ACI Materials Journal, 88, 186–196.

Park, D.C. (2008). Carbonation of concrete in relation to CO2 permeability and degradation of coatings. Construction and Building Materials, 22, 2260–2268.

Parpanesi, M. (2021). A holistic life-cycle design approach to structures with advanced cement based materials.

Pelletier, M., Brown, R., Shukla, A. & Bose, A. (2011). Selfhealing Concrete with a Microencapsulated Healing Agent.

Pelto, J., Leivo, M., Gruyaert, E., Debbaut, B., Snoeck, D. & Belie, N. De. (2017). Application of encapsulated superabsorbent polymers in cementitious materials for stimulated autogenous healing. Smart Materials and Structures, 26.

Peña, C., Civit, B., Gallego-Schmid, A., Druckman, A., Pires, A.C.-, Weidema, B., Mieras, E., Wang, F., Fava, J., Canals, L.M. i, Cordella, M., Arbuckle, P., Valdivia, S., Fallaha, S. & Motta, W. (2021). Using life cycle assessment to achieve a circular economy. The International Journal of Life Cycle Assessment, 26, 215–220.

Pennington, D.W., Potting, J., Finnveden, G., Lindeijer, E., Jolliet, O., Rydberg, T. & Rebitzer, G. (2004). Life cycle assessment Part 2: Current impact assessment practice. Environment International, 30, 721–739.

Pérez-Lombard, L., Ortiz, J. & Pout, C. (2008). A review on buildings energy consumption information. Energy and Buildings, 40, 394–398.

Petek Gursel, A., Masanet, E., Horvath, A. & Stadel, A. (2014). Life-cycle inventory analysis of concrete production: A critical review. Cement and Concrete Composites, 51, 38–48.

Piccinno, F., Hischier, R., Seeger, S. & Som, C. (2016). From laboratory to industrial scale: a scale-up framework for chemical processes in life cycle assessment studies. Journal of Cleaner Production, 135, 1085–1097.

Plank, J., Sakai, E., Miao, C.W., Yu, C. & Hong, J.X. (2015). Chemical admixtures - Chemistry, applications and their impact on concrete microstructure and durability. Cement and Concrete Research, 78, 81–99.

Plati, C. & Tsakoumaki, M. (2023). Life Cycle Assessment (LCA) of Alternative Pavement Rehabilitation Solutions: A Case Study. Sustainability, 15, 2129.

Popovics, S. (1990). Analysis of the concrete strength versus water-cement ratio relationship. ACI Materials Journal, 87, 517–529.

Poulsen, E. & Mejilbro, L. (2005). Diffusion of Chloride in Concrete Theory and Application.

Putro, W.S., Lee, V.Ya., Sato, K., Choi, J.-C. & Fukaya, N. (2021). From SiO_2 to Alkoxysilanes for the Synthesis of Useful Chemicals. ACS Omega, 6, 35186–35195.

Ravitheja, A., Reddy, T.C.S. & Sashidhar, C. (2019). Self-Healing Concrete with Crystalline Admixture—A Review. Journal of Wuhan University of Technology-Mater. Sci. Ed., 34, 1143–1154.

Regione Toscana. (2021). Prezzario dei Lavori della Toscana 2021 - Provincia di Siena. Prezzario, Regione Toscana.

Renzetti, S., Schito, M., Borgese, L., Cirelli, P., Cagna, G., Patrono, A., Peli, M., Ranzi, R., Lucchini, R. & Placidi, D. (2022). Indoor metals pollution and metabolic outcomes among Italian children. European Journal of Public Health, 32.

Richard, P. & Cheyrezy, M. (1995). Composition of reactive powder concretes. Cement and Concrete Research, 25, 1501–1511.

Rigamonti, S., Cuenca, E., Arrigoni, A., Dotelli, G. & Ferrara, L. (2019). Self-healing concrete vs. Conventional waterproofing systems in underground structures: A cradle to gate LCA comparison with reference to a case study. In: Life-Cycle Analysis and Assessment in Civil Engineering: Towards an Integrated Vision - Proceedings of the 6th International Symposium on Life-Cycle Civil Engineering, IALCCE 2018. Pp. 2277–2284.

Riordan, C., Palmer, D. & Al-Tabbaa, A. (2023). Investigation of Membrane Emulsification for the Scaled Production of Microcapsules for Self-sealing Cementitious Systems. MATEC Web of Conferences, 378, 02010.

Rivera-Corral, J.O., Fajardo, G., Arliguie, G., Orozco-Cruz, R., Deby, F. & Valdez, P. (2017). Corrosion behavior of steel reinforcement bars embedded in concrete exposed to chlorides: Effect of surface finish. Construction and Building Materials, 147, 815–826.

Robayo-Salazar, R., Mejía-Arcila, J., Mejía de Gutiérrez, R. & Martínez, E. (2018). Life cycle assessment (LCA) of an alkali-activated binary concrete based on natural volcanic pozzolan: A comparative analysis to OPC concrete. Construction and Building Materials, 176, 103–111.

Romagna, R.E. (2011). CARTA DELLA SALINITA' DEI SUOLI DELLA PIANURA EMILIANO-ROMAGNOLA STRATO 50-100 cm.

Rooij, Ma. de, Tittelboom, K. Van, Belie, N. De & Schlangen, E. (2013). Self-Healing Phenomena in Cement-Based Materials. Dordrecht: Springer Netherlands.

Roy, S.K., Northwood, D.O. & Poh, K.B. (1996). Effect of plastering on the carbonation of a 19-year-old reinforced concrete building. Construction and Building Materials, 10, 267–272.

S. Rasheeduzzafar, S.S. Al-Saadoun, A.S. Al-Gahtani Corrosion cracking in relation to bar diameter and concrete quality J. Mater. Civ. Eng., 4 (4) (1992), pp. 327-342. (n.d.). .

Sabău, M. & Remolina Duran, J. (2022). Prediction of Compressive Strength of General-Use Concrete Mixes with Recycled Concrete Aggregate. International Journal of Pavement Research and Technology, 15, 73–85.

Sáez-Guinoa, J., García-Franco, E., Llera-Sastresa, E. & Romeo, L.M. (2024). The effects of energy consumption of alumina production in the environmental impacts using life cycle assessment. The International Journal of Life Cycle Assessment, 29, 380–393.

Sala, S., Kim Cerutti, A. & Pant. Rana. (2018). JRC Technical reports - Development of a weighting approach for the Environmental Footprint.

Santhanam, M. & Otieno, M. (2016). Deterioration of concrete in the marine environment. In: Marine Concrete Structures. Pp. 137–149. Elsevier.

Sayagh, S., Ventura, A., Hoang, T., François, D. & Jullien, A. (2010). Sensitivity of the LCA allocation procedure for BFS recycled into pavement structures. Resources, Conservation and Recycling, 54, 348–358.

Schepper, M. De, Heede, P. Van den, Driessche, I. Van & Belie, N. De. (2014). Life Cycle Assessment of Completely Recyclable Concrete. Materials, 7, 6010–6027.

Schiessl, P., Bamforth, P., Baroghel-Bouny, V., Corley, G., Faber, M., Forbes, J., Gehlen, C., Helene, P., Helland, S., Ishida, T., Markeset, G., Nilsson, L.-O., Rostam, S., Siemes, A.J.M. & Walraven, J. (2006). fib Bulletin 34. Model Code for Service Life Design. fib. The International Federation for Structural Concrete.

SCHMID, Jay–Epoxy or Polyurethane Foam, Waterproof! Magazine, Spring, 2010 Available online at www.waterproofmag.com (August 2015). (n.d.). .

Selvarajoo, T., Davies, R.E., Freeman, B.L. & Jefferson, A.D. (2020). Mechanical response of a vascular self-healing cementitious material system under varying loading conditions. Construction and Building Materials, 254.

Senaratne, S., Gerace, D., Mirza, O., Tam, V.W.Y. & Kang, W.-H. (2016). The costs and benefits of combining recycled aggregate with steel fibres as a sustainable, structural material. Journal of Cleaner Production, 112, 2318–2327.

Serna, P., Roig, M., Mezquida, E., Peled, A., Regev, O., Ferrara, L., Monte, F. Lo, Cuenca, E., Reichardt, M., Schröfl, C., Mechtcherine, V., Borg, R.P., Camacho, E., Lopez, J.A. & Coll, H. (2019). D4.2 – Guidelines for mix design formulation of functionalized UHDC and adaption to different application technologies.

Seto, K.E., Churchill, C.J. & Panesar, D.K. (2017). Influence of fly ash allocation approaches on the life cycle assessment of cement-based materials. Journal of Cleaner Production, 157, 65–75.

Shafikhani, M. & Chidiac, S.E. (2019). Quantification of concrete chloride diffusion coefficient – A critical review. Cement and Concrete Composites, 99, 225–250.

Shah, S.P., Hou, P. & Konsta-Gdoutos, M.S. (2016). Nano-modification of cementitious material: toward a stronger and durable concrete. Journal of Sustainable Cement-Based Materials, 5, 1–22.

Shao, Y., Parks, A. & Ostertag, C.P. (2023). Carbon Footprint between Steel-Reinforced Concrete and UHPC Beams. Journal of Structural Engineering, 149.

Shields, Y., Mullem, T. Van, Belie, N. De & Tittelboom, K. Van. (2021). An investigation of suitable healing agents for vascular-based self-healing in cementitious materials. Sustainability (Switzerland), 13.

Shields, Y., Tsangouri, E., Riordan, C., De Nardi, C., Godinho, J. R. A., Ooms, T., Antonaci, P., Palmer, D., Al-Tabbaa, A., Jefferson, T., De Belie, N., & Van Tittelboom, K. (2024). Non-destructive evaluation of ductile-porous versus brittle 3D printed vascular networks in self-healing concrete. Cement and Concrete Composites, 145, 105333. https://doi.org/10.1016/j.cemconcomp.2023.105333

Sidiq, A., Gravina, R.J., Setunge, S. & Giustozzi, F. (2019). Microstructural analysis of healing efficiency in highly durable concrete. Construction and Building Materials, 215, 969–983.

SIKA–Waterproofing-Solutions for Water Seal, using SIKA Injection Systems in Concrete, Masonry and Natural Stone Structures (in Portuguese). SIKA Brazil Marketing Catalog. Available online at http://bra.sika.com (September 2015).

Singh, V.K., Shukla, A., Sahani, R.K., Shekhar, A.R. & Singh, R. (2022). Structural Application of Concrete Made of Recycled Aggregate Sourced from Construction and Demolition Waste. Lecture Notes in Civil Engineering. Springer International Publishing.

Snoeck, D. (2015). Self-healing and microstructure of cementitious materials with microfibres and superabsorbent polymers.

Snoeck, D., Jensen, O.M. & Belie, N. De. (2015). The influence of superabsorbent polymers on the autogenous shrinkage properties of cement pastes with supplementary cementitious materials. Cement and Concrete Research, 74, 59–67.

Snoeck, D., Roigé, N., Manso, S., Segura, I. & Belie, N. De. (2022). The effect of (and the potential of recycled) superabsorbent polymers on the water retention capability and bio-receptivity of cementitious materials. Resources, Conservation and Recycling, 177, 106016.

Snoeck, D., Steuperaert, S., Tittelboom, K. Van, Dubruel, P. & Belie, N. De. (2012). Visualization of water penetration in cementitious materials with superabsorbent polymers by means of neutron radiography. Cement and Concrete Research, 42, 1113–1121.

Snoeck, D., Tittelboom, K. Van, Steuperaert, S., Dubruel, P. & Belie, N. De. (2014). Self-healing cementitious materials by the combination of microfibres and superabsorbent polymers. Journal of Intelligent Material Systems and Structures, 25, 13–24.

Sobolev, K. & Guitierrez, M.F. (2005). SOBOLEV, Konstantin; GUTIÉRREZ, Miguel Ferrada. How nanotechnology can change the concrete world. American Ceramic Society Bulletin, 2005, 84.10: 14.

Sobolev, K. (2016). Modern developments related to nanotechnology and nanoengineering of concrete. Frontiers of Structural and Civil Engineering, 10, 131–141.

Sobolev, K. (2016). Modern developments related to nanotechnology and nanoengineering of concrete. Frontiers of Structural and Civil Engineering, 10, 131–141.

Sobolev, K., Flores, I., Torres-Martinez, L.M., Valdez, P.L., Zarazua, E. & Cuellar, E.L. (2009). Engineering of SiO_2 Nanoparticles for Optimal Performance in Nano Cement-Based Materials. In: Nanotechnology in Construction 3. Pp. 139–148. Berlin, Heidelberg: Springer Berlin Heidelberg.

Song, L., Sun, W. & Gao, J. (2013). Time dependent chloride diffusion coefficient in concrete. Journal of Wuhan University of Technology-Mater. Sci. Ed., 28, 314–319.

Souza Oliveira, A. de, Fonseca Martins Gomes, O. da, Ferrara, L., Moraes Rego Fairbairn, E. de & Toledo Filho, R.D. (2021). An overview of a twofold effect of crystalline admixtures in cement-based materials: from permeability-reducers to self-healing stimulators. Journal of Building Engineering, 41, 102400.

start2see Pty Ltd. (2016). Environmental Product Declaration - Emesh 100% Recycled Macro Poly and Virgin Macro Poly by Fibercon.

Stewart, M.G., Wang, X. & Nguyen, M.N. (2012). Climate change adaptation for corrosion control of concrete infrastructure. Structural Safety, 35, 29–39.

Stipanovic Oslakovic, I., Bjegovic, D. & Mikulic, D. (2010). Evaluation of service life design models on concrete structures exposed to marine environment. Materials and Structures/Materiaux et Constructions, 43, 1397–1412.

Summa, D. di, Parpanesi, M., Belie, N. De & Ferrara, L. (2022a). How to address sustainability and economic viability of advanced cementitious based materials by means of Life Cycle Assessment (LCA) and Life Cycle Cost (LCC) tools integrated into a holistic design-wise approach. In: ICSHM2022 Milano -8thInternational Conference on Self-Healing Materials. P. 105.

Summa, D. di, Parpanesi, M., Ferrara, L. & Belie, N. De. (2022b). Life Cycle Assessment (LCA) and Life Cycle Cost (LCC) analysis as crucial part of a holistic approach to the design of structures with advanced cement based materials. In: 76th RILEM Annual Week and International Conference on Regeneration and Conservation of Structures (ICRCS 2022).

Summa, D. di, Parpanesi, M., Ferrara, L. & Belie, N. De. (2023). A holistic life cycle design approach to enhance the sustainability of concrete structures. Structural Concrete, 24, 7684–7704.

Summa, D. di, Tenório Filho, J.R., Snoeck, D., Heede, P. Van den, Vlierberghe, S. Van, Ferrara, L. & Belie, N. De. (2022). Environmental and economic sustainability of crack mitigation in reinforced concrete with SuperAbsorbent polymers (SAPs). Journal of Cleaner Production, 358.

Szabó, L., Hidalgo, I., Ciscar, J.C. & Soria, A. (2006). CO<inf>2</inf> emission trading within the European Union and Annex B countries: The cement industry case. Energy Policy, 34, 72–87.

Talakokula, V., Bhalla, S., Ball, R.J., Bowen, C.R., Pesce, G.L., Kurchania, R., Bhattacharjee, B., Gupta, A. & Paine, K. (2016). Diagnosis of carbonation induced corrosion initiation and progression in reinforced concrete structures using piezo-impedance transducers. Sensors and Actuators A: Physical, 242, 79–91.

Talukdar, S., Banthia, N. & Grace, J.R. (2012a). Carbonation in concrete infrastructure in the context of global climate change – Part 1: Experimental results and model development. Cement and Concrete Composites, 34, 924–930.

Talukdar, S., Banthia, N., Grace, J.R. & Cohen, S. (2012b). Carbonation in concrete infrastructure in the context of global climate change: Part 2 – Canadian urban simulations. Cement and Concrete Composites, 34, 931–935.

Tang, L. & Sørensen, H.E. (2001). Precision of the Nordic test methods for measuring the chloride diffusion/migration coefficients of concrete. Materials and Structures, 34, 479–485.

Teall, O. (2016). Crack closure and enhanced autogenous healing of structural concrete using shape memory polymers. Materials Science, Engineering.

Temnikov, M.N., Anisimov, A.A., Zhemchugov, P. V., Kholodkov, D.N., Goloveshkin, A.S., Naumkin, A. V., Chistovalov, S.M., Katsoulis, D. & Muzafarov, A.M. (2018). Mechanochemistry – a new powerful green approach to the direct synthesis of alkoxysilanes. Green Chemistry, 20, 1962–1969.

Tenório Filho, J.R., Mannekens, E., Tittelboom, K. Van, Snoeck, D. & Belie, N. De. (2020a). Assessment of the potential of superabsorbent polymers as internal curing agents in concrete by means of optical fiber sensors. Construction and Building Materials, 238.

Tenório Filho, J.R., Mannekens, E., Tittelboom, K. Van, Vlierberghe, S. Van, Belie, N. De & Snoeck, D. (2021). Innovative SuperAbsorbent Polymers (iSAPs) to construct crack-free reinforced concrete walls: An in-field large-scale testing campaign. Journal of Building Engineering, 43, 102639.

Tenório Filho, J.R., Mannekens, E., Tittelboom, K. Van, Vlierberghe, S. Van, Belie, N. De & Snoeck, D. (2021). Innovative SuperAbsorbent Polymers (iSAPs) to construct crack-free reinforced concrete walls: An in-field large-scale testing campaign. Journal of Building Engineering, 43, 102639.

Tenório Filho, J.R., Snoeck, D. & Belie, N. De. (2020b). Mixing protocols for plant-scale production of concrete with superabsorbent polymers. Structural Concrete, 21, 983–991.

The Global Commision on the Economy and the climate. (2018). Unlocking the inclusive growth story of the 21st century: accelerating climate action in urgent times.

Thomas, J., Thaickavil, N.N. & Wilson, P.M. (2018). Strength and durability of concrete containing recycled concrete aggregates. Journal of Building Engineering, 19, 349–365.

Timoshenko, S. & Woinowsky-Krieger, S. (1959). Theory of Plates and Shells. Engineerin.

Tomasini, A. & León-Santiesteban, H.H. (2015). Nylon uses in biotechnology. In: Biocomposites. Pp. 319–346. Elsevier.

Tonucci, L., Mascitti, A., Ferretti, A.M., Coccia, F. & d’Alessandro, N. (2022). The Role of Nanoparticle Catalysis in the Nylon Production. Catalysts, 12, 1206.

Torres-Acosta, A.A., Presuel-Moreno, F.J. & Andrade, C. (2019a). Electrical resistivity as durability index for concrete structures. ACI Materials Journal, 116, 245–253.

Tsangouri, E. (2019). A Decade of Research on Self-Healing Concrete. In: Sustainable Construction and Building Materials. IntechOpen.

Turner, L.K. & Collins, F.G. (2013). Carbon dioxide equivalent (CO<inf>2</inf>-e) emissions: A comparison between geopolymer and OPC cement concrete. Construction and Building Materials, 43, 125–130.

Ulkir, O. (2023). Energy-Consumption-Based Life Cycle Assessment of Additive-Manufactured Product with Different Types of Materials. Polymers, 15, 1466.

UNI. (2015). UNI EN ISO 16627:2015 - Sustainability of construction works - Assessment of economic performance of buildings - Calculation methods.

UNI. (2019a). UNI EN 15804:2019, Sustainability of construction works - Environmental product declarations - Core rules for the product category of construction products.

UNI. (2019b). UNI EN 15804:2019, Sustainability of construction works - Environmental product declarations - Core rules for the product category of construction products.

UNI. (2021a). UNI EN ISO 14040:2021, Environmental management - Life cycle assessment - Principles and framework.

UNI. (2021b). UNI EN ISO 14044:2021, Environmental management - Life cycle assessment - Requirements and guidelines.

UNI. (2021b). UNI EN ISO 14044:2021, Environmental management - Life cycle assessment - Requirements and guidelines.

United States Environmental Protection Agency. (2000). Vinyl acetate [Internet document] URL https://www.epa.gov/sites/default/files/2016-09/documents/vinyl-acetate.pdf. Accessed 19/01/2024.

United States Patent. (1989). Patent nr. 4,873,365, Process for the preparation of isophorone disocyanate from sophorone dicarbamy esters using highly selective SNO2 or CUO catalysts.

United States Patent. (1996). Patent nr. 5,491,264 preparation of isophorone diamine.

Val, D. V. & Melchers, R.E. (1997). Reliability of Deteriorating RC Slab Bridges. Journal of Structural Engineering, 123, 1638–1644.

Vallance, S., Perkins, H.C. & Dixon, J.E. (2011). What is social sustainability? A clarification of concepts. Geoforum, 42, 342–348.

Vera-Agullo, J., Chozas-Ligero, V., Portillo-Rico, D., García-Casas, M.J., Gutiérrez-Martínez, A., Mieres-Royo, J.M. & Grávalos-Moreno, J. (2009). Mortar and Concrete Reinforced with Nanomaterials. In: Nanotechnology in Construction 3. Pp. 383–388. Berlin, Heidelberg: Springer Berlin Heidelberg.

Vladisavljevic, G. (2003). Influence of process parameters on droplet size distribution in SPG membrane emulsification and stability of prepared emulsion droplets. Journal of Membrane Science, 225, 15–23.

Wang, H.L., Dai, J.G., Sun, X.Y. & Zhang, X.L. (2016). Characteristics of concrete cracks and their influence on chloride penetration. Construction and Building Materials, 107, 216–225.

Wang, J.Y., Soens, H., Verstraete, W. & Belie, N. De. (2014). Self-healing concrete by use of microencapsulated bacterial spores. Cement and Concrete Research, 56, 139–152.

Wang, X.-H., Hu, D.-G., Hong, A.K.B. & Shi, D.-D. (2022). Prediction of Equivalent Chloride Ion Diffusion Coefficient in Cracked Concrete of the in-Service RC Element. KSCE Journal of Civil Engineering, 26, 2369–2380.

Warsi, Y., Kabanov, V., Zhou, P. & Sinha, A. (2020). Novel Carbon Dioxide Utilization Technologies: A Means to an End. Frontiers in Energy Research, 8.

Weerdt, K. De, Justnes, H. & Geiker, M.R. (2014). Changes in the phase assemblage of concrete exposed to sea water. Cement and Concrete Composites, 47, 53–63.

Wu, P., Xia, B. & Zhao, X. (2014). The importance of use and end-of-life phases to the life cycle greenhouse gas (GHG) emissions of concrete - A review. Renewable and Sustainable Energy Reviews, 37, 360–369.

Xing, S., Xu, Z. & Jun, G. (2008). Inventory analysis of LCA on steel- and concrete-construction office buildings. Energy and Buildings, 40, 1188–1193.

Y. Liu, R.E. Weyers Modelling the time-to-corrosion cracking in chloride contaminated reinforced concrete structures ACI Mater. J., 95 (6) (1998), pp. 675-681. (n.d.). .

Yang, G., Wei, J., Yu, Q., Huang, H. & Li, F. (2019). Investigation of the Match Relation between Steel Fiber and High-Strength Concrete Matrix in Reactive Powder Concrete. Materials, 12, 1751.

Yang, K.-H., Lim, H.-S., Kwon, S.-J. & Kim, J.-H. (2020). Repair cost estimation techniques for reinforced concrete structures located at the seashore: Considering various probabilistic service life functions and actual mix proportions. Construction and Building Materials, 256, 119469.

Yang, R., Kang, S., Ozer, H. & Al-Qadi, I.L. (2015). Environmental and economic analyses of recycled asphalt concrete mixtures based on material production and potential performance. Resources, Conservation and Recycling, 104, 141–151.

Yang, Y. & Urban, M.W. (2013). Self-healing polymeric materials. Chemical Society Reviews, 42, 7446.

Yeheyis, M., Hewage, K., Alam, M.S., Eskicioglu, C. & Sadiq, R. (2013). An overview of construction and demolition waste management in Canada: a lifecycle analysis approach to sustainability. Clean Technologies and Environmental Policy, 15, 81–91.

Zampori, L., Saouter. E., Schau, E., Cristobal, J., Castellani, V. & Sala, S. (2016). Guide for interpreting life cycle assessment result.

Zhang, J. & Mailvaganam, N.P. (2006). Corrosion of concrete reinforcement and electrochemical factors in concrete patch repair. Canadian Journal of Civil Engineering, 33, 785–793.

Zhang, J., Li, G., Ye, W., Chang, Y., Liu, Q. & Song, Z. (2018). Effects of ordinary Portland cement on the early properties and hydration of calcium sulfoaluminate cement. Construction and Building Materials, 186, 1144–1153.

Zhang, X., Zhang, Y., Liu, B., Liu, B., Wu, W. & Yang, C. (2021). Corrosion-induced spalling of concrete cover and its effects on shear strength of RC beams. Engineering Failure Analysis, 127, 105538.

Zhang, Y., Wu, S., Zhang, Y., Zhou, C. & Fu, C. (2023). Similarities and probability distributions of chloride convection zone depth in concrete exposed to cyclic drying-wetting environments. Cement and Concrete Composites, 139, 105040.

Zhao, Y., Yu, M., Xiang, Y., Kong, F. & Li, L. (2020). A sustainability comparison between green concretes and traditional concrete using an emergy ternary diagram. Journal of Cleaner Production, 256, 120421.

Zhao, Z., Qi, T., Zhou, W., Hui, D., Xiao, C., Qi, J., Zheng, Z. & Zhao, Z. (2020). A review on the properties, reinforcing effects, and commercialization of nanomaterials for cement-based materials. Nanotechnology Reviews, 9, 303–322.

Zhu, L., Zhao, C. & Dai, J. (2021). Prediction of compressive strength of recycled aggregate concrete based on gray correlation analysis. Construction and Building Materials, 273.

Zhu, Y., Yang, J., Mei, F., Li, X. & Zhao, C. (2022). Bio-based 1,4-butanediol and tetrahydrofuran synthesis: perspective. Green Chemistry, 24, 6450–6466.

CURRICULUM VITAE – Davide di Summa

Nationality: **Italian**

Date and place of birth: **17/07/1991, Taranto – Italy**

Email: **disumma.d@gmail.com**

LinkedIn: **www.linkedin.com/in/davide-di-summa-91t**

EDUCATION

PhD In Civil Engineering/Structural, seismic and earthquake and geotechnical engineering | August 2020 – July 2024

Ghent University, Ghent, Belgium – Faculty of Engineering and Architecture

Politecnico di Milano, Milan, Italy – Department of Civil and Environmental Engineering (DICA)

Fellow of Marie Skłodowska-Curie Project (European Union's Horizon 2020 research and innovation program) SMARTINCS Grant No 860006

MSc in Building Engineering | March 2014 – April 2016

Polytechnic University of Bari, Bari, Italy

Final grade: 110 cum laude/110

Final dissertation: Analysis of real estate market condition by rating scoring systems

Erasmus visiting student | September 2015 – January 2016

University of Warmia and Mazury in Olsztyn, Olsztyn, Poland

Erasmus visiting student | January 2015 – July 2015

University of Seville, Seville, Spain

BSc in Building Engineering | October 2010 – March 2014

Polytechnic University of Bari, Italy

Final grade: 110 cum laude/110

Final dissertation: The Energy retrofit of historical buildings: architectural survey and intervention guidelines for "d'Ayala Building" in Taranto (Italy)

PROFESSIONAL EXPERIENCE

Research fellow | February 2020 – July 2020

Politecnico di Milano, Milan, Italy

- development of a business plan to promote new settlements in Mogadishu, based on affordable and sustainable housing, local entrepreneurship, related social facilities and renewable energies;
- market appraisal, construction costs estimation;
- Investigation of innovative technological solutions for Mogadishu area.

Research fellow | January 2019 – January 2020

University of Bergamo, Bergamo, Italy

- development of high performance shielding building materials using mortar/concrete with a secondary conductive phase deriving from biomasses;
- study of urban development strategies using low cost sensors as tools to monitor the most important air quality indices.

Construction manager assistant | September 2017 – January 2019

SJS Engineering/DBA group, Taranto, Italy

Support to Construction managers' activities during the "*Redevelopment of the molo polisettoriale - bulk materials terminal rehabilitation*" in Taranto (Italy) and "*Port of Dammam redevelopment*" in Dammam (Saudi Arabia), carrying out the following key duties:

- bill of quantities editing;

- oversee and direct construction projects from conception to completion;
- review the project in-depth to schedule deliverables and estimate costs;
- oversee all onsite and offsite constructions to monitor compliance with construction and safety regulations;
- select tools, materials and equipment and track inventory;
- meet contractual conditions of performance;
- review the work progress on daily basis;
- prepare internal and external reports pertaining to job status.

Building and construction account manager |October 2016 – September 2017

Hilti Italia, Rimini, Italy.

- grow a loyal customer base within a defined territory through outside, business-to-business, face-to-face sales;
- participate in construction industry trade organizations to build relationships and networks;
- read and understand construction documents at a Hilti relevant level;
- analyse MS Excel report data and develop business plans to effectively maintain and grow customer sales;
- leverage multiple sales channels to maximize territory revenue;
- utilize consultative sales techniques;
- demonstrate Hilti products and services to customers on active jobsites;
- obtain appointments with decision makers at construction/ industrial companies;
- jobsite visits to identify key roles on the project as well as their responsibilities and needs;
- work across multiple departments to be a successful Account Manager (materials

management, logistics, credit, marketing, technical services, customer service).

Intern | June 2016 – August 2016

Biwater International, Dorking, United Kingdom

- use of Causeway Project Controls System to manage construction projects;
- provide assistance in the delivery of a change management programme implementing new systems and processes into Biwater International Limited, a global specialist in the provision of water facilities;
- use of electronic document management systems in construction and the implementation of change within a major organization.

PUBLICATIONS

Peer-reviewed journals

D. di Summa, M. Parpanesi, L. Ferrara, N. De Belie, A holistic life cycle design approach to enhance the sustainability of concrete structures, Structural Concrete 24 (2023) 7684–7704. https://doi.org/10.1002/suco.202300645.

V. Cappellesso, D. di Summa, P. Pourhaji, N. Prabhu Kannikachalam, K. Dabral, L. Ferrara, M. Cruz Alonso, E. Camacho, E. Gruyaert, N. De Belie, A review of the efficiency of self-healing concrete technologies for durable and sustainable concrete under realistic conditions, International Materials Reviews (2023) 1–48. https://doi.org/10.1080/09506608.2022.2145747.

N. Kannikachalam, D. di Summa, R.P. Borg, E. Cuenca, M. Parpanesi, N. De Belie, L. Ferrara, Assessment of Sustainability and Self-Healing Performances of Recycled Ultra-High-Performance Concrete, ACI Mater J 120 (2023). https://doi.org/10.14359/51737336.

D. di Summa, J.R. Tenório Filho, D. Snoeck, Philip. Van den Heede, S. Van Vlierberghe, L. Ferrara, N. De Belie, Environmental and economic sustainability of crack mitigation in reinforced concrete with SuperAbsorbent polymers (SAPs), J Clean Prod 358 (2022). https://doi.org/10.1016/j.jclepro.2022.131998.

C. Del Pero, O.E. Bellini, M. Martire, D. Di Summa, Sustainable solutions for mass-housing design in africa: Energy and cost assessment for the somali context, Sustainability (Switzerland) 13 (2021) 1–19. https://doi.org/10.3390/su13094787.

M. Yasir, D. Di Summa, G. Ruscica, I.N. Sora, P. Savi, Shielding properties of cement composites filled with commercial biochar, Electronics (Switzerland) 9 (2020). https://doi.org/10.3390/electronics9050819.

M. Renigier-Biłozor, A. Biłozor, D. di Summa, 2016. "Rating Decision Rules on the Real Estate Market in Poland and in Italy – a Case Study," World of Real Estate Journal 98 (2016). https://doi.org/10.14659/worej.2016.98.08

CONFERENCES
Proceedings

D. di summa, A. Marcucci, M. Nicolo`, F. Martignoni, A. Carrassi, F. Liberato, N. De Belie, LCA assessment related to the evolution of the earthquake performance of a strategic structure, in: F. Biondini, D.M. Frangpol (Eds.), Proceedings of the eighth international symposium on life cycle civil engineering (IALCCE 2023), 2-6 JULY, 2023, Politecnico di Milano, Milan, Italy, Milano, 2023: pp. 1169–1176.

D. di Summa, F. Soave, M. Davolio, S. Al Obaidi, L. Ferrara, N. De Belie, How to better exploit the use of LCA analysis for Ultra High Performance Concrete (UHPC) through a constitutive law which integrates chloride and sulfate attack, in: F. Biondini, D.M. Frangopol (Eds.), Proceedings of the eighth international symposium on life cycle civil

engineering (IALCCE 2023), 2-6 JULY, 2023, Politecnico di Milano, Milan, Italy, Milano, 2023: pp. 3094–3101.

D. di Summa, E. Camacho, L. Ferrara, N. De Belie, Towards a Conscious and Far-Sighted Construction Market Through the Use of Sustainability Indexes, in: Building for the Future: Durable, Sustainable, Resilient Proceedings of the Fib Symposium 2023 - Volume 1, 2023: pp. 870–877. https://doi.org/10.1007/978-3-031-32519-9_86.

D. di Summa, L. Ferrara, N. De Belie, How to account for benefits of Self-Healing concrete in design? A LCA/LCC perspective, in: M. di Prisco, A. Meda, G.L. Balazs (Eds.), Proceedings of the 14th Fib PhD Symposium in Civil Engineering, 2022: pp. 689–696.

D. di Summa, D. Snoeck, J.R.T. Filho, P. Van den Heede, S. Van Vlierberghe, N. De Belie, L. Ferrara, Sustainability and Economic Viability of Self-healing Concrete Containing Super Absorbent Polymers, in: 2023: pp. 335–343. https://doi.org/10.1007/978-3-031-21735-7_37.

D. di Summa, M. Parpanesi, N. De Belie, L. Ferrara, How to address sustainability and economic viability of advanced cementitious based materials by means of Life Cycle Assessment (LCA) and Life Cycle Cost (LCC) tools integrated into a holistic design-wise approach., in: ICSHM2022 Milano -8thInternational Conference on Self-Healing Materials, 2022: p. 105.

D. di Summa, M. Parpanesi, L. Ferrara, N. De Belie, Life Cycle Assessment (LCA) and Life Cycle Cost (LCC) analysis as crucial part of a holistic approach to the design of structures with advanced cement based materials, in: 76th RILEM Annual Week and International Conference on Regeneration and Conservation of Structures (ICRCS 2022), 2022.

P. Savi, D. di Summa, I.N. Sora, G. Dassano, G. Ruscica, R. Pelosato, Drywall coated with biochar as electromagnetic interference shielding material, in: 2021 International Conference on Electromagnetics in Advanced Applications (ICEAA), IEEE, 2021: pp. 403–404.
https://doi.org/10.1109/ICEAA52647.2021.9539791.

M. Yasir, D. di Summa, G. Ruscica, I.N. Sora, P. Savi, Shielding properties of cement composites filled with commercial biochar, Electronics (Switzerland) 9 (2020). https://doi.org/10.3390/electronics9050819.

P. Savi, D. Cirielli, D. di Summa, G. Ruscica, I.N. Sora, Analysis of shielding effectiveness of cement composites filled with pyrolyzed biochar, in: 5th International Forum on Research and Technologies for Society and Industry: Innovation to Shape the Future, RTSI 2019 - Proceedings, 2019. https://doi.org/10.1109/RTSI.2019.8895522

BOOKS
Chapters

O.E. Bellini, D. di Summa, Estimation of Construction Costs: From Technological Solutions to the Settlement Scale, in: 2022: pp. 167–182. https://doi.org/10.1007/978-3-031-00284-7_8

CONFERENCES
Organization committee

Part of the following organization committees

International Conference on Self-healing Materials, Milan, Italy |June 2023

SMARTINCS conference, Ghent, Belgium |May 2023

RILEM spring convention, Milan, Italy |April 2024

TEACHING AND TUTORING EXPERIENCE

Life Cycle Assessment of Materials and structures | Academic years: 2022/2023 – 2023/2024

Ghent University, Ghent, Belgium

Teaching activities: Life Cycle Assessment – basic principles and case studies. Use of SimaPRO software

Exercise: Life cycle assessment in SimaPRO

Precast structure | Academic years: 2020/2021 - 2021/2022 – 2022/2023 – 2023/2024

Politecnico di Milano, Milan, Italy

Seminar: Life Cycle Assessment and Life Cycle Costing for advanced construction materials

Tutor of students for MSc thesis

Academic years: 2021/2022 -2022/2023

- *Student:* Antonio Carrassi. *Thesis*: "Life Cycle Assessment and Corrosion Effects on Structural Behaviour: A Case Study of The New Water Treatment Plant in Genoa". Politecnico di Milano, 2023;
- *Student*: Francesco Soave. *Thesis*: "Valutazione della sostenibilità delle applicazioni strutturali in materiali cementizi avanzati tramite integrazione di analisi LCA e LCC in un approccio alla progettazione del tipo Durability Assessment Design". Politecnico di Milano, 2022;
- *Student*: Matteo Parpanesi. *Thesis*: "A holistic life-cycle design approach to tructures with advanced cement based materials". Politecnico di Milano, 2021.

LANGUAGES Italian – *native* | English – *fluent* | Spanish - *fluent*

“ [...] e volta nostra poppa nel mattino,
de' remi facemmo ali al folle volo.”

Dante Alighieri - Inferno, Canto XXVI

Abstract representation of a built environment and the potential impact of sustainable solutions on it.